

Curtin University of Technology
School of Chemical and Petroleum Engineering
Department of Petroleum Engineering

**GAS INJECTION IN FRACTURED RESERVOIRS:
EMPHASIS ON MASS TRANSFER**

By

Mohammad Mohammadzadeh Bahar

This thesis is presented for the Degree of

Doctor of Philosophy

of

Curtin University of Technology

March 2010

Declaration

This thesis contains no material which has been accepted for the award of any other degree or diploma in any university.

To the best of my knowledge and belief this thesis contains no material previously published by any other person except where due acknowledgement has been made.

Signature:.....

Date:.....

ABSTRACT

Mass transfer occurs in a number of Enhanced Oil Recovery (EOR) processes such as gas injection, solvent injection, Water Alternative Gas injection (WAG) processes and gas cycling. The role of mass transfer in gas injection into an oil phase at fractured media is significant. In naturally fractured reservoirs, fluid exists in two interconnected systems; the rock matrix, which contains the bulk of the volume of the oil reservoir, and the high permeability fractures medium.

Laboratory measurements of the diffusion coefficient of methane into crude oil under both unsteady-state and steady-state conditions were carried out to obtain the dissolution rates of methane during gas injection and/or flooding in the short term, and for enhanced oil recovery at thermodynamic equilibrium in the long term. The pressure drop in the core flooding cell during the contact of the methane and oil phases was used to measure the diffusion coefficient of the system under the reservoir conditions. A new empirical correlation for the diffusion coefficient was achieved using the measured experimental data at reservoir conditions. A comparison of this new correlation and previous methods shows that the current method is more accurate than other methods at high pressure and temperature conditions.

Experimental tests on fluid flow in tight carbonate porous media were carried out with single and composite core plugs. It was demonstrated that the swelling of oil strongly depended on the contact time of the oil and gas phases and heterogeneity of the system.

The two and three-phase relative permeability in tight carbonate reservoirs was a major part of this research. It was carried out on single and composite core plugs at reservoir conditions.

Modelling of the displacement of fluids in tight carbonate rocks was carried out with experimental data. Solving of the partial differential equation of displacement phenomena in porous media was carried out with the finite element method software (FLEXPDE). All of the experimental data with the new diffusion coefficient correlation were used to model the system.

In the fracture medium, an artificial fracture in synthetic rock was made and all the parameters used for carbonate rock were considered without fracture. Modelling of the system was carried out between the matrix and fracture medium. The effect of mass transfer between gas in the fracture and oil in the matrix was evaluated and the variation of saturation in the matrix by applying the boundary condition method was evaluated. As a result, it was shown that the mass transfer significantly increased the recovery from the matrix by following the condensation and evaporation mechanisms.

Dedication

To my beloved wife **Ensiyeh**

and my lovely kids **Hasti and Ali**

with love and gratitude



ACKNOWLEDGEMENTS

I would like to thank my Curtin University of Technology advisors, Associate Professor M. Reza Rezaee, and Professor Brian Evans, Head of Petroleum Engineering, for their technical guidance and support in developing this dissertation.

I wish to express my sincere gratitude and appreciation to the National Iranian Oil Company for their financial support in granting me a NIOC scholarship. My special thanks go to Dr. Keyu Liu from CSIRO Petroleum for supporting me in submitting this thesis.

I would like to express my sincere thanks to CoreLab , Australia for cleaning all the core plugs used in the experiments at no cost, and Dr. Robert G. Nelson, Technical Support of PDE Solution Inc Software Company for giving me access to the software license.

Last but not least, I would like to express gratitude to my wife, Ensiyeh, for her love, support, and understanding, without which this work would not have been accomplished.

Table of Contents

CHAPTER1: Introduction

Introduction-----	1
1.1 Diffusion coefficient measurements under reservoir conditions-----	2
1.2 The mass transfer effect-on Three-phase relative permeability measurements-----	4
1.3 The miscibility effect on enhanced oil recovery-----	6
1.3.1 Single contact miscibility-----	7
1.3.2 Multiple contact miscibility-----	7
1.3.3 Minimum miscibility pressure -----	8
1.3.4 Miscibility in fractured reservoirs -----	10
1.4 Fracture-Matrix mass transfer-----	11
1.5 Research Objectives-----	12
1.6 Thesis outline-----	15

Chapter 2 : Theory and methodology

Overview-----	16
2.1 Mass transfer phenomena in PVT cell-----	17
2.1.1 Mass transfer with constant diffusion coefficient-----	17
2.1.2 Mass transfer with variable diffusion coefficients-----	20
2.2 Mass transfer phenomena in porous media-----	23
2.2.1 Diffusion in porous media-----	23
2.2.2 Diffusion of gas into the oil phase (condensing)-----	24
2.2.3 Three-phase flow equations with mass transfer-----	26
2.2.4 Three-phase flow equations in displacement theory -----	31
2.2.5 Three-phase relative permeability with mass transfer-----	34

2.2.6 Vaporising of oil during gas injection-----	35
2.3 Mass Transfer phenomena between Fractures and the Matrix-----	38
2.4 Remarks-----	40

Chapter 3 : Experimental Equipment and Procedure

3.1 Introduction-----	41
3.2 Equipment description-----	44
3.2.1 Injection and collection pumps -----	45
3.2.2 The water, oil, and gas cylinders -----	47
3.2.3 Core holder -----	49
3.2.4 Three-phase acoustic separator -----	51
3.2.5 Rotating gas meters-----	53
3.2.6 Pressure and temperature transducers-----	54
3.2.7 Data monitoring system -----	55
3.3 Equipment set up to measure mass transfer under static and dynamic conditions-----	56
3.3.1 Measurement of the diffusion coefficient under static conditions using a PVT cell-----	56
3.3.2 Measurement of the relative permeability in the laboratory-----	59
3.3.3 Unsteady-state method for measuring two-phase relative permeability -----	60
3.3.4 The unsteady-state method for measuring three-phase relative permeability ----	64
3.3.5 Experimental equipment for measuring three-phase relative permeability and enhanced oil recovery -----	65
3.4 Calibration of the equipment for static and dynamic experiments-----	66
3.4.1 Calibration of the pressure sensors with a referenced pressure gauge -----	66
3.4.2 Temperature calibration with a referenced thermometer -----	68

3.4.3 Calibration of the volume and flow rate measurement systems -----	68
3.4.4 Measurement of the dead volume in the system-----	70
3.4.5 Calibration of the separator with collection pumps-----	71
3.4.6 Calibration of the gas meter -----	73
3.5 Material selection and preparation to perform the experiments-----	73
3.5.1 Core selection, cutting and cleaning -----	73
3.5.2 Core Plugs absolute permeability and porosity -----	74
3.5.3 Study of capillary end effect-----	75
3.5.4 Gravity effect during flooding-----	75
3.5.5 Core ordering -----	76
3.5.6 Brine treatment -----	77
3.6 Experimental Procedures and Data Collection-----	78
3.6.1 Diffusion coefficient measurement procedure at high pressure and temperature	78
3.6.2 Procedure for the measurement of two-phase relative permeability -----	79
3.6.3 Absolute permeability measurement with water -----	79
3.6.4 Relative permeability measurement -----	80
3.6.5 Procedures for core saturation and displacement experiments -----	80
3.6.6 Core preparation and core holder handling -----	81
3.6.7 Three-phase relative permeability measurements-----	84

Chapter 4: Results and discussion

4.1 Introduction-----	86
4.1.1 Mass transfer in a PVT cell under reservoir conditions -----	88
4.1.2 New correlation of diffusion coefficient at reservoir condition-----	90
4.1.3 Comparison of measured correlation diffusion coefficient with previous	

correlations-----	93
4.1.4 Modelling of the system by the finite elements method-----	94
4.1.5 Discussion-----	102
4.2 Mass transfer during displacement in carbonate reservoir-----	102
4.2.1 Experimental results for selected core plugs-----	105
4.2.2 Experimental results from the composite core plug-----	111
4.2.3 Volume of gas diffused into the oil phase by mass transfer-----	114
4.2.4 Two-phase relative permeabilities with the unsteady-state method-----	118
4.2.5 Three- phase relative permeability with the unsteady-state method-----	119
4.2.6 Simulation of fluid flow through porous media-----	125
4.2.7 Discussion-----	133
4.3Effect of mass transfer on fluid flow in a fractured medium-----	136
4. 3.1 Effect of overburden pressure on fractured media-----	136
4.3.2 Simulation of fluid flow in fractured media-----	139
4.3.3Discussion of the results-----	146

Chapter 5: Conclusions and recommendations

5.1 Conclusions-----	148
5.2 Recommendations-----	150
References-----	152
Appendix A-----	163
Appendix B-----	173
Appendix C-----	175
Appendix D-----	190
Appendix E-----	193

LIST OF TABLES

Table 2.1 The coefficient of equation 2.9 for Methane-Dodecane and Methane-crude oil system at various temperatures (Jamiyolahmadi et al., 2006) -----	22
Table 3.1: Technical specification of Pressure Transducer-----	55
Table 3.2 Absolute permeability, total porosity and pore volume of core samples-----	74
Table 4.1 Comparison of diffusion coefficient value of this research with other studies-----	93
Table 4.2 Measured properties of the core plugs used in the experiments-----	104
Table 4.3 Swelling volume of oil phases in four type core plugs-----	117
Table 4.4 Recovery of oil during gas injection -----	136
Table 4.5- Porosity and permeability of fracture porous media-----	138

LIST OF FIGURES

Figure 1.1: A schematic of forward and backward contact experiment (Whitson and Brule, 2000) -----	8
Figure 1.2: Pressure distribution in a hypothetical reservoir-----	10
Figure 1.3: Flowchart of progress of the thesis-----	14
Figure 2.1: Schematic and dimensions of a diffusion process model-----	18
Figure 2.2: Diffusion coefficient in a porous medium with fractures (Ho and Webb, 2006)-	25
Figure 2.3: Schematic of velocity profile of the gas phase in the fracture media during mass transfer taking place-----	31

Figure 2.4: Schematic of one dimensional evaporation from a liquid in a dead-end region with external convection-----	39
Figure 2.5: Fracture flow and diffusion phenomena into the rock matrix-----	39
Figure 2.6: Gas velocity profile in fracture and matrix media-----	44
Figure 3.1: The three-phase core-flooding apparatus-----	43
Figure 3.2: Schematic of the three phase core-flooding system -----	44
Figure: 3.3 : Positive displacement pumps -----	45
Figure 3.4: Gas, oil and water collection pumps -----	46
Figure 3.5: Enerpac hand pump -----	47
Figure 3.6: Gas, oil and water high-pressure vessels-----	48
Figure 3.7: Schematic of the injection point and spider pattern in inlet point of core holder -	49
Figure 3.8: Core-holder and back pressure valve at overburden pressure-----	50
Figure 3.9: High pressure separator set-up with three vessels -----	52
Figure 3.10: Gas meter, back pressure and overburden vessels -----	53
Figure 3.11: Pressure indicators and transducers -----	54
Figure 3.12: Computer data gathering display -----	55
Figure 3.13: Diffusion coefficient measurement apparatus under static conditions-----	57
Figure 3.14: Schematic of mass transfer process under static condition -----	58

Figure 3.15: A schematic of the three phase core-flooding system -----	67
Figure 3.16: Calibration curve for pressure sensor in the system -----	69
Figure 3.17: Schematic of dead volume measurement -----	71
Figure 3.18: Schematic of separator and collection pumps -----	72
Figure 3.19: Calibration of collection pumps -----	72
Figure 3.20: Effect of gas diffusion through the sleeve -----	84
Figure 4.1: Schematic of the mass transfer of gas and oil during contact time and moving boundary of the phases -----	89
Figure 4.2: Measured pressure drop during mass transfer of gas into crude oil -----	89
Figure 4.3a: Schematic of the mass transfer of gas and oil during contact time and moving boundary of the phases-----	91
Figure 4.3b: Comparison of measured and new correlation pressure drop during mass transfer of gas into crude oil-----	92
Figure 4.4a: Pressure surface maps in gas and oil phases during mass transfer of the system-- -----	95
Figure 4.4b: Pressure contour maps in gas and oil phases during mass transfer of the system-- -----	95
Figure 4.5: Profile of methane mole fraction in the oil phase at $p=200 \text{ Bar}$ and $T=87 \text{ }^\circ\text{C}$ ---	96
Figure 4.6: Saturation profile of methane in the oil phase during displacement-----	97
Figure 4.7: Concentration Profile of methane in the oil phase at $p=200 \text{ Bar}$ and $T=87 \text{ }^\circ\text{C}$ ---	98

Figure4.8: Diffusion coefficient of methane in the oil phase at T=87 °C and P=200 Bar---	98
Figure 4.9: Variation of the pressure from 206 Bar (3000 Psia) in the system at T=87 °C---	99
Figure4.10: Variation of methane concentration in the oil phase with time at 200 Bar and 87°C-----	100
Figure 4.11: Production of oil, water and gas during displacement-----	105
Figure 4.12: Water, oil and gas recoveries during the drainage process for three types of core plugs -----	107
Figure 4.13: Pressure drop during the drainage process with gas flooding-----	109
Figure 4.14: Oil Recoveries during gas flooding-----	111
Figure 4.15: The composite core plug ordering-----	112
Figure 4.16: Water recovery during the drainage process with crude oil flooding-----	113
Figure 4.17: Variation of pressure during three phase production-----	113
Figure 4.18: Oil recovery during gas flooding q=30 (cc/h)-----	114
Figure 4.19: Volume of dissolved gas into the oil phase – core plug 1-3-----	115
Figure 4.20: Volume of dissolved gas into the oil phase – core plug 2-3-----	116
Figure 4.21: Volume of dissolved gas into the oil phase core plug 2-2-----	116
Figure 4.22: Volume of dissolved gas into the oil phase – composite core plug-----	117
Figure 4. 23: Two-phase relative permeability of core plug 2-3-----	118
Figure 4.24: Two-phase relative permeability from the composite core plug-----	119
Figure 4.25: Relative permeability of water versus water saturation of core plug 1-3-----	121
Figure 4.26: Relative permeability of oil versus water saturation of core plug 1-3-----	122
Figure 4.27: Relative permeability of gas versus oil saturation of core plug 1-3 -----	122

Figure 4.28: Relative permeability of water versus gas saturation of core plug 1-3 -----	122
Figure 4.29: Relative permeability of water versus water saturation of composite core plug --- -----	123
Figure 4.30: Relative permeability of water versus oil saturation of composite core-plug-- ---- -----	123
Figure 4.31: Relative permeability of gas versus oil saturation of composite core-plug-----	124
Figure 4.32: Relative permeability of water versus gas saturation of composite core-plug--	124
Figure 4.33: 2D horizontal core flooding system mesh model-----	127
Figure 4.34: Relative permeability of gas and oil in two phase flow versus time-----	127
Figure 4.35: Relative permeability of gas and oil in two phase flow and gas saturation variation versus Time-----	128
Figure 4.36: Estimated recovery percent versus time by model-----	128
Figure 4.37: Variation of gas saturation during displacement of crude oil by gas-----	130
Figure 4.38: Variation of gas saturation during displacement of crude oil by gas -----	131
Figure 4.39: Relative permeability of gas displacement system with mass transfer-----	131
Figure 4.40: Relative permeability of gas displacement system with mass transfer-----	132
Figure 4.41: Recovery percent with low and high diffusion coefficient in comparison to experimental data-----	133
Figure 4.42: Effect of gas diffusion on swelling of crude oil-----	133
Figure 4.43: Schematic of prepared artificial fractured -----	137
Figure 4.44: Effect of overburden of fracture permeability-----	139
Figure 4.45: Schematic of fluid flow in a fracture and matrix-----	140

Figure 4.46: Dynamically generated grid after 60 minutes-----141

Figure 4.47: Contour map of gas saturation during displacement of crude oil by gas in a fractured medium-----142

Figure 4.48: Variation of gas saturation during displacement of crude oil by gas in fractured medium at time= 10, 20, 40, and 60 minute consequently -----143

Figure 4.49: Variation of gas saturation during displacement of crude oil by gas in fractured medium at time= 10, 20, 40, and 60 minute consequently-----144

Figure 4.50: Variation of gas saturation along the core holder in fractured medium after 3000 seconds-----144

Figure 4.51: Variation of gas relative permeability at outlet of core holder after 3000 seconds-----144

Figure 4.52: The percentage of recovery during displacement of crude oil by gas in fractured medium after 3000 seconds-----145

Figure 4.53: Evaporation mechanism in fracture medium and effect on permeability in the system-----147

CHAPTER 1

Introduction

Many existing oil and gas reservoirs in Iran are naturally fractured and, on average, more than two-thirds of the original oil in fractured reservoirs remains unrecovered, even after carrying out secondary recovery (Sahimi et al, 2006). New technologies may enable exploitation of these reservoirs in an efficient and cost effective manner. Enhanced oil recovery (EOR) processes and horizontal drilling are two fundamental technologies which could be used to increase the recoverable reserves in fractured reservoirs by as much as fifty percent (Sahimi et al 2006).

Production from fractured reservoirs normally occurs by diffusion or gravity drainage of oil from the matrix into the fracture network. The ability to predict the performance of enhanced oil recovery processes by gas injection requires knowledge of the mass transfer phenomena and the concept of three-phase relative permeability. Mass transfer occurs when gas and oil make contact with each other during gas injection. During gas flooding phenomena, if the saturations of water and oil are higher than their irreducible levels, all of the three phases would move toward the drainage point and their three-phase relative permeability controls the mobility of each phase. When oil is displaced by gas, considerable interaction takes place between these phases, substantially modifying the physical and chemical properties of the fluids, especially at their interfaces. These changes in fluid properties considerably affect the EOR performance. The current practice to calculate three-phase relative permeability from two-phase relative permeability in predicting the recovery using a numerical reservoir simulator might not be representative.

This study investigates the effects of mass transfer phenomena during gas injection into carbonate core plug saturated with oil under reservoir conditions. The diffusion coefficient, the three-phase flow relative permeability and the partial miscibility were considered to be the most important parameters that would have a material impact during the injection of gas into

Introduction and outline

an oil-saturated fractured carbonate reservoir. These parameters are briefly described in the following sections.

1.1 Diffusion coefficient measurements under reservoir conditions

Mass transfer occurs during a number of enhanced oil recovery (EOR) processes such as gas injection, solvent injection, water alternative gas (WAG) processes and gas cycling. Mass transfer is the migration of matter from one location to another due to concentration or partial pressure gradients. The mass transfer processes can be subdivided into two categories namely, molecular and convective. The random molecular migration of matter through a medium is called diffusion, whereas migration of the matter from a surface into a moving fluid or gas is called stream convective mass transfer. During gas injection in fractured reservoirs, diffusion and convective mass transfer occur in the matrix/fracture network. The rate of diffusion between gases and liquids is affected by temperature and pressure. Diffusion in porous media is more complex than diffusion in free gases and liquids because the molecules may travel in various directions dictated by the conditions of the porous medium.

Mass transfer can occur either under steady-state or unsteady-state conditions. Under steady-state conditions, the concentration of phases or partial pressure, the resistance to fluid and the mass transfer rate are all constant over time. Under unsteady-state conditions however, all these properties vary with time. The mathematical solution for steady-state conditions is therefore simpler than that for unsteady-state conditions.

During primary production of a fractured reservoir most of the oil is produced from the fractures, with the matrix left with unrecovered moveable oil. Gas injection helps to recover substantial quantities of the oil trapped in the matrix (Sarma, 2003). For the naturally fractured reservoirs (NFRs), it is necessary to estimate the rate of mass transfer caused by molecular diffusion in order to determine the amount of gas diffusing into the oil when gas is injected into the reservoir (Siang, 2000). The molecular diffusion is very important in miscible gas flooding since it helps gases to penetrate the oil which then inhibits viscous fingering, delays gas breakthrough, and increases the oil production rate (Denoyelle and Bardon, 1984).

Introduction and outline

Sigmund (1976), Grogan and Pinczewski (1987), Renner (1988), and Grogan et al. (1988) have discussed the importance of molecular diffusion in the study of petroleum recovery techniques. It is very important to understand the effects of molecular diffusion on the total amount and rate of gas dissolution in vertical miscible floods. The conditions at which the diffusion process is important in comparison to dispersion in porous media are discussed by Perkins and Johnston (1963). To calculate the rate of gas dissolution by diffusion, the diffusion coefficient under reservoir conditions is the most important parameter. In spite of this, there is a lack of sufficient experimental data on diffusion coefficients at high pressures for multi-component mixtures and reservoir fluids.

In general, the methods used to measure the diffusion coefficients in hydrocarbon systems can be divided into four categories. In the first category, during the experiments, samples of the reservoir fluids are taken at various times and are analysed using a gas chromatograph. For example, the methods used by Berry and Koller (1960), Sigmund (1976) and Dickson and Johnson (1988) are in this category. In the second category, the samples are not analysed, but the self-diffusion coefficients are measured using tools such as nuclear magnetic resonance (NMR) and once the measurements are made, the correlations such as those proposed by Vignes (1966) have been used to obtain the binary diffusion coefficients. The methods used by Dawson et al. (1970) and Woessner et al. (1969) fall in this category. In the third category, the volume of gas dissolved in oil versus time at a constant pressure is measured to determine the diffusion coefficient in reservoir fluids. The work of Denoyelle and Bardon (1984) and Renner (1988) are in this category. The last category considers the rate of pressure change and the interface position as a function of time, which depends on the rate of diffusion in each phase and the diffusion coefficient. Riazi (1996), Zhang et al. (2000) and Hong et al. (2000) proposed using a PVT cell to determine the diffusion coefficient of dense gases in liquids. A non-equilibrium gas is brought into contact with a liquid in a sealed container at a constant temperature, and the final state is determined by thermodynamic equilibrium.

It can be concluded that there is no single universal method for calculating the diffusion coefficient from known properties of the systems. Most conventional methods utilized for

Introduction and outline

compositional analysis of the fluids are time consuming, expensive, and tedious (Moulu, 1989).

The diffusion coefficient obtained in this section at reservoir condition will be applied for fluid flow in porous media. The suitable time of contact to get more mass transfer from gas phase into liquid will be considered in next experiment.

1.2 The mass transfer effect-on Three-phase relative permeability measurements

Reservoir engineering designs, oil recovery predictions, and evaluation of EOR processes require good quality relative permeability data. Production of petroleum reservoirs by primary, secondary, or tertiary processes usually involves the simultaneous flow of two or more fluids within the reservoir. Three-phase flow in the reservoir always occurs during gas injection into an oil reservoir. Two-phase relative permeability has been widely reported in the literature (Stone (1973), Wyllie and Gardne (1958), Corey (1956), Oak (1991), Welge (1952), and JBN (1959); however, the study of three-phase relative permeability has not been fully understood, because of the complexity of the experiments that need to be performed and the subsequent mathematical analysis. Experimental work has shown that the presence of a third phase influences the transport properties of the other two phases during the flow in a porous medium. Leverett and Lewis (1941) were the first to report the results of three-phase relative permeability experiments. They measured three-phase relative permeabilities in unconsolidated sand using the steady-state method and ignoring the capillary end effects and hysteresis. However, they attempted to minimise these end effects by using core plugs with semi permeable membranes mounted at each end. Corey (1956) measured saturations gravimetrically and avoided the hysteresis effect by using a separate core plug for each measurement rather than re-saturating the same core plug. A dynamic method using NMR techniques was used by Saraf and Fatt (1967) to determine the liquid saturation thereby minimising the end effect. It was also noted by all these researchers that the relative permeability of the wetting and non-wetting phase is primarily a function of its own saturation whereas the relative permeability of the mix-wetting phase is strongly affected by the saturation history and the saturations of the other two phases. Oak (1990) presented a study of steady-state, two-phase and three-phase relative permeability data using three fired Berea

Introduction and outline

sandstone cores of 200 mD, 800 mD and 1000 mD. This comprehensive analysis included over 30 combinations of rock and fluid systems and saturation histories. The author concluded that, while the water and gas relative permeabilities during three-phase flow were only functions of their own saturations, the oil relative permeability varied with the saturation of the other phases as well.

Virnovsky (1985) and Grader and O'Meara (1988) developed a theory to obtain three-phase relative permeability by an extension of the Welge (1950) and Johnson-Boster-Nauman (JBN) (1959) methods to three phases. Siddiqui et al. (1996) verified the theory using X-Ray computerised tomography to obtain in-situ saturations for three-phase dynamic displacement experiments. Sahni (1998) used the three-phase relative permeabilities from Grader and O'Meara's experiments to predict successfully the saturation paths and recoveries analytically using the Method of Characteristics. Sarem (1966) obtained three-phase relative permeability by unsteady-state displacement experiments which assumed that the relative permeability of each phase was a function of its own saturation. Oak (1991) presented a further steady-state study of three-phase relative permeability using the fired Berea cores. Naylor et al. (2001) obtained three-phase relative permeability from gravity drainage experiments using in-situ saturation measurements and ignoring capillary pressure. Nordvedt et al. (1996) performed displacement experiments on low-permeability chalk samples and obtained three-phase relative permeability from an optimisation technique using a general purpose three-phase simulator. Akin and Demiral (2001) obtained three-phase relative permeability from unsteady state displacement experiments using an automated history matching technique. Spronsen (1985) and Hagoort (1980) measured three-phase relative permeabilities using the centrifuge method, whereas Elment et al. (2003) used four gas and water flooding in sequences with emphasis on the hysteresis effect. They concluded that the measuring of three-phase relative permeability must consider irreversibility of hysteresis cycles, the potential for the reduction in the residual oil saturation with trapping of gas by water, and the reduction in both water and gas permeability, with the potential for the fractional flow to vary with trapped gas saturation.

Oil and gas relative permeability is a function of interfacial tension (IFT). Experimental results show (McInery et al.(2005)) that the residual oil saturation and the relative

Introduction and outline

permeability are strongly affected by IFT, especially when the IFT is lower than about 1.0mN/m. Cinar et al. (2004) presented experimental data showing that the wetting phase relative permeability was not affected by IFT, whereas the other two-phase relative permeability was affected.

During mass transfer phenomena light components of gas phase diffuse to oil phase, the composition of the oil phase convert to light components subsequently viscosity, density, and IFT of oil phase change. As explained in this section, the relative permeability strongly depend to viscosity and IFT, therefore effect of the diffusion mechanisms in porous media will be studied.

1.3 The miscibility effect on enhanced oil recovery

Miscible displacement processes are widely employed in various aspects of oil recovery. Mass transfer between fluids occurs when the chosen injection fluid is completely miscible with the oil under reservoir conditions. In this case, the residual oil saturation becomes low due to solubility and reduction of interfacial tension, and hence the displacement efficiency is increased. In the reservoir, the miscible condition between two immiscible fluid phases develops in two ways:

1. First contact miscibility – when two fluids are first contact miscible, they form a single-phase mixture in various proportions at the given conditions; and,
2. Multiple contact miscibility – this kind of miscibility develops when two fluids come in contact with each other several times. The injected gas and oil may form two different phases; therefore, they may not be first contact miscible but mass transfer between the two phases can happen after a long period of contact between the fluids to achieve miscibility.

Generally, first contact miscibility processes involving rich hydrocarbon (solvent) or high reservoir pressures are not economically feasible. The total cost of the miscible displacement,

Introduction and outline

including the cost of transporting the injection gas to the oil field, is so high that it is economically unattractive to the industry.

However, multiple contact miscibility can be developed for many reservoirs economically. Injection gases like nitrogen, carbon dioxide and natural gas are known to develop multiple contact miscibility at reservoir conditions under some conditions of pressure, compositions and temperature (Hoier and Whitson, 2000).

1.3.1 Single contact miscibility

The capillary forces and interfacial tension phenomena between fluids cause most of the oil to remain unrecovered in the reservoir. Producing trapped and residual oil in a reservoir depends on how much gas and solvent is injected into the reservoir. The injected fluid should reduce the capillary and interfacial forces of the oil until a large fraction of the trapped oil is recovered. If the critical temperature and pressure of the injected gas are near the critical state of the oil, they will mix in large proportions with the oil phase. During gas injection in the reservoir, if the gas and oil in-place mix in all proportions, the gas and the oil became single contact miscible.

1.3.2 Multiple contact miscibility

Multiple contact miscibility develops by in-situ transfer of components between oil and gas after multiple contacts between the injected gas and the oil in-place in the reservoir. Depending on the initial composition of the oil and the injected gas, the phases become either lean or rich depending on the composition of oil and injected gas. The gas drive processes can be classified under two broad categories (Orr et al., 1984).

1. Vaporising gas drives; and,
2. Condensing gas drives.

Introduction and outline

The schematic in Figure 1.1 shows the forward and backward contact for both mechanisms. The forward contact experiment follows the vaporizing gas miscible process. That is, the equilibrium gas from each contact is removed and mixed with more of the original reservoir oil. The developed gas should eventually reach miscibility with the original oil if the experiment is conducted at a pressure greater than the Minimum Miscibility Pressure (MMP).

The backward contact experiment follows the condensing gas drive and the procedure allows for enrichment of the gas miscible drive process. Here, the equilibrium oil resulting from a given contact is mixed with more of the original injection gas. In this process, the swelling and gas/oil ratio of the oil are changed during each step and miscibility should develop between the original injected gas and altered reservoir oil. Other types of gas drives can be interpreted as a combination of the vaporising and condensing gas drives.

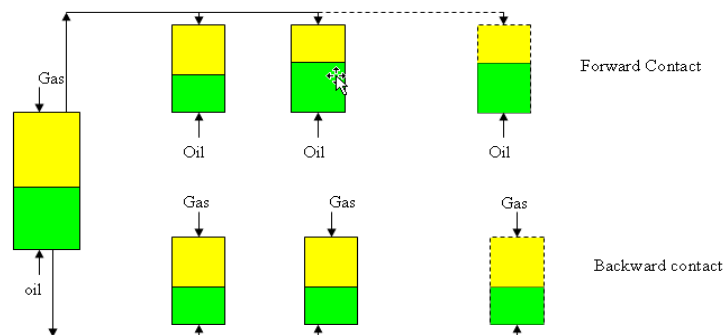


Figure 1.1 A schematic of forward and backward contact experiment (Whitson and Brule, 2000)

1.3.3 Minimum miscibility pressure

The development of the miscibility of gas into oil largely depends on the compositions of the reservoir oil and the injection gas at a given temperature and pressure in the reservoir. In other words, in a ternary diagram, the relative location of the reservoir oil, injection gases, and the extent of the two-phase region, determine whether multiple contact miscibility can occur.

Introduction and outline

However, under practical conditions, it is not possible to alter the composition of the reservoir oil and for economic reasons it is not possible to alter the injection gas composition beyond a certain point. Hence, pressure is often the only variable that can be manipulated to achieve miscibility. At a given reservoir temperature, for a given system of reservoir oil and injected gas compositions, the minimum pressure required to achieve multiple contact miscibility between the oil and gas phase is known as the Minimum Miscibility Pressure (MMP). To achieve high displacement efficiency, the pressure in the reservoir should be maintained at or above MMP. In practice, gas injection is carried out at a pressure which is slightly above the MMP, such that the pressure at the miscible front remains at or above MMP for most of the reservoir area. In any real displacement processes, however, the local pressure will vary along the displacement length (Figure 1.2) from injector to producer. This results in a pressure profile, which suggests that, in the vicinity of a production well, the pressure may decline below the reservoir MMP thus affecting the displacement efficiency (Kumar, 2004). Under some conditions, a partial miscibility occurs when the reservoir pressure is below MMP and the sweep efficiency is increased as the contact time is increased. In gas injection processes, MMP varies with time and the diffusion coefficients of the phases; therefore it covers a zone from high pressure to low pressure (Figure 1.2).

All the miscibility mechanisms were explained are independent from time of contact between phases. In this research time of contact and rate of diffusion will be monitored for partially miscible phenomena to get extra oil recovery from the system.

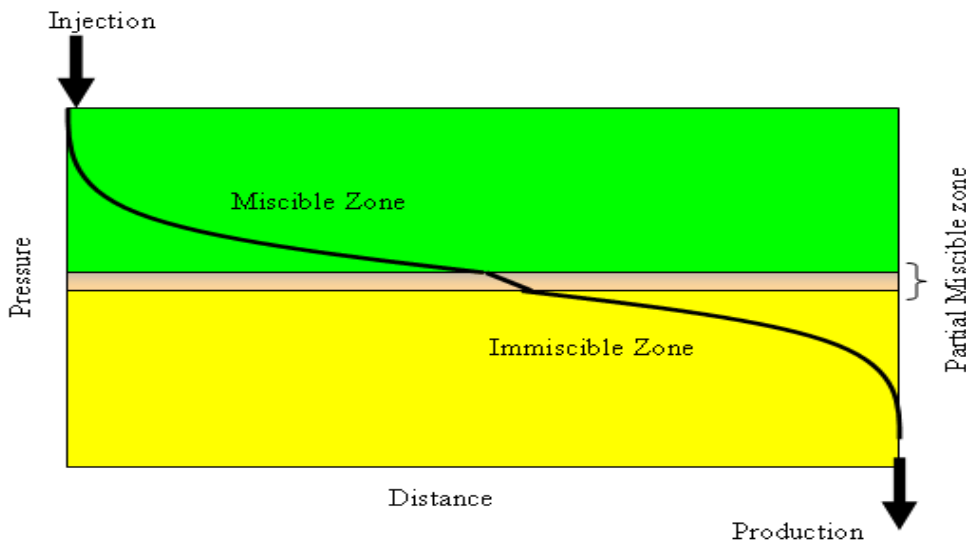


Figure 1.2 Pressure distribution in a hypothetical reservoir

1.3.4 Miscibility in fractured reservoirs

Much research has been carried out on the recovery of matrix oil in fractured reservoirs by miscible displacement. In fractured reservoirs, a major concern for miscible fluid injection is the early breakthrough and production of large quantities of the injected fluid. The capillary pressure contrast of the fracture and the matrix is a major parameter which causes low recovery efficiency in fractured reservoirs. Reduction or elimination of capillary pressure (miscibility or near miscibility) is expected to improve recovery performance of fractured reservoirs. In 1969, Thompson and Mungan reported the results of an experimental study on gravity drainage in fractured porous media under first contact miscible conditions. They showed that the fracture permeability does not affect the displacement process.

Experimental work performed by Frioosabadi (1994) showed that first contact miscibility is a very efficient displacement process. Due to a pronounced fluid cross flow process between the matrix and the fractures, a significant amount of the injected fluid flows from the fracture to the matrix. As a result, a significant amount of the matrix oil flows to the fracture.

Introduction and outline

Nitrogen is a commonly injected gas into naturally fractured reservoirs for pressure maintenance (Mungan, 2000) due to its availability and low cost. If miscibility conditions are achieved, the matrix oil can be produced using the diffusion mechanism. Another common gas injected for the same purpose is methane. Le Romancer (1994) observed that oil (pentane) recovery is twice as fast with methane as with nitrogen.

Heavier carbon fractions than methane have also been tested as injection fluids (Le Gallo, 1997). More recently, Lenormand et al. (1998) defined a transfer function for the diffusion between matrix and fracture, and Stubos and Poulou (1999) proposed a scaling equation for the same phenomenon. Both approaches might lead to field scale performance estimations.

1.4 Fracture-Matrix mass transfer

In low permeability reservoirs with small matrix porosity and high gas-oil capillary pressure, the recovery efficiency of gravity drainage is often very low. In fractured systems, the rate of mass transfer between the rock matrix and fractures usually determines the oil production. A matrix contains most of the oil due to its much higher storage capacity compared to the fracture network, but an effective matrix-fracture network is required to recover the matrix oil. Hence, recovery due to mass transfer between gas in the fracture and the gas/oil system in the matrix must be taken into account to accurately predict reservoir performance. Oil swelling due to gas dissolution in the oil phase and the vaporisation of light oil fraction, significantly improves oil recovery in such cases (Le Gallo et al.(1997)). Molecular diffusion can offset the adverse effects of viscous fingering on oil recovery by swelling (Do and Pinczewski, (1991)). On the other hand, when gas is injected into a highly fractured, under-saturated oil reservoir, it will dissolve in the oil present in the matrix resulting in an increased saturation pressure with the subsequent swelling of the oil, together with decreasing oil viscosity and interfacial tension. Under these conditions, molecular diffusion of the gas dispersed through the fractures is the main recovery mechanism of matrix oil. Generally, the mass transfer mechanisms that occur between the matrix and the fracture can be categorised into three types: (a) transport within a single phase, (b) transport across a partially immiscible phase along a single tie-line and (c) transport across partially immiscible phases across many tie-lines (lines joining

Introduction and outline

equilibrium liquid and vapor compositions of hydrocarbon components). Diffusion and dispersion mechanisms are important in all three cases. Equilibrium constants and phase behavior are important in the last two cases. Capillarity is important in the last two cases whereas it is insignificant in the first case. Gas injection is considered to be the main mechanism for oil recovery in oil and intermediate-wet fractured reservoirs as it allows for recovery of substantial quantities of oil trapped within the matrix.

Diffusion coefficient which is obtained in section (1.1), relative permeability of section and desirable time of contact for partial miscible condition in sections(1.2 and 1.3), will be carried out for simulation of fluid flow in fractured media. Also effect of the pressure on fracture aperture which affect on the permeability and mass transfer will be investigated.

1.5 Research Objectives

In spite of many published experimental studies on gas injection in fractured reservoirs, there are still several aspects which have not been researched, including:

1. Measurement of diffusion coefficients in two and three-phase flow at high pressures and temperatures (reservoir conditions);
2. The effect of mass transfer on three-phase relative permeability (miscible or near miscible under Buckley Leverett theory);
3. The capillary effect in tight carbonate composite core plugs based on Huppler, or descending order;
4. Measurement of the partial miscibility condition under mass transfer phenomena in condensing (diffusion from gas to liquid) in porous media under reservoir conditions; and
5. Measurement of the influence of mass transfer phenomena on Enhanced Oil Recovery (EOR) in fractured reservoirs.

A series of mass transfer experiments were performed at reservoir temperature and pressure using cores from a carbonate fractured reservoir in Iran. The diffusion coefficient

Introduction and outline

measurements were made using a PVT cell. The three-phase relative permeability, oil recovery and partial miscibility were measured using high pressure and high temperature core flooding equipment available from Curtin University. The expected performance of the EOR process using gas injection into a fractured carbonate reservoir was evaluated by using commercially available reservoir simulations software in the industry. These simulators use a simple dual porosity/dual permeability model to predict the EOR efficiency. Unfortunately, these software do not consider the effect of mass transfer during an EOR process on the concept of three-phase relative permeability. This leads to erroneous predictions of EOR performance in a fractured reservoir. The research performed and described in this thesis aims to understand what really happens when gas is injected into a fractured oil reservoir for the purpose of EOR.

The diffusion coefficient is critical for the estimation of mass transfer during an EOR process and should be measured in the laboratory at high pressures and temperatures. Three-phase relative permeability is another unknown in gas injection processes. It should also be measured in the laboratory at reservoir conditions. All of the available commercial simulation software uses two-phase relative permeability data to calculate three-phase relative permeability. The only way to obtain good three-phase relative permeability data is through experimental means.

Introduction and outline

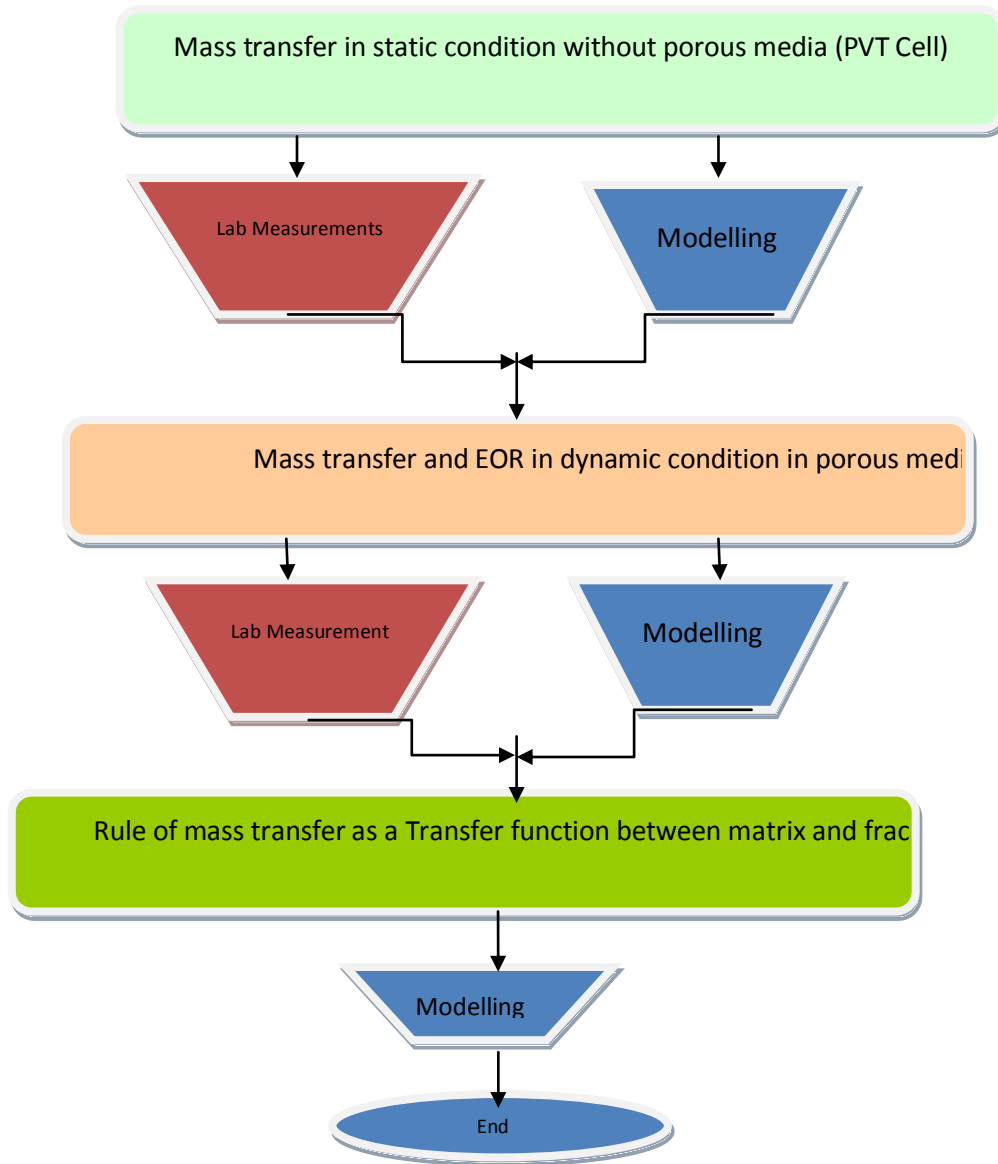


Figure 1.3 Flowchart of progress of the thesis

Finally, the additional recovery due to gas injection into fractured reservoirs was estimated, and the most important parameters strongly influencing EOR such as transmissibility of the fracture-matrix, shape factor of the fracture, immiscibility, and miscibility, were investigated

Introduction and outline

to properly estimate the efficiencies obtained by gas injection into a depleted fractured oil reservoir. Flow chart of this study is illustrated in Figure 1.3.

1.6 Thesis outline

This thesis investigates the effect of mass transfer during gas injection into a tight carbonate and fractured oil reservoir. The effect of mass transfer on relative permeability was another important factor that was investigated. Moreover, simulation of the experimental data with a finite element method using FLEXPDE software was part of this thesis.

This thesis is subdivided into five chapters. These chapters are organised in a logical order to reflect the progress made in achieving the above-mentioned objectives. Chapter one is an introductory chapter which explains some basics and thesis objectives Chapter 2 discusses the mass transfer theory at high temperatures, pressures and fluid flow in porous media .The rate of diffusion of gas from gas phase into the liquid and the rate of condensation (swelling) from the fracture into the matrix and the rate of evaporation of oil from the matrix into the fracture is presented.

Chapter 3 outlines the experimental equipment used for measuring enhanced oil recovery achieved due to the gas injected into a fractured carbonate reservoir at reservoir conditions. The procedure for measuring the unsteady-state, three-phase relative permeability at reservoir conditions is set out.

Chapter 4 contains the results and discussions of the overall experimental work. The results were carefully investigated, discussed and analysed in terms of the mass transfer phenomena between the injected phase and the displaced phases.

Finally, Chapter 5 outlines a conclusion of the research findings and recommendations. Relevant information outside the main chapters is given in the appendices at the end of the thesis.

Introduction and outline

Chapter 2 Theory and methodology

Overview

Although diffusion can occur in all three phases (gas, liquid, and solid), the mechanisms involved in each at atomic or molecular scales are likely to be quite different. For the gas phase, individual molecules are well separated and the rate of diffusion can be understood in terms of the kinetic theory of gases. For the liquid phase, the diffusion is known to occur due to a random process involving thermal fluctuation in which atoms or molecules are able to exchange positions with neighbors. For porous media, the diffusion is due to the movement of point defects such as vacancies and interstitial atoms within porous media solids.

Gas injection is presently the most-commonly used approach to enhance recovery. A gas is injected into the oil-bearing stratum under reservoir conditions. The injection pressure and diffusion of gas into the oil phase causes the oil moving into the production well and up to the surface. In addition to the beneficial effect of the pressure support, the diffusion aids recovery by reducing the viscosity, the interfacial tension (IFT) of the crude oil after mixing with the injected gas. The low IFT affects the relative permeabilities through the capillary number, which is a ratio of viscous and capillary forces. Most of the authors (Bardon and Longeron, 1980; Jerauld, 1996; and Blem et al., 2000) suggest that there is a threshold point which the dependence on the capillary number becomes more important.

In the gas injection process, the three-phase flow of gas, oil, and water are moving in a wide variety of circumstances in the petroleum reservoirs. Therefore, for understanding the simultaneous fluid movement of the three phases, measuring of three phase relative permeabilities are necessary. Mass transfer of gases into the liquid phase during gas displacement is affecting the relative permeability of each phase. The following sections are describing theory of mass transfer in PVT cell (static condition), fluid flow in porous media and fluid flow in fractured media.

2.1 Mass transfer phenomena in PVT cell

The fundamentals of diffusion were first developed based on experiments on porous media in response to a concentration gradient by Fick in 1855. Fick (1855) suggested that diffusion occurs in order to reduce the gradient. The following equation is known as Fick's second law of diffusion.

$$\frac{\partial C}{\partial t} = -\frac{\partial}{\partial z}\left(-D\frac{\partial C}{\partial z}\right) = \frac{\partial}{\partial z}\left(D\frac{\partial C}{\partial z}\right) \quad (2.1)$$

where C is the gas concentration in oil phase; z is the distance from bottom of the diffusion cell; t is the time; and D is the diffusion coefficient of the gas in oil phase.

Some researchers (Grogan and pinczewski (1987), Riazi and whitson (1993), and Zhang et al (2000)) assumed that D remains constant throughout the diffusion process. This assumption is reasonable for heavy oil and heavy component with methane gas because the gas concentration in heavy oil is generally low under the condition they have used. The analytical solution of the system with constant diffusion coefficient can be seen in Appendix A.

2.1.1 Mass transfer with constant diffusion coefficient

When a non-equilibrium gas is in contact with crude oil in a constant volume vessel, the system will move towards a state of equilibrium. However, the required time for the complete equilibrium to occur depends on the diffusion coefficient of each phase of the system. Figure 2.1 shows a non-equilibrium gas and oil system with known initial concentrations at a constant temperature.

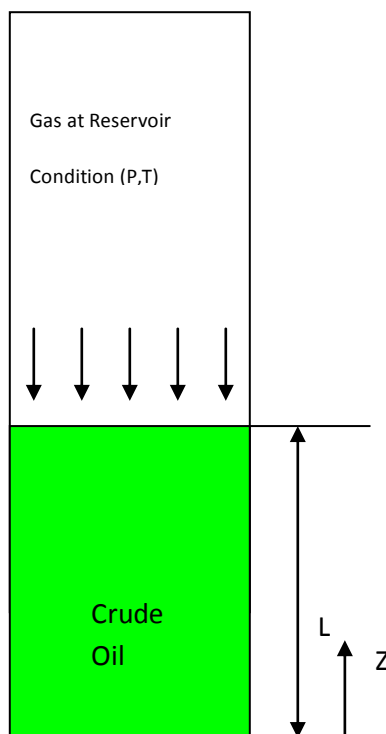


Figure 2.1 Schematic and dimensions of a diffusion process model

The amount of gas that is finally transferred into the crude oil phase depends on the gas solubility in the oil; however, the transfer rate of gas into the liquid phase depends on the diffusion coefficient. If the diffusion coefficient is independent of the concentration, the position, the pressure, the temperature, and the viscosity, it can be moved outside the parentheses and Equation 2.1 can be simplified to:

$$\frac{\partial C}{\partial t} = D \nabla \cdot (\nabla C) = D \nabla^2 C \quad (2.2)$$

The one dimensional diffusion equation is:

Theory and methodology

$$\frac{\partial C}{\partial t} = D \frac{\partial^2 C}{\partial x^2} \quad (2.3)$$

The boundary conditions are:

$$C(z,0) = 0 \quad \text{for } 0 < z < 1$$

$$C(z,t) = C_0 \quad \text{for } z=1, t>0$$

$$\frac{\partial C}{\partial z} = 0 \quad \text{for } z=0, t>0$$

where C_0 is the initial concentration of the gas phase.

Application of the Laplace transform of $C(z, t)$ with respect to time gives:

$$\frac{d^2 \bar{C}}{dz^2} - \left(\frac{s}{D}\right) \bar{C} = 0 \quad 0 < z < 1 \quad (2.4)$$

$$\bar{C}(1,s) = \frac{C_0}{s}, \left(\frac{d\bar{C}}{dz}\right) = 0$$

The solution of this differential equation is:

$$\bar{C}(z,s) = \frac{C_0 \cosh\left(z\sqrt{\frac{s}{D}}\right)}{s \cosh\left(1\sqrt{\frac{s}{D}}\right)} \quad (2.5)$$

which is in writing $\alpha = \sqrt{\frac{s}{D}}$

$$\begin{aligned}
 \bar{C}(z,s) &= \frac{C_o(e^{az} + e^{-az})}{s(e^{aa} + e^{-aa})} = \\
 &= \frac{C_o}{s} [\exp\{-a(a-z)\} + \exp\{-a(a+z)\}] \sum_{n=0}^{\infty} (-1)^n \exp(-2\pi na) \quad (2.6) \\
 &= \frac{C_o}{s} \left\{ \sum_{n=0}^{\infty} (-1)^n \exp[-a\{(2n+1)a-z\}] + \sum_{n=0}^{\infty} (-1)^n \exp[-a\{(2n+1)a+z\}] \right\}
 \end{aligned}$$

In using the Laplace inverse transform such as:

$$\ell\left\{erfc\left(\frac{a}{2\sqrt{t}}\right)\right\} = \frac{1}{s} \exp(-a\sqrt{s})$$

we can obtain the final solution:

$$\bar{C}(z,s) = C_o \left\{ \sum_{n=0}^{\infty} (-1)^n \left[erfc\left\{\frac{(2n+1)a-z}{2\sqrt{Dt}}\right\} + erfc\left\{\frac{(2n+1)a+z}{2\sqrt{Dt}}\right\} \right] \right\} \quad (2.7)$$

This solution represents an infinite series of complementary error functions.

2.1.2 Mass transfer with variable diffusion coefficients

In many systems, such as homogeneous, heterogeneous, and fractured porous media, the diffusion coefficient depends on the concentration of the diffusing substance C , pressure, porous media, viscosity, and temperature. An analytical solution for all the variables is impossible but if D depends on one variable the analytical solution would follow as is described in appendix A. The following equation explains the variation of concentration of components in a static condition.

$$\frac{\partial C}{\partial t} = \frac{\partial}{\partial x} \left(D \frac{\partial C}{\partial x} \right) + \frac{\partial}{\partial y} \left(D \frac{\partial C}{\partial y} \right) + \frac{\partial}{\partial z} \left(D \frac{\partial C}{\partial z} \right) \quad (2.8)$$

where D may be a function of x, y, z, p, T, μ and C .

Theory and methodology

There are cases in which the diffusion coefficient changes with composition. This makes the analysis of the diffusion process more complicated because one has to consider the extra variables when solving the diffusion equation. When a concentration gradient is imposed on a non-stoichiometric compound, re-equilibration of the system may occur by a diffusion process involving the propagation of a concentration gradient throughout the components fraction to minimise the concentration differences in the system. To achieve equilibrium in a system, the value of the chemical potentials of the different components of the system must be constant.

Most of the empirical correlations in isothermal systems have assumed that the diffusion coefficient varies inversely with the viscosity of the solvent. This inverse dependence originated from the Stokes-Einstein equation for a large molecule diffusing through small molecules.

Almost all correlations available for the prediction of molecular diffusion of gases in liquids show that, at a certain temperature, the diffusion coefficient depends primarily on the liquid phase viscosity. For this reason, some investigators (Bruce et al 2004, and Grogan et al 1986) have tried to model their experimental data with respect to liquid phase viscosity. The dissolution of a gas into a liquid reduces its viscosity, which results in an increase in the molecular diffusivity of the solute gas in the liquid phase. Liquid phase viscosity also decreases with increasing liquid phase temperature. As shown in the experiments, the diffusion coefficient also increases as liquid phase temperature increases (as molecules move more rapidly), even though increasing the temperature reduces the solubility of the gas phase in the liquid phase. When the pressure is further increased, the viscosity and density of the solution are also increased and, as a result, the diffusion coefficient gradually decreases.

Many efforts have been made by several investigators (Riazi et al., 1993; Hayduk, 1973; Swapan and Butler, 1996; McManamey and Woollen, 1973 and Grogan et al., 1986) to correlate the molecular diffusion of gases in liquids in terms of liquid phase viscosity. The general model proposed by these investigators can be expressed as:

$$D(T, P) = Q\mu^q \quad (2.9)$$

Theory and methodology

where Q and q are constants and must be obtained from experimental data. The coefficient Q varies from 3.0×10^{-6} to 3.0×10^{-4} (Bruce et al., 2004). On the other hand, almost all researchers have reported that the coefficient q is negative and varies from 0.5 to -1.0. This indicates that the diffusion coefficient has an inverse relationship with liquid phase viscosity. There is no doubt that the liquid phase viscosity is the main operational parameter affecting the diffusivity, but fitting all the experimental data obtained at various operational conditions to Equation 2.9 is impractical. Other parameters such as molar volumes of gas and liquid phases also have an effect on the diffusion coefficient even though this effect is not as pronounced as the liquid phase viscosity. The coefficients of Equation 2.9 at various temperatures are summarised in Table 2.1.

Table 2.1 The coefficient of equation 2.9 for Methane-Dodecane and Methane-crude oil system at various temperatures (Jamiyolahmadi et al., 2006)

Coefficients	Methane-Dodecane system			Crude oil	
	T=45 °C	T=65 °C	T=81 °C	T=25 °C	T=50 °C
Q	0.24719e-8	0.26309e-8	0.27494e-8	0.2304e-8	0.25028e-8
q	-1.0006	-1.00012	-1.00024	-1.009	-1.00717

It is interesting to note that, for a methane-crude oil system, the coefficient q is almost independent of temperature and remains constant at the value of one across all different temperatures. This is in agreement with the equation of Stokes-Einstein which is the basis for almost all mathematical models developed for the prediction of diffusivity of gases in liquids:

$$D = \frac{K_B T}{3\pi\mu d} \quad (2.10)$$

Theory and methodology

where T is the liquid temperature in degree Kelvin, K_B is the Boltzmann constant 1.38×10^{23} J/K, μ is the liquid phase viscosity and d is the solute molecule diameter.

2.2 Mass transfer phenomena in porous media

Under certain conditions, the diffusion of the gas phase into the oil phase can be important. During both secondary and tertiary displacement of the oil reservoir by gas, the development of the multiple contacts (transition zone) strongly controls the efficiency of the ultimate recovery. On a microscopic scale, molecular diffusion is the mechanism by which the molecular diffusion of gas into the oil occurs. With a long contact time between the phases, intermediate components will increase in the gas phase and the gas phase enriches. The transition zone, through a partial miscible zone with the initial oil, is developed by the multiple-contact condensing mechanism. Mass transfer diffusion plays an important role in the condensing mechanisms (see Section 2.5.2). However, a significant oil saturation may exist in the dead-end zone, or be trapped by the water film in a water wet porous medium. This can efficiently traverse the surrounding water barriers to contact and swell the trapped oil. The injected gas also diffuses the oil by molecular diffusion which joins the small fingers together (Sahimi et al., 2006). Diffusion causes a delay in gas breakthrough and, therefore, it increases oil recovery.

2.2.1 Diffusion in porous media

Mass transfer in a porous media can be explained by applying Fick's Law with the addition of some porous characterisation factors such as β ,

$$D_{OG} = \beta D_{og} \quad (2.11)$$

where, β is defined as:

$$\beta = \phi S_g \tau \quad (2.12)$$

D_{OG} is the effective diffusion coefficient for the oil-gas system in porous media, D_{og} is the diffusion coefficient of oil-gas in the PVT cell in the absence of any porous media, ϕ is the porosity, S_g is the gas saturation and τ is the tortuosity of the porous system.

The tortuosity factor τ , is defined as the ratio of the length of the tortuous path in a porous medium, divided by the length of the porous medium under consideration. In other words, the path the fluid must flow through can be considerably longer than the distance between the inlet and outlet of the core sample used in the experiment. The most widely used correlation for calculating the tortuosity factor is described by Millington and Quirk (1961) as follows:

$$\tau = \phi^{1/3} S_g^{7/3} \quad (2.13)$$

2.2.2 Diffusion of gas into the oil phase (condensing)

Injected gas in the reservoir will not only be transported in the gas phase, but the gas will also be transported as a dissolved component in the liquid phase. Since the dissolved gas in the liquid is of low concentration (see Section 2.1), Fick's Law can be adequately applied to estimate the amount of diffused gas into the liquid phase. However, the diffusion flux of gas in the liquid phase can be larger than in the gas phase (Ho and Webb, 2006). The ratio of the gas concentration in the liquid and gas phases is known as the dimensionless Henry's Constant, K_H :

$$K_H = \frac{C_g}{C_o} \quad (2.14)$$

Theory and methodology

where C_g is the concentration of the gas phase, and C_o is the concentration of the oil phase. A low value of the dimensionless Henry's Constant indicates that a significant concentration of dissolved gas is in the oil phase compared to the gas phase values.

In 1983, Jury et al. developed a simplified model to calculate the effective ordinary diffusion coefficient of gas under unsaturated conditions including gas diffusion. The model neglected advection and only considered ordinary diffusion with tortuosity included. The resulting expression for the diffusion coefficient in an under-saturated porous medium is given as:

$$D_{GO} = \phi^{4/3} (S_g^{10/3} D_{go} + S_o^{10/3} D_{go} / K_H) \quad (2.15)$$

This equation provides a simple way to estimate the diffusion coefficient for gas in the oil phase. Figure 2.2 illustrates the diffusion of gas in a fracture medium through the matrix. Diffusion in the gas phase dominates at low oil saturation values, while dissolved gas diffusion in the oil phase dominates at higher oil saturation values.

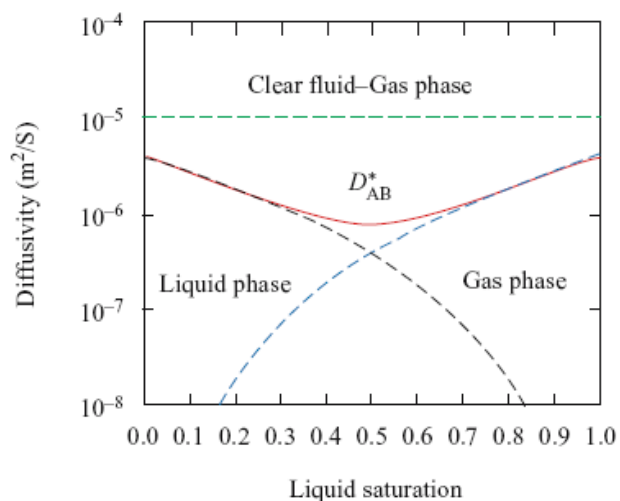


Figure 2.2 Diffusion coefficient in a porous medium with fractures (Ho and Webb, 2006)

2.2.3 Three-phase flow equations with mass transfer

The balance equation for the flow of three phases in a porous medium is given by conservation of mass and momentum in terms of the extended Darcy's Law as:

$$\frac{\partial(S_x \phi \rho_\beta)}{\partial t} + \text{div}(\rho_\beta v_\beta) - \rho_\beta Q_\beta = 0 \quad (2.15)$$

$$v_\beta = \frac{KK_{r\beta}}{\mu_\beta} \left(\frac{\partial P_\beta}{\partial x} - \rho_\beta g \frac{dz}{dx} \right) \quad (2.17)$$

where, the subscript β denotes a given phase ($\beta = w, o, g$) in equations (2.30) and (2.31).

The rest of the variables in the above equations are described below:

S_β - phase saturation`

ϕ - porosity

ρ_β - density of the phase

t - time

v_β - phase velocity

Q_β - phase flow rate from either a sink or a source

$K_{r\beta}$ - relative permeability of the phase

μ_β - dynamic viscosity of the phase

Theory and methodology

Inserting equation (2.30) into equation (2.31) yields the three-phase flow equation:

$$\frac{\partial(S_{\beta}\phi\rho_{\beta})}{\partial t} - \text{div}(\rho_{\beta}\lambda_{\beta}k(\text{grad}P_{\beta} - \rho_{\beta}g)) = 0 \quad (2.18)$$

$$\lambda_{\beta} = \frac{k_{r\beta}}{\mu_{\beta}}$$

Summation of the mass conservation equations for all the phases (oil, gas and water) gives:

$$\frac{\partial(V_w + V_o + V_g)}{\partial x} + \phi \frac{\partial(S_o + S_g + S_w)}{\partial t} = 0 \quad (2.19)$$

$$S_o + S_g + S_w = 1 \quad (2.20)$$

$$V_t = V_w + V_o + V_g \quad (2.21)$$

$$\frac{\partial V_t}{\partial x} = 0 \quad (2.22)$$

Therefore, the total velocity at a given time is constant with respect to the location. Regarding to Settari and Aziz (1976), saturation formula for the water phase it can be written as :

$$\phi \frac{\partial(S_w\rho_w)}{\partial t} + \text{div}(\rho_w V_w) - \rho_w Q_w = 0 \quad (2.23)$$

the oil phase:

Theory and methodology

$$\phi \frac{\partial(S_o \rho_o)}{\partial t} + \text{div}(\rho_o V_o) - \rho_o Q_o = 0 \quad (2.24)$$

the gas phase:

$$\phi \frac{\partial(S_g \rho_g)}{\partial t} + \text{div}(\rho_g V_g) - \rho_g Q_g = 0 \quad (2.25)$$

Darcy's Law for each phase is:

$$V_w = -\lambda_w K(\text{grad}(P_w) - \rho_w g) \quad (2.26)$$

$$V_o = -\lambda_o K(\text{grad}(P_o) - \rho_o g) \quad (2.27)$$

$$V_g = -\lambda_g K(\text{grad}(P_g) + \text{grad}(p_{diff}) - \rho_g g) \quad (2.28)$$

$$\text{grad}(P_c) = \text{grad}(P_o) - \text{grad}(P_w) \quad (2.29)$$

$$\text{grad}(P_c) = \text{grad}(P_o) - \text{grad}(P_g) \quad (2.30)$$

For two- phase flow of water and oil in the system, if the equation for V_o (Equation 2.41) is multiplied by $-\frac{\lambda_w}{\lambda_o}$ and then subtracted from the equation for V_w , (Equation 2.40), and

using Equation 2.43, can be re-arranged as:

$$V_w - V_o \frac{\lambda_w}{\lambda_o} = -\lambda_w K(\text{grad}(P_c) - \rho_o g + \rho_w g) \quad (2.31)$$

$$V_w = V_o \frac{\lambda_w}{\lambda_o} + \lambda_w K(\text{grad}(P_c) - \rho_o g + \rho_w g) \quad (2.32)$$

The total volume, V_t , is given by,

Theory and methodology

$$V_t = V_o + V_w$$

And therefore,

$$V_o = V_t - V_w$$

Substituting the above for V_w into Equation 2.46 results in:

$$V_o = \frac{1}{1 + \frac{\lambda_w}{\lambda_o}} [V_t - \lambda_w K(\text{grad}(P_c) + (\rho_w - \rho_o)g)] \quad (2.33)$$

The fractional flow for oil phase can be defined as:

$$f_o = \frac{\lambda_o}{\lambda_o + \lambda_w} = \frac{\frac{K_{ro}}{\mu_o}}{\frac{K_{rw}}{\mu_w} + \frac{K_{ro}}{\mu_o}} \quad (2.34)$$

and the mean mobility of the system as:

$$\bar{\lambda} = \frac{\lambda_o \lambda_w}{\lambda_o + \lambda_w} = \quad (2.35)$$

Substituting of Equation 2.48 into Equation 2.47 gives the oil velocity as:

$$V_o = f_o V_t - \bar{\lambda} K(\text{grad}(P_c) + (\rho_w - \rho_o)g) \quad (2.36)$$

For two-phase flow of oil and gas in the system, if the equation for V_g is multiplied by $-\frac{\lambda_o}{\lambda_g}$

and then subtracted from the Equation 2.50 for V_o , and using Equation 2.44, it can be rewritten as below:

Theory and methodology

$$V_o - V_g \frac{\lambda_o}{\lambda_g} = -\lambda_o K(\text{grad}(P_c) - \text{grad}(P_{diff}) + \rho_g g - \rho_o g) \quad (2.37)$$

and when considering $V_g = V_t - V_o$, the velocity equation for gas becomes:

$$V_g = \frac{1}{1 + \frac{\lambda_o}{\lambda_g}} [V_t - \lambda_o K(\text{grad}(P_c) - \text{grad}(P_{diff}) + (\rho_o - \rho_g)g)] \quad (2.38)$$

The fractional flow for the gas phase is:

$$f_g = \frac{\lambda_g}{\lambda_o + \lambda_g} = \frac{\frac{K_{rg}}{\mu_g}}{\frac{K_{ro}}{\mu_o} + \frac{K_{rg}}{\mu_g}} \quad (2.39)$$

And mean mobility of the system is:

$$\bar{\lambda} = \frac{\lambda_o \lambda_g}{\lambda_o + \lambda_g} = \quad (2.40)$$

The velocity equation for the gas phase, using Equation 2.53:

$$V_g = f_g V_t - \bar{\lambda} K(\text{grad}(P_c) - \text{grad}(P_{diff}) + (\rho_o - \rho_g)g) \quad (2.41)$$

Figure 2.3 shows the velocity profile of the gas phase into the fracture media during gas diffusion through the oil phase and transition zone. The partial miscible zone increases at the same time.

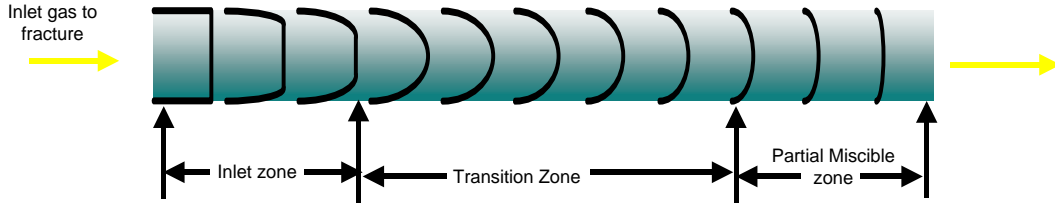


Figure 2.3 Schematic of velocity profile of the gas phase in the fracture media during mass transfer taking place

If we insert Equations 2.50 and 2.55 into Equations 2.38 and 2.39 respectively, with the assumption that the density of each phase remains constant, we obtain:

$$-\phi \frac{\partial S_o}{\partial t} = \text{div}[f_o V_t - \bar{\lambda} K(\text{grad}(P_c) + (\rho_w - \rho_o)g)] - Q_o \quad (2.42)$$

$$-\phi \frac{\partial S_g}{\partial t} = \text{div}[f_g V_t - \bar{\lambda} K(\text{grad}(P_c) - \text{grad}(P_{diff}) + (\rho_o - \rho_g)g)] - Q_g \quad (2.43)$$

2.2.4 Three-phase flow equations in displacement theory

A derivation can be formed from the governing equation of a mathematical formula for multiphase flow in porous media with the assumptions of one-dimensional flow, non-compressible fluids, negligible capillary and gravitational forces, homogeneous rigid porous media, and immiscible fluids. The assumption of immiscible fluids prevents mass transfer between phases and the one-dimensional mass conservation for each phase is driven as follows:

$$\partial_t(m_i) + \partial_x(q_i) = 0 \quad (2.44)$$

Theory and methodology

where, m_i is the mass density and q_i is the mass flow rate flux of each phase. In three-phase flow, the system includes water, oil and gas, and the mass density of each phase can be defined as the mass per unit bulk volume of porous media, where:

$$m_i = \rho_i S_i \phi \quad (2.45)$$

In the above equation, ρ_i is the density of the i^{th} phase, s_i is the saturation and ϕ is the porosity. Assuming that the phase density and the porosity are constants and, by applying Darcy's Law for multiple phase flow, we have:

$$q_i = -K \frac{K_{ri}}{\mu_i} \rho (\partial_x p_i + \rho_i g \partial_x z) \quad (2.46)$$

Relative permeability is a function of the phase saturations. By ignoring gravitational force, capillary effect and defining the relative mobility of i^{th} phase we have:

$$\lambda_i = \frac{K_{ri}}{\mu_i} \quad (2.47)$$

The mass conservation equation for the i^{th} phase is:

$$\partial_t S_i + \partial_i \left(-\frac{1}{\phi} k \lambda_i \partial_x p \right) = 0 \quad (2.48)$$

Since the fluids invade all the pore space, the total saturation is one:

$$S_w + S_o + S_g = 1 \quad (2.49)$$

The total mobility is:

$$\lambda_w + \lambda_o + \lambda_g = \lambda_T \quad (2.50)$$

Considering conservation equations for all phases and applying saturation constraints, the pressure equation can be written as:

Theory and methodology

$$\partial_x \left(-\frac{1}{\phi} k \lambda_T \partial_x p \right) = 0 \quad (2.51)$$

From the above equation, the total velocity can be defined as:

$$v_T = \partial_x \left(-\frac{1}{\phi} k \lambda_T \partial_x p \right) \quad (2.52)$$

which is at most, a function of time. The individual phase velocity can now be defined as:

$$V_i = \frac{\lambda_i}{\lambda_T} v_T \quad (2.53)$$

The fractional flow of the i^{th} phase is:

$$V_i = \frac{v_i}{v_T} = \frac{\lambda_i}{\lambda_T} \quad (2.54)$$

With the definition above, the three-phase flow equation in the 2 x 2 system of conservation laws is:

$$\partial_t \begin{pmatrix} S_w \\ S_g \end{pmatrix} + v_T \partial_x \begin{pmatrix} f_w \\ f_g \end{pmatrix} = \begin{pmatrix} 0 \\ 0 \end{pmatrix} \quad (2.55)$$

The solution of the above equation is restricted to lie in the saturation triangle and can also be written in vector notation defining the vector of unknown $u = [S_w, S_g]$ and the flux vector $f = [f_w, f_g]$. It could be written such that:

$$\partial_t u + v_T \partial_x f = 0 \quad (2.56)$$

with the initial conditions:

$$u(x,0) = \begin{cases} ul & \text{if } x < 0 \\ ur & \text{if } x > 0 \end{cases} \quad (2.57)$$

where ul is the left side boundary and ur is the right side boundary.

With considering of diffusion phenomena (Equation 2.43), Riemann problem (Equation 2.56) and porous media (Equation 2.11) we have:

$$\phi \frac{\partial S_o}{\partial t} + V_t \frac{\partial f_o}{\partial S_o} \frac{\partial S_o}{\partial x} + \frac{\partial}{\partial x} \left(D \frac{\partial S_o}{\partial x} \right) = 0 \quad (2.58)$$

The solution of the Riemann problem with diffusion term in three-phase flow can be obtained by using the finite element method which is discussed in the Results and Discussion chapter (Chapter 4).

2.2.5 Three-phase relative permeability with mass transfer

In tight carbonate reservoirs, the flow velocity is low enough for the displacement process to be controlled by diffusion. The fractional flow as a function of the saturation phase during incubation period is almost a 45° line from partial miscible to miscible phenomena. The diffusion of gas into the oil phase changes the relative permeabilities of the system, and it causes the mobility ratio of the system to change, i.e., the change in viscosity of the oil and gas phases. The viscosity of the transition zone depends on the concentrations of the displacing phase (gas) and the displaced phase (oil). In many cases, the viscosity of the transition zone is estimated from the following empirical correlation offered by Koval in 1963:

$$\mu_{tran} = \frac{C_g}{\mu_g^{1/4}} + \frac{1 - C_g}{\mu_o^{1/4}} \quad (2.59)$$

When the gas phase diffuses within the oil phase a transition zone is created. The fluid properties of this zone are different from the gas and oil phases. In partial miscible displacement of the three-phase flow by gas, the Buckley Leverett equation could be used

Theory and methodology

where the gravity and capillary pressures are negligible as in the case of tight carbonate rocks. The fractional flow for each phase can be written as follows:

$$f_i = \frac{\frac{K_i}{\mu_i}}{\frac{K_o}{\mu_o} + \frac{K_w}{\mu_w} + \frac{K_g}{\mu_g} + \frac{K_{tran}}{\mu_{tran}}} \quad (2.60)$$

where f_i is the fractional flow of the i^{th} phase, μ_{tran} is the viscosity of the fluid mixture in the transition zone and K_{tran} is the permeability of the transition zone.

2.2.6 Vaporising of oil during gas injection

The rate of evaporation of oil in the porous media depends on a number of factors, including oil composition, gas concentration in oil, gas velocity, extent of the dead-end zone, and curvature of the oil/gas interface. In a porous medium, the curvature of the interface between the oil and gas phases affects the equilibrium between the phases. Very small pores can produce a very large capillary pressure for the wetting fluid. The resulting tension in the liquid phase tends to reduce the equilibrium partitioning of compounds in the gas phase and is referred to as vapour pressure lowering (Ho and Webb, 2006). The equilibrium partial pressure of gas, P_g , over the liquid capillary tension can be expressed by Kelvin's equation as follows:

$$P_v = P_{sat} \text{Exp}\left(\frac{-P_c}{\rho RT}\right) \quad (2.61)$$

$$P_c = \sigma \left(\frac{1}{r_1} + \frac{1}{r_2} \right) \quad (2.62)$$

Theory and methodology

where, P_v , P_{sat} , P_c are partial pressure of vapour, saturation pressure, and capillary pressure respectively, R is the gas constant, T is the absolute temperature and σ is the surface tension between oil and gas. r_1 and r_2 are the radii of curvature of the oil and gas interface. Based on Equation 2.75, as the radii of curvature are reduced (smaller pores), the capillary pressure is increased and the resulting partial pressure in the gas phase is decreased.

For oil evaporation in a porous medium to occur during gas injection into an oil reservoir, a transition zone with a moving boundary of the evaporating source must exist. The diffusion mechanism controls the evaporation of oil in the trapped or dead-end regions (Figure 2.4). The concentration at the surface of the liquid is a constant, C_o , and the concentration at the boundary of the region is C_s and the average concentration in the gas flow region is C_{flow} . During the initial periods of contact between the two phases, mobile oil is drawn to the interface between the gas flow and dead-end regions by capillarity, keeping the evaporating surface stationary at the interface. When the oil reaches residual saturation and becomes immobile, the evaporating surface begins to reduce into the dead-end region (Ho and Webb, 2006).

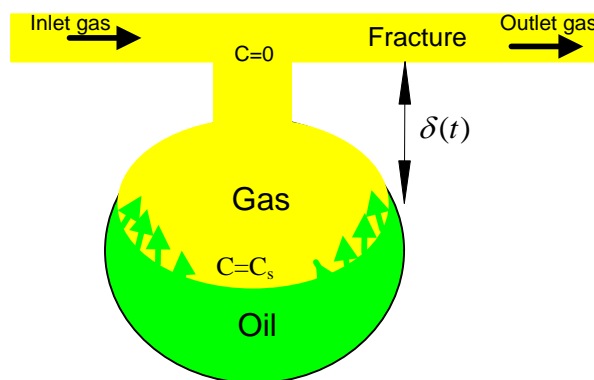


Figure 2.4 Schematic of one dimensional evaporation from a liquid in a dead-end region with external convection

Theory and methodology

The evaporation rate at time, t , can be written as follows:

$$\frac{dm}{dt} = -DA \frac{C_s - C_o}{dt} = -QC_{flow} \quad (2.63)$$

where, A is the cross-sectional area available for diffusion and Q is the flow rate. Equation 2.63 equates the evaporation rate to the rate of diffusion through the dead-end region and to the rate of mass advection away. The rate of change in the mass of the oil can be written as follows:

$$\frac{dm}{dt} = -\phi S_o \rho_o A \frac{d\delta(t)}{dt} \quad (2.64)$$

Where $\delta(t)$ is the distance of the oil level in the matrix from the fracture. The combination of Equations 2.63 and 2.64 gives the following equation:

$$\frac{DAC_s}{\delta(t)} = \phi S_o \rho_o A \frac{d\delta(t)}{dt} \quad (2.65)$$

The above equation can be integrated and solved for $\delta(t)$:

$$\delta(t) = \sqrt{\frac{2DC_s t}{\phi S_o \rho_o}} \quad (2.66)$$

Equation 2.63 can then be used to calculate the gas concentration, C_{flow} and the transient evaporation rate $\left(\frac{dm}{dt}\right)$ of the oil phase that reduces the volume of oil into the dead-end region.

2.3 Mass Transfer phenomena between Fractures and the Matrix

Fractures are the principal paths for fluid flow in tight carbonate reservoirs. The matrix adjacent to the fractures plays an important role in the fluid flow process. The saturated fracture media with oil is displaced by the gas during gas flooding. When injected gas fills the fracture, it comes into contact with oil in the matrix and the gas starts diffusing into the oil. This process was modelled as part of this research and is illustrated in Figure 2.5, which schematically shows the constant concentration of gas (C_g) transported through a fracture. Figure 2.6 schematically shows the velocity profile of the gas phase through the fracture and the matrix.

It is a known fact that the effect of gas diffusing from the fracture into the matrix, causes the contacted oil to swell and move into the fracture. The rate of swelling of the matrix oil is related to Fick's Law which was described in before. The net effect of matrix diffusion is to retard the contact time of the gas phase in the fracture and the crude oil in the matrix. If the gas flow is discontinued, the swelled volume will be flushed into the fracture and the concentration will be reversed, thus moving the swelled crude oil from the matrix into the fracture medium. Therefore, swelling of the oil and evaporation of oil from the matrix into the fracture increases the oil recovery (see more in Appendix c)

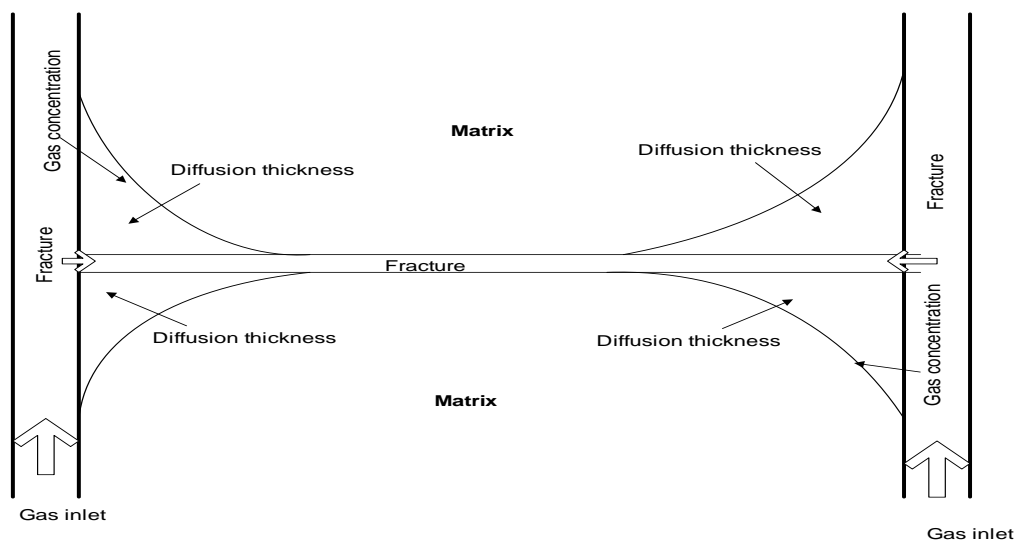


Figure 2.5 Fracture flow and diffusion phenomena into the rock matrix

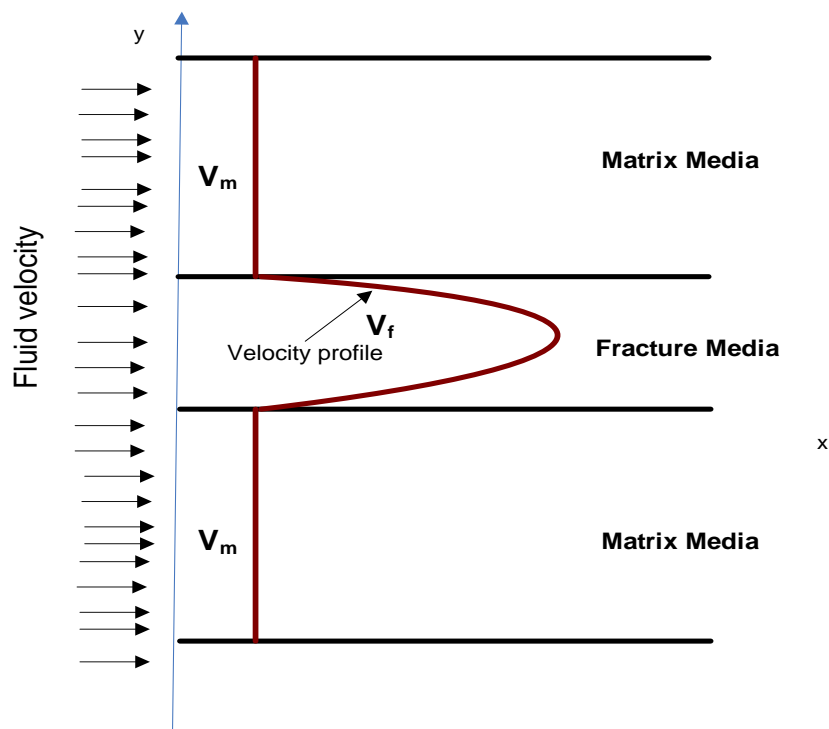


Figure 2.6 Gas velocity profile in fracture and matrix media

2.4 Remarks

The experimental measurements of the gas diffusion in porous media and effect of mass transfer on the 3-phase relative permeability are crucial for the understanding of the EOR process when the partially miscible gas injection method is adopted. Diffusion coefficient of Methane (gas phase) was measured in static condition, and new correlation for diffusion coefficient in high pressure and temperature regarding to experimental data was offered. Rate of mass transfer through porous media controls by diffusion coefficient, regarding to theory in this chapter and suitable finite element software, fluid flow in porous media was modelled and variation of other parameters along core holder was analysed. Considering incubation time of

Theory and methodology

contact and getting best match of fluid flow in carbonate rocks were supported to generate a model for fractured media.

In fractured media, effect of overburden on fracture permeability was main difference with carbonate rocks. Effect of the overburden on artificial made fracture was measured, and then physical model of fracture with considering effect of mass transfer was prepared (see theory in Appendix c).

The effect of mass transfer on relative permeability was another important factor that was investigated. Moreover, simulation of the experimental data with a finite element method using FLEXPDE software was part of this thesis.

Chapter 3 Experimental Equipment and Procedure

3.1 Introduction

The main objective for conducting gas flooding experimental studies was to measure critical parameters using special chosen methods. The chosen parameters such as diffusion coefficient, relative permeability, and oil recovery focused on the mass transfer that takes place between the oil and gas phases during gas injection into a porous medium, especially during the process of enhanced oil recovery from a depleted fractured carbonate oil reservoir. To facilitate the understanding of the experiments performed and to measure three-phase relative permeabilities, this chapter is divided into three sections, namely:

1. description of the basic equipment used;
2. equipment set up and calibration; and
3. description of the experimental procedures.

Initially, the equipment had to be set up to measure the mass transfer under static and dynamic conditions in order to measure the relative permeability. This process was then repeated under reservoir conditions (reservoir temperature and pressure). A new, state-of-the-art, three-phase fluid flow apparatus at the Department of Petroleum Engineering, Curtin University of Technology, was used. The equipment had to be calibrated using a state-of-the-art pumping system and a three-phase separator system was used as part of the overall set up. It was completely automated and controlled by the computer system.

The flooding apparatus was designed for simultaneous injection of one, two or three phases at reservoir conditions. A set of very high precision-positive displacement pumps injected oil, water and gas in separate phases, virtually pulse free, into the core-holder where a single core plug, or a set of multiple core plugs, was placed in series. The fluids injected into the core-

Experimental Equipment and Procedure

holder then passed through the core plugs and entered a sophisticated, acoustic three-phase separator. Volumes of individual phases exiting the core-holder were then measured after being separated in the acoustic separator at the prescribed pressure and temperature. Along with the production data, the pressure drop across the core samples was also measured as a function of time, using differential pressure transmitters. All the data measured were automatically recorded and analysed using the online computer system.

Before any meaningful experiments could be performed, all the equipment needed to be calibrated. The data obtained during the calibration process was collected by the online computers. To ensure accuracy of the data collected, all the components of the equipment were calibrated with highly accurate references.

Once the equipment was pressure tested to ensure that there were no leaks in the system and calibrated against accurate reference data, the planned unsteady-state fluid flow experiments could be performed. The experiments mainly focussed on the measurement of two-phase relative permeabilities initially and were then followed by the measurement of three-phase relative permeabilities with an emphasis on the measurement of mass transferred between the phases during the gas injection into the porous medium filled with oil and water.

Three-phase core-flooding equipment, which can perform under typical reservoir conditions up to a pressure of 103 Bar and at temperatures up to 200°C , is shown in Figure 3.1.

To measure the outlet saturations during the displacement process, a visual high pressure and high temperature separator was used. This separator could maintain each phase at constant levels. Three collection pumps were then used to collect the individual phases exiting the separator.



Figure 3.1 The three-phase core-flooding apparatus

Experimental Equipment and Procedure

3.2 Equipment description

The schematic of the experimental setup for the core-flooding system is shown in Figure 3.2. The equipment consisted of three cylinders containing the individual phases, a set of three positive displacement injection pumps, a core-holder encapsulating the core plugs, a high pressure separator with a light source, and a collection system consisting of three cylinders and pumps.

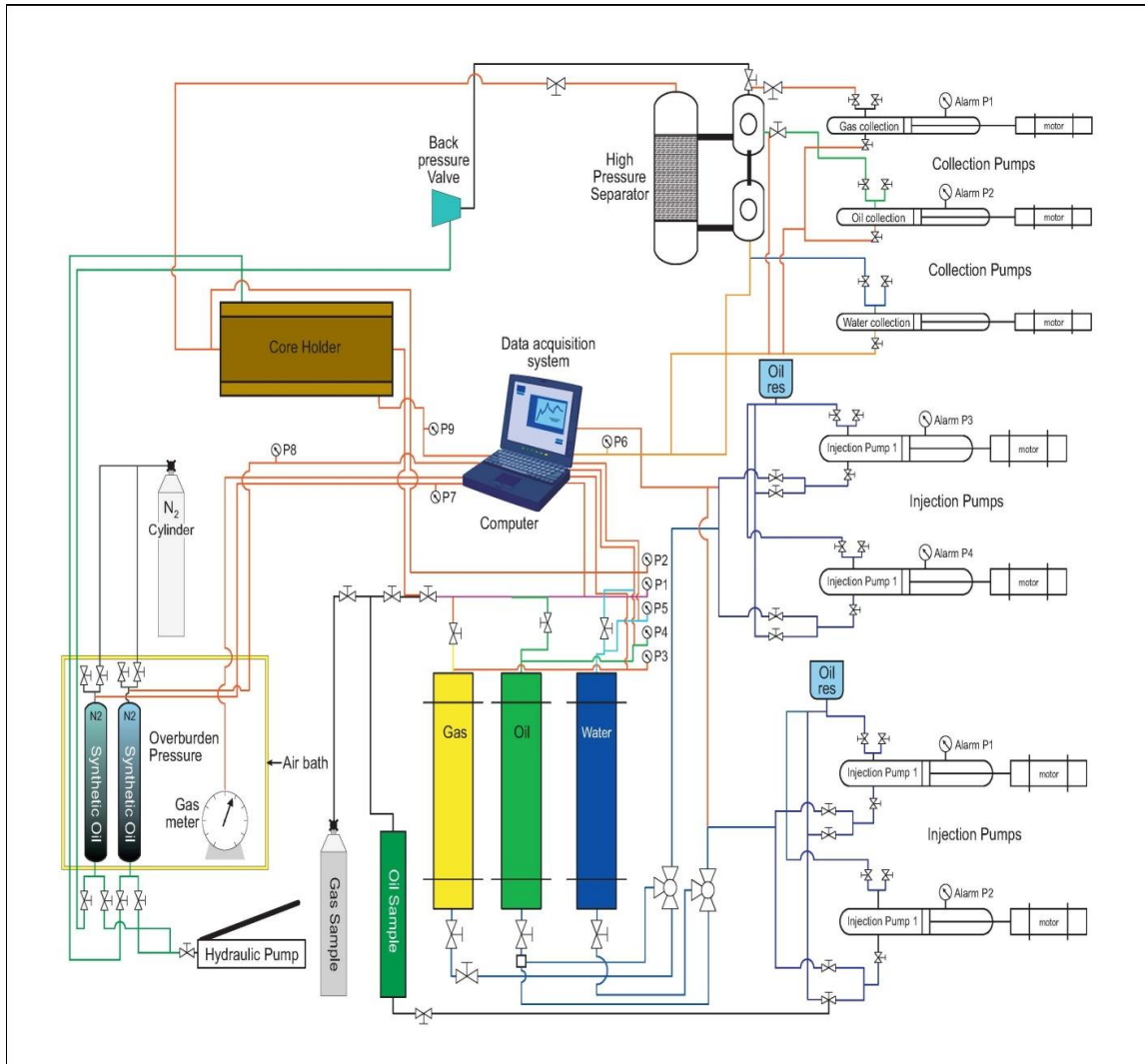


Figure 3.2 Schematic of the three phase core-flooding system

Experimental Equipment and Procedure

3.2.1 Injection and collection pumps

The system consisted of three injection and three collection pumps (Sanchez Technology which were of the positive displacement type), an Enerpac hand pump and a vacuum pump. Figure 3.3 shows the Sanchez digital positive displacement pumps which are driven by positive gear transmissions and are capable of injecting at rates ranging from 0 *cc/hr* to 650 *cc/hr*. The Sanchez digital collection pumps are shown in Figure 3.4. These pumps control the water-oil level and gas-oil level in the separator by injecting and collecting the excess volume from each phase. The collection pumps connected to the high-pressure oil and water vessels at the top in order to keep the cylinders topped up in case of any leaking during the three phases. The Enerpac hand pump shown in Figure 3.5 has an injection cylinder with a capacity of 300 *cc* and a choke valve at the outlet and is rated for pressures up to 2,757 Bar. This pump was used to control the pressure of the backpressure valve and the overburden vessels. The vacuum pump was used to vacuum the system and core plugs.

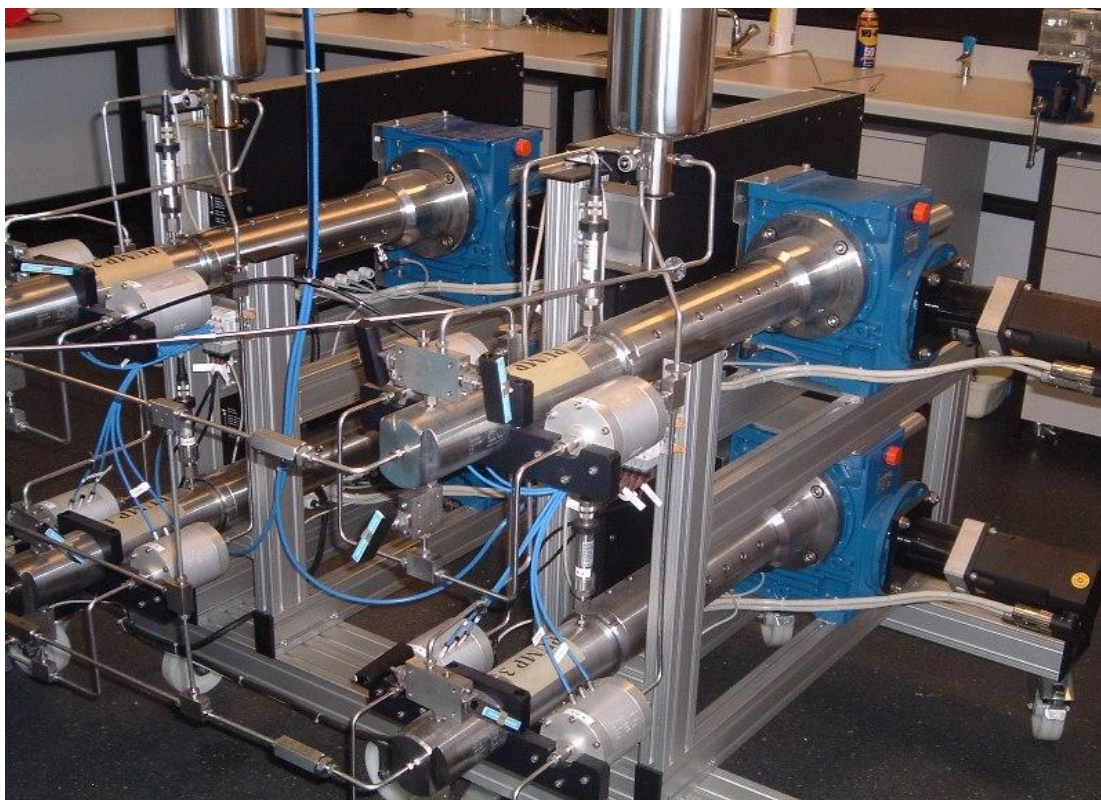


Figure 3.3 Positive displacement pumps. These pumps can inject fluids at the rate 0.0 to 650 *cc/hr*

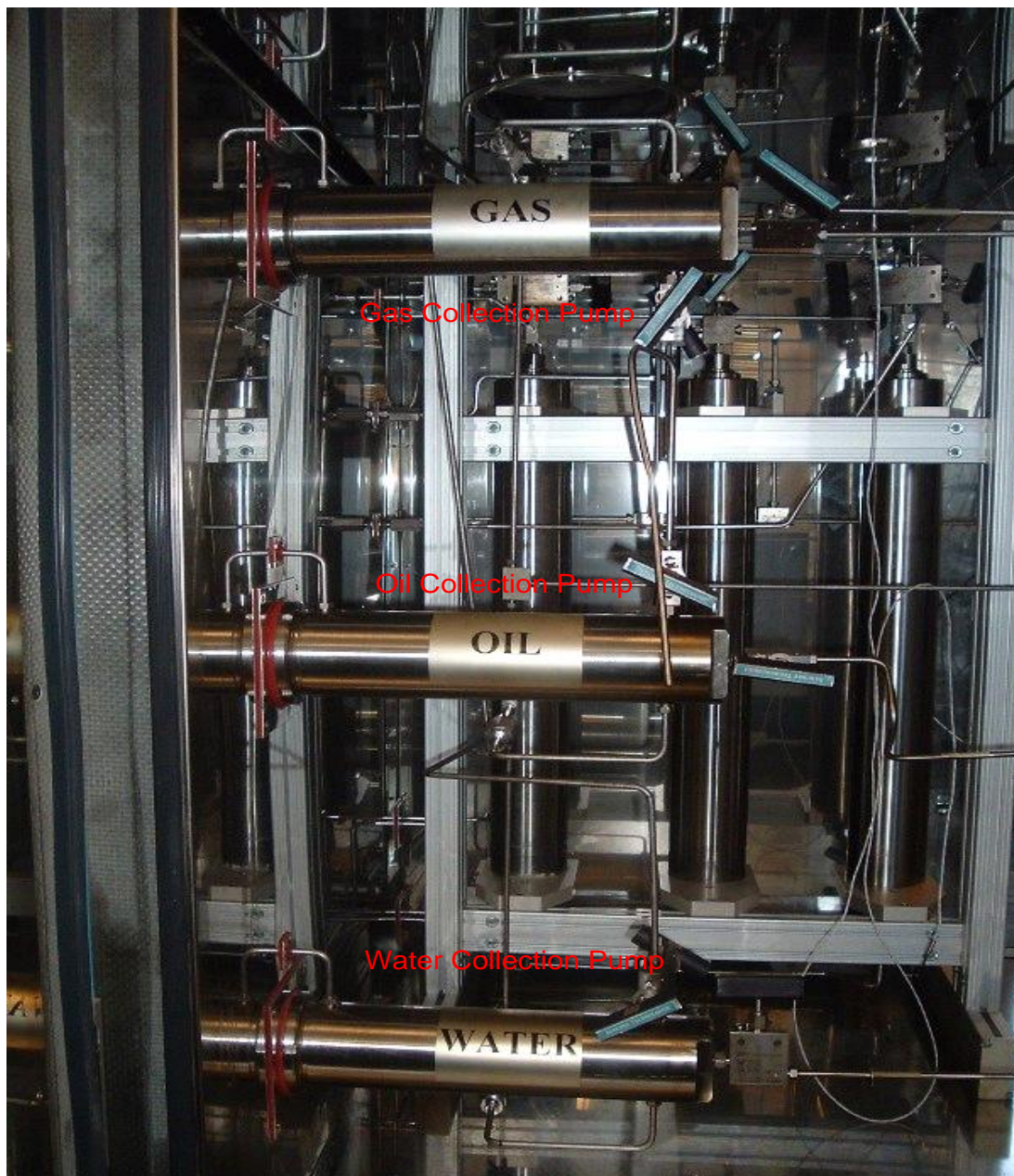


Figure 3.4 Gas, oil and water collection



Figure 3.5 Enerpac hand pump pumps which is rated for pressure up to 2557 Bar

3.2.2 The water, oil, and gas cylinders

Three high pressure titanium vessels, each with a capacity of 1.5 litres, consisting of pistons that help with the compression, were used as the reservoirs for the three phases. These vessels were located inside the heating cabinet and were operated at high pressures and high temperatures (Figure 3.6) to replicate the actual reservoir conditions.



Figure 3.6 Gas, oil and water high-pressure vessels

Experimental Equipment and Procedure

3.2.3 Core holder

The core holder used in the experiments was designed such that the outlet saturation of each phase could be measured. Applying the common radial and axial confining pressure on the core plugs achieved the hydrostatic condition that exists in the reservoir. The same confining pressure was applied radially along the core plugs as well as axially to the floating distribution plug. A variety of core lengths could be accommodated by varying the length of the sleeve placed in the core holder. All flow lines and internal volumes were kept to a minimum so that accurate flow data could be obtained. The parts of the core holder that came into contact with the fluid had to be chemically inert. It was also important to eliminate any fluid bypass around the core holder and for this reason, a heat shrunk Teflon sleeve was used to encapsulate the core plugs. The Teflon sleeve also provided the mechanical strength to contain the core plugs firmly.

There were four ports at the inlet to the core holder. One port was used for the pressure gauge, one used for injection and the other two were blanked off. The injection port was fitted with a distribution device which had $1/16$ inch grooves placed in a spider web pattern to enable a homogeneous distribution of the injected fluids. The pattern is shown in Figure 3.7. The core holder which contained the core plug or plugs is shown in Figure 3.8.

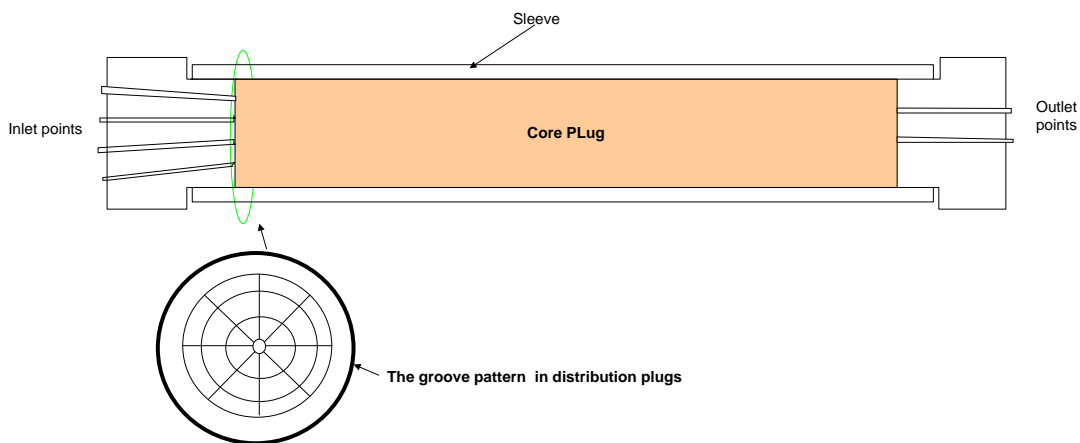


Figure 3.7 Schematic of the injection point and spider pattern in the inlet point of the core holder

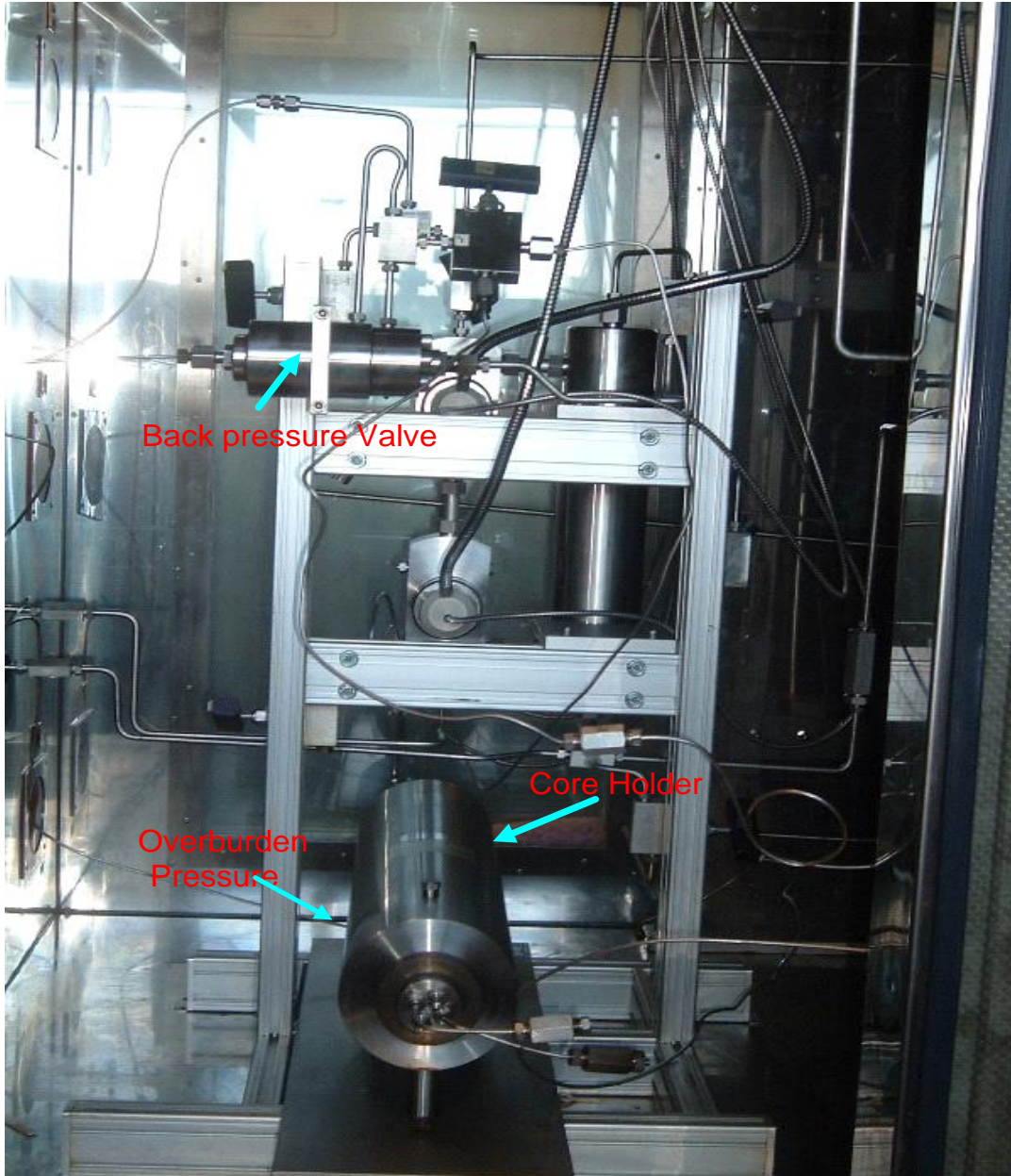


Figure 3.8 Core-holder and back pressure valve at overburden pressure

3.2.4 Three-phase acoustic separator

The three-phase separator is a vital part of the core flooding equipment. Its function is to determine the volume of each phase produced from the core sample and is shown in Figure 3.6. The three-phase separator consists of three vessels as shown in the schematic in Figure 3.9. The fluids exiting the core holder entered the main separator vessel at the top. The three phases were separated here and, through two outlets at the top half of the main vessel, oil and gas flowed into the second separator chamber which was fitted with a visual port. The visual port was used to maintain the gas oil interface by taking off gas and oil by the collection pumps. The second chamber was also connected to the third chamber to drain any water that may have entered the second chamber. The lower part of the main separator chamber was connected to the third separator vessel to remove the water phase from the main separator chamber. Here again the visual port was used to maintain the oil water interface by removing the water.

The volumes of the phases in the second two chambers of the separator system were controlled by means of the acoustic transducers installed as part of the visual port by determining the distance from the transducers to the interfaces formed in the measurement chambers. This distance was determined by measuring the time taken for an acoustic pulse to echo off the interface and return to the transducer. One of the transducers faced upwards towards the oil/gas interface in the upper chamber which measured the distance from the transducer to the interface. The second transducer installed in the lower chamber faced downwards and measured the distance to the oil/water interface from the transducer. From the measurements of volumes produced by each phase, the respective phase saturations could be calculated.

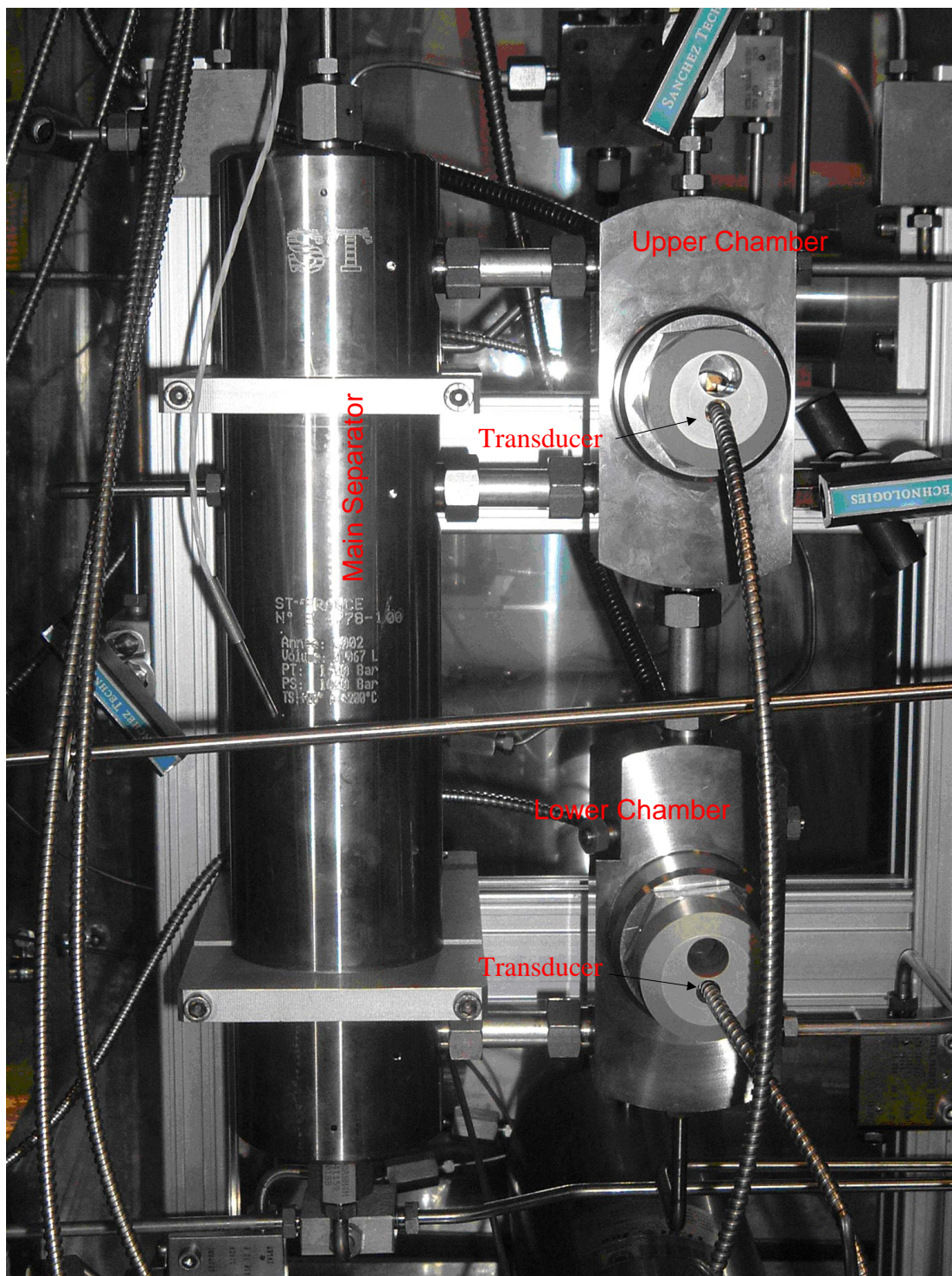


Figure 3.9 High pressure separator set-up with three vessels

Experimental Equipment and Procedure

3.2.5 Rotating gas meters

Rotating gas meters are commonly used when positive displacement pumps are employed. They consist essentially of a gas tight casing containing a measuring drum, with many components mounted on a spindle that is free to rotate. The calibration of the measuring drum is determined by the height of the water in the casing. The normal calibration point of all meters is shown by a water level indicating the point that is visible in the sight box located on the right side of the meter casing. The spindle through the drum is connected via a gearbox to a main pointer; a revolution counter then records the quantity of gas passing through the meter. The set point and the volume of the gas are controlled by the computer which uses software developed by Falcon. Figure 3.10 shows the main parts of the gas meter as described.

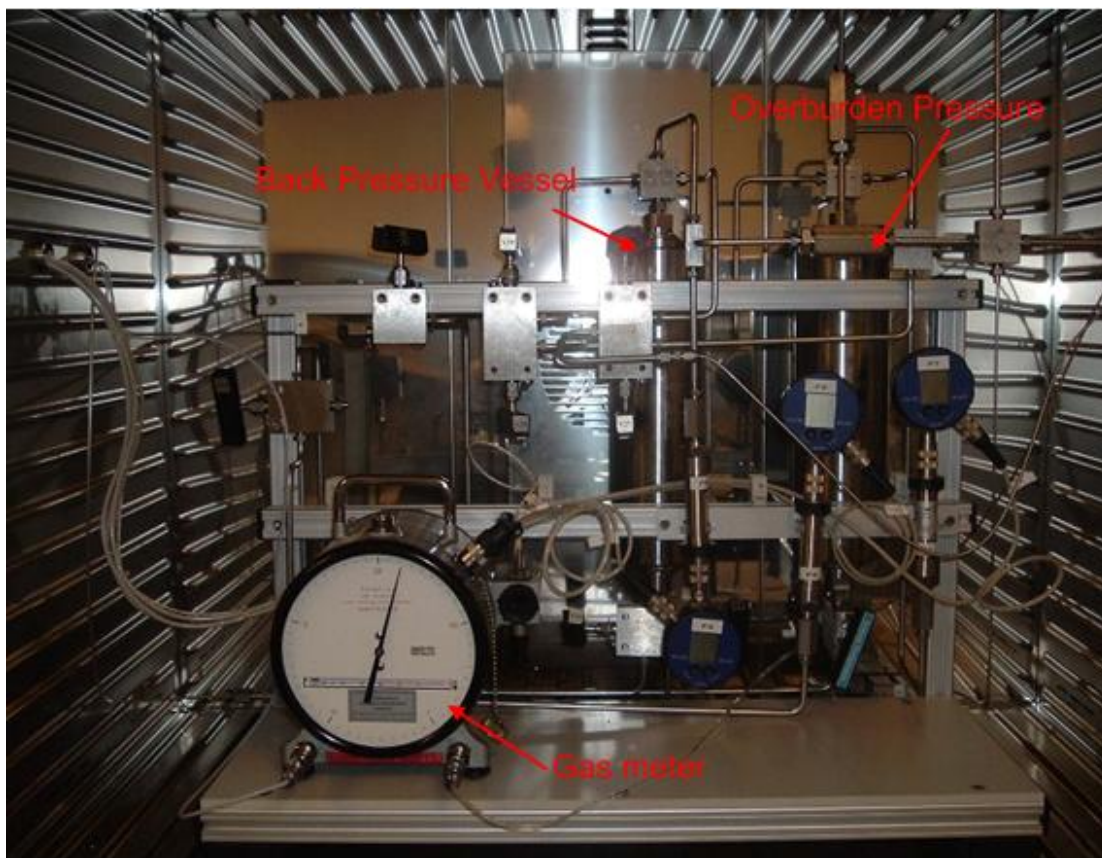


Figure 3.10 Gas meter, back pressure and overburden vessels

Experimental Equipment and Procedure

3.2.6 Pressure and temperature transducers

All the pressure transducers and indicators used in these experiments were manufactured by Keller . The pressure transducers are able to operate up to a pressure of 1,034 Bar. The transducers consist of two main components, a pressure gauge with an indicator and a transmitter which sends the data to the online computer. The pressure is transmitted by a voltage change from a special diaphragm and the voltage is then converted to a digital value by the indicator. These two instruments provide a highly precise pressure measurement. The transducers are displayed in Figure 3.11 and Table 3.1 provides their specifications. Two installed thermocouples were used to measure the temperature of the system.



Figure 3.11 Pressure Indicators and Transducers

Experimental Equipment and Procedure

Table 3.1 Technical specification of Pressure Transducer

Product name	Pressure transducer
Company name	Keller
Model of product	EV-120 and Series 30 transmitter
Pressure range	0-1034 Bar
Accuracy	<+- 0.02 % of FS(TEB)

3.2.7 Data monitoring system

Falcon software was used for data acquisition, controlling and reporting on the facilities. A continuous display of measurements versus time in the form of trends and values were displayed online by two computers, as shown in Figure 3.12.

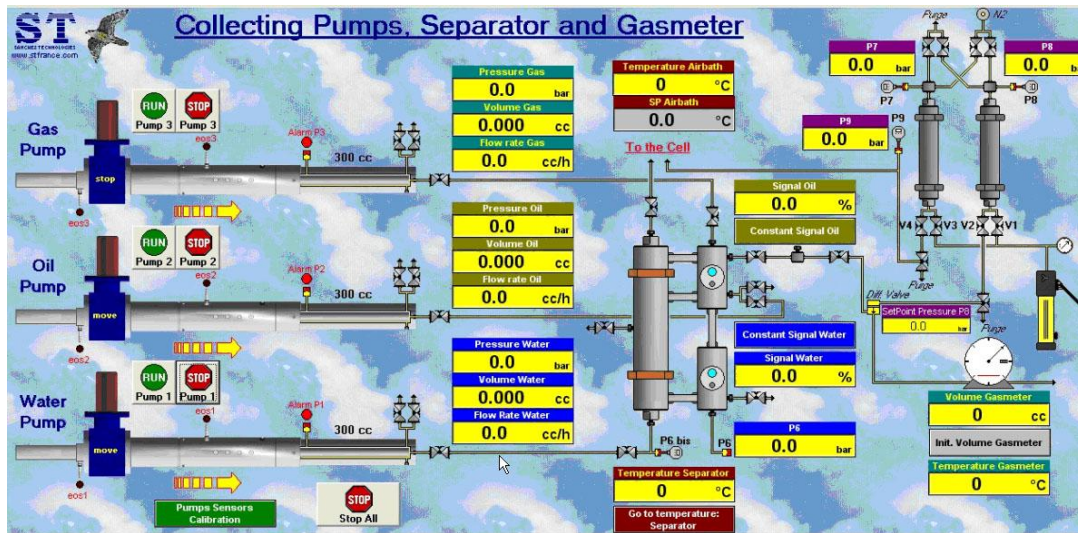


Figure 3.12 Computer data gathering display

3.3 Equipment set up to measure mass transfer under static and dynamic conditions

In this section, some of the equipment was modified to measure the incubation time for mass transfer under reservoir conditions. The pressure drop measured, which indicated that mass transfer was taking place, was the key parameter during the contact of the two phases. During all the experiments, the core holder was placed in a horizontal position so that the effect of gravity could be ignored.

3.3.1 Measurement of the diffusion coefficient under static conditions using a PVT cell

An experimental system was designed and installed as part of this study as shown in Figure 3.13. This equipment can be used to conduct measurements of the diffusion coefficient at reservoir conditions. The PVT cells in Figure 3.14 were designed such that the pressure and temperature of the system could be measured while the mass transfer phenomena were taking place. The PVT cell enabled the measurement of the oil volume increase due to swelling as a result of the mass transfer taking place between the oil and gas. The main components of the experiment are described in detail in the following sections. High accuracy positive displacement pumps, as shown in Figure 3.2 were used to increase the pressure of the system. Two computers with the Falcon software were used for monitoring the experiments and data collection.

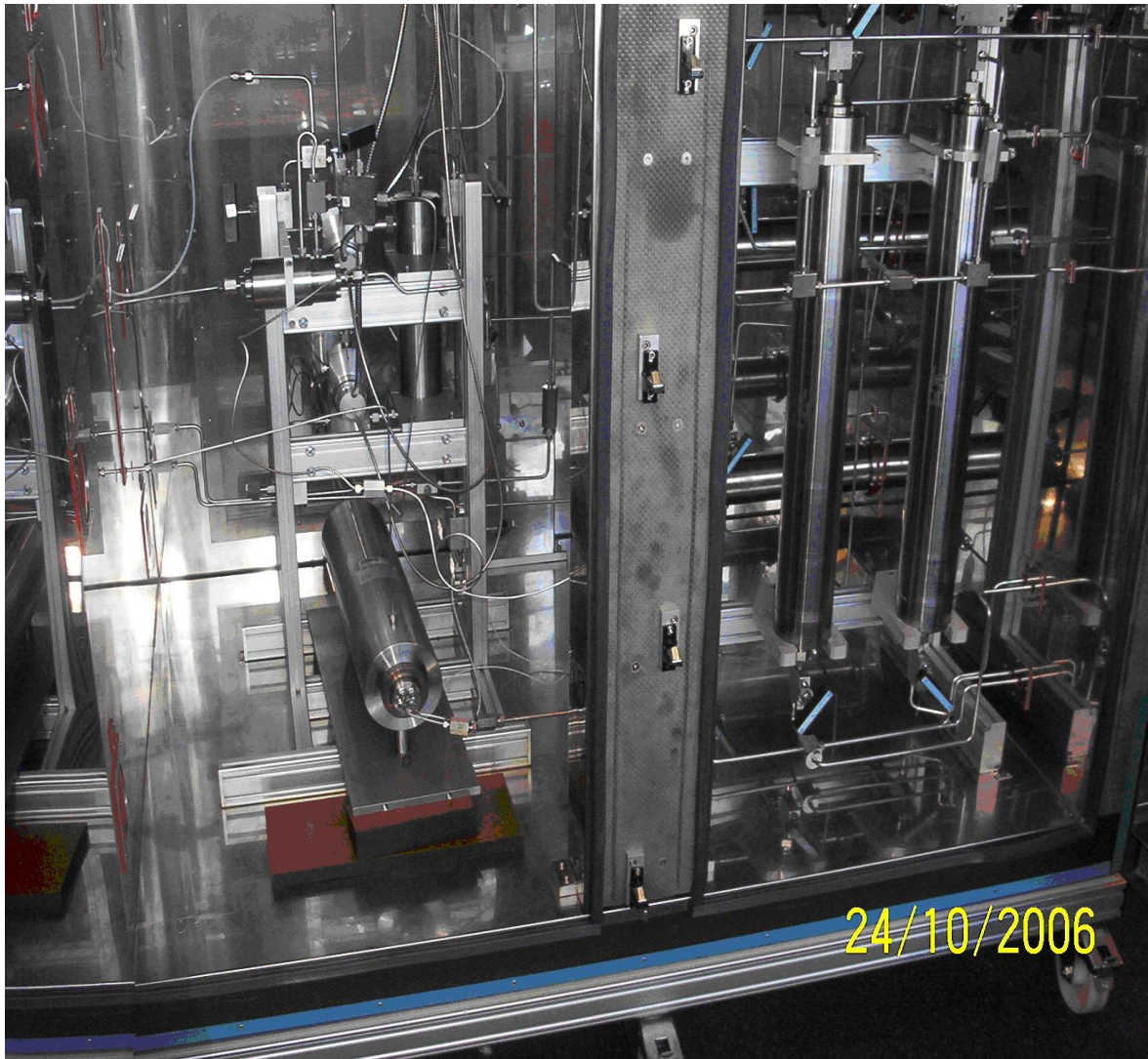


Figure 3.13 Diffusion coefficient measurement apparatus under static conditions

Experimental Equipment and Procedure

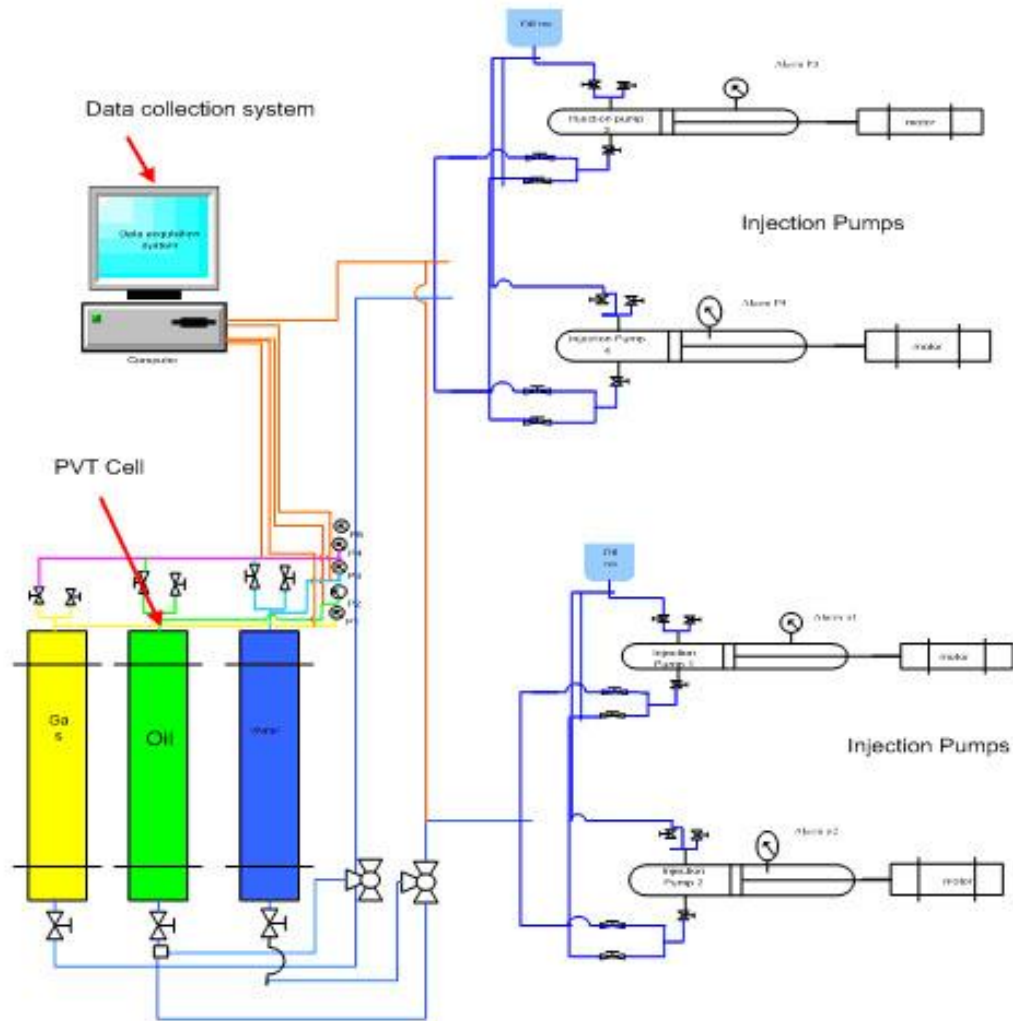


Figure 3.14 Schematic of mass transfer process under static condition
($P=200 \text{ bar}$ & $T=87.7^\circ\text{C}$)

3.3.2 Measurement of the relative permeability in the laboratory

The relative permeability can be measured at ambient and/or reservoir conditions using either ‘steady-state’ or ‘unsteady-state’ methods. At reservoir conditions, it is obvious that reservoir core samples and fluids need to be used and restorations of these conditions need to be performed carefully.

In the steady-state method, generally a fixed ratio of wetting and non-wetting phases is injected through the core sample until the pressure equilibrium and saturation are established; in other words, the production ratio is equal to the injection ratio. The pressure drop across the core along with the fluid viscosity and flow rates are used in Darcy’s Law to calculate the effective permeability. Many of the techniques have been successfully applied to obtain a uniform saturation. The primary concern when designing the experiment is to eliminate or reduce the saturation gradient which is caused by capillary pressure effects at the outflow boundary of the core (Honarpour, 1994).

In the steady-state method, the fluid saturation, the pressure gradient, and the individual phase flow rate in the core need to be measured. The steady-state methods are time-consuming because equilibrium achievement may require several hours or days at each saturation level. In addition, these methods require independent measurements of fluid saturations in the core. The advantages are greater reliability and the ability to determine relative permeability for a wide range of saturation levels. A comprehensive review of the methods is given by Honarpour et al. (1994). One disadvantage of this method is that residual saturation in the core has to be measured by other methods or calculated from material balance. Another disadvantage is the capillary end effect, but by increasing the flow rate or using a porous disk, this problem can be overcome.

In 1952, Welge presented the unsteady-state technique, which comprised the quickest laboratory method for obtaining relative permeability data and which also mimicked what really happens in a reservoir. However, saturation equilibrium is not attained with this method. Thus an entire set of relative permeability versus saturation curves can be obtained in a few hours. A typical run involves displacing in-situ fluids by a constant flow rate or constant

Experimental Equipment and Procedure

pressure injection of a driving fluid while continuously monitoring the effluent volumes. The production data are analysed and a set of relative permeability curves are obtained using various mathematical methods.

The Buckley Leverett equation for linear displacement of immiscible and incompressible fluids is the basis for all the analyses (refer to Section 2.2.3). This equation relates the saturation levels, at each point in time, to the capillary pressure, the ratio of fluid viscosities, the flow rates, and the relative permeability. Numerous studies have been carried out to examine the steady-state and unsteady-state methods with core samples of water, oil and intermediate wettabilities.

This study, the unsteady-state method was used to measure the relative permeabilities and the diffusion process between the phases. The oil phase was displaced from the core by injecting the gas phase, and the relative permeability ratio was calculated from the produced fluid ratio.

3.3.3 Unsteady-state method for measuring two-phase relative permeability

Unsteady-state relative permeability measurements can be made more rapidly than steady-state measurements, but the mathematical analysis of the unsteady-state procedure is more difficult. The theory developed by Buckley and Leverett and extended by Welge is generally used for the measurement of relative permeability under unsteady-state conditions. The mathematical basis for interpretation of the test data can be summarised as follows. Leverett combined Darcy's Law with a definition of capillary pressure in a differential form to obtain:

$$f_{we} = \frac{1 + \frac{k_o}{q_i \mu_o} \left(\frac{\partial P_c}{\partial x} - g \Delta \rho \sin \theta \right)}{1 + \frac{k_o}{k_w} \frac{\partial^2 \Omega}{\partial v^2} \cdot \frac{\mu_w}{\mu_o}} \quad (3.1)$$

Experimental Equipment and Procedure

where f_{we} is the fraction of water in the outlet stream; q_t is the volumetric flow rate of the total fluid leaving the core; θ is the angle between direction x and horizontal; and $\Delta\rho$ is the density difference between the displacing and the displaced fluids. In a flooding experiment with horizontal flow, the capillary pressure and gravitational effects can be neglected. Based on these assumptions, Welge showed that Equation 3.1 can be simplified to the form:

$$S_{w,av} - S_{we} = f_{oe} Q_w \quad (3.2)$$

where, the subscript e is the outlet end of the core; $S_{w,av}$ is the average saturation; and Q_w is the cumulative water injected, measured in pore volumes. Since Q_w and $S_{w,av}$ can be measured experimentally, the fraction of oil in the outlet stream, f_{oe} can be determined from the slope of a plot of Q_w as a function of $S_{w,av}$ by definition:

$$f_{oe} = \frac{q_o}{(q_o + q_w)} \quad (3.3)$$

By combining this equation with Darcy's Law, it can be shown that:

$$f_{oe} = \frac{1}{1 + \frac{\mu_o}{\mu_w} \frac{k_{rw}}{k_{ro}}} \quad (3.4)$$

Since μ_o and μ_w are known, the relative permeability ratio $\frac{k_{ro}}{k_{rw}}$ can be determined from

Equation 3.2. The work of Welge was extended by Johnson et al. (1959) to obtain a technique

Experimental Equipment and Procedure

for calculating individual phase relative permeabilities from unsteady-state test data. The equations which were derived are:

$$k_{ro} = \frac{(f_{oe})d\left(\frac{1}{Q_w}\right)}{d\left(\frac{1}{Q_w I_r}\right)} \quad (3.5)$$

and

$$k_{rw} = \frac{f_{we} \mu_w}{f_{oe} \mu_o} k_{ro} \quad (3.6)$$

where, I_r is the relative injectivity, and defined as:

$$I_r = \frac{\text{Injectivity}}{\text{initial injectivity}} = \frac{(q_{wi}/\Delta p)}{(q_{wi}/\Delta p) \text{ at start of injection}} \quad (3.7)$$

For determining gas-oil relative permeability in a core sample using an unsteady-state method, gas is flooded through the core initially saturated with oil and connate water. The injected volume and produced volume is then measured and the relative permeability for gas-oil is calculated. Welges's equation, based on the theory of Buckley Leverett states that:

$$S_{g,av} - S_{g(out)} = f_{o(out)} Q_g \quad (3.8)$$

where $S_{g,av}$, is the average gas saturation, $f_{o(out)}$ is the fraction of water at the outlet stream, and Q_g is the cumulative gas injected.

Experimental Equipment and Procedure

$$S_{g,av} = \frac{N_p}{V_p} \quad (3.9)$$

where, N_p is the cumulative water produced and V_p is the pore volume.

In the above equations, Q_g and $S_{g,av}$ can be measured experimentally, $f_{o(out)}$ can be determined from the plot of Q_g as a function of $S_{g,av}$:

$$f_{o(out)} = \frac{dS_{g,av}}{dQ_g} \quad (3.10)$$

Gas saturation at the outlet can be calculated from Equation 3.9. The fraction of oil and gas at the outlet can be defined as follows:

$$f_{o(out)} = \frac{q_o}{q_o + q_g} \quad (3.11)$$

$$f_{g(out)} = 1 - f_{o(out)} \quad (3.12)$$

By combining Equations (3.56) with Darcy's Law, it can be shown that:

$$f_{o(out)} = \frac{1}{1 + \frac{K_{rg}\mu_o}{K_{ro}\mu_g}} \quad (3.13)$$

Since viscosities are known, the relative permeability ratio K_{rg}/K_{ro} can be calculated from Equation 3.12 and the gas relative permeability can be calculated from the following equation:

$$K_{rg} = \frac{\Delta G_{inj}}{\Delta t} \left(\frac{\mu_g LC_1}{AK\Delta P} \right) \quad (3.14)$$

where C_1 is the ratio of the atmospheric pressure and the mean pressure and ΔG_{inj} is injected gas volume (cm^3) for the time interval Δt (s).

3.3.4 The unsteady-state method for measuring three-phase relative permeability

Sarem (1966) formulated the three-phase relative permeability based on fractional flow as follows:

$$K_{ro} = \frac{f_{oe} d\left(\frac{1}{Q}\right)}{d\left(\frac{\Delta P K A}{L \mu_o q_t Q}\right)} \quad (3.15)$$

$$K_{rw} = \frac{f_{oe} d\left(\frac{1}{Q}\right)}{d\left(\frac{\Delta P K A}{L \mu_w q_t Q}\right)} \quad (3.16)$$

$$K_{rg} = K_{ro} \frac{f_g \mu_g}{\mu_o f_o} \quad (3.17)$$

Experimental Equipment and Procedure

Where:

$$f_i = \frac{\frac{K_i}{\mu_i}}{\frac{K_o}{\mu_o} + \frac{K_w}{\mu_w} + \frac{K_g}{\mu_g}} \quad (3.18)$$

$$f_o + f_w + f_g = 1 \quad (3.19)$$

Average saturations, fractional flow at the outlet end and cumulative injection volume were measured in the laboratory.

3.3.5 Experimental equipment for measuring three-phase relative permeability and enhanced oil recovery

A schematic of the core flooding apparatus used is shown in Figure 3.2. The individual components of the equipment were discussed earlier in this chapter. In summary, the core flooding apparatus consisted mainly of the following:

- a positive displacement pumping system for fluid injection and pressure maintenance;
- a core holder to contain the cores at the overburden pressures;
- a three-phase acoustic separator to maintain individual phase production;
- three collection pumps for measuring the volume of each phase produced separately; and
- a thermal bath, including a gas meter and high pressure bottles for applying pressure on the core holder to maintain the overburden pressure, and a back pressure regulator.

3.4 Calibration of the equipment for static and dynamic experiments

The equipment needed to be calibrated and comprehensively tested prior to each experiment if meaningful results were to be obtained. As all the calculations that needed to be performed to estimate the diffusion coefficients and to develop the relative permeability curves were heavily dependent on pressure drops and saturations, great care and attention was given to get accurate data from the core flooding equipment.

In this research, as in any other, the accuracy of the pressure sensors, pumping volumes and temperature measurements were calibrated using high accuracy reference systems. Finally, the accuracy of the saturation determinations obtained by the collection pumps were verified and all other parameters, such as offset and gain, (obtained using the Falcon software) were adjusted to match the experimental measurements.

3.4.1 Calibration of the pressure sensors with a referenced pressure gauge

One of the transducers connected to the cylinders was calibrated against a reference pressure gauge. The following procedure was applied to calibrate the system.

1. Offset adjustment.

In this section, the offset of transducers was adjusted in two ways as follows:

- a. Through relative pressure sensor: Measurement of the atmosphere pressure P_{atm} , and calculation of the difference Δp between P_{atm} and standard atmospheric pressure ($P_{\text{std}} = 1.013 \text{ Bar}$), was applied to adjust the offset. The displayed pressure must be equal to $\Delta p = 0$ because Perth is at sea level.

Experimental Equipment and Procedure

- b. Through measuring absolute pressure sensor: the vacuum pump was connected to the system and carried out vacuuming for three hours. The displayed pressure was equal to zero in both the referenced gauge and transducer.

2. Adjustment of the gain.

The referenced gauge was connected to the system and the pressures measured with the sensor and the referenced pressure gauge were recorded. The two indicated pressure values had to be equal for the pressure sensors to be accepted as properly calibrated. This process was repeated at least ten times with the pressure increasing and for at least five times with the pressure decreasing. At each pressure measurement, the pressure displayed by the sensors had to be equal to that indicated by the referenced pressure gauge. A calibration curve was then produced by plotting the pressures recorded, as shown in Figure 3.15.

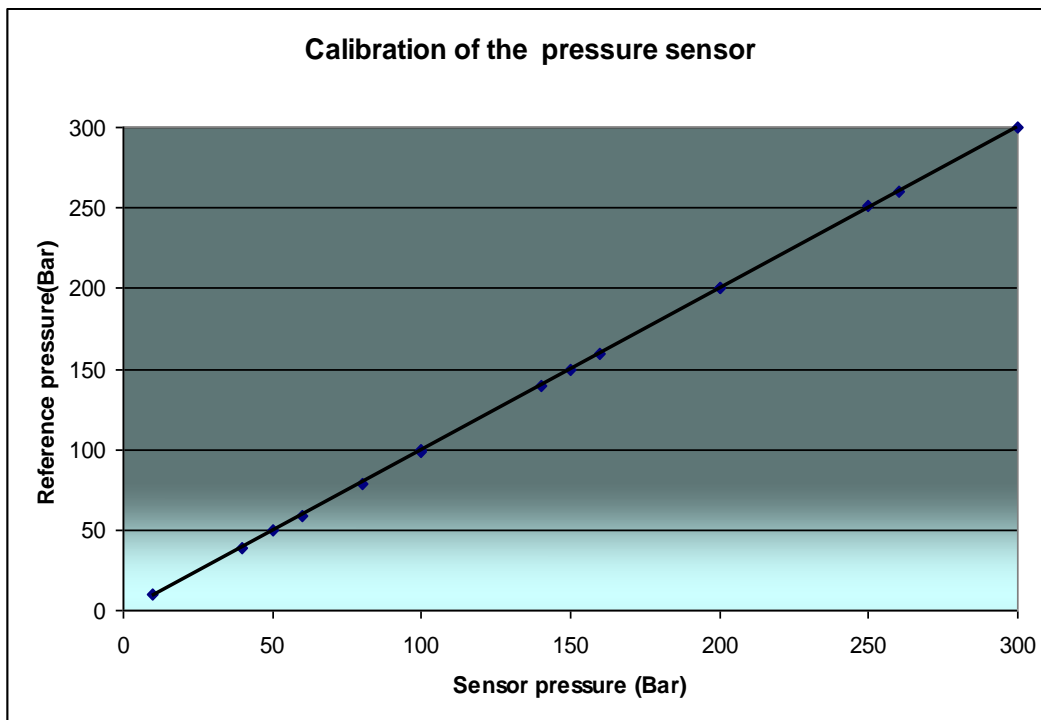


Figure 3.15 Calibration curve for pressure sensor in the system

3.4.2 Temperature calibration with a referenced thermometer

The calibration of the thermocouple used for temperature measurement was carried out by performing the following steps. The thermocouple and the thermometer were placed into an ice-water mixture. If the temperature recorded by the thermo couple was not zero, an offset was applied to adjust the recording to zero to make its measurement the same as that displayed by the referenced thermometer. The temperature of the system was then increased in 10 steps and the temperatures measured by the thermocouple and the thermometer were recorded. The gain from the system was then adjusted, based on the recorded data.

3.4.3 Calibration of the volume and flow rate measurement systems

The displaced volumes indicated by the highly accurate positive displacement pumps were compared to the actual volumes of the fluids produced. This was done with the use of one of the three cylinders (1.5 litre capacity) discussed earlier (Figure 3.4). These two sets of volumes measured were then plotted. The procedure to obtain the necessary data to calibrate the volume throughout the measurement system was as follows:

1. One of the cylinders was filled with 1.5 litres of distilled water at room temperature.
2. The pressure of the system was then increased to 100 Bar to make sure that the cylinder was 100 percent full with water. The pressure was then released until the cylinder was at 7 Bar and this was followed by the gradual increase of the pressure to 10 Bar. This was done to nullify any mechanical friction between the piston and the cylinder wall and also any expansion of the liquid caused by the sudden reduction of pressure from 10 Bar down to 7 Bar.
3. The pressure of the system was released to atmospheric conditions and the exit valve of the cylinder was left open.

Experimental Equipment and Procedure

4. A pre-determined volume of water was then pumped into the cylinder and the water exiting the cylinder was collected in a graduated beaker and the volume recorded. Also for accuracy, the beaker was weighed before and after, using a high precision balance. Knowing the density of the distilled water, the volume was calculated.
5. If there were any discrepancies between the pumped volumes and the volumes measured, the online computer was adjusted such that the future pumped volumes could be corrected.

The produced volume of water measured using the balance was compared against that initially injected into the cylinder. During the actual calibration performed as part of this research, normally four to five different volumes were injected and then produced as described earlier and shown in Figure 3.16.

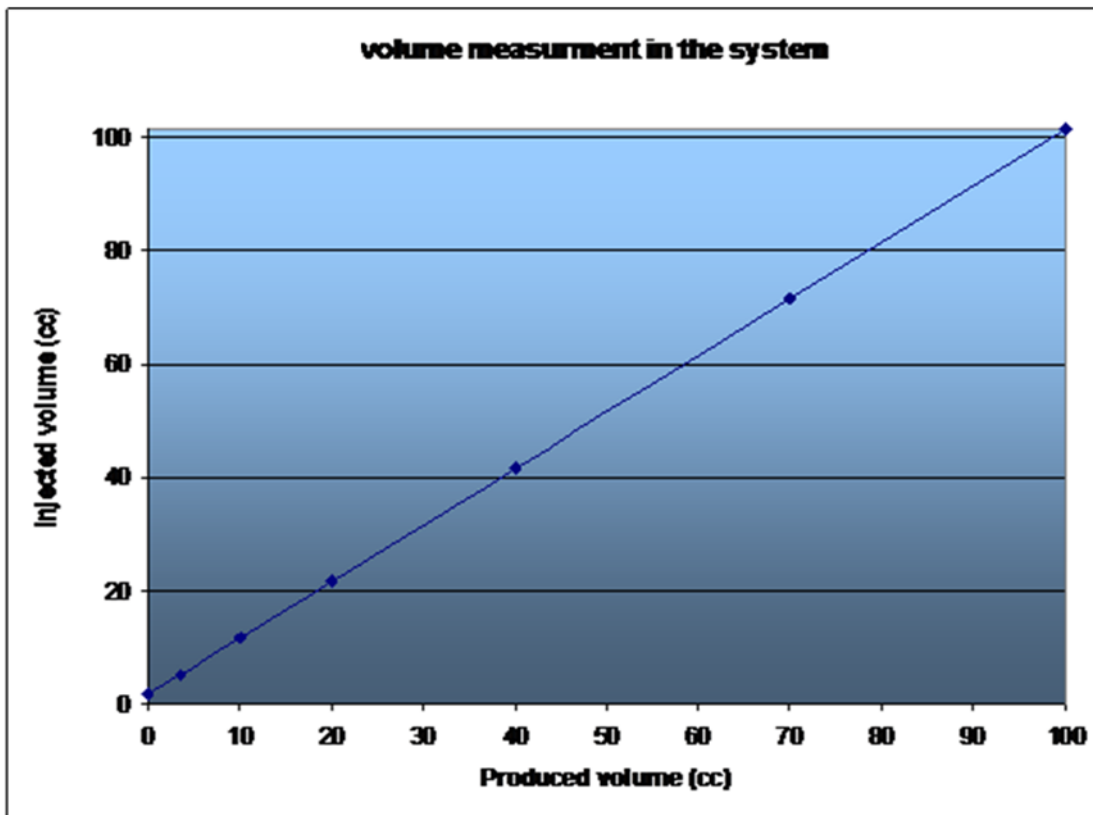


Figure 3.16 3 Calibration of the volume with distilled water

3.4.4 Measurement of the dead volume in the system

The dead volume of the system was measured using the following procedure:

1. The vacuum pump was connected to the top of one of the cylinders discussed earlier and it was put under a vacuum using a vacuum pump.
2. A specific volume of water in a beaker was then charged into the cylinder.
3. The pressure of the system was then increased to 200 Bar for complete saturation to occur (100 percent liquid), then decreased to 7 Bar, and then gradually increased to 10 Bar for the same reasons mentioned earlier.
4. The specific volume charged earlier into the cylinder was then purged from the cylinder into the beaker. The volume of water collected was then measured accurately by weighing as before.

The upstream dead volume between the three-way valve at the top of the cylinders (Figure 3.17) and the inlet to the core holder was measured by attaching the plug to the injection system and alternately sending synthetic oil and distilled water through it. The liquid displaced from the dead volume was measured several times in a beaker and was weighed with a high accuracy digital balance.

Experimental Equipment and Procedure

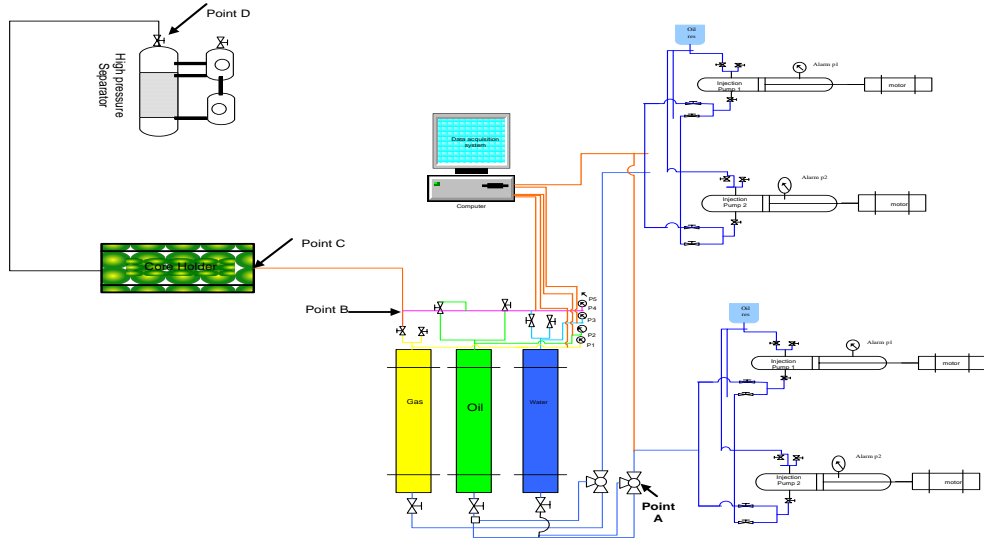


Figure 3.17 Schematic of dead volume measurement

3.4.5 Calibration of the separator with collection pumps

The procedure for the calibration of the separator system was performed by collecting and measuring the volume of the produced oil or water from the collection pumps and then comparing that against the pump's estimate of the volume pumped and noting the difference in volumes obtained through the two measurements.

The calibration process started by filling the separator with known quantities of distilled water, synthetic oil and air at atmospheric pressure. Additional distilled water was then injected into the separator to increase the volume of water and as a consequence, air was produced from the separator. The injected water was then collected by the collection pumps and the volumes collected were then compared to the volumes injected. Figure 3.18 shows the schematic of the separator and the collection pumps. As can be seen from Figure 3.19, the linearity was good between the injected volume and the collected volume. This procedure was repeated for the oil pumps as well. Note that at high temperatures and pressures, the measured

Experimental Equipment and Procedure

volumes of water would be affected due to the influence of surface tension, especially at temperatures above 100 °C.

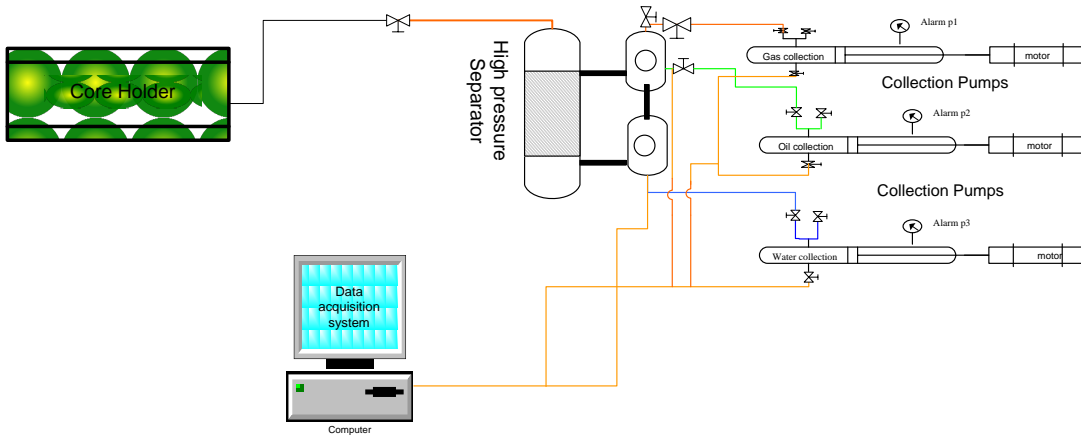


Figure 3.18 Schematic of separator and collection pumps

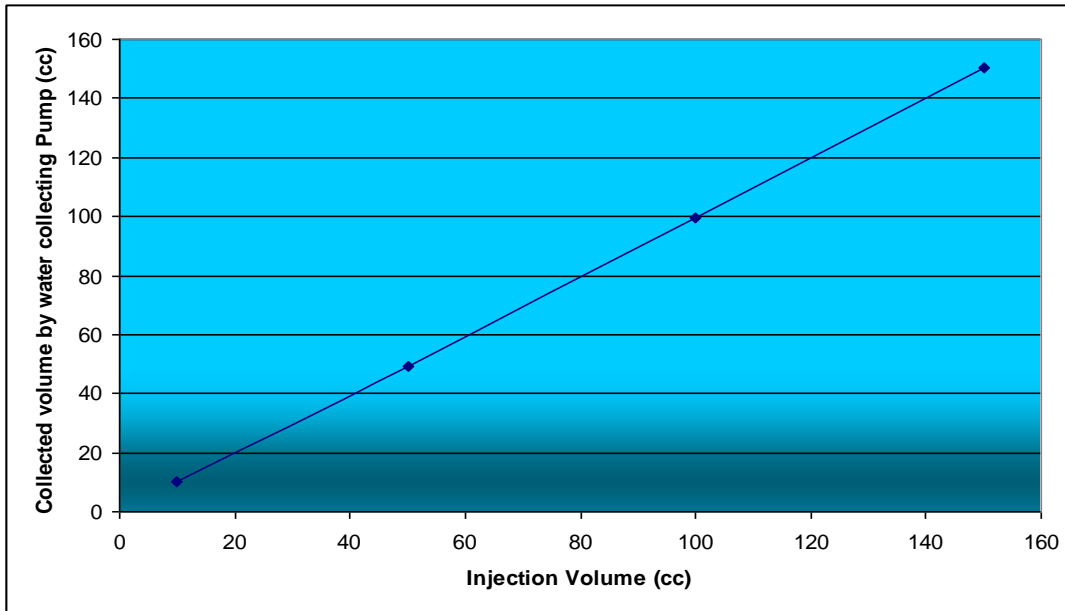


Figure 3.19 Calibration of collection pumps

Experimental Equipment and Procedure

3.4.6 Calibration of the gas meter

The gas meter must be kept in a perfectly horizontal position using the level adjuster that comes with the set up. The gas coming out of the gas meter must be vented through the fume cupboard. These processes should be adhered to strictly before commencement of the equipment calibration. The procedure for the calibration of the gas meter was as follows:

1. The high pressure vessel was first filled with methane gas at 7 Bar.
2. The gas was then purged through the line connected to the gas meter in five steps of pressure reduction and the released gas volume was measured using the gas meter.
3. The purged gas volume was also calculated by applying the equation of state (PV) for the pressure changes made during each step above.

The measured and calculated values were compared and the difference was compensated for via the online computer.

3.5 Material selection and preparation to perform the experiments

The cutting and cleaning of the core plugs, the measurement of the rock absolute permeability and porosity, and the ordering of the composite cores before mounting in the core holder are discussed in this section. In addition, the selection of the fluids (oil, water and gas) is also discussed.

3.5.1 Core selection, cutting and cleaning

All the core plugs used in the experiments were either 1.5 inches in diameter and approximately 2 inches in length and were cut from a whole core. The full core samples were brought from Iranian carbonate oil reservoirs. The cutting and cleaning of all the core plugs used in the experiments was generously performed at no cost by the CoreLab Company.

Experimental Equipment and Procedure

3.5.2 Core Plugs absolute permeability and porosity

The core samples used were from an Iranian carbonate oilfield where a gas injection EOR project had been proposed. The core absolute permeability and porosity measured by CoreLab/Perth are listed in table 3.2. The CoreLab Company in Perth, Western Australia, measured the porosity and absolute permeability.

Table 3.2 Absolute permeability, total porosity and pore volume of core samples

Sample Number	55 Bar Net Overburden (NOB) Pressure			Pore Volume (PV)
	Absolute Permeability(k)		Porosity (%)	
	$K_{inf}(mD)$	$K_{air}(mD)$		
2-1	0.00277	0.00646	2.5	1.385
2-2	3.67	4.87	20.5	10.316
2-3	3.41	4.61	20.6	11.12
3-1	0.0136	0.0172	2.4	1.319
1-1	0.00143	0.00357	2.0	1.069
1-2	2.58	3.51	19.5	10.55
1-3	2.51	3.41	19.9	10.632

3.5.3 Study of capillary end effect

To reduce the capillary end effect in the laboratory, the pressure drop along the core plug needed to be high to reduce the capillary end effect. There are three methods by which this can be achieved:

1. by increasing the total injection rate;
2. by using high viscosity crude oil; and,
3. by selecting core plugs with a low permeability.

In this research, since all of the studied core plugs have very low permeability, the capillary end effect would be minor and can be neglected.

3.5.4 Gravity effect during flooding

During all the experiments performed, the core holder was placed horizontally, hence negating the influence of gravity during flooding of the core plugs.

3.5.5 Core ordering

When a composite core is used to perform a flooding experiment, it is only natural to expect that each core plug would have different properties, such as permeability and porosity, unless the core was obtained from a homogeneous reservoir. In order to minimise the capillary end effects, the core plugs in a composite core set up must be ordered in descending value of absolute permeability. Typically, the core plugs can be arranged using any one of the following:

1. ascending order of permeability;
2. descending order of permeability; or,
3. the method suggested by Huppler (1969).

Huppler (1969) presented an ordering criterion for the individual cores assembled in a composite system. Huppler defined the harmonically averaged permeability as the highest 'H' in the outlet:

$$K_j = \frac{\sum L_i}{\sum \frac{1}{K_n}} \quad (3.20)$$

The variable, Huppler (H), is then calculated using equation (3.2):

$$H = \frac{k_a}{N} \sum \left[\frac{1}{K_j} - \frac{1}{K_n} \right] \quad (3.21)$$

where K_a is based on core plugs with similar air permeability, and K_n is the air permeability of individual core plugs, L is individual core lengths and N is the number of segments. He suggested that the core plugs be arranged in an ascending order of the Huppler (H), with the lowest 'H' core plug placed at the inlet of the composite set of core plugs.

Experimental Equipment and Procedure

The objective behind the ordering of the core plugs is to provide the largest possible pressure drop across the composite core to minimise the capillary end effects. Longaast et al. (1998) reported that the best ordering to achieve this is by arranging the core plugs in a descending order of permeability along the flow direction. Therefore, the core plug with the lowest permeability is placed at the outlet and the one with the highest permeability is placed at the inlet. Based on their experimental data, Zekri and El-Mehaideb (2002) concluded that when arranged in descending order of permeability, the measured relative permeability was lower than that measured using the Huppler arrangement when ordered ascendingly. In this research, the permeability was arranged in a descending order so the capillary end effects could be ignored.

3.5.6 Brine treatment

Nitrogen was blown into the three bottles of distilled water to reduce the oxygen concentration in the water and also to remove the oxygen from the air space in the bottles. In one litre of distilled water, 50 grams of NaCl (five percent by weight) was added and stirred. This solution was then poured into the Pyrex bottle, which was sealed between loadings to prevent oxygen contamination of the air space above the water. During each step of the experiment, approximately one litre of brine at a time was loaded into the salt water pressure vessel by vacuuming the system.

Table 3.3 Physical properties of fluids which are used

Component name	Viscosity (cp)	Molecular weight
Crude oil	45	250 *
Methane	0.001896	16
Water	1.04	18

* this value is estimated by empirical correlation

3.6 Experimental Procedures and Data Collection

3.6.1 Diffusion coefficient measurement procedure at high pressure and temperature

Pressure drop has the most influence when two non equilibrium phases are left in contact under static conditions. A PVT cell was used to measure the diffusion coefficient under static reservoir conditions. The pressure of the system is a function of the time and composition of each phase. By measuring the pressure drop while the two phases were in contact in the PVT cell the following procedure was used to measure the diffusion coefficient:.

1. The high pressure cylinder (PVT cell) was cleaned, dried and connected to the displacement pumps.
2. The PVT cell was vacuumed for two hours.
3. The PVT cell was filled with oil.
4. The high pressure gas cylinder was filled with pure methane at 345 Bar.
5. The top of the PVT cell was connected to a gas cylinder through a valve.
6. The valve was then closed when the pressure in the PVT cell reached 206 Bar.
7. The pressure drop measurement began once the top valve was closed.

The equipment was left to stand for a period of time until the system pressure dropped and reached equilibrium. The amount of the mass of transferred gas was calculated based on the pressure drop in the PVT cell using the method as discussed in Chapter 2.

Experimental Equipment and Procedure

3.6.2 Procedure for the measurement of two-phase relative permeability

The absolute permeabilities of the core plugs were measured by passing a fluid of known viscosity and volume through a core sample. The pressure drop across the core plug was measured when the fluid was injected at a constant rate. The measurement of the absolute and relative permeability for oil and water is one of the most important tasks undertaken in core laboratories. The tested sample plug was initially saturated with a wetting phase using a vacuum pump, then the absolute permeability for the wetting phase was measured. The relative permeability measurements were conducted under two-phase flow using the unsteady-state method. Based on the data collected, the absolute and relative permeabilities were calculated.

The unsteady-state method, also referred to as Welge's Method, uses the theory of Buckley and Leverett for the one-dimensional immiscible displacement of the non-wetting phase (oil) by the wetting phase (water) (Section 3.3.3). The experiments performed during this research were carried out on carbonate rock plugs by injecting oil and water using the unsteady-state method, at a constant injection rate. The fractional flow of the two phases flowing out of the core plug was measured during the flooding process (Equations 3.10). Absolute permeability was then used to calculate the relative permeabilities. The first stage of these experiments was the measurement of the absolute permeability of water using Darcy's Law.

3.6.3 Absolute permeability measurement with water

The following steps were performed during the unsteady-state approach to core flooding for checking the absolute permeability.

1. The cleaned and dried core plug was weighed.
2. The dimensions (diameter D and length L) of the core plug were measured using a calliper.
3. The core plug was then vacuumed and saturated with the NaCl (five percent concentration v/v) brine and weighed again.

Experimental Equipment and Procedure

4. The core plug was placed in the core holder and a known volume of water was injected through the core plug.
5. Measurement of the pressure drop across the core plug during the injection was taken.
6. The absolute permeability was calculated using Darcy's Law.

3.6.4 Relative permeability measurement

Using the unsteady-state method, the core plug was saturated with 100 percent brine. The sample was then displaced by injecting the oil until no further production of water was obtained at the outlet of the core holder which resulted in the core plug being saturated with oil and connate water. The total amount of water produced during the oil displacement was recorded and, using this value and the volume of brine contained in the core plug when it was 100 percent saturated with brine, the connate water saturation, S_{wc} , was then calculated.

Effective oil permeability was calculated at the S_{wc} . The next step was to inject the brine at a constant rate through the oil saturated core plug. The fractional flow of oil and water at the exit of the core plug and the pressure drop across the core plug were recorded. Relative permeability could then be calculated using the cumulative brine injected, the pressure drop across the core plug, and the volume of oil produced and applying Welge's Method in reverse. The unsteady-state process was relatively simple, fast, and adaptable to reservoir conditions, with minimal fluid requirements.

3.6.5 Procedures for core saturation and displacement experiments

At the beginning of each displacement experiment, the oil-water and the gas-oil contacts were adjusted in the separator vessels by clicking on the water and oil signals in the main menu provided in the online computer control software. The detailed procedure was carried out as follows:

Experimental Equipment and Procedure

1. Care was taken to ensure the water and oil vessels (Figure 3.4) were filled with salt water and crude oil.
2. The core plug was weighed and the dimensions, (length and diameter) were measured using the callipers.
3. The plug was placed in a vacuum chamber and vacuumed for three hours.
4. The saturated liquid was connected to the vacuum chamber, then the core plug was saturated with five percent of NaCL brine and weighed again.
5. The core plug was loaded into the core holder.
6. The overburden and back pressures were applied to the system.
7. Water was then injected at a constant rate through the core plug to measure the absolute permeability.
8. The water saturated core plug was then displaced by injecting the oil through the core plug at a constant rate.
9. The total water produced when the first drop of oil reached the exit of the core plug was recorded. The volume of water and oil produced was then measured every 60 seconds.
10. Calculations of the oil and water relative permeabilities were made based on Equations 3.15, 3.16, and 3.17 (Section 3.3.4).
11. The core was weighed and the residual water saturation calculated.

3.6.6 Core preparation and core holder handling

At the beginning of a set of displacement experiments, the core flooding equipment should be calibrated as discussed earlier (Section 3.4). The core plug was loaded into the core holder and the latter was then securely installed in the system. The oil, water and gas reservoirs were then filled with the corresponding fluids. The system was then brought up to the reservoir pressure and temperature. The procedure to prepare the equipment and the core samples to perform a core flooding experiment is described below in six steps.

1. The core plug was placed in an oven for 24 hours at 100 °C to remove any fluids present. It was then weighed with a digital balance and placed in a vacuum chamber. The

Experimental Equipment and Procedure

vacuum chamber was connected to a vacuum pump for five hours to remove any air from the core plug and chamber. The vacuum chamber was then filled with brine and the core holder was suspended for one day in order to achieve total saturation of the core plug. The core plug was weighed again and the weight of the water contained in the saturated core plug was calculated. The core plug was then bandaged with a Teflon tape to prevent leaking into the core holder and then placed into the sleeve. The core holder has one fixed end and the other end can be adjusted using a piston to make the sleeve containing the core plug fit tightly into the core holder.

The overburden and back pressure vessels were filled with synthetic oil and purged with nitrogen from the top to achieve more stability during the experiments. The overburden pressure valve was then released, and all the synthetic oil passed into the annulus of the sleeve from the bottom point upward through to the top point. The top point plug was opened to purge the air from the system. The annulus pressure of the sleeve was increased to 14 Bar by a hand pump and the overburden pressure was purged from the upstream point of the core-holder to release the gas phase in the annulus of the sleeve.

2. The valve between the backpressure cylinder and the backpressure valve was opened to apply the required pressure of the system using the backpressure regulator. The stability of the backpressure valve is most important and is usually reliable if the top of the backpressure vessel is filled with nitrogen or another gas due to the high compressibility of gases.
3. In the next step, all the connecting lines and valves from the top of the formation water cylinder to the downstream of the core-holder were vacuumed and then filled with formation water. By injecting water into the porous medium using a positive displacement pump, the pressure of the core-holder was slowly increased and at the same time, the overburden pressure was increased (the overburden pressure during the experiments performed was always held at 14 Bar above the pore pressure). The

Experimental Equipment and Procedure

difference between the overburden pressure and the pore pressure was kept small to reduce the impact on the rock compressibility and the pressure drop across the core plug.

4. The core holder annulus between the outer diameter of the sleeve and the inner diameter of the core holder body, was filled with a synthetic hydraulic oil, or clean water. It was filled from the bottom end of the core holder to allow the displaced air in the system to exit through the top of the core holder. Hydraulic oil is strongly recommended for filling the annulus between the sleeve containing the core plug and the body of the core holder and gas should never be used for this purpose because, in the event of a system failure, gas could be very dangerous at high pressures. In addition, gas would diffuse through the rubber sleeve into the core sample making the experiments invalid. Figure 3.20 shows the effect of gas on the rubber sleeve containing the core plug.
5. Once the annulus was filled with the synthetic oil, the outlet drain valve was shut. The core holder was then pressurised until the desired pressure was achieved. The pressurisation of the system was carried out in 35 Bar increments, while continuously checking for any leaks, as the pressure was increased. During the de-pressurisation process, performed after the experiment was completed, the pressure of the system was reduced gradually to prevent any damage being caused to the core sample.

Experimental Equipment and Procedure

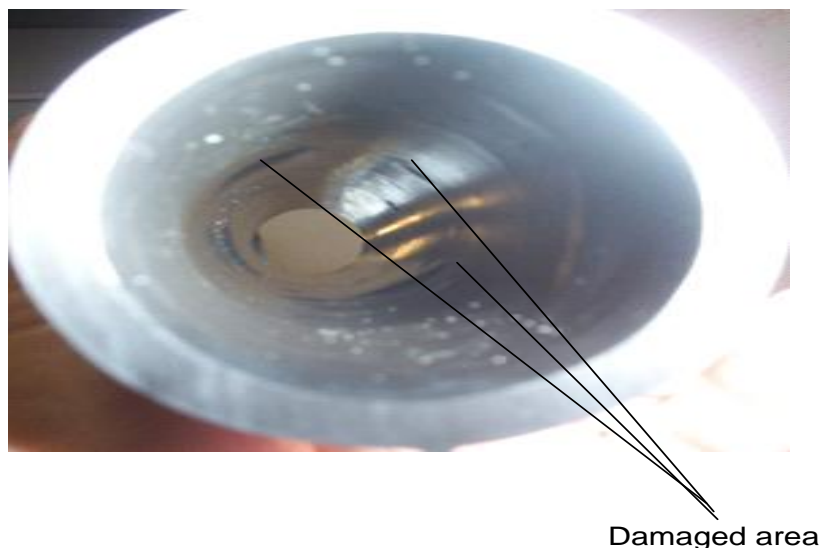


Figure 3.20 Effect of gas diffusion through the sleeve

3.6.7 Three-phase relative permeability measurements

During an unsteady-state gas displacing liquid relative permeability test, the objective was to measure the resistance to viscous flow of each phase in a porous medium as a function of their respective saturations. Viscous forces control the fluid flow. When mass transfer takes place between oil and gas, as the gas is absorbed into the liquid phase, the pressure of the system drops along the core holder. In carbonate reservoirs, differential pressures exerted by the injected gas are much more than the capillary force and hence the capillary end effects could be ignored during these experiments Benston (1978) (see more on appendix B).

The objective of this experiment was to determine the three phase (gas, oil and water) relative permeability in a core sample by means of the unsteady-state method. A carbonate core plug, 1.5 inches in diameter and 2.3 inches in length was drilled from a whole core. The pore

Experimental Equipment and Procedure

volume, bulk volume and air permeability were then measured. The viscosities of the oil, water and gas at reservoir conditions (operating condition) were then calculated. The following procedure was then followed to measure the three-phase relative permeability:

1. The oil, water and gas cylinders were filled with the relevant fluids.
2. The flow of oil, water and gas was facilitated with the use of the positive displacement pumps at a constant rate.
3. A brine-saturated core plug was then placed into the rubber sleeve and loaded into the horizontal core holder.
4. The absolute permeability of the rock to water was then measured.
5. The over burden pressure was then applied to the core holder. This depended on the core permeability and hardness of the sleeve material used in the experiment relating to the reservoir conditions.
6. The pressure, temperature, and the overburden pressure were allowed to achieve equilibrium conditions.
7. The saturated core with the brine was then displaced by oil until breakthrough of oil occurred at the exit of the core holder.
8. The core containing oil and water was then injected with gas at a constant rate.
9. A large volume of gas, more than three pore volumes, was injected through the core to reduce the oil and water saturation adequately.
10. All the data, such as pressure drop, water, and oil and gas saturations were calculated based on the respective volumes of fluids collected at the exit of the core holder using the collection pumps as a function of time.
11. The core was then flooded with water to measure the residual oil volume.

CHAPTER 4

Results and Discussion

Introduction

This chapter presents the results and discussion of the laboratory experiments performed to study the behaviour of oil and gas under reservoir conditions in a PVT cell and in the presence of a porous medium. This study focused on the fluid behaviour in a fractured, carbonate porous medium (see the objectives in Section 1.5). The laboratory experiments and the subsequent modeling of the findings were carried out in three stages:

1. mass transfer in a PVT cell;
2. mass transfer during displacement in carbonate rock; and,
3. mass transfer during displacement in a fractured media.

In stage one, the mass transfer between oil and gas in a PVT cell was examined by measuring the diffusion coefficient under reservoir conditions (Section 3.6.1). An empirical correlation, to calculate the diffusion coefficient, based on the experimental results was then developed (Equation 4.5 in Section 4.1.1). The developed empirical correlation was then used to model the fluid flow behaviour in porous media (Section 4.2).

In the carbonate reservoirs which have been depleted after primary oil recovery, and EOR gas injection is used to improve the oil recovery, the mass transfer phenomena during displacement process strongly depends on the time of contact and directly increases oil recovery of the system. In stage two, the following key parameters that determine such EOR process during different time of contacts were measured:

- a. Absolute permeability and porosity – They are influenced by the distribution of pore and throat sizes in the formation matrix (Das and Hassanizadeh, 2005). For carbonate reservoirs, the fractures can have a dominant effect (Yu shu et al., 2008) in displacements. The measurements of the absolute permeability and porosity of core

plugs were necessary prior to the measurement of two- and three-phase relative permeabilities.

- b. Two-phase relative permeability – It is one of the essential parameters required when designing an EOR process, i.e., the injection of gas into a fractured carbonate reservoir containing residual and by-passed oil after primary recovery. However, there is insufficient published data available on EOR processes with gas injection in tight carbonate reservoirs (see Section 1.2 for a review of the literature). The mechanism of displacement in this type of reservoir is quite complicated. Two-phase relative permeabilities in a tight carbonate rock were measured in this research.
- c. Three-phase relative permeability – In the case of enhanced oil recovery achieved through gas injection into a fractured carbonate rock, the use of three-phase relative permeability is absolutely vital when attempting to predict the reservoir performance. This is because the absorption of gas into the oil phase in the presence of water is what determines the efficiency of the recovery. The mass transfer of gas into oil makes the oil molecules swell and makes them mobile. There is hardly any published data on three-phase relative permeabilities (Section 2.5.5) and hence, the major focus of this research was the measurement of three-phase relative permeability in core plugs that were obtained from a tight carbonate reservoir in Asmary Formation in Iran.
- d. Mass transfer during displacement – The quantification of the mass transfer process that takes place when gas is injected into a depleted oil reservoir (after primary recovery) is the major component of this research (Section 1.5). All the experiments were performed to evaluate the mass transfer process carried out in the incubation period. The experimental results were then compared with the model predictions, developed in stage two of mass transfer taking place between the residual oil present in the porous media and the injected gas. This was achieved through the measurement of the three-phase relative permeabilities.

In stage three, modelling of the fractured system with a new diffusion coefficient correlation (developed as part of this research in Stage One, Section 4.6) was carried out. The results were compared with the diffusion and without diffusion mechanisms during the EOR process (Section 4.4). Evaporation and condensation phenomena, which take place when gas is injected into an oil phase under reservoir conditions between the fractures and the matrix, were also studied as part of this research.

4.1 Mass transfer in a PVT cell under reservoir conditions

The diffusivity of gas into a liquid phase has been measured at low pressures and temperatures since the early 1900s (Section 2.2). There are no reliable experimental data available in the literature of diffusion coefficients at high pressures and temperatures that represent typical reservoir conditions. The diffusion coefficient plays the most important role in the mass transfer that takes place between gas and oil during gas flooding (Sahimi et al., 2006; Riazi, 1996).

Figure 4.1 shows a schematic of the system with the PVT cell, 1.5 litres in volume, designed to contain 800 cm^3 of oil and 200 cm^3 of gas. From this set-up, all data were collected with high precision every minute using the two online computers driven by the Falcon software.

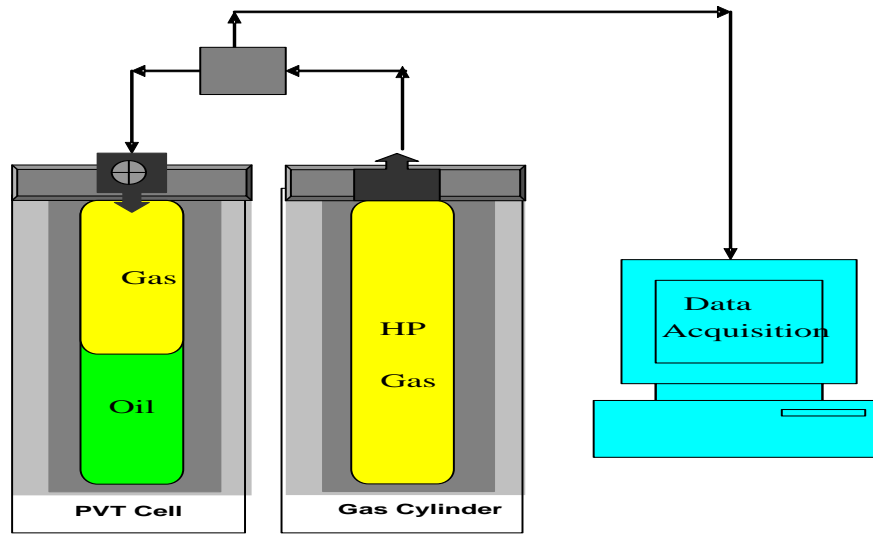


Figure 4.1 A schematic of the equipment used to measure the pressure drop during gas diffusion into an oil sample.

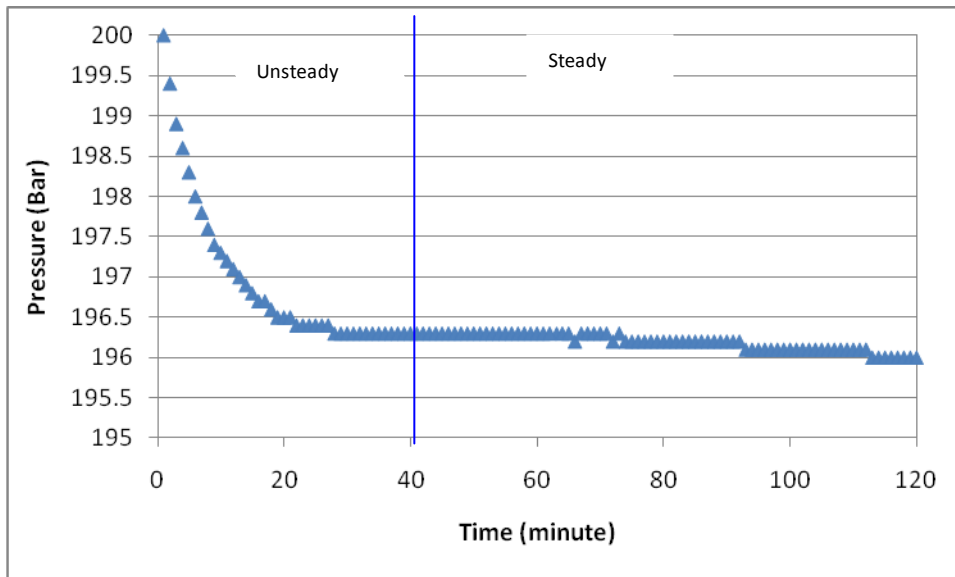


Figure 4.2 Measured pressure drop during mass transfer of gas into crude oil.

The results are presented in Figure 4.2, which shows two regions that were measured in the PVT cell. The unsteady-state process took place in Region 1, while the steady-state process took place in Region 2. The mass transfer rate was higher in unsteady state region than that in steady state. During the experiments, the diffusion coefficient which controls the rate of

diffusion, varied with time under the unsteady-state process. Some investigators (e.g. Renner, 1988) have called the incubation period the unsteady-state region. When pressure and temperature were low, the incubation period was found to be short and has hence been neglected by Riazi (1996), Zhang et al. (2000) and Hong et al. (2001) In this–study with running the generated model, it was found that the incubation period increased as the pressure and temperature of the system increased.

4.1.1 New correlation of diffusion coefficient at reservoir condition

The pressure of the two-phase system is strongly dependent on the more compressible gas phase. During the contact between the oil and gas phases in the closed system (PVT cell), if the liquid phase components evaporate into the gas phase through the interface, the pressure of the system increases. During the condensation process, when the lighter components of the gas phase dissolve into the liquid phase, the pressure of the system reduces until equilibrium is achieved between the two phases. This was clearly demonstrated during the experiments performed. In this research, a dead oil was selected for the liquid phase and 100% methane as the gas phase. By applying the material balance on each phase, the following mathematical equation could be developed. For instance, the moles of methane removed from the gas phase were equal to the moles of methane diffused into the liquid phase and this could be calculated using the following equation:

$$\text{Number of moles removed from gas phase over unit time} = \frac{V}{Z_g RT} \frac{dP(t)}{dt} \quad (4.1)$$

$$\text{Number of moles diffused into the liquid phase over unit time} = -D_{go} A \left(\frac{dC_g}{dZ} \right) \quad (4.2)$$

$$\frac{V}{Z_g RT} \frac{dP(t)}{dt} = -D_{go} A \left(\frac{dC_g}{dZ} \right) \quad (4.3)$$

When the volume of gas and cross section of the PVT cell are constant then Equation 4.3 can be simplified to:

$$\frac{dP(t)}{dt} = -\frac{Z_g RT}{h} D_{go} \left(\frac{dC}{dZ}\right)_{z=z_0} \quad (4.4)$$

In the equations above, D_{go} is the diffusion coefficient, which depends on the concentration, pressure, temperature, and the distance between molecules. The classical diffusion coefficients are considered constant under steady-state conditions (Taylor, R., and Krishna, R. 1993).

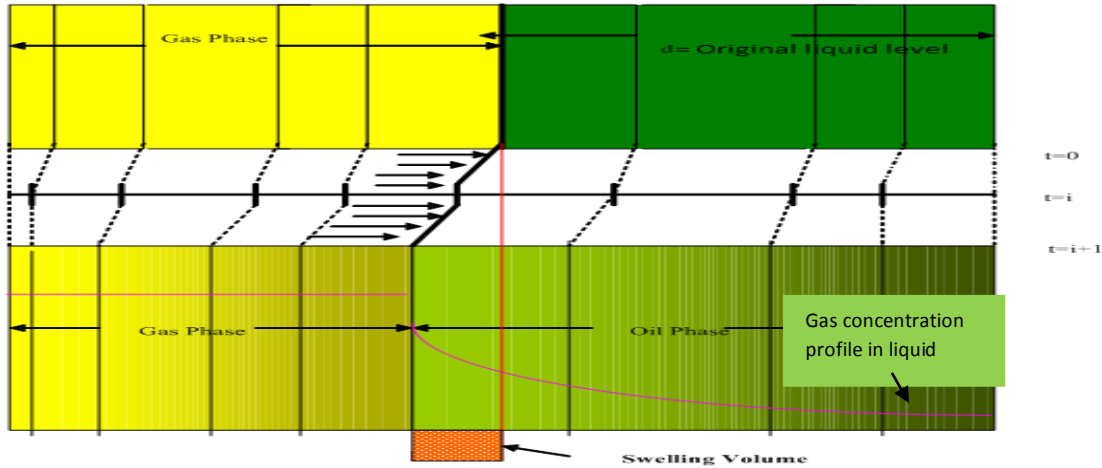


Figure 4.3a Schematic of the mass transfer of gas and oil during contact time and moving boundary of the phases.

During gas injection into an oil reservoir, the mass transfer occurs under unsteady-state conditions and hence the diffusion coefficient role becomes important. To measure the diffusion coefficient in a PVT cell, the diffusion coefficient was obtained from the gradient of the pressure/time profiles based on the mathematical analysis of the diffusion process (Equation 4.4). The initial and final molar concentration of the gas phase was calculated with the equation of state. A considerable amount of gas was transferred into the crude oil during the unsteady-state process depending on the gas solubility (Figure 4.3a). However, the rate of gas transfer into the crude oil was controlled by the diffusion coefficient of the gas.

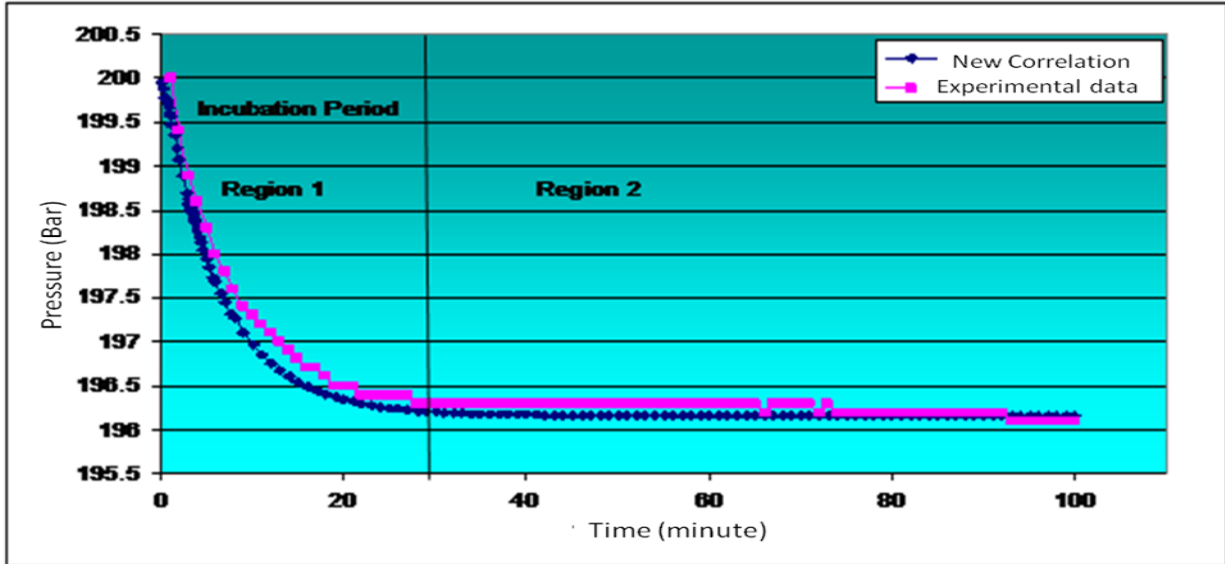


Figure 4.3b Comparison of measured and new correlation pressure drop during mass transfer of gas into crude oil.

Using the PVT cell, the diffusion coefficient was obtained under static conditions, by matching the experimental pressure drop and that predicted by the new empirical correlation (which was developed using the finite elements method as part of this research; see Section 4.1.4):

$$D_{go} = 1.3678 \times 10^{-7} \frac{T^{1.47} MW^{2.2}}{V^{0.5} P \mu_o} \quad (4.5)$$

where, P and T are temperature and pressure of the system and MW , and μ_o are the molecular weight, and viscosity of the oil phase respectively and V is the molar volume of gas phase.

For example:

$$T = 648 \text{ }^\circ\text{R}$$

$$\text{Molar volume of gas} = 0.72134$$

$$P = 3000 \text{ Psia}$$

$$MW = 250$$

$$\mu_o = 45 \text{ cp}$$

$$D_{go} = 2.2339 \times 10^{-3} \text{ (cm}^2\text{/s)}$$

4.12 Comparison of measured correlation diffusion coefficient with previous correlations

Table 4.1 compares diffusion coefficient obtained during this study with those previously reported. The diffusion coefficient of the methane in the unsteady-state appears to be larger than that of the steady-state. The duration of the unsteady-state appears to strongly depend on the pressure of the system when comparing with the previous studies.

Table 4.1 Comparison of diffusion coefficient value of this research with other Studies

Diffusion Coefficient $D_{AB}(m^2/s)$	Pressure (psi)	Components	Reference
9.2×10^{-9} 10.6×10^{-9} 9.4×10^{-9}	113.85	Methane-Crude oil	Hong S.Loh (year)
9.8×10^{-9}	500	Methane – Crude oil	Zhang (2000)
1.37×10^{-8}	1029	Methane-N-Pentane	Riazi-Whitson (1993)
1.5×10^{-8}	1480	Methane-N-Pentane	Riazi (1996)
2.238×10^{-7}	3000	Methane-Crude oil	This study

4.1.3 Modelling of the PVT system by the finite elements method

A general-purpose partial differential equation (PDE) solver, namely FlexPDE (2006) by Pdesolution company (www.pdesolutions.com) was used for solving the complicated diffusion equation mathematical model. FlexPDE, is a finite elemental software, specially designed, for the solution of PDEs or systems of PDEs. It offers an integrated solution environment, including problem description language, numerical modeling, and graphical output of solutions. However, it could be programmed to output numeric data also, when graphs need to be plotted using a different graphical software package. FlexPDE uses a Galerkin finite element model, with quadratic or cubic functions involving nodal values of system variables only. FlexPDE assumes that the dependent variables are continuous (in most physical situations, this is true) over the problem domain, but does not require or impose continuity of derivatives of the dependent variables. Second-order terms in the equations will give rise to various forms of flux continuity (through surface integrals generated by integration by parts), and these conditions will be imposed in an integral sense over the cells.

There are several useful empirical correlations available for obtaining the diffusion coefficient. In this research, the correlation was developed by applying the FlexPDE software to match the experimental data with the theory of the partial differential equation explained in Chapter Two (Section 2.3 and Equations 2.8). The empirical correlations were developed for both static (Figure 4.3b) and dynamic conditions (Figure 4.15). The software yielded high levels of accuracy and was user friendly. The strength of the software lies in the automatic mesh generation, mesh refinement during the solution process, and automatic time step control. In this study, a two-dimensional problem in space was divided into triangular elements and the variables were approximated by third order polynomials in each element.

Figures 4.4a and 4.4b show the modeling results about the pressure contour and surface distribution of the PVT system during mass transfer between the phases. It demonstrates that the pressure reduction (Equation 4.4) of the gas phase at the interface is far greater than in any other region.

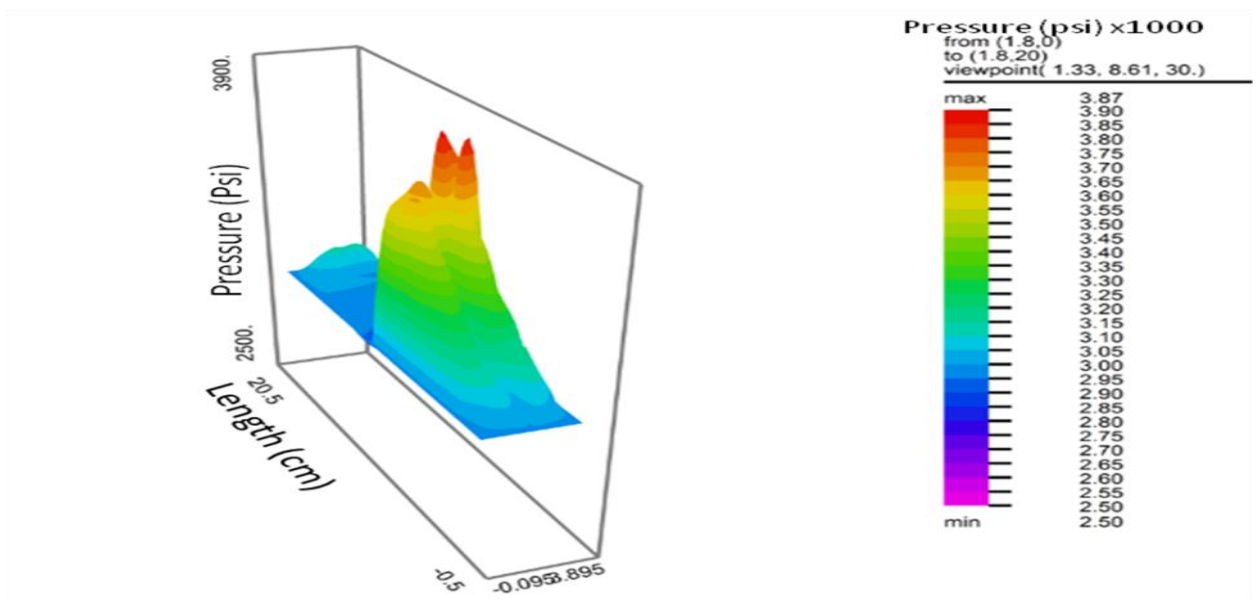


Figure 4.4a Pressure surface maps in gas and oil phases during mass transfer of the system

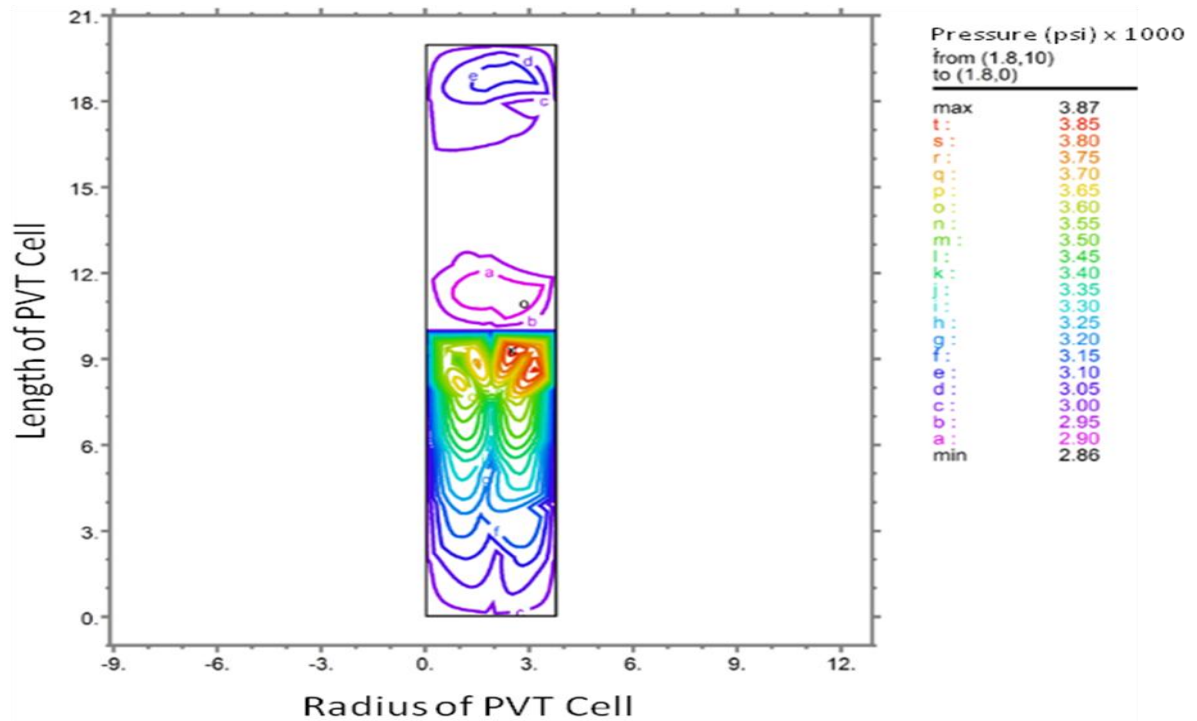


Figure 4.4b Pressure contour maps in gas and oil phases during mass transfer of the system

Figure 4.5 shows the methane concentration profile during contact between the phases of gas and oil. The concentration of methane was higher at the interface and reduced farther away from the interface within the liquid phase. The concentration of the methane was considered constant in the gas phase. There were two types of diffusion taking place in the system namely; (a) diffusion of the gas phase into the oil phase and (b) diffusion of the light liquid phase (top of the liquid phase) into the liquid in the heavy, bottom part of the liquid phase.

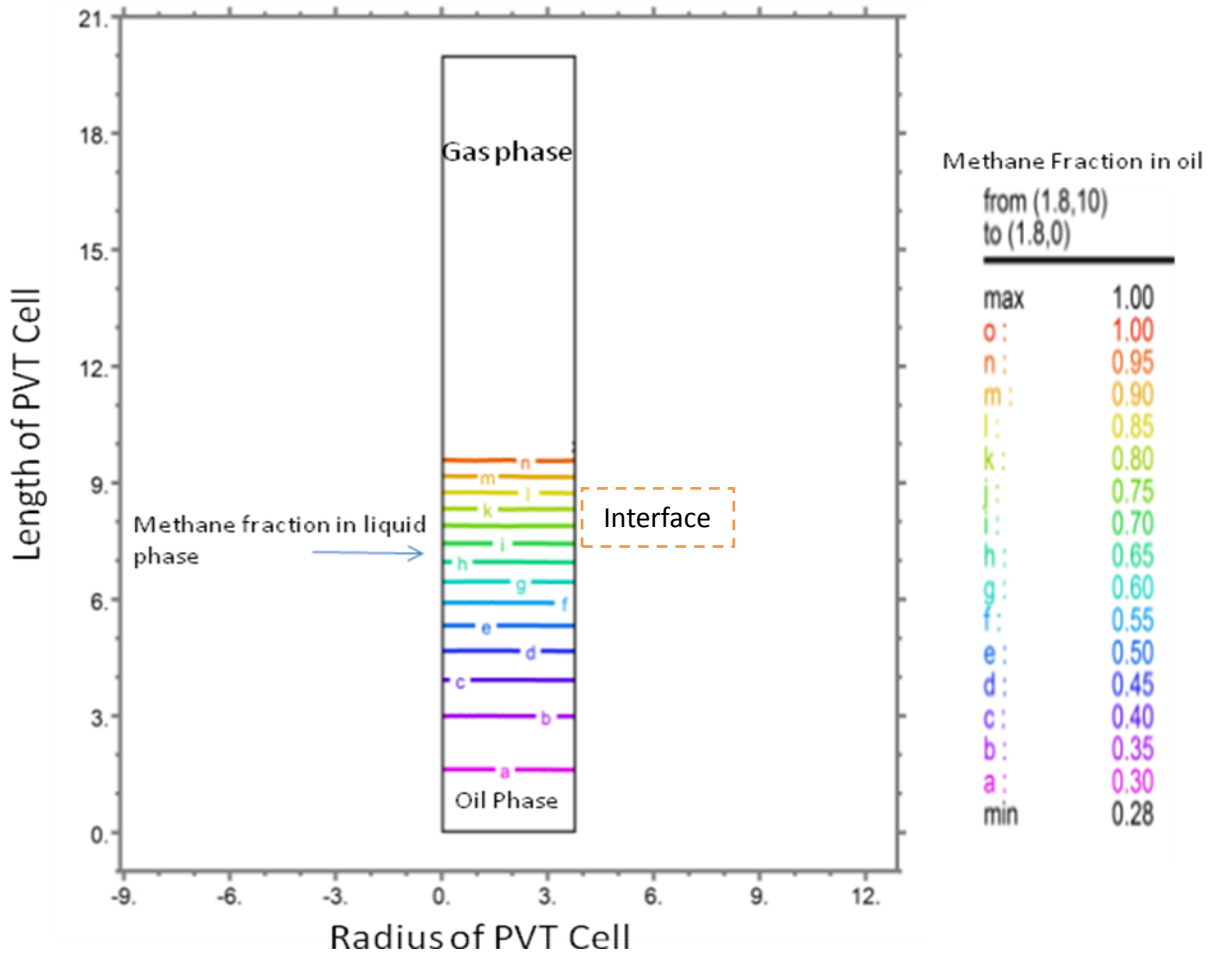


Figure 4.5 Profile of methane mole fraction in the oil phase at $p=200 \text{ Bar}$ and $T=87 \text{ }^\circ\text{C}$

Figure 4.6 shows the methane saturation variation in the oil phase where diffusion occurred mainly in the region close to the gas/oil interface. This means the upper region in the PVT cell achieved equilibrium quicker than in the lower region of the cell. The main diffusion occurred between the oil and gas phases, then diffusion took place between the light and heavy oil phases because of the concentration gradient present in the oil phase. Note that there was no methane present in the oil phase prior to the diffusion.

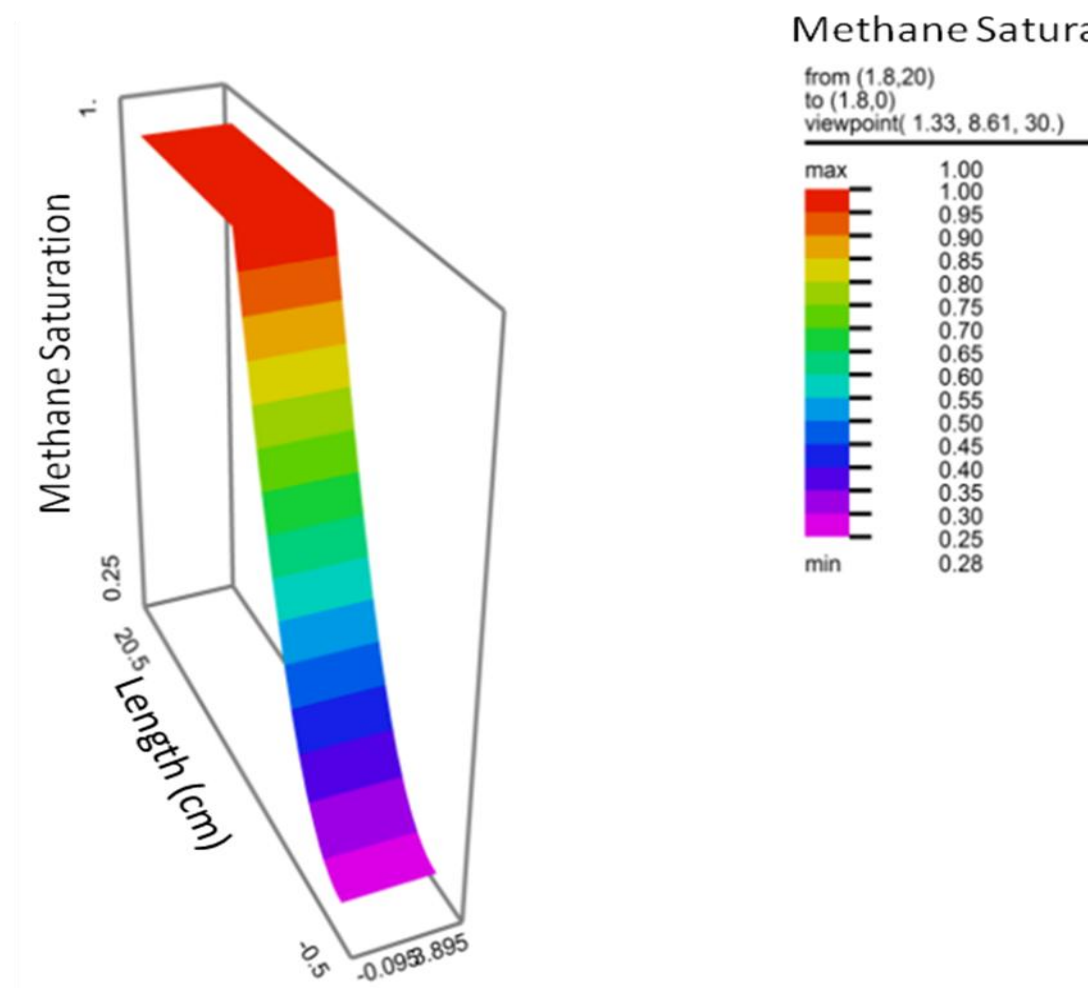


Figure 4.6 Saturation profile of methane in the oil phase during displacement

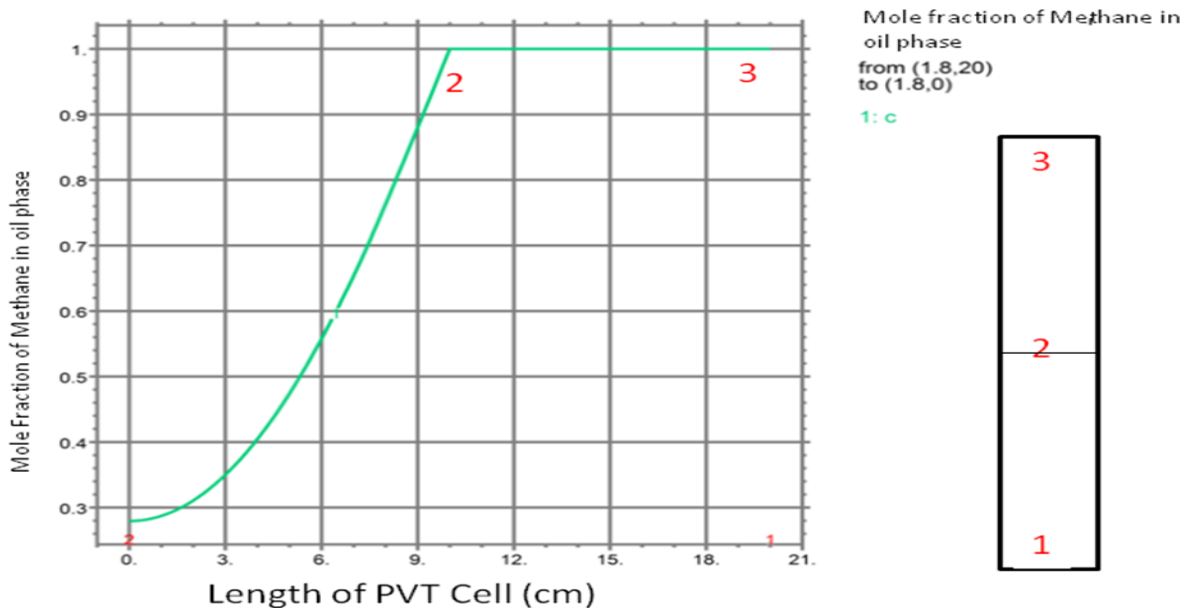


Figure 4.7 Concentration Profile of methane in the oil phase at $p=200\text{Bar}$ and $T=87\text{ }^\circ\text{C}$

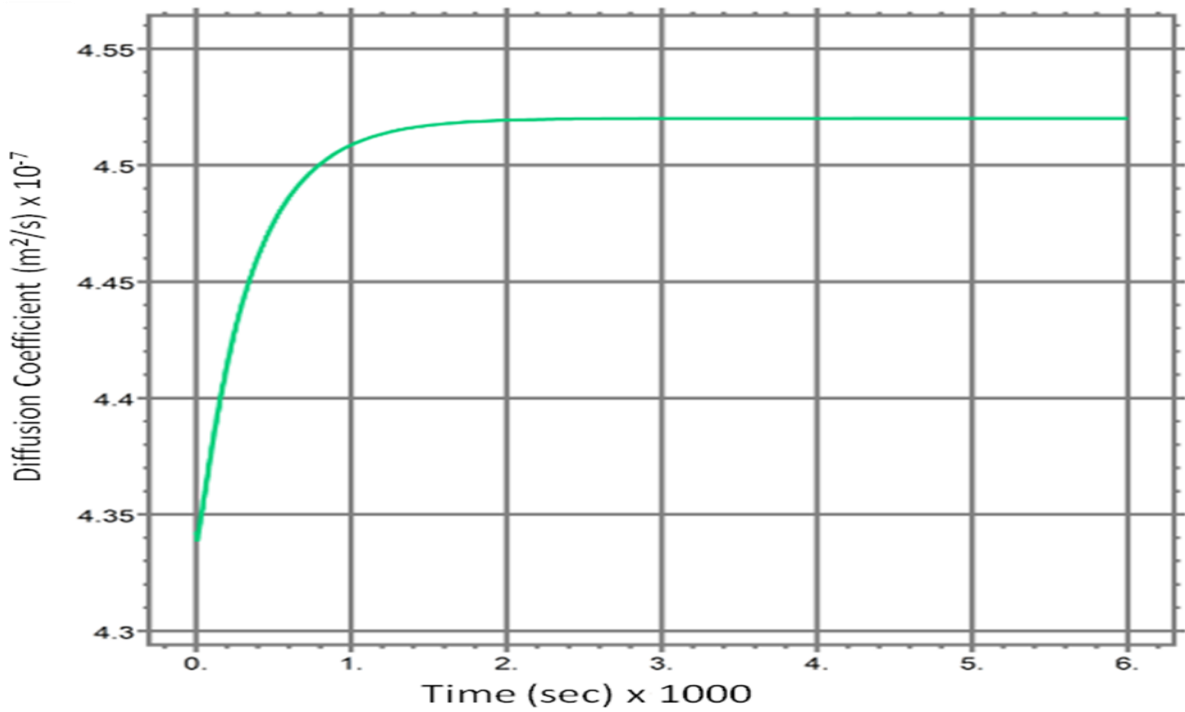


Figure 4.8 Diffusion coefficient of methane in the oil phase at $T=87\text{ }^\circ\text{C}$ and $P=200\text{ Bar}$

The methane concentration profile in the oil phase after 46 minutes is shown in Figure 4.7. The 2300 seconds were the incubation time for the mass transfer phenomena at $P=200$ Bar and at a temperature of 87 °C. Figure 4.8 shows that the flux between the phases was reduced during the contact time but was constant near the equilibrium condition.

The diffusion coefficient of gas into the oil phase was calculated from the empirical correlation (Equation 4.5), developed as part of this research and was used for modeling of the PVT system. Pressure of the system was reduced due to mass transfer phenomena and the new empirical correlation was implemented for pressure reduction, concentration of the gas and liquid phases. The variation of the diffusion coefficient as a function of time is shown in Figure 4.8. This parameter in the oil phase strongly depended on the methane concentration in the oil phase. The diffusion coefficient varied, from start of the contact period at the interface until the end of the incubation period, between 2.28×10^{-3} and 2.4×10^{-3} seconds.

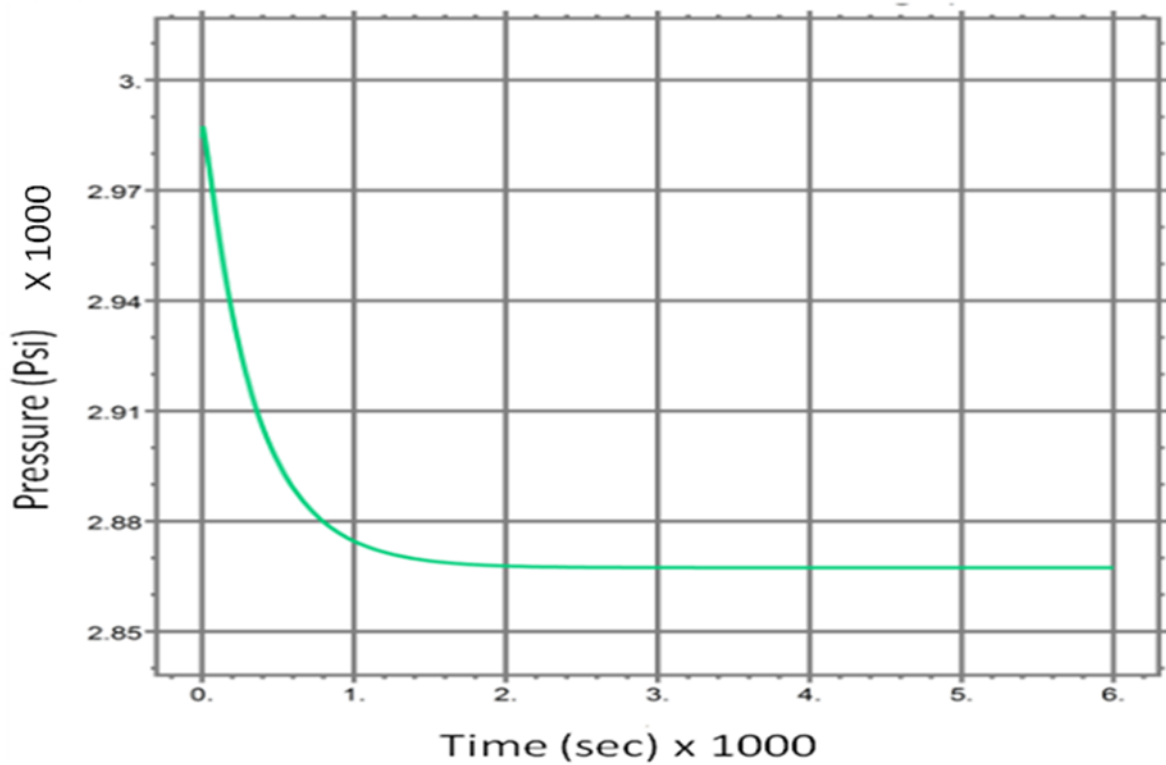


Figure 4.9 Variation of the pressure from 206 Bar (3000 Psi) in the system at $T=87$ °C

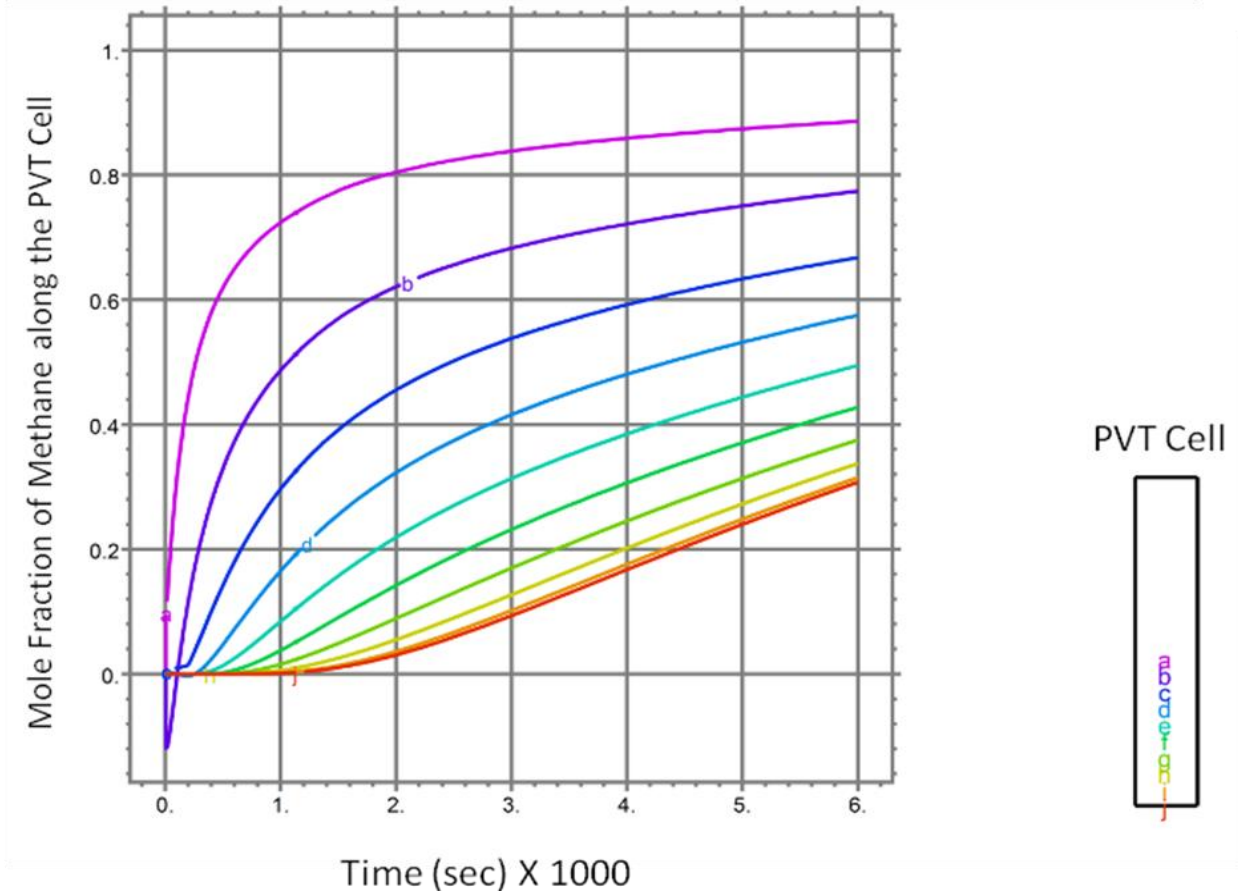


Figure 4.10 Variation of methane concentration in the oil phase with time at 200 Bar and 87 °C

Figure 4.9 shows the pressure profile during the contact period between the oil and the gas phase. It can be seen that the pressure reduction that took place depended on the rate of gas diffusion into the oil phase.

Figure 4.10 shows the variation of methane concentration along the oil phase from $Z=10$ to $Z=0$. The modelling results show methane concentration approached quasi-equilibrium over time (6000 seconds) in the oil phase interface. Curve 'a' in Figure 4.10 is the top of the oil phase where the gas phase diffused through the interface into the oil phase and curve 'j' is the bottom of the oil phase where it had little effect. The dissolution of the methane into the oil phase resulted in the oil having a lower viscosity, density and interfacial tension. With increased pressure of the system, the density and viscosity of the solution gradually increased.

Several approaches to solve the initial and boundary-value problems for the diffusion model have been explored. In all cases, the solution is obtained either in analytical or semi-analytical form. In all cases, the diffusion coefficient is considered to be dependent on just one variable such as pressure, temperature, concentration, porous media, or viscosity. In the real world, diffusion coefficient depends on all of the above variables, but the structure of this solution is quite complicated. Therefore, the finite element method can help to get acceptable results in such a complicated condition. The FLEXPDE software is used to simulate the diffusion system with the diffusion coefficient considering all reservoir parameters. The model shows that the diffusion coefficient during incubation time is affected significantly by the rate and pressure drop in the system (Figure 4.8). The finite element method solution of nonlinear Partial Differential Equation (PDE) is a good approximation at incubation time and steady state condition.

The diffusion coefficient of methane into crude oil is measured at reservoir condition and simulation model is generated by finite element method by using the FLEXPDE software. In both area of unsteady state and steady state region, the predicted pressure decay profile are very similar using both measured and modelled diffusion coefficient (Equation 4.5), (Figures 4.3b and 4.9). It was found that the rate of diffusion in the unsteady state is more than the steady stated. This shows that the multiple contacts of phases has the main rule in rate of gas diffusion into the oil phases.

The measured values of diffusion coefficient for the gas-oil mixture at temperature of 87 °C and 3000 Psia varies from 2.28×10^{-7} to 2.452×10^{-7} m²/s. This differences caused by pressure variation during time of contact between phases. In the Methane and oil system, it is seen from Figures 4.8 and 4.10 the diffusion coefficient increases with the methane concentration due to a reduced viscosity of crude oil. It means that the methane molecules can pass relatively easily through the transition zone of crude oil and diffuses into the bulk crude oil phase.

4.1.4 Discussion

The amount of mole fraction of diffuses into oil phase and causes the unsaturated crude oil gas/oil ratio to increase due to the swelling of the oil by diffusion of the gas can be calculated by Equation 4.1 (Section 4.1.2). The value of the diffusion coefficient in the incubation period was measured and found to be larger than that measured in the steady-state period through pressure drop of the system (Section 4.1.1). The estimated diffusion coefficient value with new correlation gave a better match on experimental data (Figure 4.3b).

The diffusion process takes place in two regions, the incubation region and the steady-state region. The main transfer occurred in the incubation region, which helped the transition zone to grow, thereby making it a partial miscible zone which in turn, helped to increase the displacement process. Figure 4.10 shows variation of the methane concentration along the liquid phase and it is clear that in the contact zone, the methane concentration is higher than bottom of the PVT cell. Besides, it is obvious that the diffusion coefficient depends on the concentration, temperature, viscosity of oil, pressure of the system, and the length of the PVT cell used in the experiments (Section 4.1.3).

The new correlation (Equation 4.5) developed through this research takes into consideration all the parameters discussed in Chapter Two. Advantage of the new correlation in comparing with others method (Table 4.1) is applicability of the current method at high pressure and temperature conditions (Section 4.1.2). The solution of the PDE was carried out using the finite elements method, which provided estimates of mass transfer rate and pressure drop, and were found to be valid for all diffusion times. The FlexPDE software was used to model the diffusion of the system and it provided the best match for the experimental measurements made.

4.2 Mass transfer during displacement in carbonate rock

In this section, the major findings and measurements from the core flooding experiments of four cases are summarised. Section 3.5.2 has a summary of the available core plug properties.

Three core plugs with 5, 4.8 and 4.5 cm in length and 3.8 cm in diameter were selected (Table 4.2), and they were weighed and dried in the oven for 48 hours. Then, the core plugs were saturated, by applying a high-vacuum pressure for at least eight hours, with five percent NaCl brine. Section 3 has a detailed description of the procedures. Finally, several experiments were conducted to measure the three-phase flow behaviour.

Three experiments were performed with single carbonate core plugs and one experiment was carried out with a composite core plug. Three carbonate core plugs with relatively higher permeability (plug 1-3, plug 2-2 and plug 2-3) were selected with rock properties provided in Table 4.2. The whole core plugs from Asmari Formation in Iran (Firoozabadi 2000)) transferred to Australia and eight core plugs had been taken by Corelab company. Three relatively high permeable plugs have selected for this study. Each plug was tested separately by three-phase flooding under reservoir conditions and also during displacement of water by oil two phase relative permeability was measured. During each experiment, the volume of water, oil and gas injected and produced was measured. The pressure drop during displacement of the fluids was also measured. The overburden pressure was always maintained at 30 Bar more than the reservoir pressure. The temperature for all experiments was kept at 87.5 °C. To evaluate the mass transfer that took place under the unsteady-state method, dead-oil was used to help measure the diffused gas oil ratio (GOR) during the displacement in the core holder.

All of the core plugs were cleaned in the traditional manner before being used in the experiments (Section 3.6.6). Drying and vacuuming of the core plugs was carried out before each test to measure the irreducible saturation of water. The measured properties of the core plugs are given in Table 4.2.

Table 4.2 Measured properties of the core plugs used in the experiments

Core Sample	Test pressure (Bar)	Absolute Permeability (mD)	Porosity %	pore volume (cc)
Core 1-3	55	3.41	19.9	10.632
Core 2-3	55	4.61	20.6	11.12
Core 2-2	55	4.87	20.5	10.316
Composite Core plug	55	4.778	20.33	32.068

The Peclet number (see Section 4.2.5) is less than one (0.29) in this system, therefore diffusion phenomena dominates. And also, all of the displacement tests were conducted within the incubation period of the diffusion process (injection rate was 30 cc/h), as explained in the previous section on diffusion. During the incubation period in PVT cell, mass transfer played the main role (Section 4.1.2 – the PVT cell experimental results), dissolving gas into the oil phase and during this process the pressure of the system reduced.

Figure 4.11 shows a typical example of the data from the displacement experiments performed in a core plug saturated with a five percent NaCl brine solution. The displacement experiment was conducted at 200 Bar pressure and 87 °C temperature where gas was injected into the core plug to displace the oil and residual water. Figure 4.11 is divided into four main parts; (a) saturation with brine and stabilisation at the pressure (200 Bar) and temperature (87.5°C), (b) displacement by oil until breakthrough, (c) continued displacement of oil with gas to produce the movable volumes of oil and water and (d) the imbibition process for calculating the residual gas saturation.

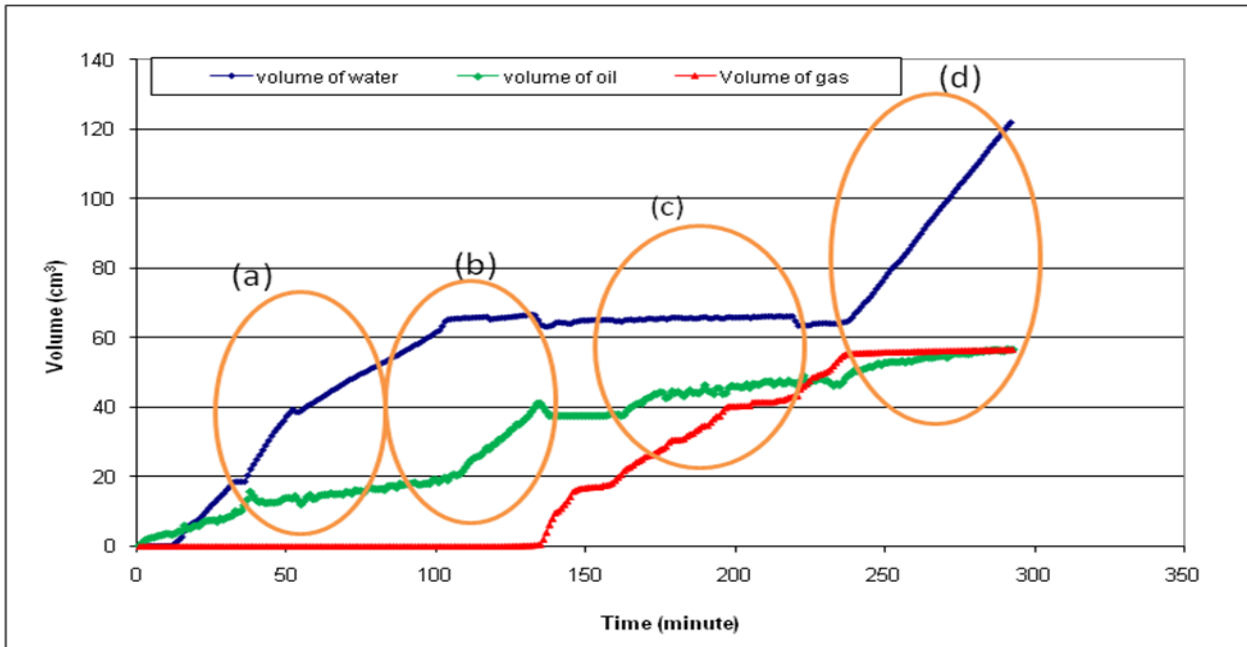


Figure 4.11 Production of oil, water and gas during displacement sample of whole systems

4.2.1 Experimental results for selected core plugs

Three carbonate core samples were chosen for study. The porosity and permeability of the samples were shown in Table 4.2. They had been water, oil, and gas flooded under reservoir conditions at an oil/water viscosity ratio of 19.73 and gas/oil viscosity ratio 0.0001235. The oil and gas breakthrough were observed in all tests. The plugs were initially saturated with a five percent NaCl brine solution representing the water phase. The flooding tests were conducted at 200 Bar, with the overburden pressure at 250 Bar, and a temperature of 87.7°C. The laboratory measured three phase recovery percentage of water, oil, and gas are plotted versus time in Figures 4.12 (a, b, c).

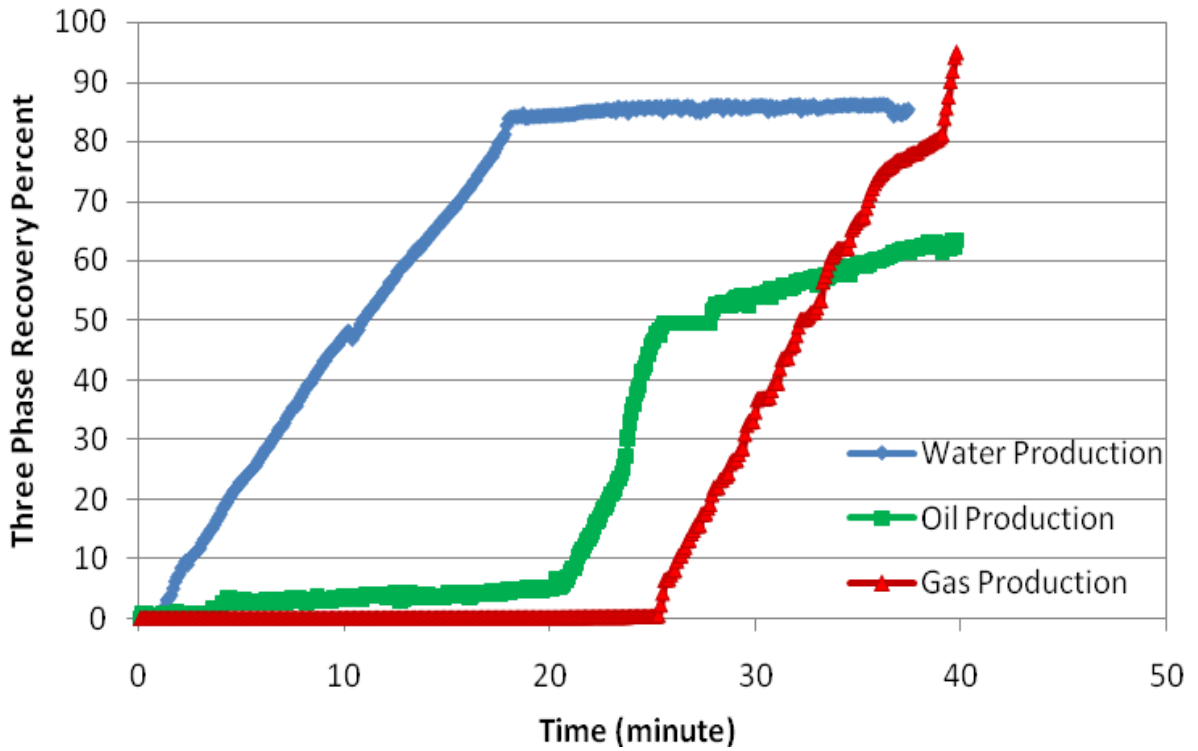
All the tests were conducted at 200 Bar pressure and 87.7°C temperature with different rates of injection, where oil displaced water until breakthrough and gas displaced both oil, and water phase after oil breakthrough in the porous media. During displacing of water by oil phase, the outlet saturation of water and oil was measured, therefore, two phase relative

permeability by using measured value of oil and water saturation, pressure drop along the core, and time were calculated. Figure 4.12 (a, b, c) show how all of the phases (water, oil, gas) were moved through the end-point of the core-holder. Core plug 1-3 was conducted with 60cc/h rate of injection and core plugs 2-2 and 2-3 were conducted with 30 cc/h rate of injection. The rate of the produced water phase became constant after gas breakthrough in a short time. The oil phase rate continued to increase and then gradually reduced after 1.2 pore volume of gas injection. The rate of gas production sharply increased and the pressure drop of the system reduced during the single gas phase production. In other hands, as the pressure is fixed at the outlet by applying back pressure regulator, it makes the inlet pressure increase.

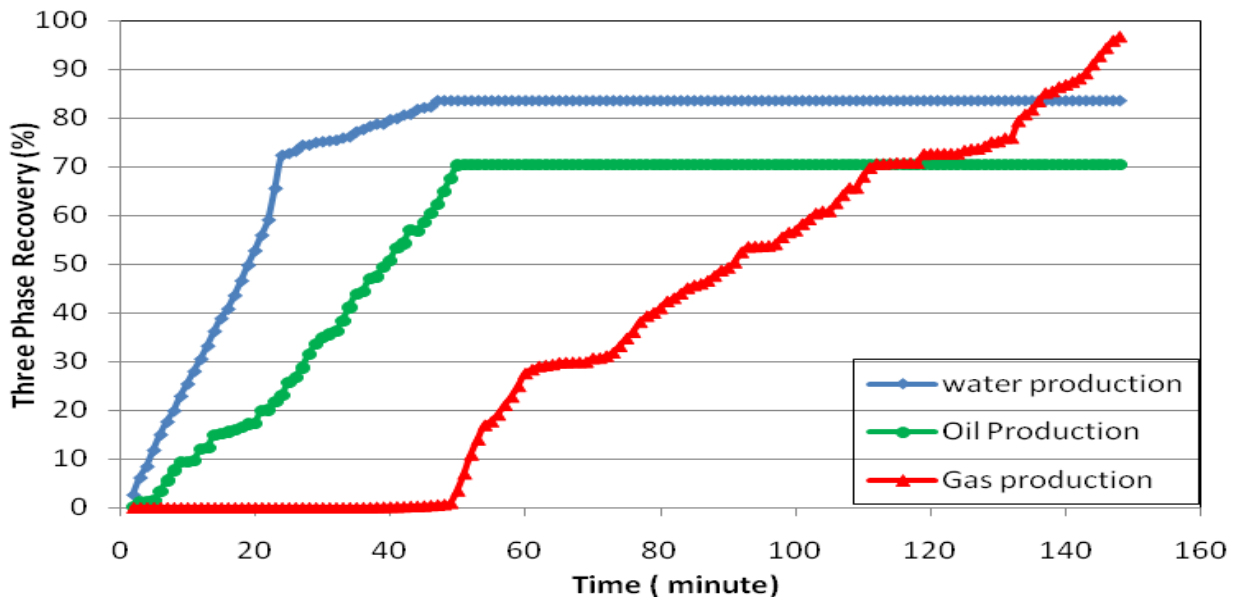
The pressure drop data were plotted for all of the carbonate core plugs during displacement by oil and gas (which were conducted using the unsteady-state flooding method). Figures 4.13 (a, b, c) and 4.17 show the relationship between inlet and outlet pressure of the system during the drainage process when the gas was injected into the saturated core plug with oil and brine. It was found that in the short time of contact between phases, after gas breakthrough was occurred the pressure dropped shapely. It shows the volume of swollen oil in transition zone is smaller than long time of contact.

Figure 4.14 (a, b, c) provides the data for the oil recovery versus injected pore volume during the displacement of crude oil when the gas phase (methane) was injected into the core-holder. The effect of the contact time on oil recovery was measured for 1.2 pore volume of injection. It was found that for long contact time or low injection rate (0.5cc/60 sec), total oil recovery was increased by 10 percent in comparing with injection rate of (1cc/60 sec).

(a)-Core plug 1-3



(b)- Core plug 2-3



(c) -Core plug 2-2

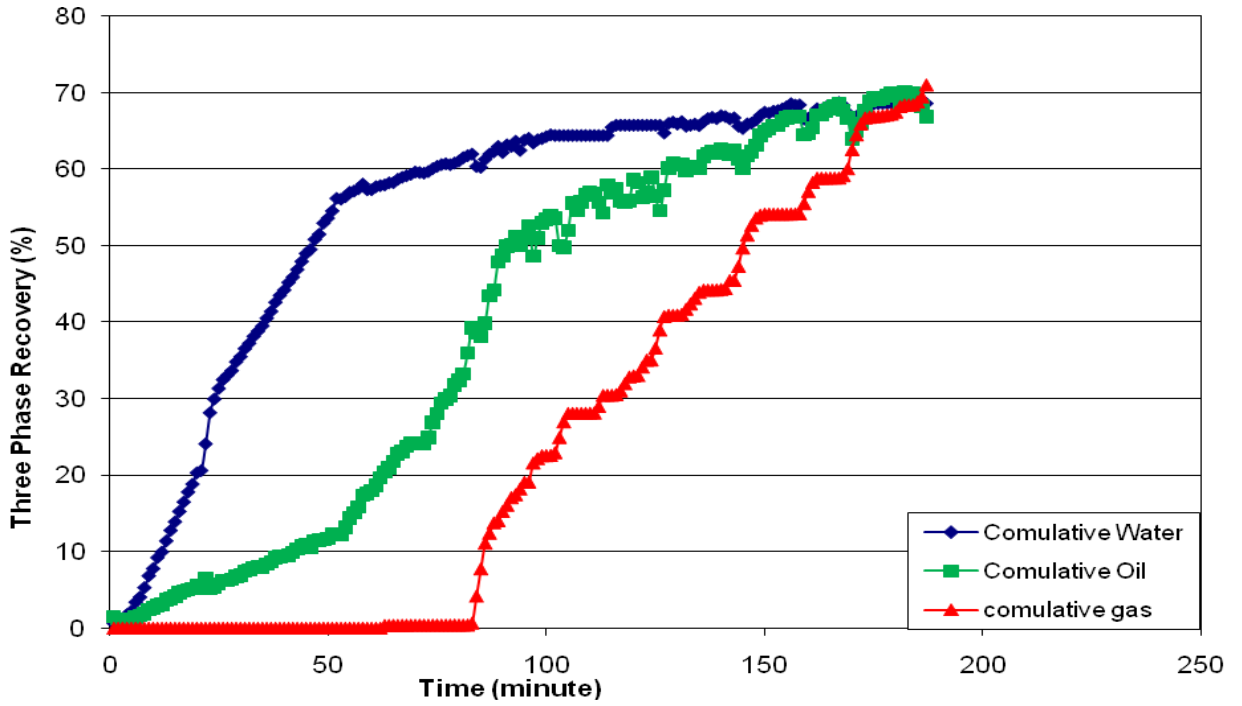
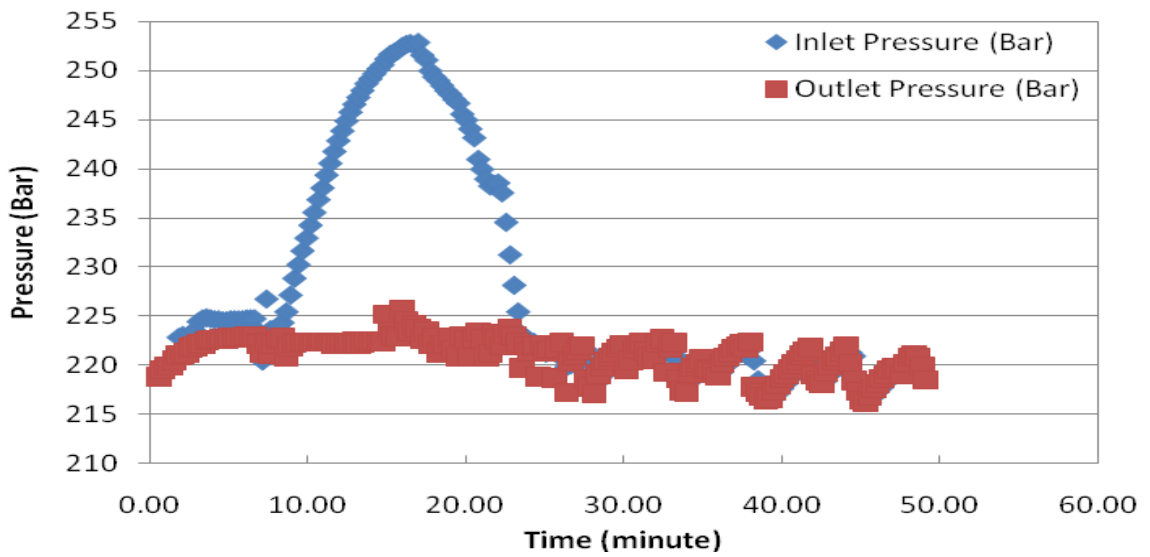
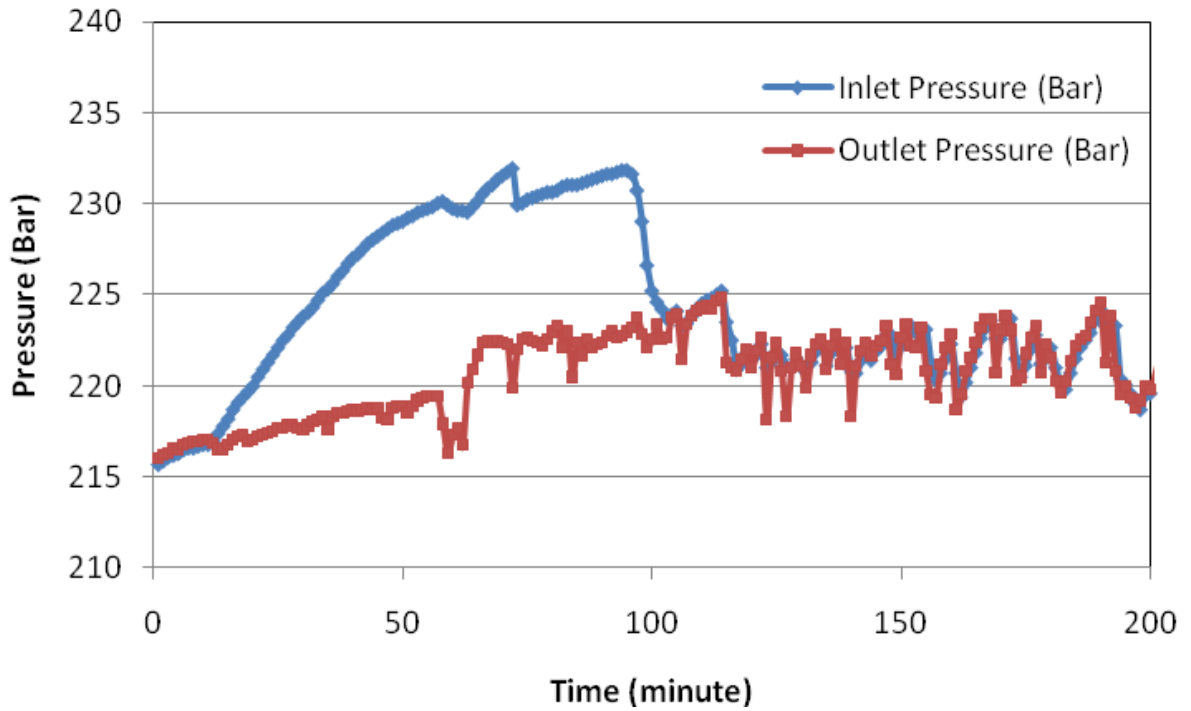


Figure 4.12 Water, oil and gas recoveries during the drainage process for three types of core plugs

(a)- Core plug 1-3



(b)- Core plug 2-2



(c)- Core plug 2-3

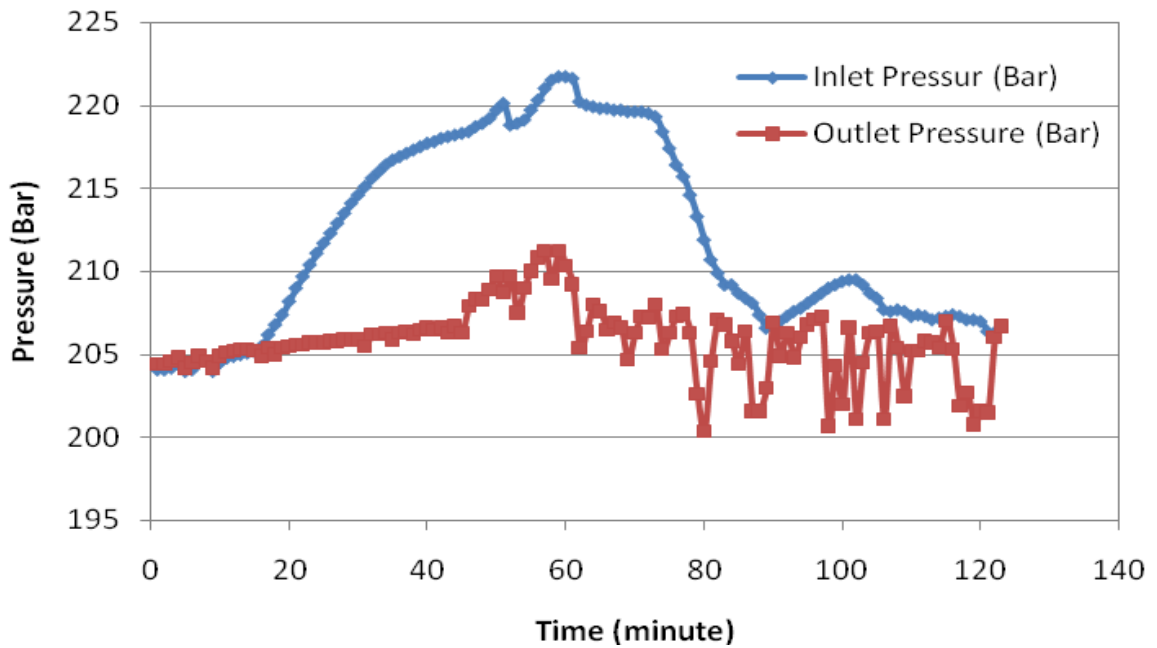
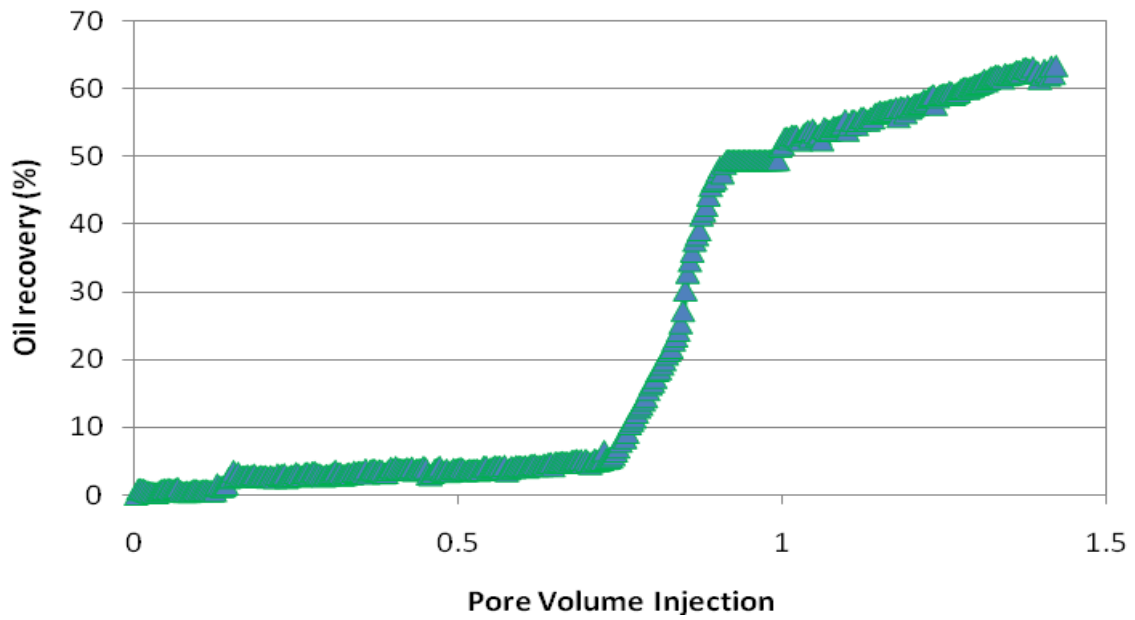
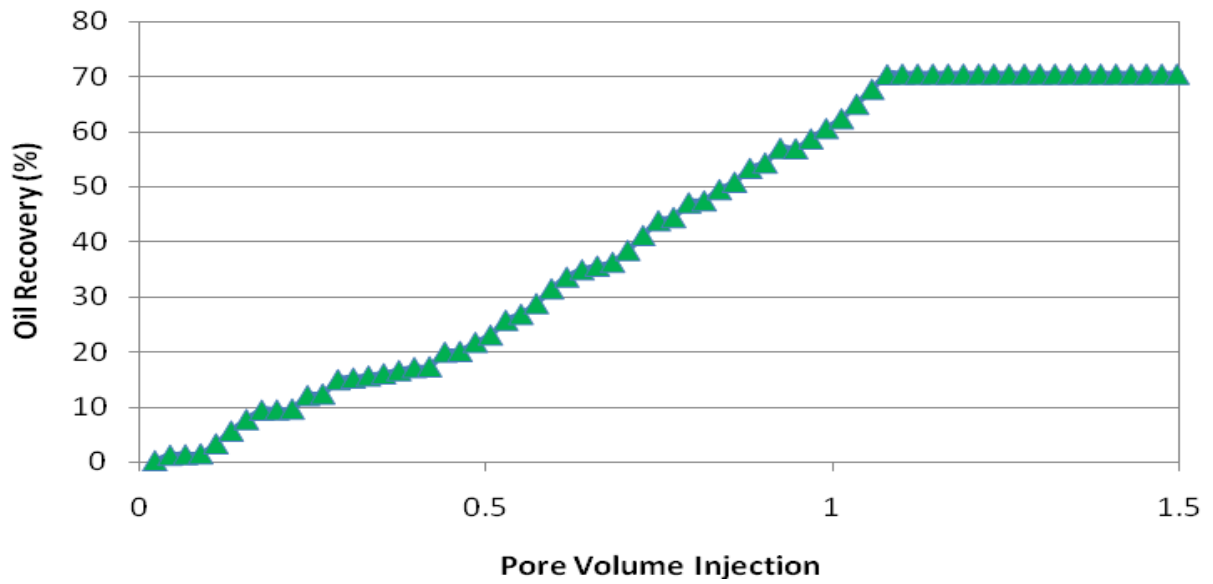


Figure 4.13 Pressure drop during the drainage process with gas flooding

(a)- Core plug 1-3 (Injection rate 60cc/h)



(b)- Core plug 2-2 (Injection rate 30 cc/h)



(c)- Core plug 2-3 (Injection rate 30 cc/h)

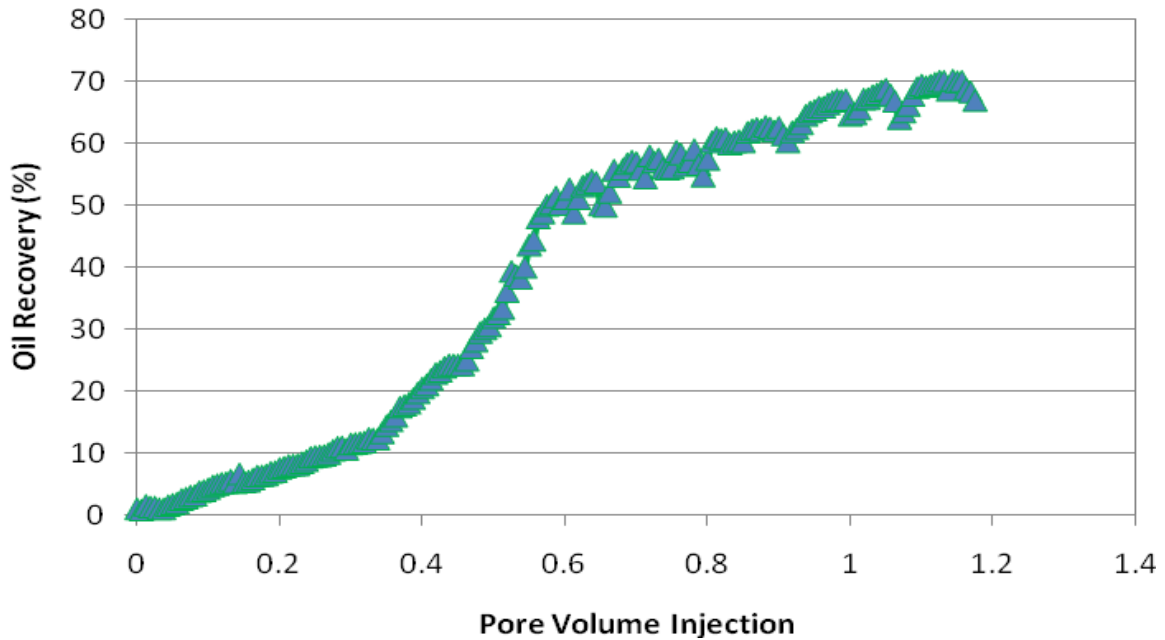


Figure 4.14 Oil Recoveries during gas flooding

4.2.2 Experimental results from the composite core plug

In this section, the experimental composite core flooding results are presented. The experiments were designed to test how mass transfer of gas into the oil phase during the incubation period influenced the swelling of the oil. This part of the project was conducted by arranging the core plugs in a descending order of permeability to reduce the capillary end effects and to improve the oil recovery, as explained in Section 3.5.5.

The composite core ordering is shown in Figure 4.15. A tissue was placed for capillary continuity at the interface between the core plugs. The core permeability ranged from 4.87 to 3.41 mD and the porosity varied from 19.9% to 20.5%. The oil used in these experiments was the same as that used with the single core plugs. The contact time was increased due to increasing of the length of the core, therefore oil recovery is maximised to 88% of original oil

in place in comparing with short core recovery (59%). Transition zone between phases was increased then the sharpness of the inlet pressure after breakthrough was decreased (Figure 4.17).

Oil volume is increased by the diffusion of gas molecules into the oil during the contacting of gas phase with the residual oil. The pores are preferentially wetted by water and oil and in the constant rate of gas injection, the pressure drop caused by viscous force between residual oil and gas, therefore a difference in pressure exists between the residual oil and gas. The pressure in the oil phase is higher than gas, therefore, the magnitude of the pressure gradient is higher to mobilize residual oil from the pore space. The mass transfer of gas molecules into the oil phase reduces the interfacial tension (IFT) and the swelling of the oil phase increases the oil film in the pore space, therefore based on the Laplace law (Equation 2.75) both of these phenomena are helping oil to move from porous media toward the outlet. Figure 4.18 shows significant increment in oil recovery of the system. Multiple contact of oil and gas along the composite core plug helps to increase transition zone and finally oil recovery to 88 percent in comparing with single core plugs. If experiment carried out with long core plug or composite core plugs, the oil recovery is increased due to long contact time.

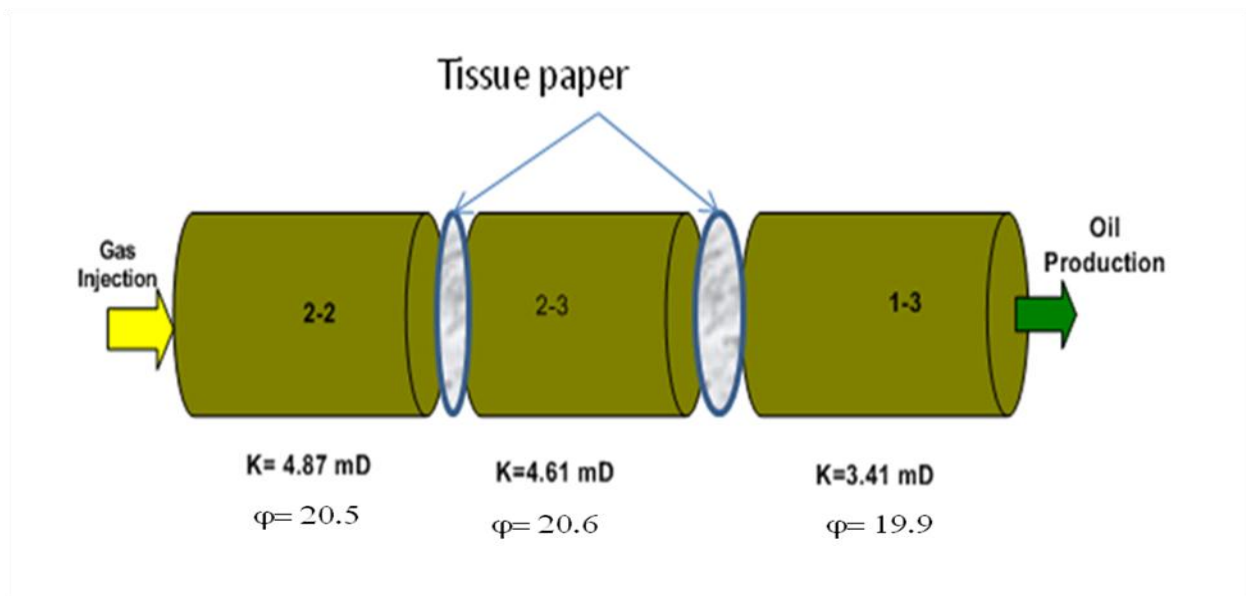


Figure 4.15 The composite core plug ordering

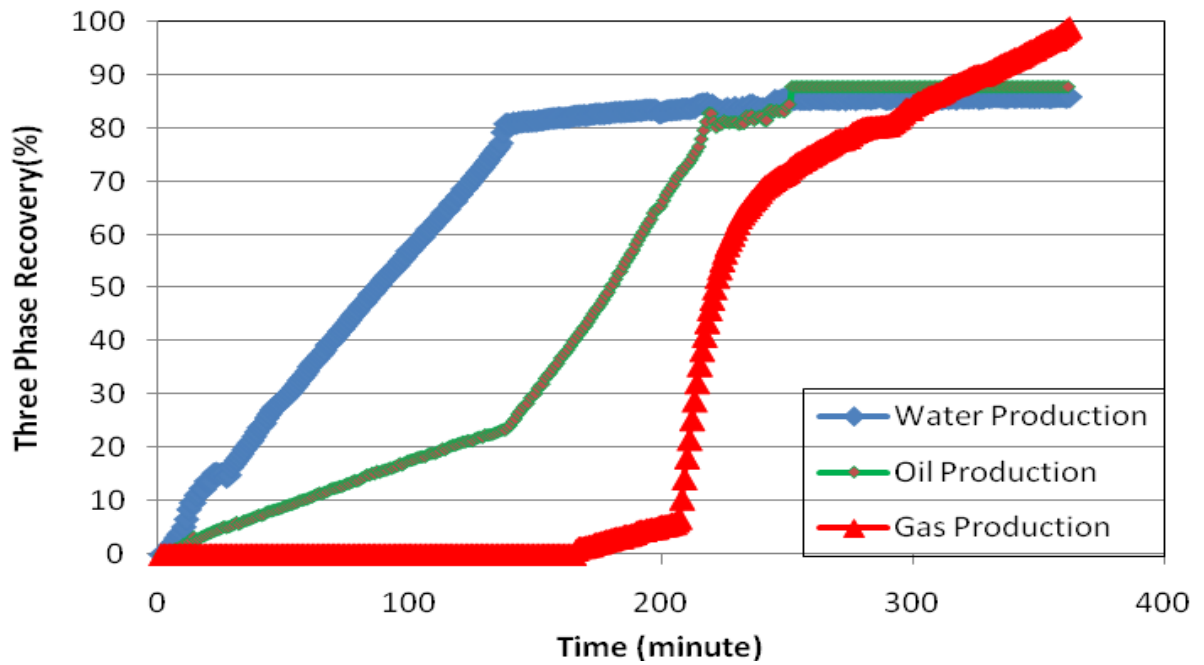


Figure 4.16 Water recovery during the drainage process with crude oil flooding

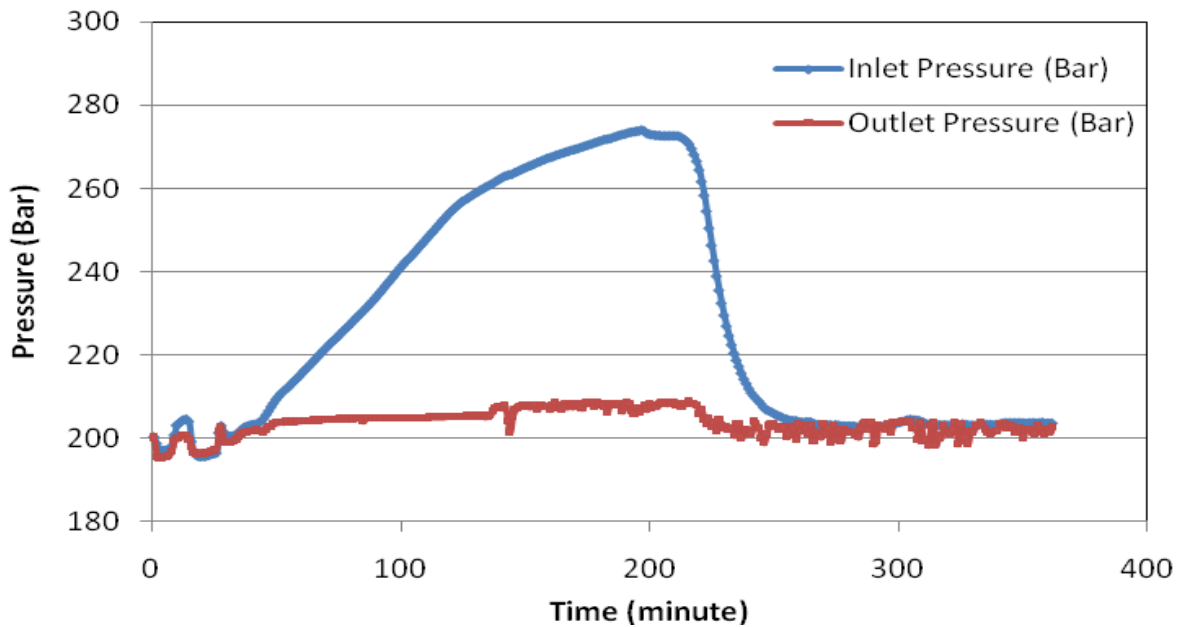


Figure 4.17 Variation of pressure during three phase production

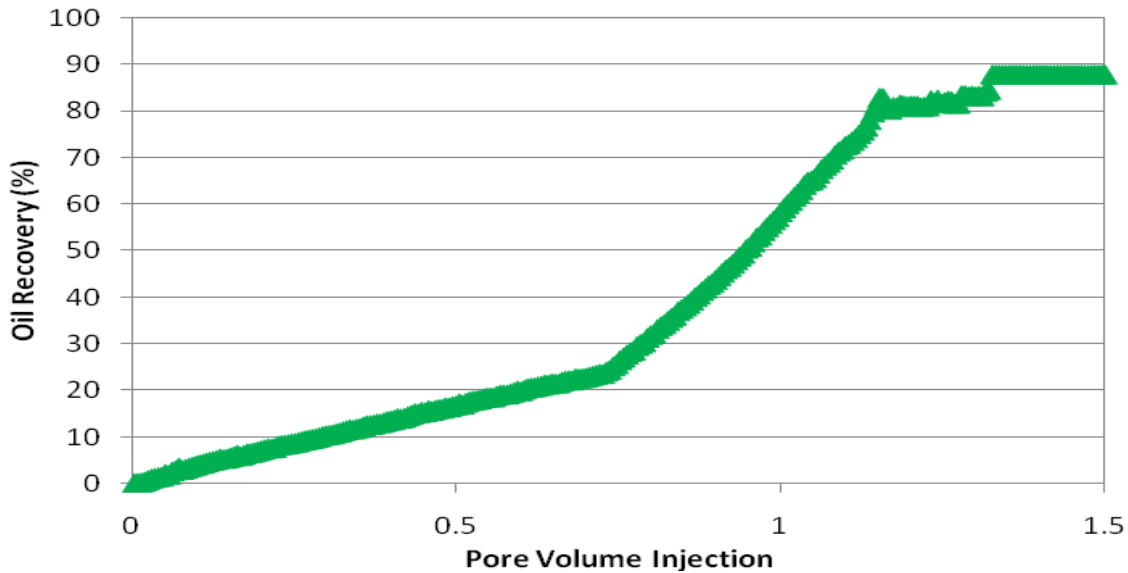


Figure 4.18 Oil recovery during gas flooding $q=30$ (cc/h)

4.2.3 Volume of gas diffused into the oil phase by mass transfer

In all the experiments, dead oil was used for displacing water and gas (methane) was used for displacing oil phase, therefore, when gas was diffused into the oil phase, produced oil was contained significant gas. High pressure oil phase was flashed during all experiments and the volume of dissolved gas was measured. Figures 4.19, 4.20, 4.21 and 4.22 show the volume of gas that diffused into the oil phase during contact of the two phases. Figure 4.19 shows that a short incubation time has little effect on the diffusivity of gas into the oil phase. The data shown in Figure 4.19 were obtained during the displacement test with 1 cc/min gas injection rate. Figures 4.20 and 4.21 show the volume of gas which diffused into the oil phase during a long incubation time (0.5 cc/min injection rate). As a result, the diffused gas volume increased during this period. All of the figures are shown after gas breakthrough volume of gas phase slightly was increased; it means width of transition zone is extended during mass transfer. In

short contact time (Figure 4.19) after gas breakthrough, the volume of gas steeply increased. The data shown in Figure 4.22 were obtained from the composite core plug at 0.5 cc/min injection rate and shows that the amount of gas that diffused into the oil phase increased with the increasing time and the length of the core plug. Table 4.3 show the swelled volume of dead oil during mass transfer of gas phase. Maximum volume was occurred in composite core plugs, because of contact time and multiple contacts of phases. Gas Oil Ratio (GOR) is another parameter which was indicated mass transfer phenomena in the system. Slightly mass transfer was occurred in sample 1-3 which had high injection rate and short time of contact. The majority of mass transfer was occurred in composite core plugs which had enough time of contact.

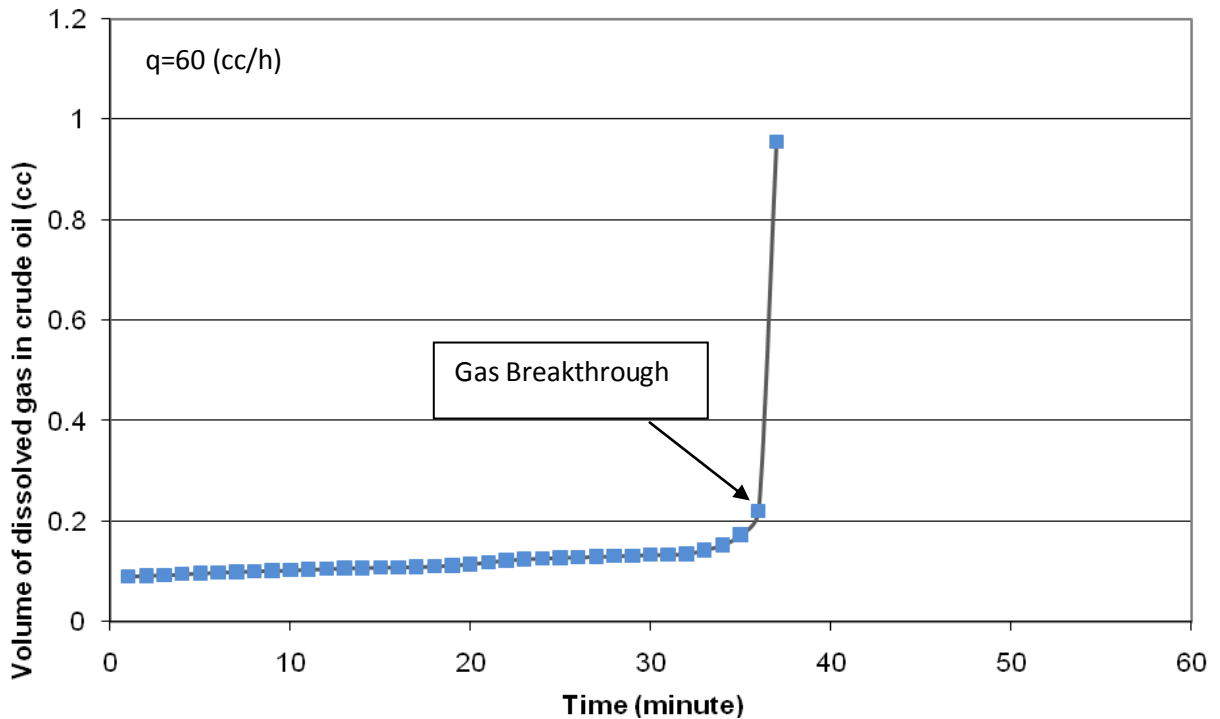


Figure 4.19 Volume of dissolved gas into the oil phase – core plug 1-3

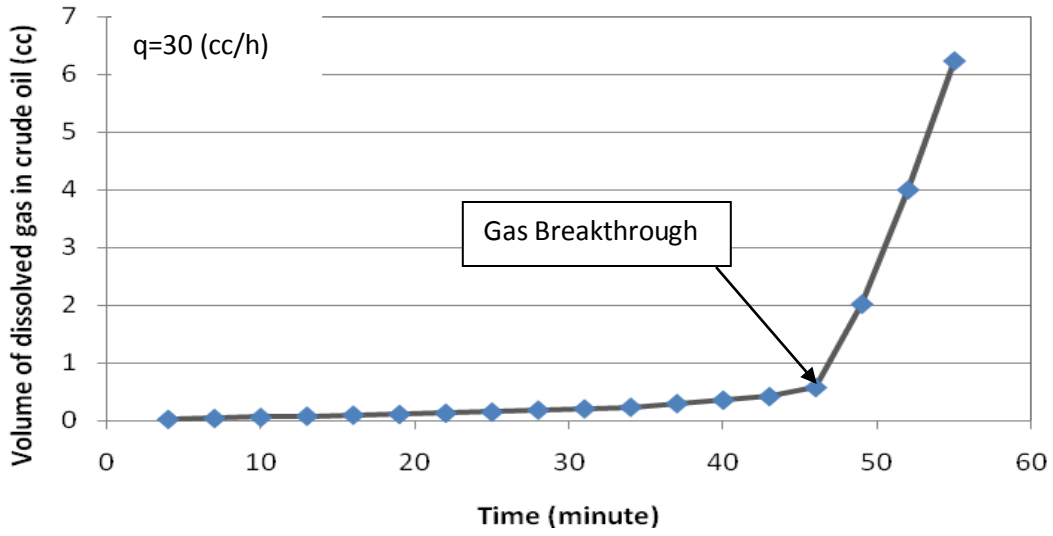


Figure 4.20 Volume of dissolved gas into the oil phase – core plug 2-3

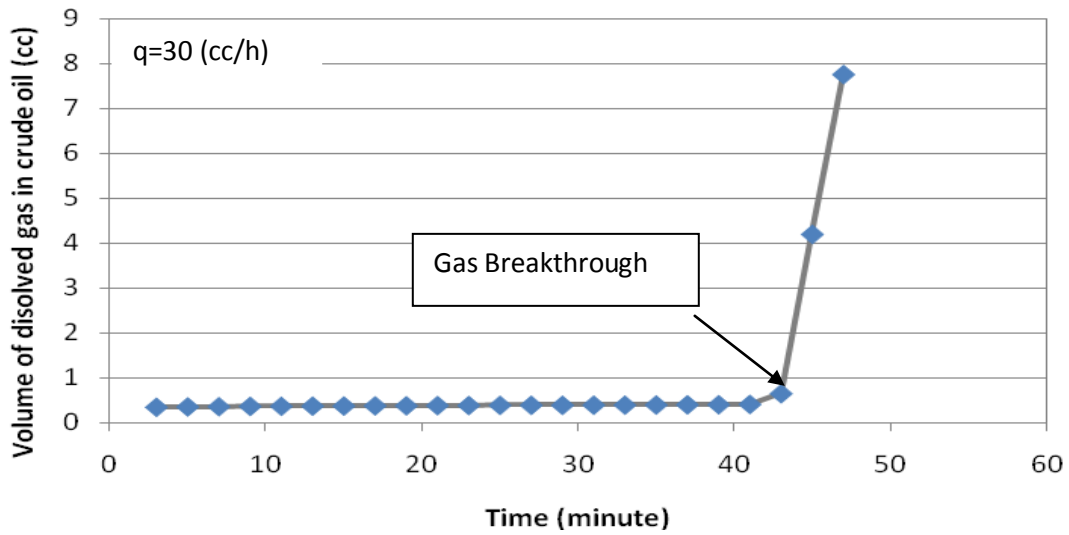


Figure 4.21 Volume of dissolved gas into the oil phase – composite core plug

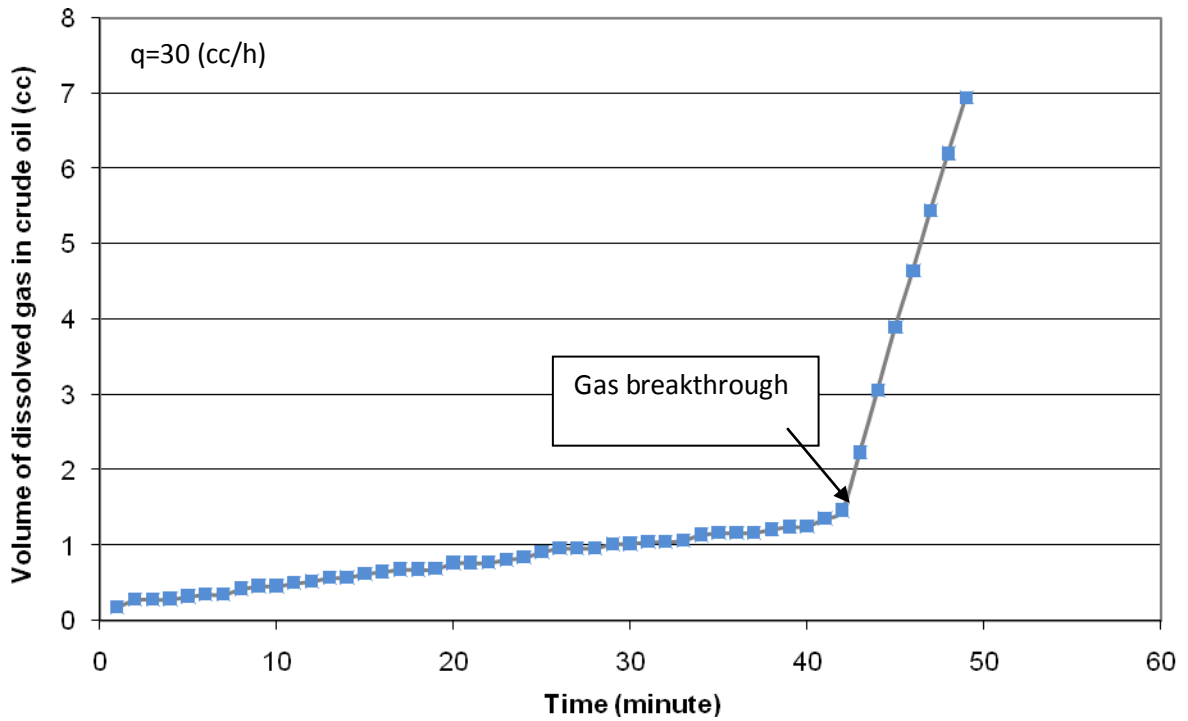


Figure 4.22 Volume of dissolved gas into the oil phase – composite core plug

Table 4.3 Swelling volume of oil phases in four type core plugs

Core Plug	Swelling volume (cc)	Swelling Volume percent	GOR Variation
Plug 1-3	0.219	0.97	Steepest increased
Plug 2-2	0.655	2.80	Sharply increased
Plug 2-3	0.568	2.41	Sharply increased
Composite Core plug	1.480	2.59	Slightly increased

4.2.4 Two-phase relative permeabilities with the unsteady-state method

For the carbonate core plugs, the relative permeabilities were measured in the laboratory based on the unsteady-state method. The procedures to measure the two-phase relative permeability using the unsteady-state method have been explained in Chapter Three (Section 3.6.2). During displacing of water by oil, some parameters such as, water saturation at outlet part of core, pressure drop, time and oil saturation were measure. Relative permeability for two phases was calculated by measured data in this stage. Figure 4.23 shows the relative permeability for a two-phase system through the tight carbonate rock. As discussed earlier in (Section 3.5.2), the capillary end-point effects were ignored because of the high pressure drop across the core plug. Figure 4.24 shows the relative permeability measured (red dot points) using the composite core plug. The blue curve shows trend of the experimental data and there is no scattering of data in the system before gas injection.

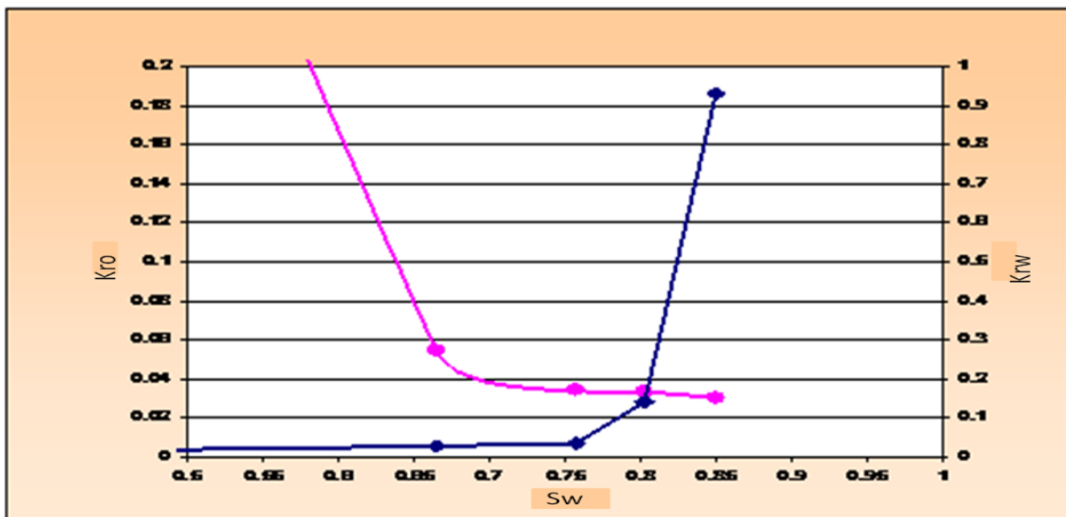


Figure 4. 23 Two-phase relative permeability of core plug 2-3

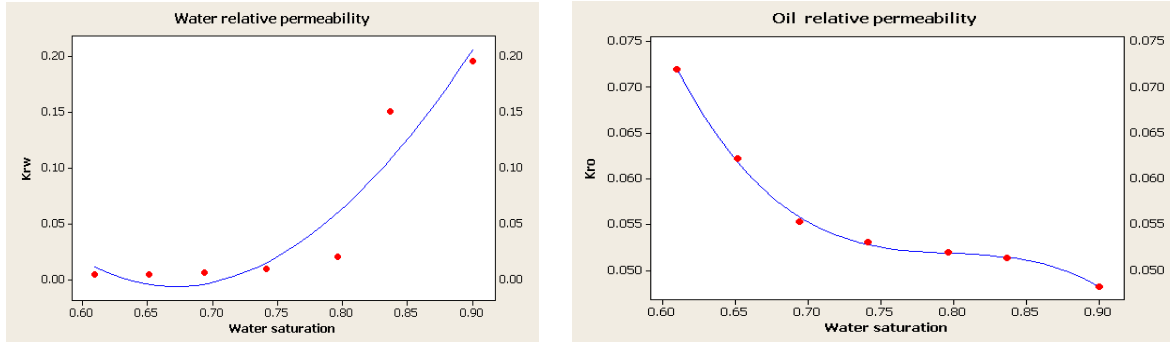


Figure 4.24 Two-phase relative permeability from the composite core plug

4.2.5 Three- phase relative permeability with the unsteady-state method

The procedures to measure the three-phase relative permeability using the unsteady-state method have been explained in Chapter Three (Section 3.6.7). A constant flow rate ($1\text{cm}^3/\text{min}$ for core plug 1-3 and $0.5\text{ cm}^3/\text{min}$ for composite core) was maintained. These rates were chosen to minimize capillary end effect and promoting diffusion domain in the system. The capillary end effect is minimal when the scaling factor ($L\mu V$) is greater than 2, based on scaling criteria proposed by Ropoport and Leas (1953). The Peclet number ($\frac{V.L}{D}$) is representing diffusion and convection domain during displacement phenomena. If Peclet number is greater than 1.0, convection occurs in the system and if less than 1.0 diffusion control the system, in this study, for both rate of injection was less than 1.0. L is the core length (cm), μ is displacing phase viscosity (cp), V is the flow velocity of flow (cm/s), and D is the diffusion coefficient of two phases (cm^2/s). Figures 4.25 to 4.32 show the measured three-phase relative permeabilities using the single core plug 1-3, and the composite core used in the experiments discussed elsewhere in this chapter.

Figure 4.25 show a plot of water, oil and gas relative permeabilities against their saturation. From Figures 4.26, 4.27, and 4.28 can be seen, there was considerable scatter in the data of relative permeability of water against oil and gas saturation. It can be concluded that, relative permeability of water was a function of water saturation alone.

Oil relative permeability against oil saturation showed more scatter compare to the water and gas relative permeability plots. There is some consistent trend between oil saturation and water relative permeability but the gas relative permeability against oil saturation was proximally constant. Therefore it was concluded that the oil relative permeability is a function of oil and water no gas.

All plots of gas relative permeability against water and oil (Figures 4.25, 4.26, 4.27, and 4.28) were shown there is no trend with their saturation and is close to constant, therefore it was concluded in this system with low mass diffusion, the gas relative permeability is function of own saturation only.

Mass transfer affects on relative permeability of three phases, therefore the long time of contact was selected to compare the results with short time of contact. Figures 4.29 to 4.32 show the measured three phase relative permeability in composite core plug. A plot of relative permeability of water, oil, and gas versus their saturation is shown in Figure 4.29. There was some trend between relative permeability of each phase with their saturation and also, there was some consistent trend with other phases. Therefore, it was concluded that the mass transfer during displacement affect on other phases saturation and movements. Figure 4.30, 4.31, and 4.32 were shown these consistencies between data. In all of the Figures (4.24- 4.31), the blue curve shows trend of the experimental data.

In the gas injection phenomena, mass transfer causes to evaporate water and oil into the gas phase and change their saturation during contact time. Also, some of gas molecules condense to the oil phase and change oil saturation in porous media. It was concluded, that in three phase relative permeability depend to all phases saturation. In other hand, water relative permeability depend to own, oil and gas saturation and oil and gas relative permeability depend to own, and other phases saturation.

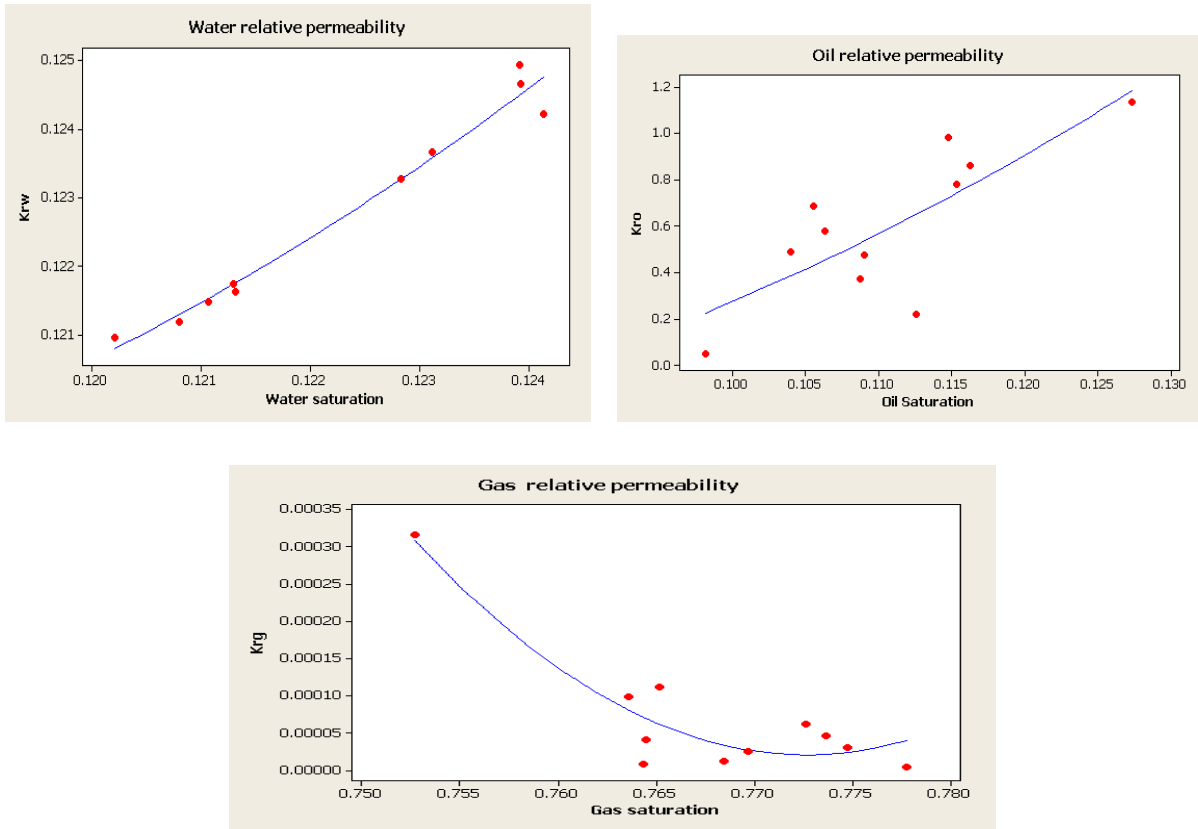


Figure 4.25 Relative permeability of water versus water saturation of core plug 1-3

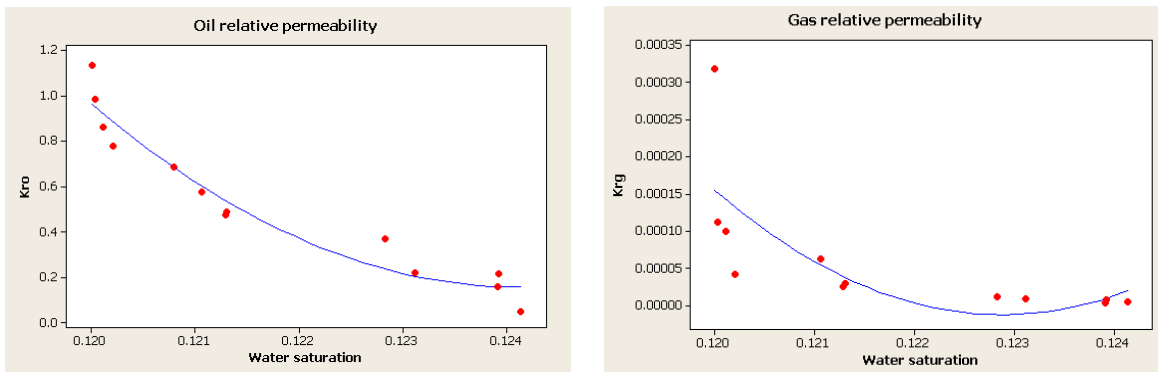


Figure 4.26 Relative permeability of oil versus water saturation of core plug 1-3

RESULTS AND DISCUSSION

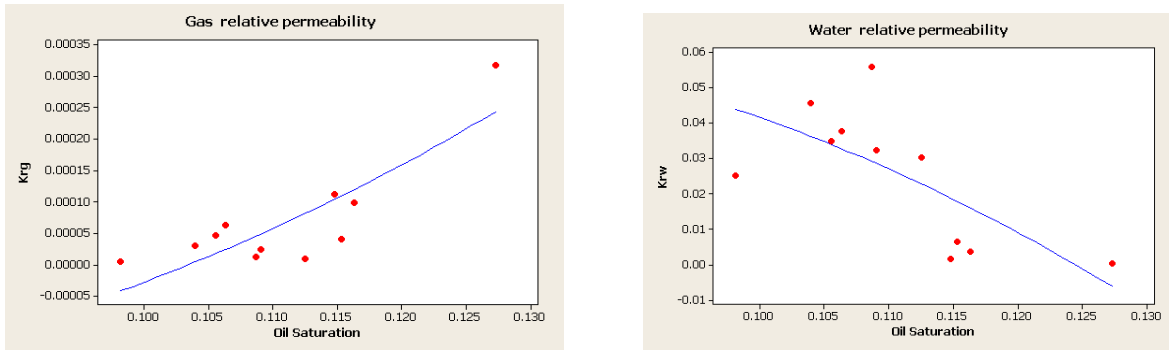


Figure 4.27 Relative permeability of gas versus oil saturation of core plug 1-3

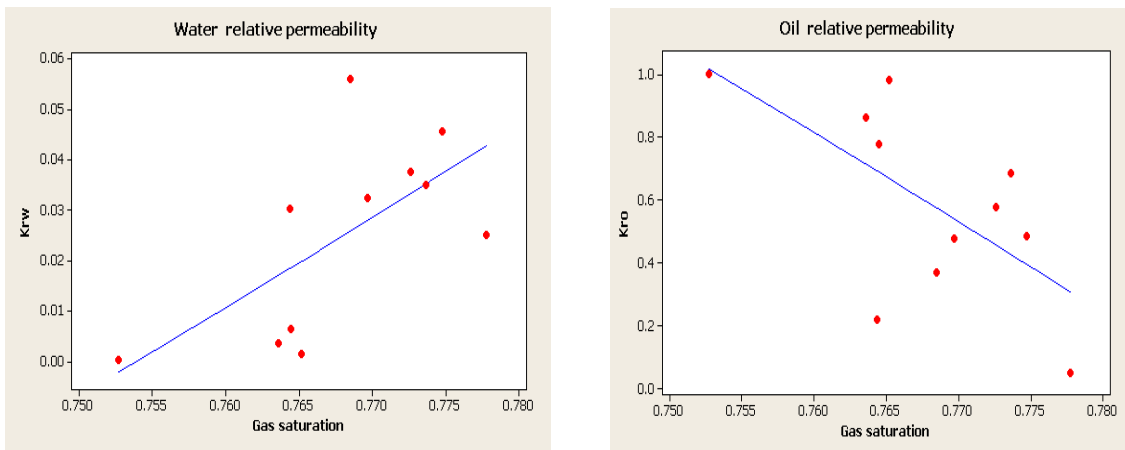
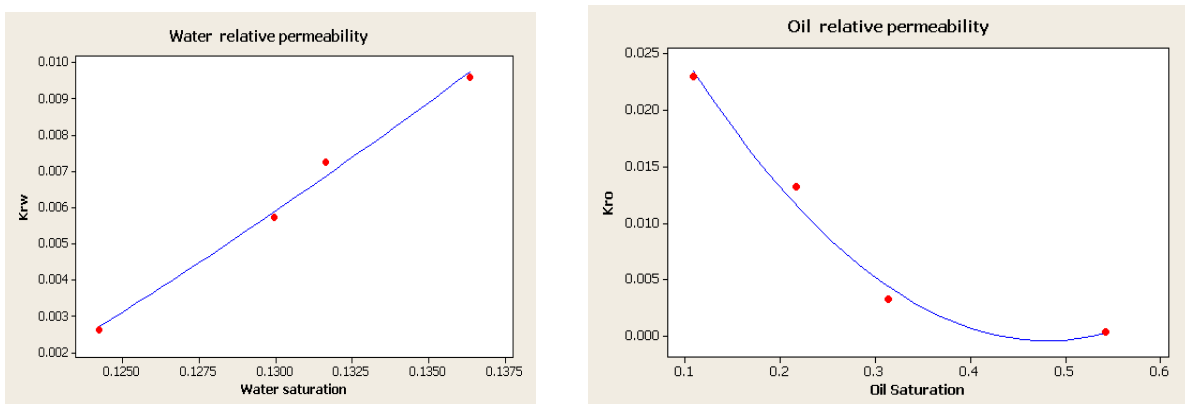


Figure 4.28 Relative permeability of water versus gas saturation of core plug 1-3



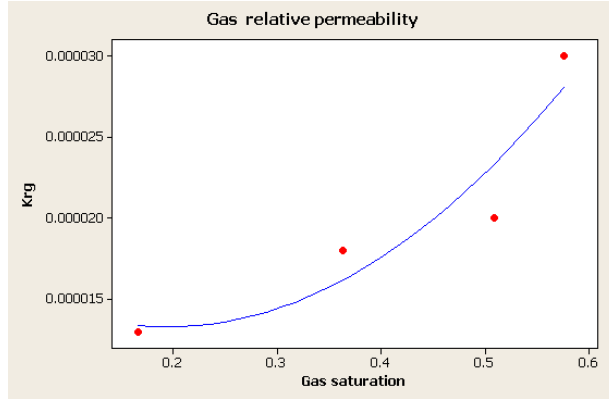


Figure 4.29 Relative permeability of water versus water saturation of composite core-plug

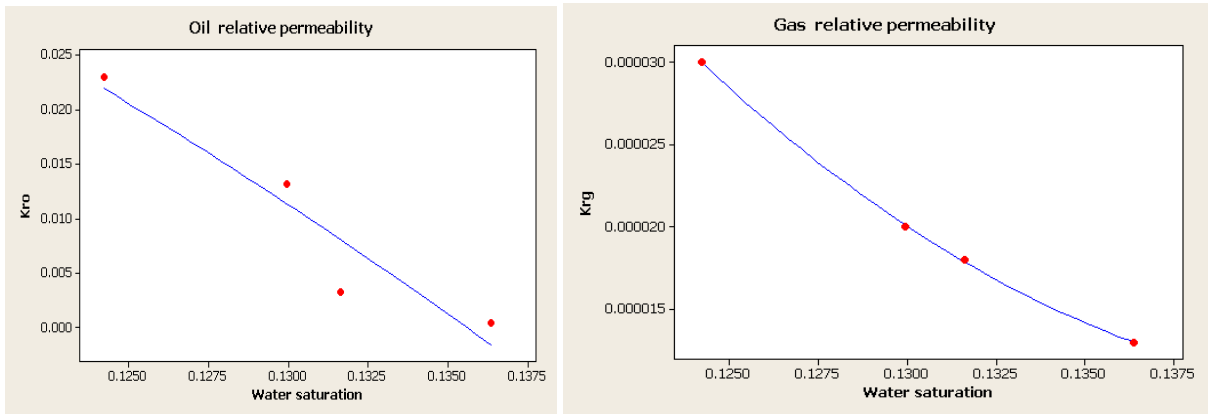


Figure 4.30 Relative permeability of water versus oil saturation of composite core-plug

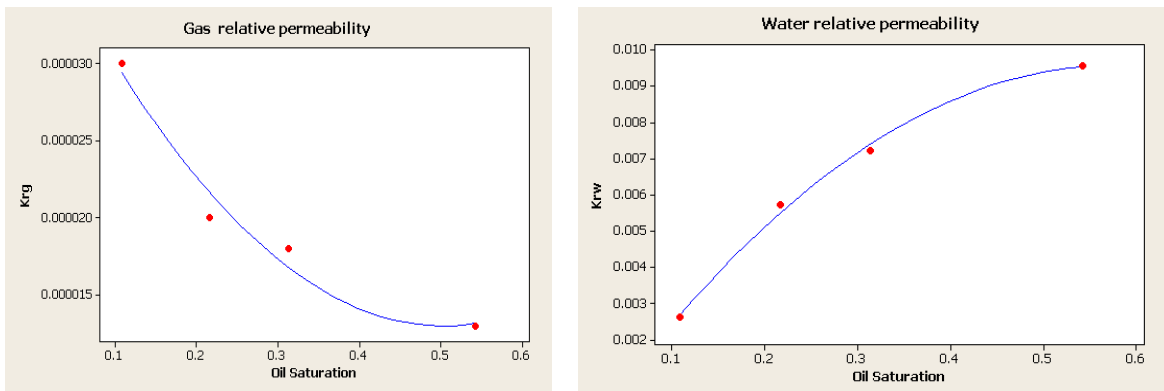


Figure 4.31 Relative permeability of gas versus oil saturation of composite core-plug

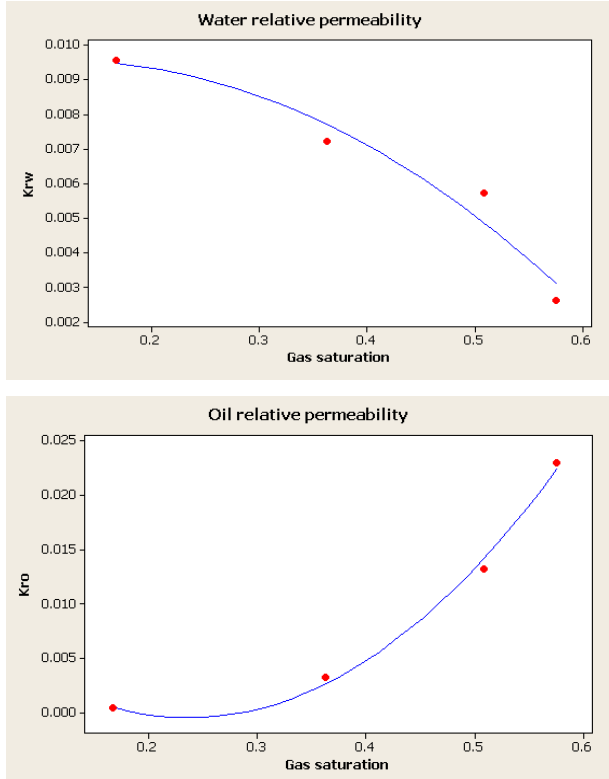


Figure 4.32 Relative permeability of water versus gas saturation of composite core-plug

4.2.6 Simulation of fluid flow through porous media

In this section, the new correlation of diffusion coefficient (Equation 4.7) (see section 4.1.2) was used to simulate fluid flow in porous media for predicting the amount of oil recovery in carbonate rocks. All simulations are carried out on a uniform mesh with a refinement level of maximum. As described in Section 2.2.4, a hyperbolic partial differential equation (Riemann's problem) can be handled by using the finite element method. The saturation formulation of the three phase flow equations can be derived as follow as:

$$\phi \frac{\partial S_i}{\partial t} + V_t \frac{df_i}{dS_i} \frac{\partial S_i}{\partial x} + \frac{\partial}{\partial x} \left(D \frac{\partial S_i}{\partial x} \right) = 0 \quad (4.7)$$

Where D is the diffusion coefficient between phases, V represents the velocity of fluid and ΔL is the core length in the system. In all of the simulation run the experimentally measured diffusion coefficient is used by unsteady state method at reservoir conditions and the new correlation is considered for the displacement equation. Handy (1960) showed that the consideration of a diffusion term reduced the capillary-pressure gradients and also oscillations which appears in front shape.

A black oil model for gas-oil-water system is formulated as described in Sections 2.2.4 and 2.2.5. The problem is an idealized gas–oil, water drive on 2-D horizontal cylindrical domain (Ω) with zero gravitational forces. The flow equation system is described by the mean flow Equation 4.7. Residual fluxes are averaged second – order statistical fluctuation terms, that contribute to the rate of change of the mean flow equation. The capillary end effect and gravitational are taken to be negligible (see Section 3.5.3). In the core flooding system, 1-D flow, therefore, the velocity (V) is considered constant and Equation 4.7 yields the well-known Riemann Problem (see Section 2.2.4) with diffusion term in three phase flow system such as:

$$\phi \frac{\partial S_i}{\partial t} + V_i \frac{df_i}{dS_i} \frac{\partial S_i}{\partial x} + \frac{\partial}{\partial x} (D \frac{\partial S_i}{\partial x}) = 0$$

$$\text{div}(V) = 0$$

Initial condition

$$S=0 \text{ on } \Omega,$$

$$P=3000 \text{ Psi}$$

Boundary conditions:

The boundary of Γ_1 is impermeable (sleeve of core holder). That is, the outward normal component of the flow velocity, $V \cdot n$, vanishes over Γ_1 which translates to the pressure

$$\text{BC}, \frac{\partial P}{\partial n} = 0, \text{ where } n \text{ is the outward normal vector to fractional flux.}$$

$$\text{On } \Gamma_1 : V.n = \frac{\partial P}{\partial n} = 0$$

On Γ_2 : $P=3000$ Psi, and $S_r=1$ for $t>0$

On Γ_1 : $P=2700$ for $t>0$

The model is constructed by using the specifications and data collection from the core flooding apparatus (Sections 3.3.5 and 3.5.1). The core is a composite core which is explained in section 4.2.2. The intrinsic permeabilities of three carbonate cores are 4.87, 4.61 and 3.41 mD respectively and the harmonic average (4.1818 mD) was used for simulation. The cross section of the core was 11.3 cm^3 , and the average porosity was 0.2033. The viscosity of oil, water and gas were 8.439, 0.76, and 0.01826 cp respectively and 2 percent residual water saturation was used. The rate of injection was 15 cc/hr for high diffusion rate and 60 cc/hr for low diffusion rate is considered.

Figure 4.36 shows the typical finite elemental grids of the domain under study. Only half the core holder was shown in the grid because the problem was axisymmetric. The optimization of grid was done automatically by the software. The density of grid nodes is high all along the current location of the moving oil saturation front and also near the injection port, where the saturation gradient is the steepest.

The optimization of elements can be observed especially near the center, toward the inlet where steep pressure gradients were observed. The cylinder was cut along the centerline which extends from (0,0) to (L,0). In the figures, this is the bottom line where symmetry condition was applied.

Figures 4.37 and 4.38 show relative permeability of oil and gas and saturation of gas versus time. In the constant residual water (0.2), the oil saturation is decreased during gas displacement and gas saturation is increased. Viscosity of oil is greater than gas phase, therefore the average permeability of gas reduced by the presence of highly viscous oil. Since, in this scenario and according to Equation 2.60, the gas relative permeability changes too rapidly as S_g increase from zero.

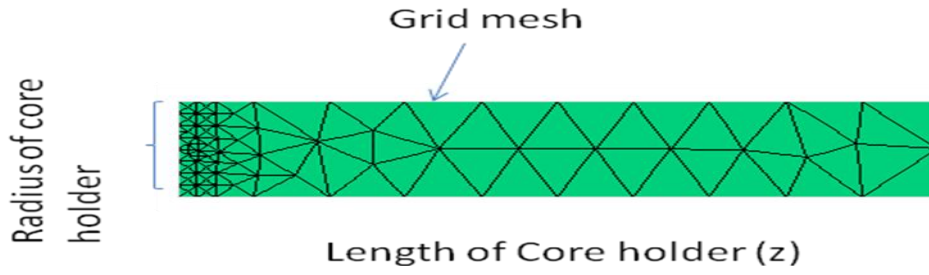


Figure 4.36 2D horizontal core flooding system mesh model

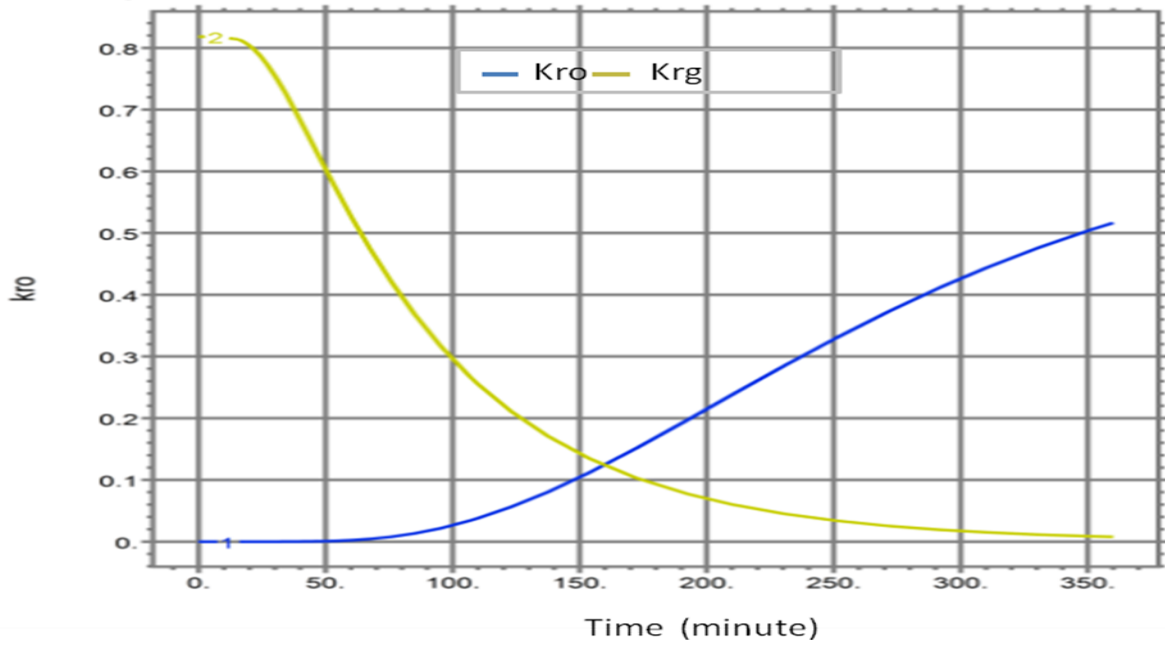


Figure 4.37 Relative permeability of gas and oil in two phase flow versus time

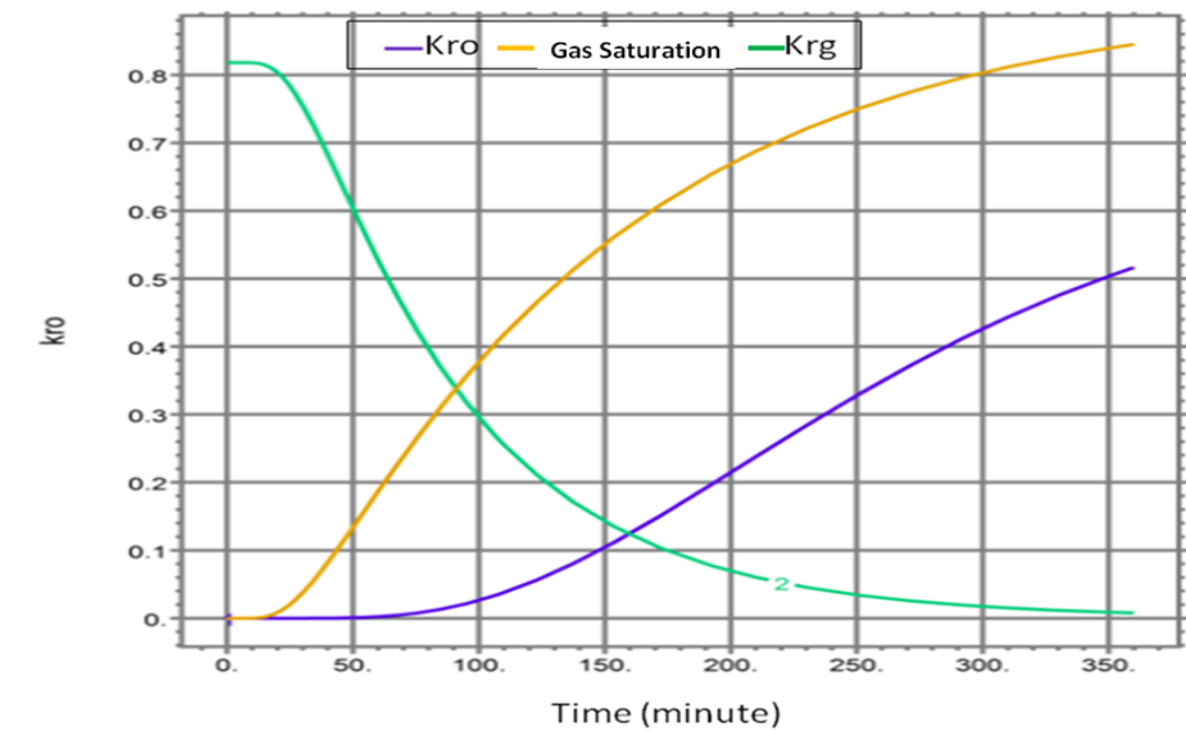


Figure 4.38 Relative permeability of gas and oil in two phase flow and gas saturation variation versus time

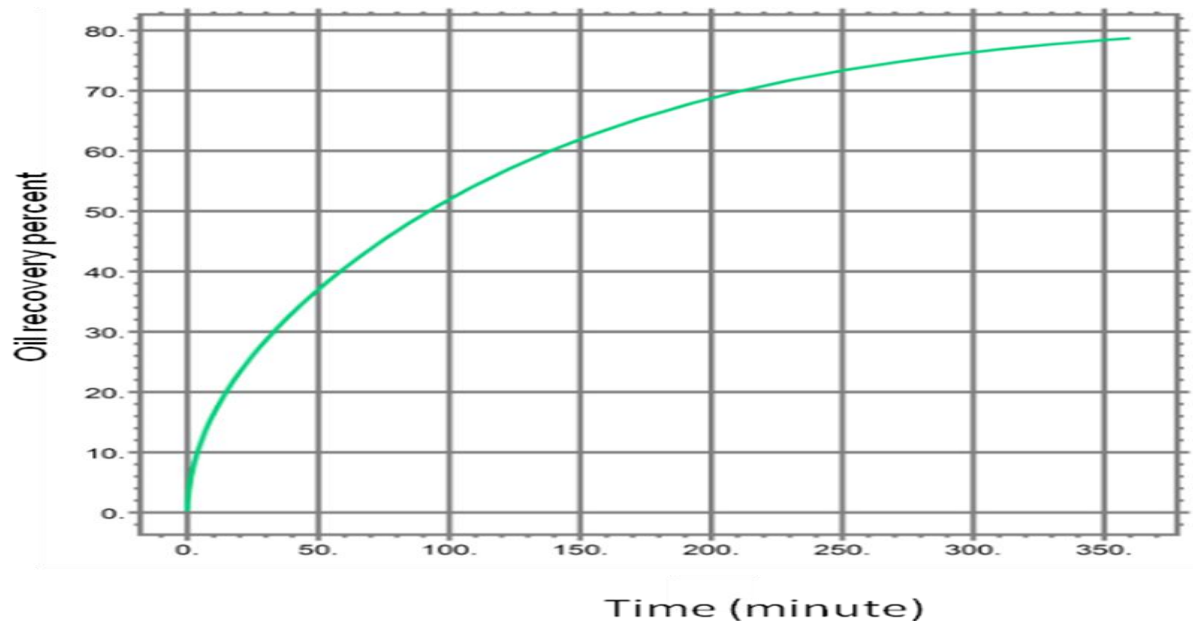


Figure 4.39 Estimated recovery percent versus time by model

Figures 4.40 and 4.41 show the variation of saturation during displacement phenomena with mass transfer phenomena which was generated by model. Effect of diffusion was considered during displacement by gas. In all of scenarios, saturation of gas is changing by time and the transition zone which is created by diffusion prevents front shock wave.

For great success, the fluid front must remain stable and oil is swept along the most advantageous path way via optimal injection rate. In carbonate and fracture reservoirs, optimal rate can be obtained by considering Peclet number which is depending on the diffusion coefficient. Mass transfer causes the front phase (transition zone) to be extended and helps to keep stable front. If the front phase becomes unstable, the injected fluids can breakthrough and leave too much oil behind and possible make a large area of reservoir unavailable for future recovery efforts. Figure 4.41 shows that the displacement phenomena in this case were completely piston displacement and mass diffusion in front phase was kept stable.

Figure 4.42 and 4.43 show variation of relative permeability with mass transfer and without mass transfer phenomena. Diffusion of light component into oil phase changes viscosity, density and IFT of the system and causes increase oil recovery of the system. Cinar et al (2004) showed at determined saturation value of gas, relative permeability as a function of IFT and increases with high saturation of gas.

RESULTS AND DISCUSSION

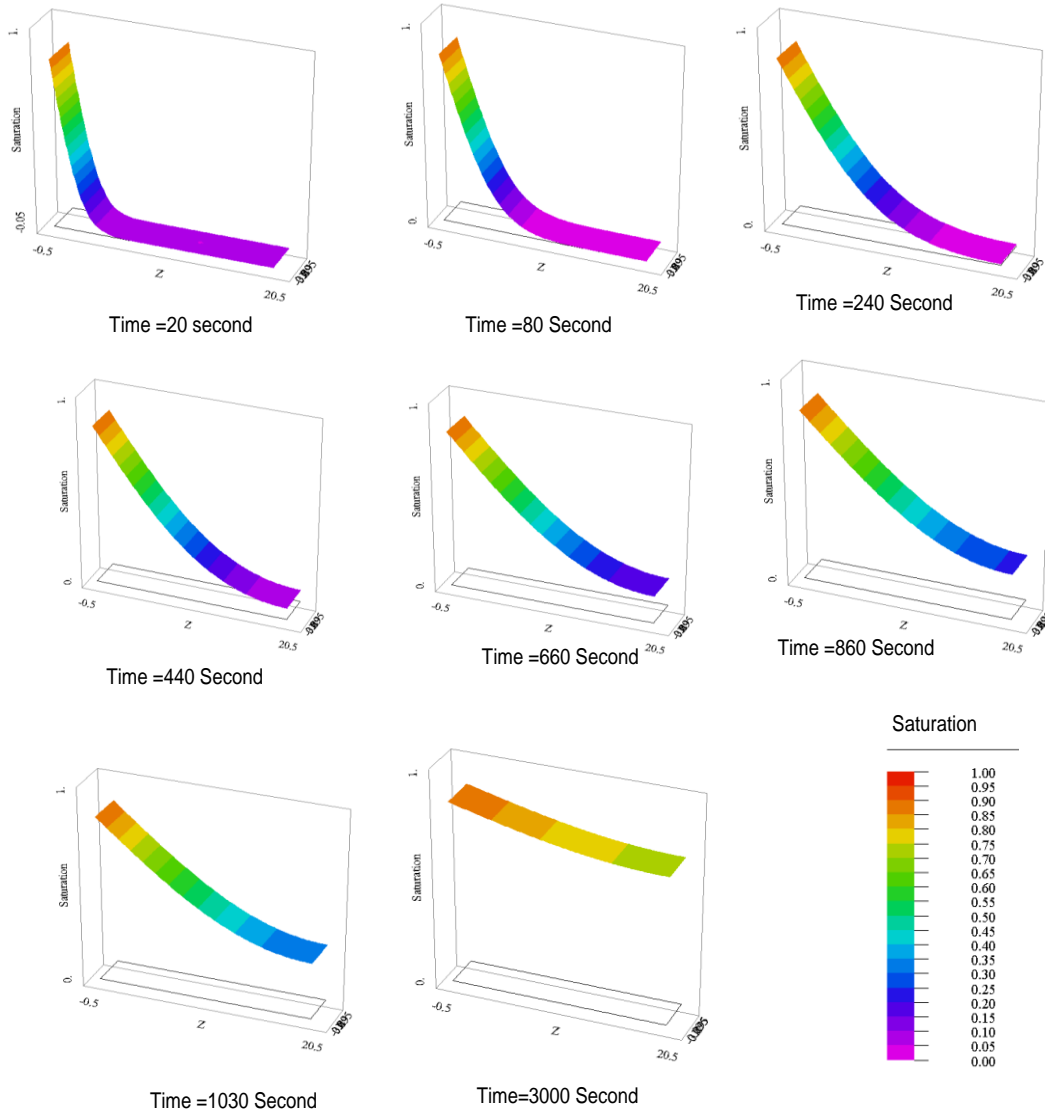


Figure 4.40 Variation of gas saturation during displacement of crude oil by gas

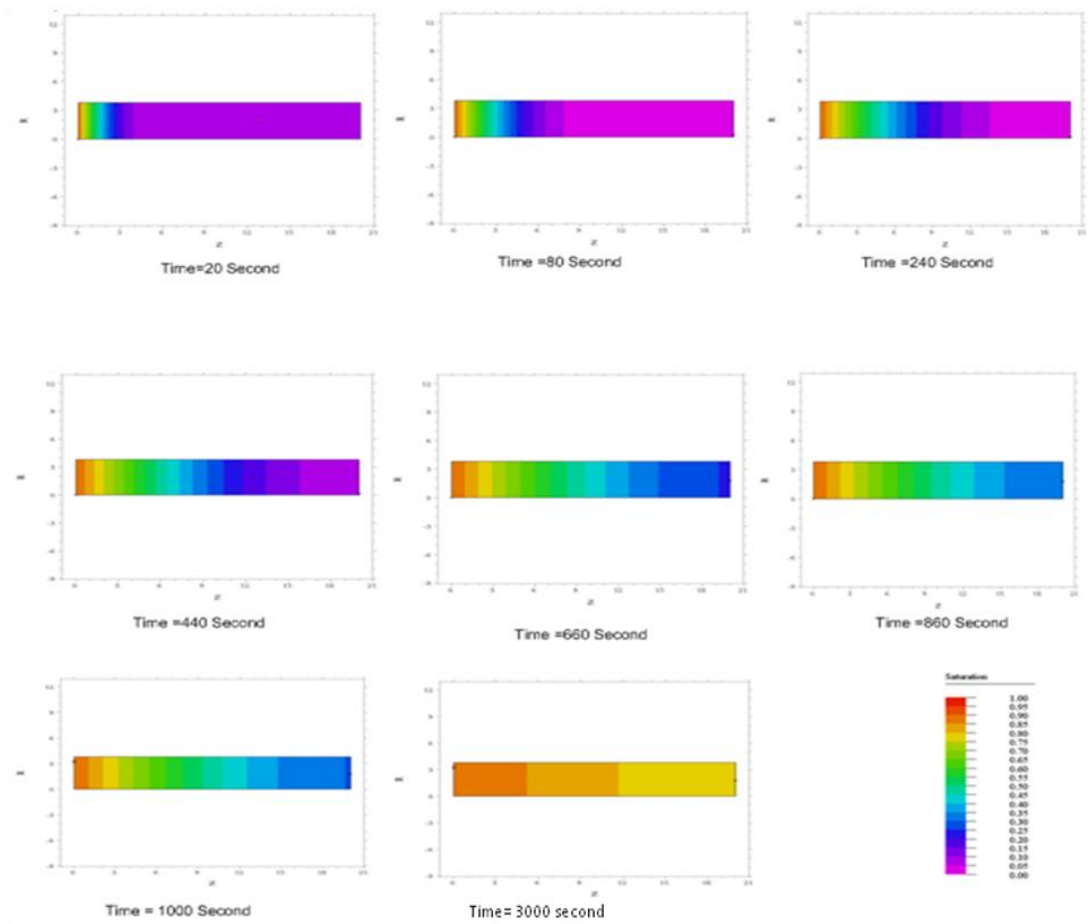


Figure 4.41 Variation of gas saturation during displacement of crude oil by gas

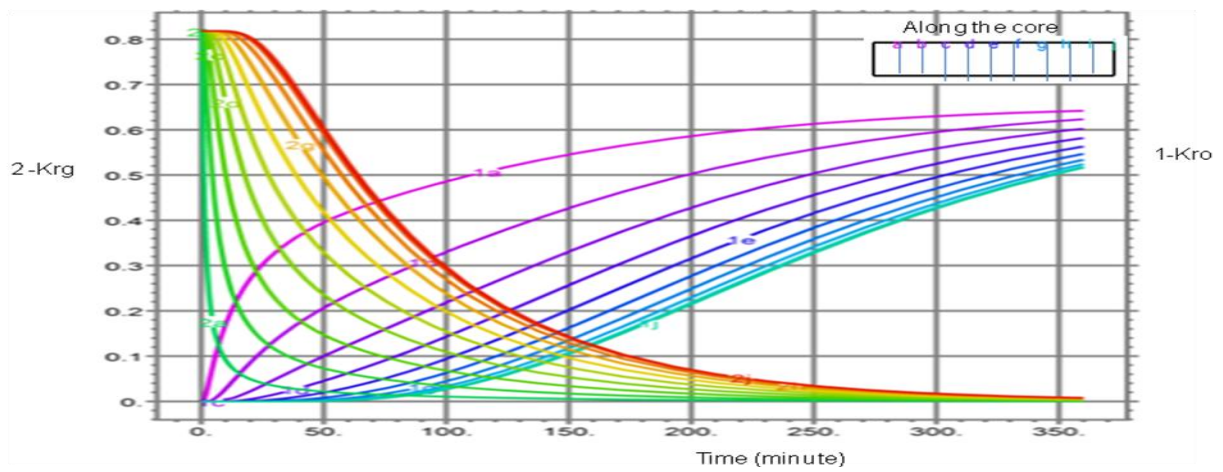


Figure 4.42 Relative permeability of gas displacement system with mass transfer

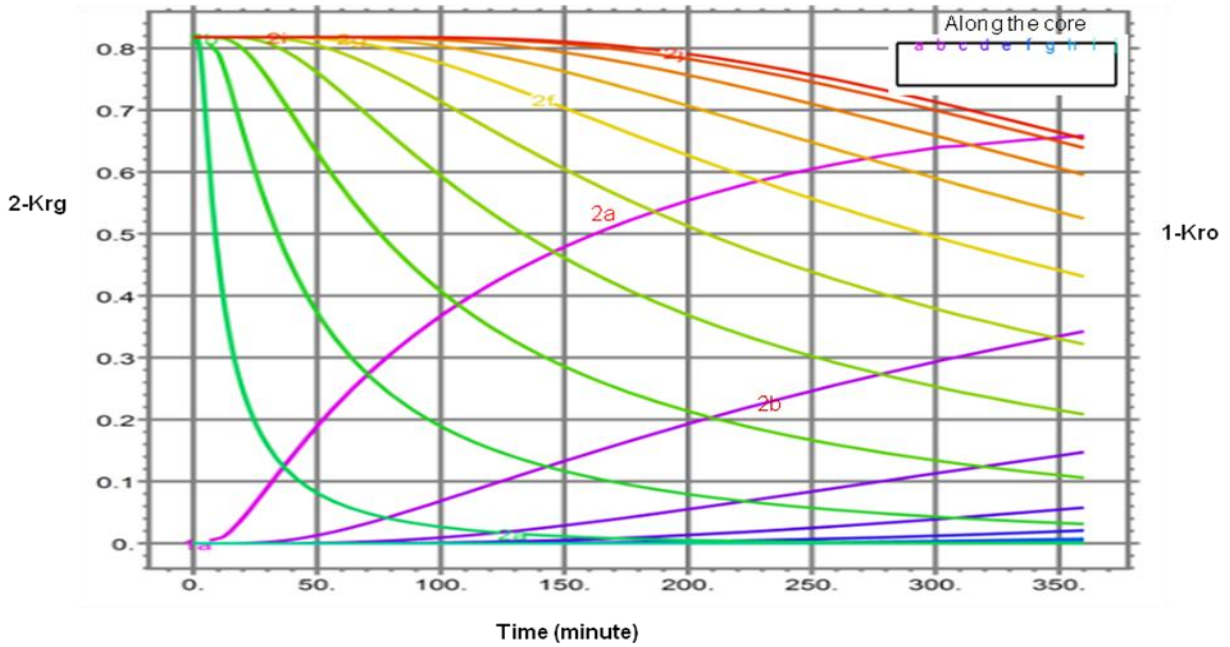


Figure 4.43 Relative permeability of gas displacement system without mass transfer

Figure 4.44 shows the recoveries of the composite core and simulated model with and without mass diffusion process. The new diffusion correlation has been applied for simulation and without considering diffusion coefficient, the Riemann's equation with specified initial and boundary condition not be able to converged. Therefore in this case for comparing effect of mass transfer on recovery in the system, considering real diffusion coefficient and low diffusion coefficient have been applied. Comparing recovery with high diffusion coefficient and low diffusion in Figure 4.44, it can be seen that our experimental data is close to the high diffusion value. It is clear that the high diffusion coefficient is increased the recovery of oil and the simulation results is covering the late behaviour of the system because the outlet of the core holder was measuring point in all core flooding system. Monitoring the system by CT-Scan could help to get more data along the core plugs. In short time or low diffusion coefficient, the experimental data with simulation results is completely matched, because there was no more phenomena happened during displacement.

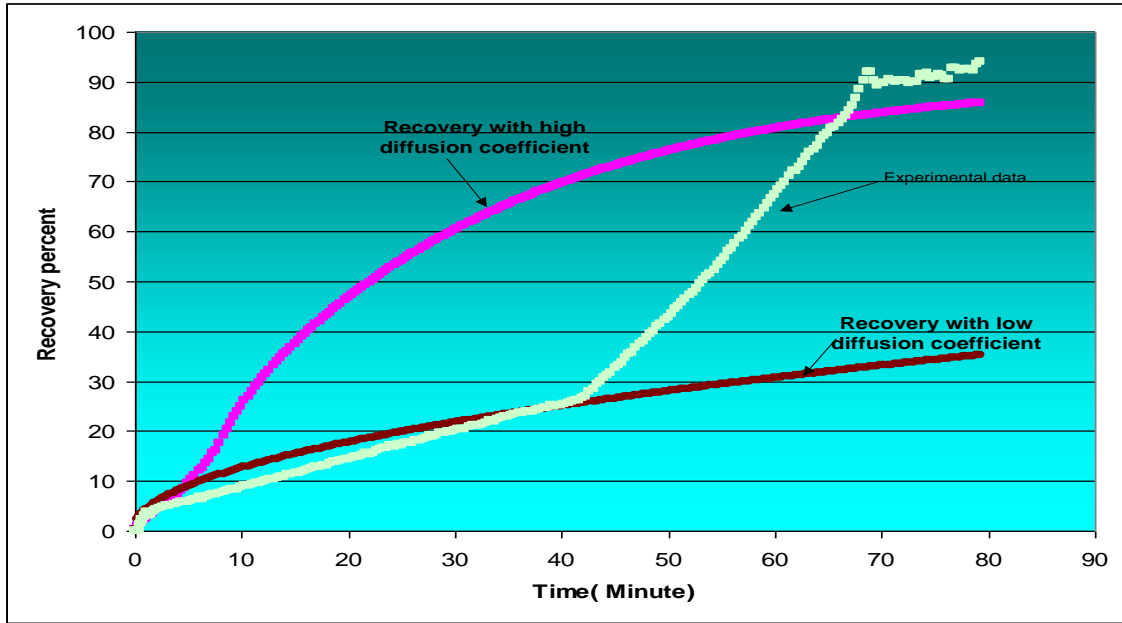


Figure 4.44 Recovery percent with low and high diffusion coefficient in comparison to experimental data

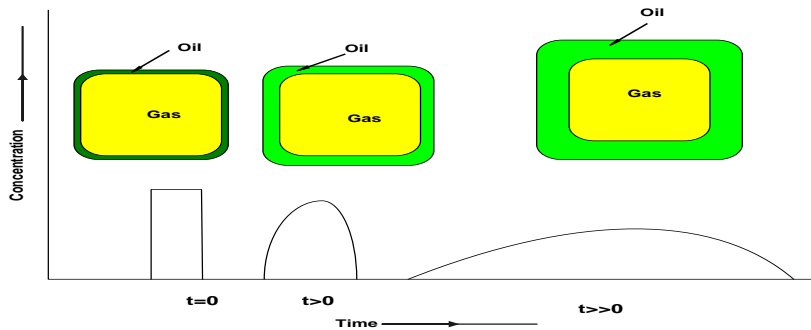


Figure 4.45 Effect of gas diffusion on swelling of crude oil

4.2.7 Discussion

4.2.7.1 Incubation time effect on the oil recovery

Laboratory transient state displacement processes are affected by mass transfer phenomena during the time of contact, which is referred to as the unsteady state diffusion. During displacement of liquid by gas, the end effect is minimized by using tight carbonate core plugs and gravitational effect can be ignored by installation of core holder at horizontal position (see more explanation in Section 3.5.4). Figures 4.16, 4.17, and 4.18 show the three phase fluid

recovery, inlet and outlet pressure, and oil recovery measured during three phase production. The pressure fluctuations seen on all the graphs indicate instability in the system. The pressure of the system was reduced after gas breakthrough in all the tests (Figures 4.13a, b, c and 4.17). During this fluctuation period, the sharply pressure drop indicated the low diffusion between phases and slightly pressure drop shows that diffusion is affected on swelling and condensation process. Therefore, it can be stated that a long incubation period contributes to the more diffusion in the system. And also, the measured dissolved gas volume was indicated which in long contact time was higher than short contact time.

4.2.7.2 Effect of viscosity ratio on relative permeability

In this research, the ratio of crude oil viscosity, water, and gas were such high ratio (see Section 4.2.6). It is affecting on relative permeability of each phases (Odeh 1959). Hypothetically, water and oil occupy the whole internal of pore volume and the gas is displacing the liquid phase. Since the carbonate rocks are wet with liquid, both of the water and oil are attached on the surface of the rock and gas phase is non wet and passing and diffusing into the liquid phase. During gas displacement, all the pores space contain high viscosity liquid, the overall pressure gradient must increase to maintain the constant flow rate (Section 4.2.1), since the high viscosity liquid are harder to move more than gas phase. The flow rate of each phase is calculating by using the Equation 2.60 (see Section 2.5.4).

When the porous media contain high viscosity liquid during oil displacement phenomena; at the beginning, inlet and outlet pressure remain parallel, this part corresponds to a constant low pressure drop along the core. As soon as the injection of gas phase is started, the overall pressure gradient must increase to maintain the constant fluid flux since the high viscosity liquid is harder to move than the gas phase. As the pressure is fixed at the outlet, it means the inlet pressure increase. This trend continues until gas breakthrough at the outlet part of core (see Section 4.2.1). As shown in Figures 4.13 a, b, c, and 4.17, at a length scale equivalent to the core apparatus, the average relative permeability of gas is dramatically reduced by the presence of highly viscous liquid (Figure 4.37) Since, in this scenario and according to Equation 2.58 the gas relative permeability changes too rapidly as S_o and S_w decrease to zero. Since the relative permeability of oil is dramatically affected by the diffusion of gas phase and

viscosity ratio is decreasing then relative permeability of gas slightly decrease (Figure 4.42 and 4.43).

Figure 4.45 shows the mechanisms of swelling of oil in oil wet and mixed wet oil reservoirs and also table 4.3 Show the amount of dissolved gas volume into oil phase. The concentration of the gas phase into the oil phase increased with time which caused the mobility of oil on the solid surface to change Figure 4. 5 and 4.7 (see section 4.1.3).

4.2.7.3 Variation of produced Gas Oil Ratio (GOR) with time of contact

As discussed earlier (Section 2.3), the incubation time for diffusion depends on the concentration of the gas phase into the oil phase, pressure, temperature and heterogeneity of porous media Long core plugs provide a significant amount of gas diffusivity into the oil phase and a reduction in interfacial tension due to a higher residence time (see Table 4.4). Hence, the long incubation period is beneficial from a recovery point of view.

Figure 4.14 (a) shows that a short incubation time has little effect on the diffusivity of gas into the oil. In this test, the rate of injection was carried out twice (30cc/hr and 60cc/hr) compared to just once (30cc/hr) for the other experiments; this caused a decrease in the contact time of the phases. In Figure 4.14 (b) (core plug 2-3), the injection rate used was the same as that used for the composite core plug but the experiment was performed on a single core plug and hence resulted in the incubation time being much shorter

Figure 4.21 shows the diffusivity of the gas phase into the oil phase during the displacement experiment. In this test, the incubation period was increased (due to the test being performed on a composite core plug) and it was also increased when the rate of injection decreased. As a consequence, the time of contact of each phase was increased resulting in the mass flux of gas into the oil.

Table- 4.4 Recovery of oil during gas injection

Core plug	Pore volume	Rate of injection	Percent of EOR
1-3	10.632	60 cc/hr	59
2-2	10.316	30 cc/h	79
2-3	11.12	60 cc/hr	62
Composite	32.068	30 cc/hr	85

The development of transition zone by gas diffusion into oil phase creates zone of low interfacial tension (IFT) between gas and oil phase in the presence of water. Bardon and Longeron observed that the oil relative permeability increase linearly as IFT was reduced from 12.5 mN/m to 0.04 mN/m and for IFT below 0.04 the oil relative permeability curves began to shift more rapidly with further reduction in IFT. Table 4.4 shows the amount of gas diffused into the oil phase, light components change the physical properties of oil during dissolving process, therefore IFT of new phase with injected gas is reduced and relative permeability curve shifted up (Figure 4.43 and 4.44).

4.3 Effect of mass transfer on fluid flow in a fractured medium

4.3.1 Effect of overburden pressure on fractured media

Success in oil phase mass removal from matrix is very sensitive to the effective fracture spacing (Esposito et al. 1999), and simulating a fractured model needs more technical data about dual permeability, dual porosity, diffusion, and fluid flow through porous media at real condition of the reservoirs. There were a gap of data and empirical correlation about the effect of overburden pressure on fracture permeability. Pore pressure is decreased during the

production of the oil from reservoir at constant overburden pressure. The permeability of the fracture media changes due to difference between overburden and pore pressure.

A core plug with 75 degree decline with 0.1 cm fracture artificially from synthetic core plug (high permeable plug) is provided (Figure 4.46). The reduction in permeability with different overburden pressure is measured. Table 4.5 and Figure 4.47 show the results of the measured permeability and a range of overburden pressures.

The reduction of the permeability clearly has a significant effect on the reservoir productivity. Reduction of fluid flow through the fracture is caused by the reduction in the fracture permeability. Reduction of fracture permeability due to pore pressure may be compensated by the increase of permeability due to reduction of liquid film.

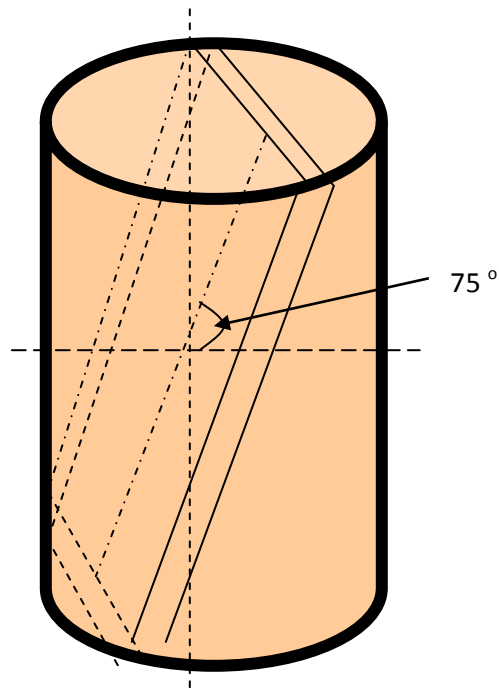


Figure 4.46 Schematic of prepared artificial fractured

Table 4.5- Porosity and permeability of fracture porous media

Overburden Pressure(psi)	Pore volume (cm ³)	Porosity (%)	Permeability Absolute(mD)	Kelinkenberg effect(mD)
524.61	13.901	20.6	7376	7347
1013.75	13.579	20.4	5394	5298
2002.74	13.579	20.1	4262	4242
3002.64	13.487	20.0	3701	3681
4008.80	13.424	19.9	3343	3325

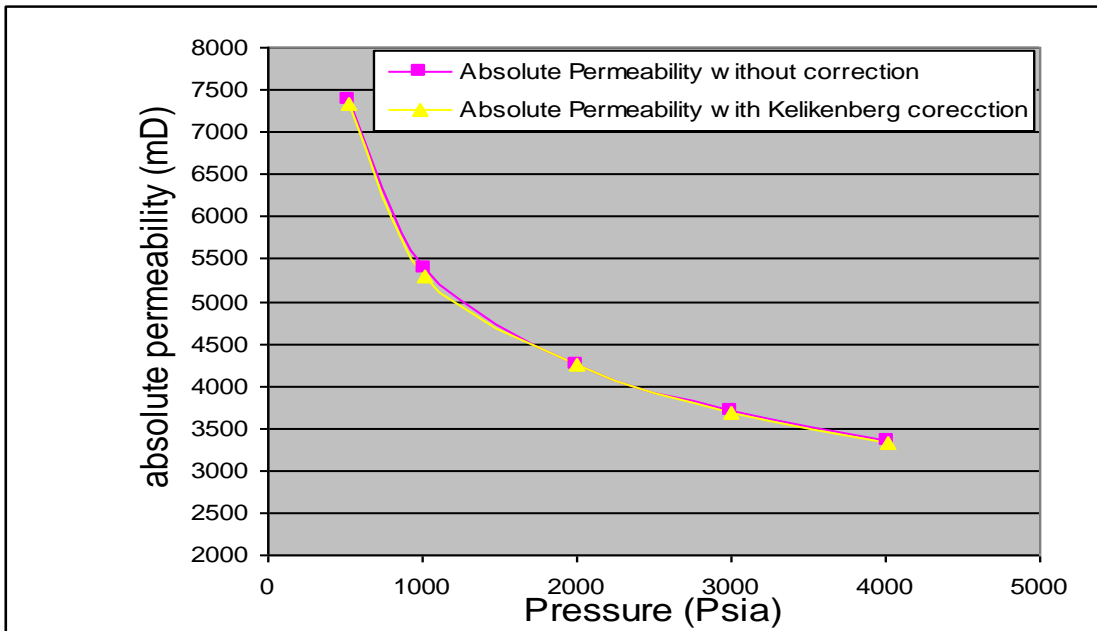


Figure 4.47 Effect of overburden of fracture permeability

4.3.2 Simulation of fluid flow in fractured media

A major objective in this model was to determine the effect of diffusion coefficient which was offered by this study (Equation 4.5) on oil recovery by using finite element method. A core flooding system with fractured media with diffusion coefficient was considered. The experimental data about compressibility effect on permeability in fractured media (Table 4.5) were applied to yield credible results for real simulations with FlexPDE software.

The diffusion phenomena in fractured carbonate rock vary by many orders of magnitude. The problem considered in this case is identical to case of carbonate rocks, except that fractured media is here taken with 25 degree from the core axis (Figure 4.46). A single fracture with mass transfer between the gas in the fracture and the oil in the matrix was investigated. Fractures in tight carbonate rocks are necessary for the flow of fluids from the matrix, yet their numerical quantification is difficult. The two-phase flow equations with mass transfer and the corresponding relationships are already highly non-linear. When fracture and matrix domains, (Section 2.5.7) with contrasting physical properties such as relative permeability, rate of diffusion, boundary conditions of each domain, it made the numerical solution even more challenging. In Figure 4.48, the set up of a simple model of fracture and matrix is shown.

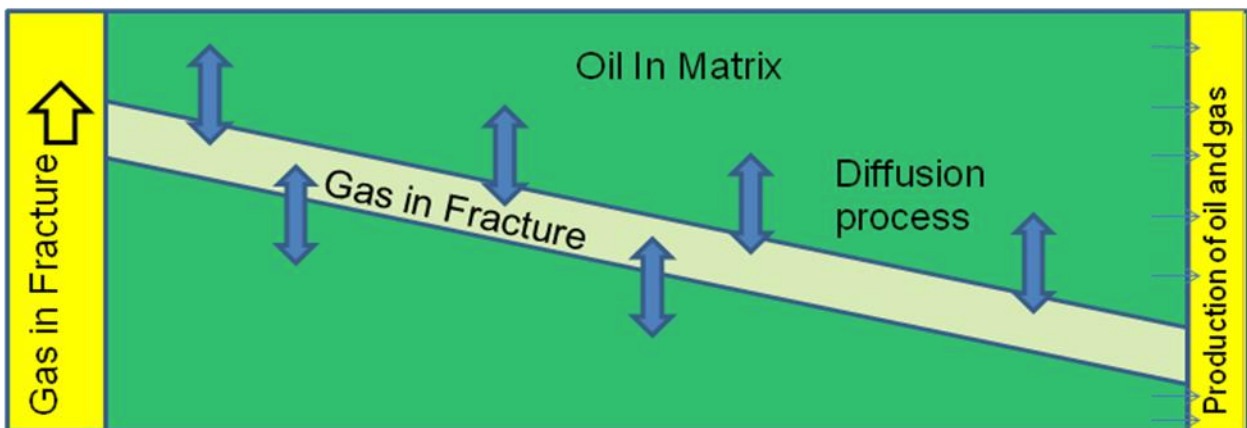


Figure 4.48 Schematic of fluid flow in a fracture and matrix

Figure 4.49 indicates how the unstructured numerical solution grid adapts dynamically to anticipate, and follow the moving saturation fronts simultaneously with pressure gradients near the outlet of core plug. The numerical grid undergoes both refinement near large gradients and un-refinement in part of the domain that do not contain large gradients. The rock and fluid properties were selected the same as Section 4.2.6.

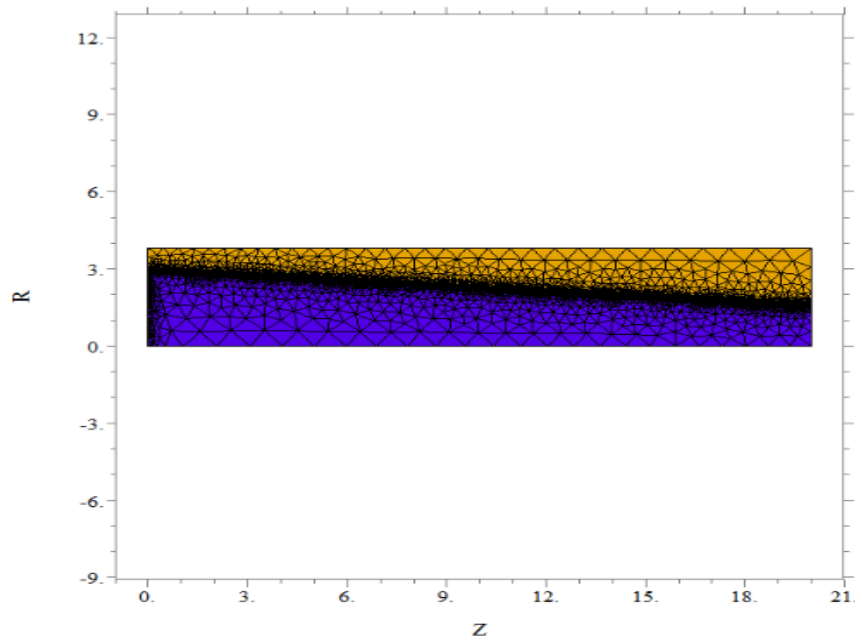
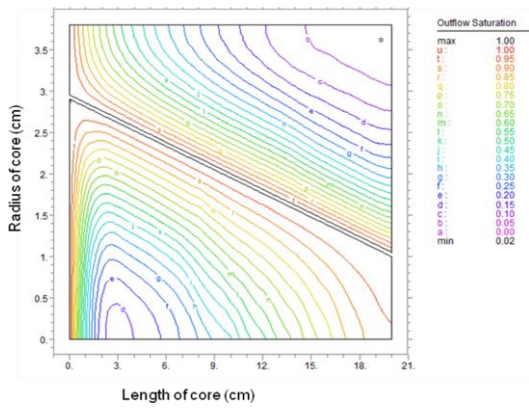


Figure 4.49 Dynamically generated grid after 60 minutes

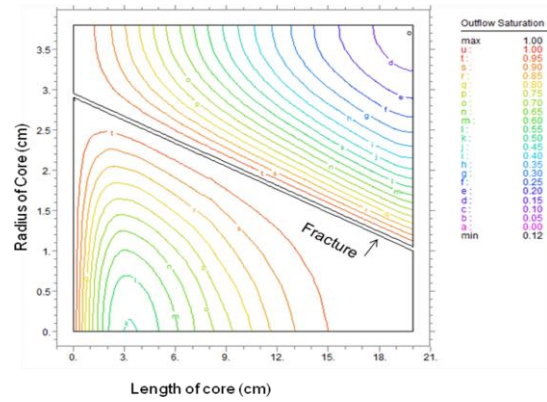
The simulation was carried out over a time period of 4000 seconds with parameters as presented in Table 4.1 and also using a partial differential equation (Riemann's problem) (see Section 2.2.4). The finite element method was applied to solve the PDE equation with the domain boundary condition method of each phase. FlexPDE software from the PDEsolution Company was selected for this purpose.

The results shown in Figures 4.50 (a,b,c,d) indicate that the mass diffusion in matrix at lower part of fractured media which has more contact area with injected gas phase was higher, therefore gas saturation has penetrated more in comparing with matrix at upper part. Retardation effect which oil resides for some significant of time in the matrix was shown in upper part of the Figure 4.50d.

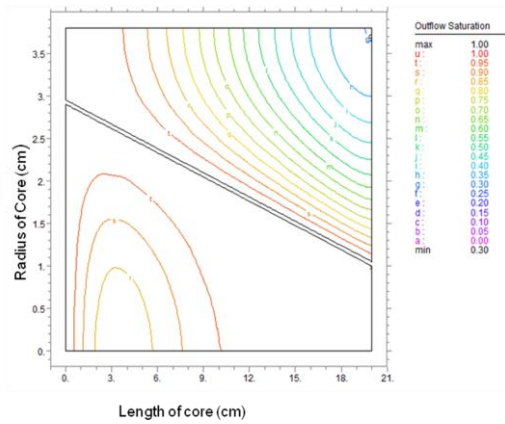
A time=10 minute



(B) time=20 minute



(C) time=40 minute



(D) time=60 minute

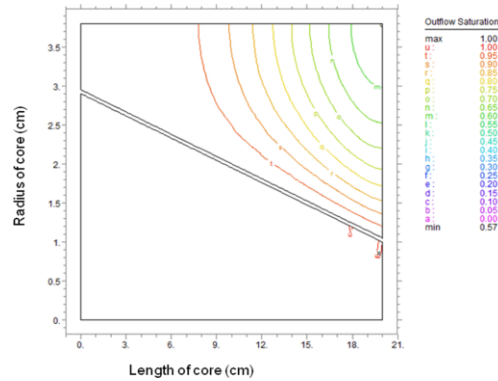


Figure 4.50 Contour map of gas saturation during displacement of crude oil by gas in a fractured medium

Figures 4.51 (a, b, c, d) show snapshot of the saturation distribution after 10, 20, 40, and 60 minutes. Gas diffusion in lower part of fracture was increased significantly and after 60 minute the gas saturation is equal to 85 percent at dead region of core plug (Figure 4.51 d). Two dimensional of gas saturation is shown in Figure 4.52 (a, b, c, d). The saturation of gas in fracture media is constant (red colour in the top) and it is vary in matrix with time. Gas saturation in fracture (middle part) is higher than matrix and the equilibrium condition of fracture and matrix is reached after 3000 second of contact time for lower part. In Figure

4.52d shows the left side of the fracture which had more contact area is swept very well at the same time with right side.

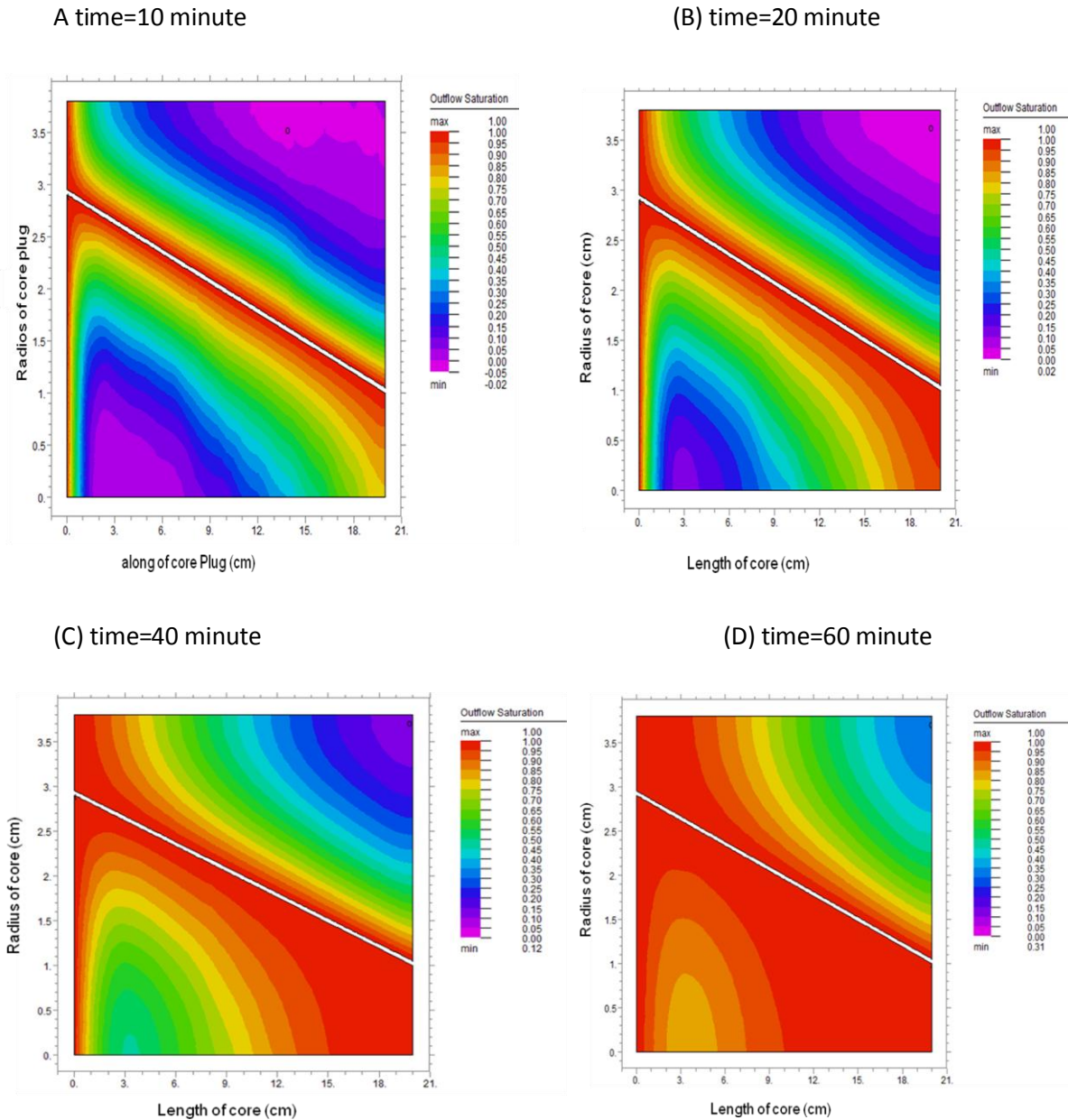
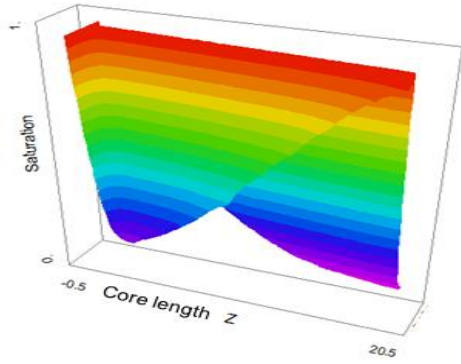
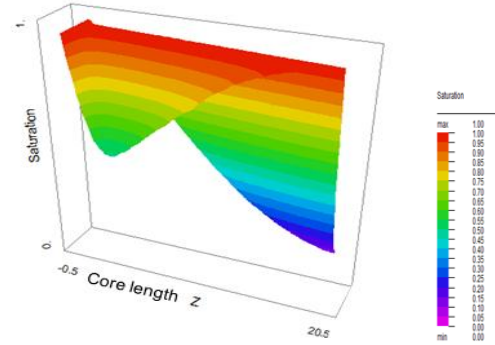


Figure 4.51 Variation of gas saturation during displacement of crude oil by gas in fractured medium after 3600 second

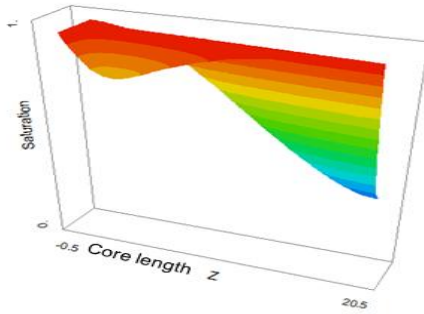
A time=10 minute



(B) time=20 minute



(C) time=40 minute



(D) time=60 minute

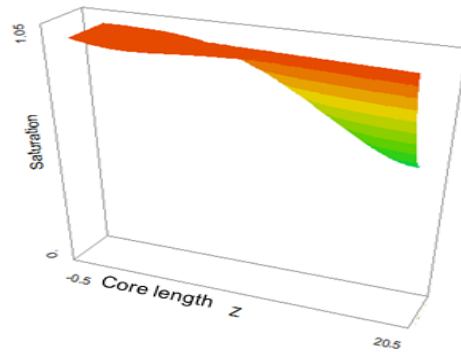


Figure 4.52 Variation of gas saturation during displacement of crude oil by gas in fractured medium after 3600 seconds

Figure 4.53 shows the saturation variation along the core plug which is clear at the inlet part of the core gas saturation is higher than end part. Time of contact between gas and oil was more than end part and diffusion played the main role for displacing oil from matrix.

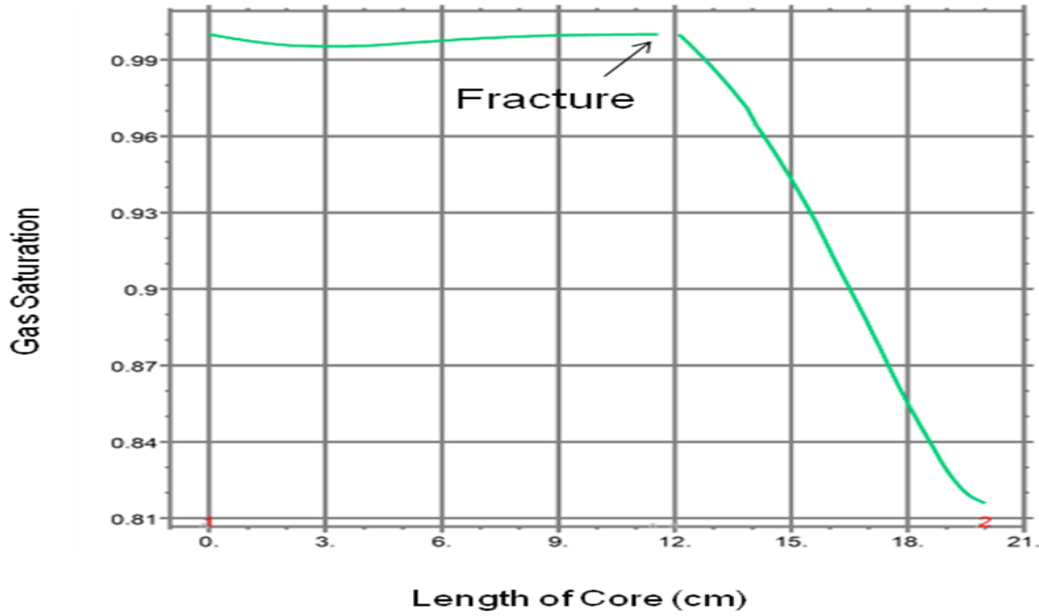


Figure 4.53 Variation of gas saturation along the core holder in fractured medium after 3000 seconds

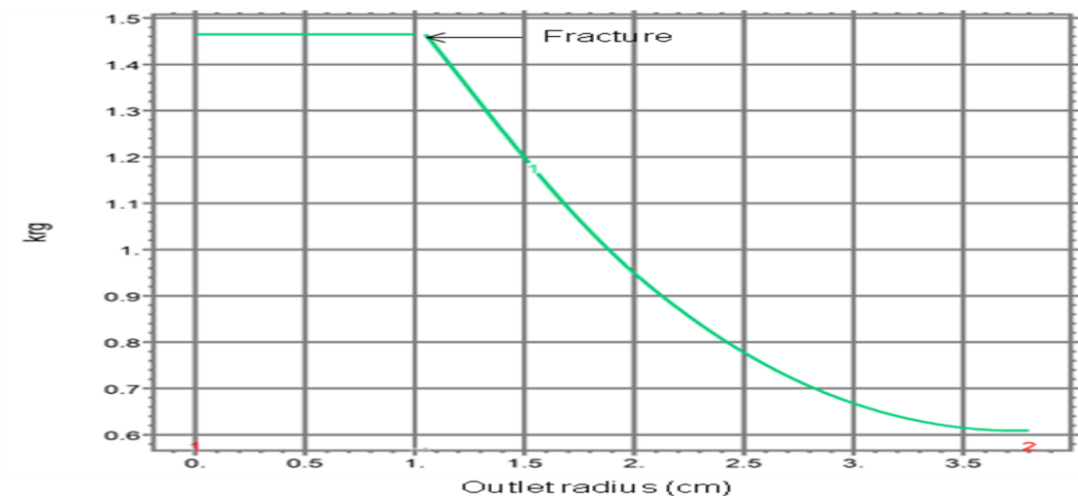


Figure 4.54 Variation of gas relative permeability at outlet of core holder after 3000 seconds

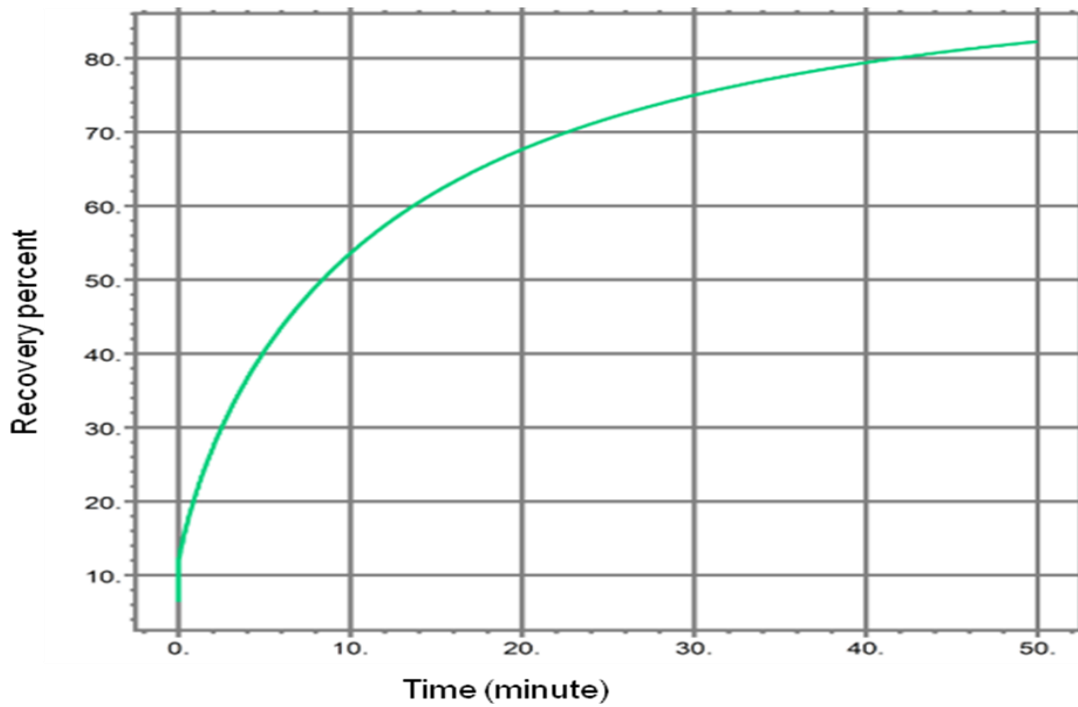


Figure 4.55 The percentage of recovery during displacement of crude oil by gas in fractured medium after 3000 seconds

4.3.3 Discussion of the results

Mass transfer affects both microscopic and macroscopic efficiency because mass transfer changes IFT and in this case microscopic efficiency is affected and also mass transfer changes the viscosity which affects the sweep efficiency. Reductions in the interfacial tension help to move the residual oil from the porous media. Diffusivity of the gas into the oil phase causes the oil phase to swell and this reduces the viscosity and density of the crude oil and makes it more mobile. The swelled oil is drained to the fracture media and it is easily moving or evaporating with the gas carrier.

Density of fractures in reservoir has linear relation to mass diffusion in matrix. It can be seen at lower part of fractured media Figure 4.48 which has more contact area with injected gas phase was higher, therefore gas saturation has penetrated more in comparing with matrix at upper part. The recovery of oil in the lower part is much more than upper part (see saturation of gas in lower part, Figure 4.52).

Modelling of the system shows that the diffusion coefficient significantly is controlling the fluid flow from matrix to fracture and vice versa. The oil swelling and evaporation mechanisms are two phenomena which is affecting on EOR in the system. Figure 4.56 shows hypothetical of evaporation of drained oil from fracture which is reduced by contacting time between carrier gas and drained oil. The permeability of the fractured media is increased during evaporation mechanisms therefore the gas flow rate of the fracture is increased which causes more mass transfer between phases. This process has been approved during passing high pressure through low pressure gas meter. Significant oil has been seen inside of the gas meter.

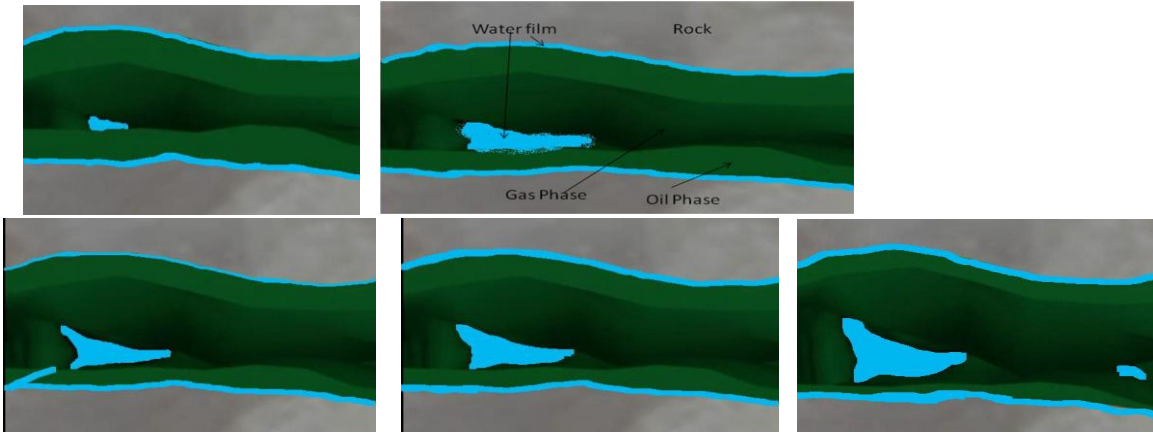


Figure 4.56, Evaporation mechanism in fracture medium and effect on permeability in the system

The world average oil recovery factor is estimated to be 35 percent of OOIP (Babadagli, 2005) and it is less for carbonate reservoirs. For instance, the estimated average oil recovery of initial water flooding in San Andres (West Texas) is about 25.88 percent of OOIP and much of the oil remains in the ground unrecoverable.

The results of the core flooding experiments are shown for the single in Figure 4.13 (a,b,c) and composite core plugs in Figure 4.18. It can be seen that the ultimate recovery in a single core plug is less than in a composite core plug. An effective displacement of oil was obtained in a composite core plug due to the contact time of the gas and oil phases.

The simulated ultimate recovery by FlexPDE software, in the case of with and without mass transfer is shown in Figure 4.44. The experimental data were matched with the simulation result, which shows the maximum recovery of the system obtained when mass transfer occurred. The deviation between the experimental and simulated result is usually within some uncertainty of three phases relative permeability correlation and precision of measuring data in tight carbonate rocks are used.

Chapter 5

Conclusions and Recommendations

5.1 Conclusions

Based on the results and discussion of this research, which investigates the effect of mass transfer phenomena during the injection of gas into a fractured carbonate oil reservoir, the following conclusions can be drawn.

- For the PVT cell experiment, the mass transfer of gas into oil causes the unsaturated crude oil gas/oil ratio to increase due to the swelling of the oil by diffusion of the gas (Section 4.1.1). The value of the diffusion coefficient in the incubation period was measured and found to be larger than that measured in the steady-state period (Section 4.1.1). This diffusion coefficient value gave a better match on experimental data. Therefore, during gas injection into the oil reservoirs, the transition zone (swelled zone) grew and the produced GOR increased. In addition, the heavy oil firstly changed into a medium oil and then into a light.
- In the PVT cell experiment, it is confirmed that the diffusion process takes place in two regions, the incubation region and the steady-state region. The main transfer occurred in the incubation region, which helped the transition zone to grow, thereby making it a partial miscible zone which in turn, helped to increase the displacement process. During running multiple experiments, It was obvious that the diffusion coefficient depends on the concentration, temperature, viscosity of oil, pressure of the system, and the length of the porous medium used in the experiments (Section 4.1.2).
- The new correlation (Equation 4.5) developed through this research takes into consideration all the parameters discussed in Chapter two. Advantage of the new correlation in comparing with others method (Table 4.1) is applicability of the current method at high pressure and temperature conditions (Section 4.1.3).The solution of the partial differential equation (PDE) with variable diffusion

coefficients was solved (refer Chapter Two) with respect to any one parameter (this could be viscosity, pressure, concentration gradient, temperature, or porous media), but the analytical solution was impossible to define as it depended on different parameters such as concentration, pressure, temperature, viscosity and reservoir characterisation. The solution of the PDE was carried out using the finite elements method, which provided estimates of mass transfer rate and pressure drop, and were found to be valid for all diffusion times. The FlexPDE software was used to model the diffusion of the system and it provided the best match for the experimental measurements made (Section 4.1.4).

- Mass transfer from a flowing region to a dead region is a condensation mechanism, whereas mass transfer from a dead region to a flowing region is made during the evaporation process. (Sections 4.3.3 and 2.2.6) This is considered a very important function of gas and oil behaviour when the oil and gas are in contact under reservoir conditions. It can be concluded that this mechanism played a major role in this research towards an understanding of enhanced oil recovery by partially miscible conditions.
- The interfacial tension between two phases in a miscible region is close to zero, but in the partially miscible region it is greater than zero and less than 10 mN/m (Section 4.2.6). Interfacial tension describes the phenomena or resistance between phases and most of the mass transfer occurs at transition phase then IFT will be change rapidly during mass transfer. In other hand, diffusion of gas into oil phase reduces viscosity of oil in overall, but this reduction in comparing with interfacial tension could not be significant. Therefore, this research showed that the mass transfer of gas into the oil phase reduced the interfacial tension and increased the capillary number directly. Therefore, an increasing of the capillary number significantly increases oil production from trapped and dead oil zones.
- Gas phase can vaporise the lighter oil fraction and condense into the residual oil phase. These phenomena can lead to the two phase fluids that become partially miscible, resulting in favorable residual oil and viscosity reduction. Diffusion causes

the mobility ratio of the system to change due to the change in viscosity of the oil and gas phases. The viscosity of the transition zone therefore depends on the concentrations of the displacing gas and the displaced oil. See Section 4.2.7.2.

- In tight carbonate reservoirs, the flow velocity is low enough that the displacement process is controlled by diffusion. The fractional flow versus the saturation curve during the incubation period is close to a 45° line from partial miscible to miscible phenomena. It is therefore concluded that the diffusion of gas into the oil phase changes the curvature of the relative permeabilities in the system. In three-phase flow, relative permeabilities of the gas phase depend on the saturation of the oil and gas phases (see section 4.2.6).
- It can also be concluded that the mass transfer between the gas and oil increased the recovery of the oil left behind in the porous media after primary depletion (as a result of evaporation of the residual oil film taking place). This reduced the IFT of oil and made it mobile (see section 4.2.3). Mass transfer between fracture and matrix caused the oil in the matrix to swell. If the gas flow discontinued, the swelled volume of oil would be flushed into the fracture and the concentration would be reversed, thus the swelled crude oil would move from the matrix into the fracture medium. Also, swelling of oil and evaporation of oil from the matrix into the fracture increased the oil recovery. After that, the oil begins to gradually evaporate from the matrices into the gas phase, helping to enrich the dry gas and increase the partial miscible zone.

5.2 Recommendations

Based on this research, there are other areas open to investigation that could help develop the mass transfer phenomena further during gas injection into the oil reservoirs. These include:

- The diffusion phenomena process between two phases occurs from both sides, the gas component into the oil phase and the oil component into the gas phase. The rate of diffusion for both phases is different; the light component velocity is higher than the heavy component and the diffusivity is higher. It is therefore recommended that an online Gas Chromatograph be used in future research to help understand more details of these phenomena.
- The incubation time of diffusion increases when using long core plugs or composite core plugs, resulting in more mass transfer taking place. The ordering of the core plugs is important in order to achieve more recovery. In this study, descending order was used to increase incubation time, but other ordering methods such as Huppler and ascending methods are recommended in further studies.
- Measurement of the viscosity and density of a transition zone can help to model three-phase flow in porous media. In further studies it is recommended that measurement of the physical properties along the core holder be undertaken using online property measurements to increase the accuracy of the mass transfer measurements.
- As no measurements were taken of the IFT under reservoir conditions during this research, it is recommended that these measurements are made and further research conducted to find the effect of mass transfer on IFT under reservoir conditions. This could help to analyse the possibility of producing oil from the trapped and dead-end zones and also residual oil from the swept area.

References

- Akin, S., and Demiral, B., (2001) *Effect of flow rate on imbibition three phase relative permeabilities and capillary pressures*. Energy sources, 23, 127-135.
- Al-Huthali A. And Gupta, A. D. (2004) *Streamline simulation of counter-current imbibition in naturally fractured reservoirs*. Journal of petroleum science and engineering 43, 271-300.
- Amyx, J. W., Bass, D.M., and Whiting, R.L. (1960) *Petroleum reservoir engineering*, McGraw Hill, New York.
- Armin Iske, A. T. R. (2000) *Mathematical methods and modelling in hydrocarbon exploration and production*, Springer, Berlin Heidelberg-New York, ISBN_3-540-22536-6
- Ayirala, S.C., (2002) *Surfactant-induced Relative Permeability Modifications for Oil Recovery Enhancement*, M.S. Thesis, The Craft and Hawkins Department of Petroleum Engineering, Louisiana State University and A and M College, Baton Rouge, LA (Dec).
- Aziz, K. and Settari A., (1979) *Petroleum Reservoir Simulation, Applied Science Publishers LTD, London*.
- Bentson, R. G. (1978) *Conditions under which the Capillary Term may be Neglected*. JCPT 25-30.
- Denoyelle, L and Bardon, C., (1984) *Influence of diffusion on enhanced oil recovery by CO₂ injection*, *Proceedings International Symposium on CO₂ Enhanced Oil Recovery*, Budapest, Hungary
- Berry, Jr. V.J. and Koeller, R.C., (1960) *Diffusion in compressed binary systems*.
AIChE J., 6(2): 274-279.
- Buckley, S. E., and Leverett, M.G. (1942) *Mechanism of fluid displacement in sands*, Trans AIME 146.
- Brooks, R.H. and Cory, A. T., (1966) *Properties of porous media affecting fluid flow*, J. Irrig. Drain. Div., 6, 61

- Cinar, Y., Franklin, M., and Orr, J. (2004) *Measurement of three phase relative permeability with IFT variation*. SPE paper Number 89419, SPE/DOE, Presented at the fourteenth symposium on improved oil recovery held in Tulsa. Oklahoma.
- Civan, F., Rasmussen, M.L. (2002) *Improved measurement of gas diffusivity for miscible gas flooding under non-equilibrium vs. equilibrium conditions*. SPE Paper Number 75135.
- Chen, J., Miller, M. A. and Sepehmooi, K.: 1995, *Theoretical investigation of counter-current imbibition in fractured reservoir matrix blocks*, SPE 29141 Proceedings of the 13th SPE Symposium on Reservoir Simulation, San Antonio, TX, USA, February 12–15, 1995.
- Chen, Z. X., Bodvarson, G. S. and Witherspoon, P. A.: 1990, *An integral equation formulation for two-phase flow and other nonlinear flow problems through porous media*, in: SPE 20517 Proceedings of the SPE Annual Technical Conference and Exhibition, New Orleans, September 23–26, 1990.
- Corey, A. T., Rathjens, C.H., Henderson, J.H. and Wyllie, M.R.J. (1956) *Three phase relative permeability*. Trans AIME, 207,349.
- Craft, B. C., Hawkins, M.F. And Terry, R.F. (1991) *Applied petroleum reservoir engineering*, Prentice-Hall Inc, ISBN 0-13-039884-5.
- Crank, J. (1995) *The mathematics of diffusion*, (2nd Edition) Clarendon Press, Oxford.
- Dawson. R., Khoury, F. and Kobayashi, R., (1970) *Self-diffusion measurements in methane by pulsed nuclear magnetic resonance*. AIChE J. 16(5): 725-729.
- Danckwerts, P. V. (1950) *Unsteady-state diffusion or heat conduction with moving boundary*, Trans Faraday Soc., 46, 701.
- Dean, R.H. and Lo, L.L., (1988) *Simulation of naturally fractured reservoirs*, SPERE, 638-648.
- Delshad, M., and Pope, G. A. (1989) *Comparison of three-phase oil relative permeability models*, *Trans. Porous Media*, 4, 59-83.

- Denoyelle, L., and B.C. (1984) *Diffusivity of carbon dioxide into reservoir fluids*, 86th Annual congress, Canadian Institute of Mining and Metallurgy. Ottawa.
- Dietrich, P., Helmig, R., Sauter, M., Hotzl, H., Kongeter, J., Teutsch, G. (2005) *Flow and transport in fractured porous media*, Springer Press, Nederland
- Dickson, K.B. and Johnson. J.P., (1988) *Measurement of Nitrogen Diffusion into Ekofisk Chalk*. Phillips Petroleum Company, Drilling and Production Division, Bartiesville
- Do, D. D. and Rice, R.G., (1986) *Validity of the parabolic profile assumption in adsorption studies*. AIChE Journal, 32, 149-154.
- Do, H. D., Pinczewski, W.V., Ruskauff, G.L., and Orr, F.M (1991) *Diffusion controlled swelling of reservoir oil by direct contact with injection gas*. Chem. Eng. Sci, 46, 1259-1270.
- Dria, D. E., Pope, G. A. and Sepehrnoori, K. (1993) *Three-phase gas/oil/brine relative permeabilities measured under carbon dioxide flooding conditions*. SPE Reservoir Engineering, 8, 143–150
- Element, D. J., Sargent, N.C. and Jayasekera, A.J. (2003) *Assessment of three phase relative permeability model using laboratory hysteresis data*. SPE Number 84903, SPE international improved oil recovery. Asia Pacific in Kuala Lumpur, Malaysia.
- Fatt, I. and Dykstra, H., (1951) *Relative permeability studies*, Trans. AIME, 192,249
- Firoozabadi, A. and Markeset, T.I. (1994) *Miscible displacement in fractured porous media: Part-I-Experiments*. SPE Paper number 27743.
- Firoozabadi, A. and Aziz, K. (1991) *Relative permeabilities from centrifuge data*. JCPT, 30, 33-42. Fung, L. S.-K. (1991) *Simulation of Block-to-Block processes in naturally fractured reservoirs*. SPERR, 477-484.
- Geffen, T. M., Owens, W.W., Parrish, D.R. and Morse, R.A. (1951) *Experimental investigation of factors affecting laboratory relative permeability measurements*. Trans AIME, 192,99.
- Grader, A. S. and O'Meara D.J. (1988) *Dynamic displacement measurement of three phase relative permeabilities using three immiscible liquids*. SPE Paper 28293, Proceeding of the SPE Annual technical conference and exhibition of the SPE,. Houston, TX ,October 2-5.

- Grogan, A. T. and Pinczewski, W.V. (1987) *The role of molecular diffusion processes in tertiary CO₂ flooding*. Journal of petroleum technology, 39, 591-602.
- Grogan, A. T., Pinczewski, W.V. and Ruskauff, G.J. (1988) *Diffusion of the CO₂ at reservoir conditions: Model and measurements*. SPE Paper 14897.
- Hagoort, J. (1980) *Oil recovery by gravity drainage*. SPE Paper number 7424.
- Hassanzadeh, H. and Polladi-Darvish, M. (2005) *Effect of fracture boundary conditions on matrix-fracture transfer shape factor*. Transport in porous media 64, 51-71.
- Hayduk, W., Castaneda, R., Bromfield, H. and Ray, R.R. (1973) *Diffusivities of propane in normal paraffin, Chlorobenzene and butanol solvents*. AIChE J., 19, 598.
- Honarpour, M., Koederitz, L., and Harvey, A.H (1982) *Empirical equations for estimating two-phase relative permeability in consolidated rock*. Trans AIME 273,2905.
- Honarpour M. , L. K. and Harvey H. (1994) *Relative permeability of petroleum reservoirs*, The Society of Petroleum Engineering, Inc.
- Hong S.L (2000) " Measurement of Gas Diffusivity in Three Australian Light Crude Oils" Msc Thesis, University of Queensland Brisbane, Queensland, Australia,
- Hoier L. and Whitson C.H., (2000) *Composition grading theory and practice* , SPE paper number 63085, Presented at the SPE annual technical conference and exhibition Dallas, Texas, USA,
- Ho, C.K. and Webb S.W. (2006) *Gas Transport in Porous Media* ISBN 978-1-4020-3961-4 (Print) 978-1-4020-3962-1 (Online), Springer Netherlands press.
- Huan, G. E., R.E., Qin, G. And Chen, Z.C. (2005) *Numerical simulation for fractured porous media. Current trends in high performance computing and its applications*, Shanghai, China, Springer-Verlag Heidelberg, 47-58.
- Huppler, J. D. (1969) *Water relative permeabilities in composite cores* JPT, 539-540.
- Huppler, J. D. (1970) *Numerical investigation of the effect of core heterogeneities on water-flood relative permeability*. SPE Journal, 10,381.

- Illingworth, T. C. and Golosnoy, I.O. (2005) *Numerical solution of diffusion controlled moving boundary problems which conserve solute*. Journal of Computational Physics, 209, 207-225.
- Islam, M. R. and Bentsen, R. G. (1986) *A dynamic method for measuring relative permeability*. JCPT, 39-50.
- Jamialahmadi, M., Emadi, M. and Steinhagen, M. (2006) *Diffusion coefficient of methane in liquid hydrocarbons at high pressure and temperature*. Journal of Petroleum Science and Engineering, 53, 47-60.
- Johnson, E. F., Bossler, D.P. and Neumann, V.O. (1959) *Calculation of relative permeability from displacement experiments*. Trans AIME, 216, 370-372.
- Jon Kleppe and Svein M. S. (1992) *Recent advances in improved oil recovery methods for North sea sandstone reservoir*, SPOR Monograph, Norwegian Petroleum Directorate.
- Jury, W.A. Spencer W.A. and Farmer, W.J. (1983) *Behavior assessment model for trace organics in soil: I. model description*, J. Environ. Qual. **12** (1983), pp. 558–564
- Kazemi, H., Merrill, L.S., Porterfield, K.L. and Zeman, P.R. (1976) *Numerical simulation of water-oil flow in naturally fractured reservoirs*. SPE Journal, 317-326.
- Kazemi, H., (1969) *Pressure transient analysis of naturally fractured reservoirs with uniform fracture distribution*. Soc. Pet. Eng. J., 451-62. Trans., AIME, 246.
- Kleppe, J., Berg, E.W., Buller, A.T., Hjelmeland, O. and Torsaeter, O., (1985) *North sea oil and gas reservoirs*. Graham & Trolman Lim Press.
- Koval, E.J. (1963), *A method for predicting the performance of unstable miscible displacement in heterogeneous media*, J. SPE, 3(6), 145-154
- Kulkarni, R., Watson, A. T., Nordtvedt, J. E. and Sylte, A. (1998) *Two-phase flow in porous media: Property identification and model validation*. AIChE J., 44(11), 2337-2350.
- Kulkarni, Madhav M., 2003. *Immiscible and miscible gas-oil displacements In porous media*, M.S. Thesis, The Craft and Hawkins Department Of Petroleum Engineering, Louisiana State University and Agricultural and Mechanical College, Baton Rouge, LA.

- Kummar Srivastava, N. (2004) *Effects of pressure gradients on displacement performance for miscible/near miscible gas floods*, Petroleum Engineering Department. Stanford University
- Langaas K.1, Ekrann S., Ebeltoft E. (1998) *A criterion for ordering individuals in a composite core*, Journal of Petroleum Science and Engineering 19, 21-32.
- Le Gallo, Y. Le Romancer, J.F., Bourbiaux, B. and Fernandes, G. (1997) *Mass transfer in fractured reservoirs during gas injection: Experimental and numerical modelling*, SPE Paper 38924.
- Lenormand, R., Kalaydjian, F., Bieber, M. T. and Lombard, J. M. (1998) *Use of a multifractal approach for multiphase flow in heterogeneous porous media: Comparison with CT-Scanning experiment*, 65th Annual technical conference and exhibition of the society of petroleum engineering held in New Orleans, LA
- Leverett, M. S., and Lewis, W.B. (1941) *Steady flow of gas-oil-water mixtures through unconsolidated sands*, Trans AIME, 207,349.
- Lewis, R. W. and Ghafouri, H.R. (1997) *A novel finite element double porosity for multiphase flow through deformable fractured porous media*, International journal for numerical and analytical methods in geomechanics, 21, 289-816.
- Lincoln, P., Ji-Youn, L., and Pinczewski, W.V. (1997) *Three phase relative permeability in heterogeneous formations*, SPE Paper number 38882.
- LeGallo, J.F. LeRomancecer and B. Bourbiaux, (1997) *Mass transfer in fractured reservoirs during gas injection: experimental and numerical modelling*, SPE paper number 38924
- Mcinerney, M. J., Duncan, K.E., Youssef, N., Fincher, T., Maudgalya, S.K., Flomsbee, M.J., Knapp, R., Simpson, R.R., Ravi, N. And Nayle, D. (2005) *Development of microorganisms with improved transport and biosurfactant activity for enhanced oil recovery*, Report # DE-Fc-02NT15321R02. University of Oklahoma.
- McManamey, W.J. and Woollen, J.M. (1973) *The diffusivity of carbon dioxide in some organic liquids at 25 and 50°C*, AIChE J. 19, pp. 667–669

- Millington, R.J., and J.M. Quirk. (1960) *Transport in porous media*. p. 97–106. In F.A. Van Beren et al. (ed.) *Trans. Int. Congr. Soil Sci.*, 7th, Vol. 1, Madison,WI. 14–24 Aug. 1960. Elsevier, Amsterdam.
- Mungan, N. (2000) *Enhanced oil recovery with high pressure nitrogen injection*, SPE Paper 62547, SPE/AAPG Western regional meeting held in Long Beach, California.
- Mungan, N. (2003) *High pressure nitrogen injection for miscible/immiscible enhanced oil recovery*, SPE Paper number 81008.
- Naimi-Tajdar, R., Sepehrnoori K., Arbogast T.J., and Miller M.A. (2006) *A fully implicit compositional parallel simulator for IOR processes in fractured reservoirs*, SPE Number 100079.
- Naylor, P., Mogford, D. and Smith, R. (2001) *Relative permeability measurements for post-water flood depressurisation of the Miller field*, North Sea.
- Nordtvedt, J. E., Ebeltoft, E., Sylte, A., Urkedal,H., Vatnek.O. and Watson, A.T. (1996) *Determination of three-phase relative permeabilities from displacement experiments*, SPE Paper 36683, Proceeding of the 1996 Annual technical conference and exhibition, Denver, Ca, October.
- O'Meara, D. J. J. and Crump, J.G. (1985) *Measuring capillary pressure and relative permeability in a single centrifuge experiment*, SPE paper number 14419 presented at the 60th Annual Technical Conference of the SPE held in Las Vegas, NV. (Sep. 22-25, 1985).
- Oak, M. J. (1991) *Three-phase relative permeability of intermediate-wet Berea sandstone*, 66th Annual technical conference and exhibition of the society of petroleum engineering held in Dallas, TX. October 6-9.
- Oak, M. J., Baker, L. E. and Thomas, D. C. (1990) *Three-phase relative permeability of Berea sandstone*, *J. Pet. Technol.*, 42(8), 1054-1061.
- Oak, M. J. (1990) *Three-phase relative permeability of water-wet Berea*, presented at the 1990 Society of Petroleum Engineers/Department of Energy Symposium on Enhanced Oil Recovery, Tulsa, April 22–25. Paper SPE/DOE 20183.
- Owens, W. W. and Archer, D. L., The effect of rock wettability on oil-water relative permeability relationship, *Trans. AIME*, 251, 8j3, 1951.

- Orr F.M. and Jensen C.M.,(1984) *Interpretation of pressure–composition phase diagrams for CO₂/Crude-oil systems*, SPE 11125, SPE-Journal.
- Parmeswar, R., and Maerefat, N.L. (1986) *A comparison of methods for the representation of three phase relative permeability data*, SPE Paper 15061.
- Perkins, T. K. and Johnston, O.C. (1963) *A review of diffusion and dispersion in porous media*, SPE Journal, 3, 70-84.
- Poling, B. E., Prausnitz, J.M. and O'connell, J-P., (2004) *The properties of gases and liquids*, MacGraw-Hill.
- Purcell, W. R. (1949) *Capillary pressures–Their measurement using mercury and the calculation of permeability therefrom*, Trans AIME, 186.
- Qadeer, S. (2006) *Techniques to handle limitations in dynamic relative permeability measurements*, PhD Thesis. Stanford University.
- Rapoport, L. A. and Leas, W.J. (1953) *Properties of linear waterfloods*, Trans AIME, 198, 139-148.
- Renner, T. A. (1988) *Measurement and correlation of diffusion coefficients for CO₂ and rich gas applications*, SPE Paper 15391.
- Riazi, M. R. (1996a) *A new method for experimental measurement of diffusion coefficients in reservoir fluids*, Journal of Petroleum Science and Engineering, 14, 235-250.
- Riazi, M. R. and Whitson, C.H (1993) *Estimating diffusion coefficient of dense fluids*, Ind. Eng.Chem. Res, 32.3081-3088
- Riazi, M. R., Whitson, C.H and de Silva, F., (1994) *Modelling of diffusional mass transfer in naturally fractured reservoirs*, Journal of Petroleum Science and Engineering 10-230-253
- Romance, R. L. J., Fernandes, X., and Gerard (1994) *Mechanism of oil recovery by gas diffusion in fractured reservoir in presence of water*, SPE Paper 22746 SPE/DOE Ninth symposium on improved oil recovery held in Tulsa, Oklahoma, USA.
- Saedi, A. M. (1982) *Simulation of naturally fractured reservoirs*, SPE Paper number 12270.

- Sahimi, M., Rasaei, M.R., and Haghghi, M. (2006) *Gas injection and fingering in porous media. Gas transport in porous media*, 133-168.
- Sahni, A. (1998) *Measurement of three phase relative permeability during gravity drainage using CT-Scanning*, Petroleum Engineering Department. Stanford.
- Sano, Y., Yamamoto, S. (1990) *Calculation of concentration-dependent mutual diffusion coefficient in desorption of film*, Journal of chemical engineering of Japan, 23 (3), 331-338.
- Saraf, D. N. and Fatt, I. (1967) *Three phase relative permeability measurement using a NMR technique for estimating fluid saturation*, SPE Journal, 235–242.
- Saraf, D. N. and Mccaffery, F.G. (1982a) *Two and three phase relative permeabilities: A review*, Report Number 81-80. Calgary, Alberta, Canada, Petroleum Recovery Institute.
- Saraf, D. N., Batycky, J.P., Jackson, J.H. and Fisher, D.B. (1982b) *An experimental investigation of three-phase flow in water-oil-gas measuresthrough water wet sandstones*, SPE 10761 presented at the 1982 California Regional Meeting of SPE, San Francisco, CA.
- Sarem, A. M. (1966) *Three-phase relative permeability measurments by unsteady-state methods*, SPE Journal, 9, 199.
- Sarma, P. (2003) *New transfer function for simulation of naturally fractured reservoirs with dual porosity models*, Petroleum Engineering Department. Stanford.
- Sigmund, P. M. (1976) *Prediction of molecular diffusion at reservoir condition, part I: Measurment and prediction of binary dense gas diffusion*, Journal of Canadian Petroleum Technology, 48-57.
- Siang, L.H. (2000) *Measurment of gas diffusivity in three Australian light crude oils*, Chemical Engineering Department, University of Queensland.
- Siddiqui S., Hicks, P.J. and Grader, A.S.,(1996) *Verification of Buckley-Leverett Three Phase Theory Using Computerised Tomography*, The Journal of Petroleum Science and Engineering, Vol. 15, No. 1.
- Spronsen, E. V. (1985) *Three phase relative permeability measurements using the centrifuge method*, SPE Paper 10688, SPE/DOE Proceedings of the third joint symposium on enhanced oil recovery , Tulsa, Oklahoma, April 4-7.

- Stone, H. L. (1973) *Estimation of three-phase relative permeability and residual oil data*, Journal of Canadian Petroleum Technology, 12(4), 53–61.
- Stubos, A. K. (1999) *Oil recovery potential from fractured reservoirs by mass transfer processes*, SPE Paper 56415.
- Swapan, K. and Buttler, R.M.,(1996) *Diffusion coefficients of propane and butane in Peace River Bitumen*, Can. J. Chem. Eng. 74, pp. 985–992
- Taylor, R. and Krishna, R. (1993) *Multicomponent mass transfer*, John Wiley & sons.
- Thompson, J.L., Mungan, N.(1969) *A laboratory study of gravity drainage in fractured systems under miscible conditions*, paper SPE 2232 presented at the 1969 Annual Fall Meeting, Houston, Sep 29 – Oct 2
- Van der Zanden A.J.J., (1998) *An iterative procedure to obtain the concentration dependency of the diffusion coefficient from the space-averaged concentration vs time*, Chemical Engineering Science 53 pp. 1397–1404.
- Vignes, A. (1966) *Diffusion in binary solutions*, Ind. Eng. Chem. Fund.,, 5, 189-196.
- Virnovsky, G.A., (1985) *Determination of relative permeabilities in a three-phase flow in a porous medium*, Izv. Akad. Nauk SSSR, Meh. Zidk. Gaza **5** (1985), pp. 187–189.
- Warren, J. E. and Root, P. J., (1963) *The behaviour of naturally fractured reservoirs*, SPE Journal, 245-255.
- Welge, H. J. (1952) *A simplified method for computing oil recovery by gas or water drive*, Trans AIME, 195, 91-98.
- Whiteman, W. G. (1923) *The two-film theory of gas absorption*, Chem. Metall. Eng., 29, 146-148.
- Whitson, C.H.,and Brule, M.R., (2000) *Phase Behaviour*, SPE Monograph, Volume 20.
- Woessner, E., George R.A. and Melrose, J.C. (1969) *Dense gas diffusion coefficient for the methane-propane system*, Ind. Eng. Chem. Fund.,, 8, 780-787.
- Wyckoff, R. D. and Botset H.G. (1936) *Flow of gas liquid mixtures through sands*, Physics, 7,325.

- Wyllie, M. R. J. and Gardner, G.H.F. (1958) *The generalized Kozeny–Carman equation. Its application to problems of multiphase flow in porous media*, World Oil, Apr 1958, 210-228.
- Zekri, A. Y. and Almehaideb R.A. (2002) *Relative permeability measurements of composite cores, an experimental approach*, SPE Asia Pacific Oil and Gas Conference and Exhibition Melbourne, Australia.
- Zhang, Y., and Maini, B.B. (2000a) *Measurement of gas diffusivity in heavy oils*, Journal of Petroleum Science and Engineering, 25, 37-47.
- Zhang, Y. P., Hyndman, C.L. and Maini, B.B.. (2000b) *Measurement of gas diffusivity in heavy oils*, Journal of Petroleum Science and Engineering, 20, 20-47.
- Zhangxin Chen, G. H. and Yuanle Ma (2005) *Computational method for multiphase flow in porous media*, Southern Methodist University, Dallas, Texas.

Appendix A

A1- Mass transfer with variable diffusion coefficients

In many systems, such as homogeneous, heterogeneous, and fractured porous media, or the diffusion of organic vapours in high-polymer substances, D depends on the concentration of the diffusing substance C . In this case, and also when the medium is not homogeneous, D varies from point to point as shown in equation (2.52).

$$\frac{\partial C}{\partial t} = \frac{\partial}{\partial x} \left(D \frac{\partial C}{\partial x} \right) + \frac{\partial}{\partial y} \left(D \frac{\partial C}{\partial y} \right) + \frac{\partial}{\partial z} \left(D \frac{\partial C}{\partial z} \right) \quad (\text{A:1})$$

where D may be a function of x , y , z , and C .

If D depends only on the time during which diffusion has been taking place but not on any of the other variables:

$$D = f(t)$$

Then on introducing a new time-scale T such that:

$$dT = f(t)dt$$

the diffusion equation becomes:

$$\frac{\partial C}{\partial T} = \frac{\partial^2 C}{\partial x^2} + \frac{\partial^2 C}{\partial y^2} + \frac{\partial^2 C}{\partial z^2} \quad (\text{A:2})$$

which is the same as equation (A:1) for a constant diffusion coefficient equal to unity.

The molar flux of a gas diffusing into a liquid column can be expressed using the following equation based on Fick's law:

$$\frac{\partial(C)}{\partial t} = \nabla \cdot (D\nabla C) + v \frac{\partial(C)}{\partial z} \quad (\text{A:3})$$

where C is the molar concentration of the gas phase. During gas injection, the pressure in the cell may vary with position. However, at a later time, the pressure in the vessel is assumed to be independent of position, and only changes with time, i.e.

$$\frac{\partial P}{\partial z} = 0$$

By writing equation (A:3) in cylindrical coordinates, for the two-dimensional case, we have:

$$\frac{\partial(C)}{\partial t} = \frac{1}{r} \frac{\partial}{\partial r} \left(D \frac{\partial(C)}{\partial r} \right) + \frac{\partial}{\partial z} \left(D \frac{\partial(C)}{\partial z} \right) + v \frac{\partial(C)}{\partial z} \quad (\text{A:4})$$

For the solution of equation (A:4), the following initial and boundary conditions can be used:

$$C = C(r, z) \quad \text{for } t = 0 \quad (\text{A:5})$$

$$C = C_0 \quad \text{for } t > 0 \text{ at the surface of the liquid}$$

$$\frac{\partial(C)}{\partial r} = 0 \quad \text{for } z = 0 \text{ for every } t \quad (\text{A:6})$$

In equation (A:6), since there is nothing taking place during the experiment, the molar average velocity, v is equal to zero. Therefore, the diffusion problem reduces to the unsteady-state one-dimensional diffusion equation in a slab as follows:

$$\frac{\partial(C)}{\partial t} = \frac{\partial}{\partial z} \left(D \frac{\partial(C)}{\partial z} \right) \tag{A:7}$$

The boundary and initial conditions, applicable to the system shown in Figure 1 are:

$$C = C_o \text{ for } t \Rightarrow 0 \text{ and } Z = z_o \tag{A:8}$$

$$\frac{\partial(C)}{\partial z} = 0 \text{ for } r = 0 \text{ for every } t$$

$$\text{For } 0 < Z < Z_o, \quad t = 0, \quad Z_o = 0$$

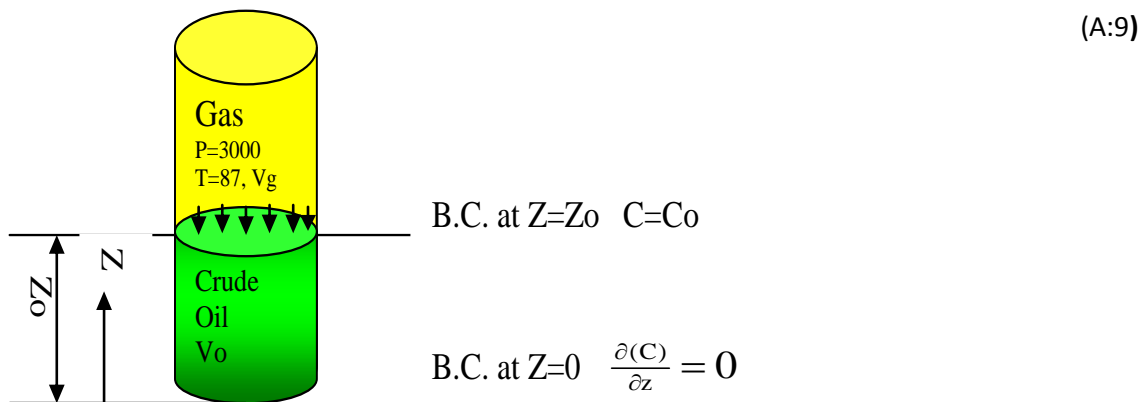


Fig 1 Schematic and dimension of the PVT Cell

A-2 Factors affecting the Diffusion Coefficient

A large number of factors, the most important ones being concentration, chemical composition, pressure, porous media and temperature, can affect the diffusion coefficient.

A-2.1 Dependency of the diffusion coefficient with chemical composition

There are cases in which the diffusion coefficient changes with composition. This makes the analysis of the diffusion process more complicated because one has to consider the extra variables when solving the diffusion equation. When a concentration gradient is imposed on a non-stoichiometric compound, re-equilibration of the system may occur by a diffusion process involving the propagation of a concentration gradient throughout the components fraction to minimise the concentration differences in the system.

To achieve equilibrium in a system, the value of the chemical potentials of the different components of the system must be constant. Let us consider a system with component, i , in it. Gradients of the chemical potential, μ in the solution will generate a flux expressed by the equations:

$$J_i = L_i \frac{\partial \mu_i}{\partial x} \quad (\text{A:10})$$

where the L_i is the transport coefficient of i and μ_i is the chemical potential of the component ($x = i$).

The chemical potential can be expressed as:

$$\mu_i = \mu_i^{\circ} + RT \ln a_i$$

where μ_i° is the chemical potential of i at $T = 0$ K and a_i is its activity. The self diffusion coefficient can be considered a measure of the rate at which atoms diffuse in an ideal solution. Therefore the activity of the diffusing components can be expressed as its mole fraction in the system, $a_i = x_i$, and the chemical potential becomes:

$$\mu_i = \mu_i^{\circ} + RT \ln x_i$$

Substituting in the flux equation (Eq. A:10) for both cases we have:

$$J_i = -D_i \frac{\partial \ln a_i}{\partial x} \tag{A:11}$$

Chemical component diffusion:

$$J_i = D_{io} \frac{\partial \ln x_i}{\partial x} \tag{A:12}$$

Assuming that the transport coefficients are the same in both cases and definition of the activity coefficient is $\gamma_i = a_i/x_i$ it gives:

$$D_i = -D_{io} \frac{\partial \ln a_i}{\partial \ln x_i} = -D_{io} \left(1 + \frac{\partial \ln \gamma_i}{\partial \ln x_i} \right) \tag{A:13}$$

Onsager (1931) stated that, based on the theory of the thermodynamics of irreversible processes, which proposes that the flux is proportional to the rate of entropy production in the system, at

constant pressure and temperature, and in the absence of external forces, the one dimensional flux for a binary system is proportional to the gradient of the chemical potential given by:

$$J_i = D_i \frac{dc_i}{dz}$$

For constant density it can be expressed as:

$$J_1 = -D_0 \left[\frac{d \ln \alpha_1}{d \ln x_1} \right] \frac{dc_1}{dz} \quad (\text{A:14})$$

Thus the Fickian coefficient can be related to the diffusion coefficient based on a chemical potential driving force by the following equation:

$$D_{12} = D_0 \left(\frac{d \ln \alpha_1}{d \ln x_1} \right) \quad (\text{A:15})$$

Gullian (1985) extended this approach and was able to develop an explicit equation with no adjustable parameters for the prediction of the variation of diffusion coefficients with temperature and composition.

$$D_{12} = \frac{kT}{2\pi\eta V^{\frac{1}{3}}} \left[1 + \frac{1}{2\pi x_1 x_2} \left(\frac{d \ln x_1}{d \ln \alpha_1} - 1 \right) \right]^{-0.5} \quad (\text{A:16})$$

Riazi (1996) used Fick's Law to describe the diffusion in dense fluids. It can be justified by considering that the diffusion coefficient should be corrected by a thermodynamic factor for non-ideal mixtures.

$$D_{oi} = D_{oie} \left(1 + \frac{\partial \ln \phi_i}{\partial \ln x_i} \right) \quad (\text{A:17})$$

Where D_{oie} and ϕ_i is effective, diffusivity and the fugacity coefficient of component i in the mixture, respectively, x_i is mole fraction of component i in the liquid phase and for dilute systems the thermodynamic correction factor $\left(1 + \frac{\partial \ln \phi_i}{\partial \ln x_i} \right)$ is unity. Dimensionless parameters have been used by this method. A constant diffusion coefficient for each time step has also been used. The dimensionless form of the liquid and gas phase is as follows:

$$\frac{\partial C_{oi}^*}{\partial t_{oi}^*} = \frac{\partial^2 C_{oi}^*}{\partial Z_o^{*2}} \quad (\text{A:20})$$

$$\text{where } t_{oi}^* = \frac{D_{oi} t}{L_o^2} \text{ and } Z_o^* = \frac{Z_o}{L_o} \quad (\text{A:21})$$

the corresponding boundary conditions are:

$$\text{at } t^* = 0 \quad C_{oi}^* = C_{oi}^{*T} \quad (\text{A:22})$$

$$\text{at } z_o^* = 0 \quad \frac{\partial C_{oi}^*}{\partial z_o^*} = 0 \quad (\text{A:23})$$

$$\text{at } Z_o^* = 1 \quad C_{oi}^* = C_{obi}^* \quad (\text{A:24})$$

To solve the above equation it is necessary to assume that, during each time step, D_{oi} is constant. The procedure for this type of problem is the same as in the previous section. The dimensionless form of the above equation (2.69) applied for the gas phase is shown in Figure 2.6 as follows:

$$\frac{\partial C_{gi}^*}{\partial t_{gi}^*} = \frac{\partial^2 C_{gi}^*}{\partial z_g^{*2}} \quad (\text{A:25})$$

$$\text{Where } t_{gi}^* = \frac{D_{gi}t}{L_g^2}, \quad C_{gi}^* = \frac{C_{gi}}{C_{oi}^1 - C_{gi}^l} \text{ and } Z_g^* = \frac{Z_g}{L_g} \quad (\text{A:26})$$

$$\text{at } t_{gi}^* = 0 \quad C_{gi}^* = C_{gi}^{*T} \quad (\text{A:27})$$

$$\text{at } z_g^* = 0 \quad C_{gi}^* = C_{gbi}^* \quad (\text{A:28})$$

$$\text{at } Zg^* = 1 \quad \frac{\partial C_{gi}}{\partial z_g^*} = 0 \quad (\text{A:29})$$

In the above equations, T is the time step. The cumulative time is obtained from the summation of these time steps. In only the first time steps the initial condition is $C_i^* = C_i^*$. In addition, for the subsequent time intervals, the initial condition becomes $C_i^* = C_i^{*T}$ and after the first time step, C_i^{*T} is a function of Z^* .

A2.2 Dependency of the diffusion coefficient with concentration

The equation for one-dimensional diffusion when the diffusion coefficient D is a function of concentration C is:

$$\frac{\partial(C)}{\partial t} = \frac{\partial}{\partial x}(D(c))\frac{\partial(C)}{\partial x} \quad (\text{A:30})$$

Boltzmann (1894) showed that, for certain boundary conditions, provided D is a function of C only, C may be expressed in terms of a single variable $\xi = \frac{x - x_m}{2\sqrt{t}}$ and (2.64) may therefore be reduced to an ordinary differential equation by the introduction of a new variable ξ where:

$$\frac{\partial C}{\partial x} = \left(\frac{\partial C}{\partial \xi} \right) \left(\frac{\partial \xi}{\partial x} \right) = \frac{1}{2\sqrt{t}} \left(\frac{\partial C}{\partial \xi} \right) \quad (\text{A:31})$$

The corresponding time derivative is:

$$\frac{\partial C}{\partial t} = \left(\frac{\partial C}{\partial \xi} \right) \left(\frac{\partial \xi}{\partial t} \right) = -\frac{x - x_m}{4t^{3/2}} \left(\frac{\partial C}{\partial \xi} \right) = -\frac{\xi}{2t} \left(\frac{\partial C}{\partial \xi} \right) \quad (\text{A:32})$$

Writing in terms of ξ and using the chain rule, then:

simplifying the equation by substituting for $\left(\frac{\partial \xi}{\partial x} \right) = \frac{1}{2\sqrt{t}}$

The simplified result is a nonlinear form of ODE with the independent variable ξ . Hence, the solution of the ordinary differential equation is as follows:

$$-2\xi \left(\frac{dC}{d\xi} \right) = \frac{d}{d\xi} \left(D(c) \left(\frac{dC}{d\xi} \right) \right) \quad (\text{A:34})$$

Where the given boundary conditions are reduced to:

$$C = C_0 \quad , \quad (\xi = 0)$$

the initial conditions are:

$$C = C_1 \quad (\xi \rightarrow \infty)$$

To find the solution, it is convenient to write 2.68 with $\bar{C} = \frac{C}{C_0}$ and $\tilde{C} = 1$ on $\xi = 0$ in the form:

$$-\frac{2\xi}{D} \cdot D \cdot \frac{d\tilde{C}}{d\xi} = \frac{d}{d\xi} \left(D \frac{d\tilde{C}}{d\xi} \right)$$

(A:35)

We solve this equation subject to the condition $C = \text{zero}$, as $\xi \rightarrow \infty$. Integrating equation (2.69) twice, we obtain:

$$\tilde{C} = 1 - A \int_0^{\xi} \frac{1}{D} \exp \left[- \int_0^{\xi} \left(\frac{2\xi}{D} \right) d\xi \right] d\xi \quad (\text{A:36})$$

where A is a constant of integration to be determined, so that:

$$A \int_0^{\infty} \frac{1}{D} \exp \left[- \int_0^{\xi} \left(\frac{2\xi}{D} \right) d\xi \right] d\xi = 1 \quad (\text{A:37})$$

in order that $\tilde{C} = \frac{C_1}{C_0}$ as $\xi \rightarrow \infty$ is satisfied and where $D=D(\bar{C})$ is a known function.

The solution (2.69) satisfies the condition $\tilde{C} = 1$ on $\xi = 0$.

Appendix B

B-1 Effect of capillary on three-phase relative permeability

The effect of the capillary force on the displacement process was introduced in 1953 by Ropopertand and Leas. They introduced the scaling factor, $L\mu\nu$, for the range of flow rates in which the capillary forces had an affect on the flow in linear systems. In addition, they concluded that the injection fluid

becomes stabilised if the scaling factor was greater than 10 *cm-cp/min*. In this case, the recovery from the core becomes independent of the flow rate and hence the Buckley Leverett theory becomes applicable. Benston (1978) found that the capillary term can be neglected in the flow equation if the value of the capillary number, Nc , defined as $\frac{\sigma AK_{rw}}{\mu_w l q}$ is less than 0.01 and in which case, the Buckley Leverett solution can be applied.

Normally, to determine oil-water relative permeability data in the laboratory, cores from the reservoir under consideration are used. In the author's study, core samples were brought from carbonate reservoirs in Iran. Since reservoir cores are relatively short in length (4-8 cm), employing these cores to obtain the relative permeability for any given reservoir will often result in significant errors. These errors are due to both the capillary end effect and errors associated with inaccuracies in volume measurements which become significant for small cores. To overcome these shortcomings, several such cores can be arranged together to form a composite core for relative permeability experiments. To reduce the capillary end effect in the laboratory, the following equations need to be discussed. The capillary pressure in an immiscible flooding system is related to the injection rate. The fractional flow (Leverett) equation is given as follows:

$$f_w = \frac{1 + \frac{K_o A}{\mu_o q_r} \left(\frac{\partial P_c}{\partial x} - \Delta \rho \sin \theta \right)}{1 + \frac{K_o}{K_w} \frac{\mu_w}{\mu_o}} \quad (B:1)$$

The two terms in brackets are the capillary force ($\frac{\partial P_c}{\partial x}$) and the gravity force ($\Delta \rho \sin \theta$) and where $\Delta \rho$ is the density difference between water and oil and θ is the dip angle. In the laboratory, the effect of the gravitational term can be neglected since the core-holder is positioned horizontally. Under typical reservoir conditions, this assumption is still valid unless the dip angle is very high. With the above reasonable assumptions, equation (3.43) can be simplified to:

$$f_w = \frac{1 + \frac{K_o A}{\mu_o q_r} \left(\frac{\partial P_c}{\partial x} \right)}{1 + \frac{K_o \mu_w}{K_w \mu_o}} \quad (\text{B:2})$$

To evaluate the capillary end effect in the laboratory, three options need to be discussed and they are:

1. increasing injection velocity;
2. using high viscosity crude oil; and
3. a core sample with low permeability for keeping the injection velocity and crude viscosity constant (Zekri, 2002).

Appendix C

C-1 Derivation of the flow equation for dual porosity systems

The Darcy equations for laminar and multiphase flow in porous media are defined as follows:

$$u_w = -\frac{KK_{rw}}{\mu_w} \nabla(P_w - \rho_w g \sin \theta) \quad (\text{C:1})$$

$$u_w = -\frac{KK_{ro}}{\mu_o} \nabla(P_o - \rho_o g \sin \theta) \quad (\text{C:2})$$

The primary fluid flows through the fracture media in dual porosity systems and the formulation for this is:

$$u_{wf} = -\frac{K_f K_{r_{wf}}}{\mu_{wf} B_{wf}} \nabla(P_{wf} + \rho_w g \sin \theta) \quad (C:3)$$

$$u_{of} = -\frac{K_f K_{r_{of}}}{\mu_{of} B_{of}} \nabla(P_{of} + \rho_o g \sin \theta) \quad (C:4)$$

The water phase pressure can be expressed in terms of oil phase pressure based on the capillary pressure definition as follows:

$$P_{cf} = P_{of} - P_{wf} \quad (C:5)$$

Equation (c:4) can then be re-written as follows:

$$u_{wf} = -\frac{K_f K_{r_{wf}}}{\mu_{wf} B_{wf}} \nabla(P_{of} - P_{cf} + \rho_o g \sin \theta) \quad (C:6)$$

The continuity equation is based on the principle of mass conservation, and states that the temporal change of mass in a control volume, is the sum of the mass flux across the volume boundaries and the mass flux due to sources and sink. The temporal change of the mass in the control volume is described as follows.

The rate of mass change in water phase in the x direction is:

$$u_{wx} \rho_w \Delta y - (\rho_w u_{wx} + \frac{\partial}{\partial x} (\rho_w u_{wx}) \Delta x) \Delta y \quad (C:7)$$

The rate of mass change in the water phase in the Y direction is:

$$u_{wy} \rho_w \Delta x - (\rho_w u_{wy} + \frac{\partial}{\partial y} (\rho_w u_{wy}) \Delta y) \Delta x \quad (C:8)$$

The rate of accumulation of water is:

$$\frac{\partial}{\partial t} (\phi S_w \rho_w \Delta x \Delta y) + \xi = 0 \quad (C:9)$$

where, ξ is the rate of water flow from the matrix into the fracture. For the fracture system, the conservation of mass can be written in the following form:

$$\begin{aligned} \frac{\partial}{\partial t} (\phi S_w \rho_w \Delta x \Delta y) + \xi = u_{wy} \rho_w \Delta x - (\rho_w u_{wy} + \frac{\partial}{\partial x} (\rho_w u_{wy}) \Delta y) \Delta x + u_{wx} \rho_w \Delta y \\ - (\rho_w u_{wx} + \frac{\partial}{\partial x} (\rho_w u_{wx}) \Delta x) \Delta y \end{aligned} \quad (C:10)$$

Equation (C.10) it can be simplified to:

$$\phi \frac{\partial}{\partial t} (S_w) + \xi_o = \nabla(u_w) \quad (C:11)$$

It can also be written for the oil phase as follows:

$$\phi \frac{\partial}{\partial t} (S_o) + \xi_o = \nabla(u_o) \quad (C:12)$$

Substituting equations (C.3) and (C.4) into equations (C.11) and (C.12), the following can be obtained:

$$\frac{\partial}{\partial t} (\phi S_{wf}) + \xi_w = \nabla \left(-\frac{K_f K_{rwf}}{B_{wf} \mu_{wf}} \nabla (P_{of} - P_{cf} + \rho_w g \sin \theta) \right) \quad (C:13)$$

$$\frac{\partial}{\partial t} (\phi S_{of}) + \xi_o = \nabla \left(-\frac{K_f K_{rof}}{B_{of} \mu_{of}} \nabla (P_{of} + \rho_o g \sin \theta) \right) \quad (C:14)$$

In two-phase flow (water and oil), the sum of the saturation is unity. Then:

$$S_o + S_w = 1, \quad \frac{\partial S_o}{\partial t} = -\frac{\partial S_w}{\partial t} \quad (C:15)$$

Equations (C.13) and (C.14) can be simplified using equation (C.15) as follows:

$$\phi \frac{\partial}{\partial t} (S_{wf}) + \xi_w = \nabla \left(-\frac{K_f K_{rwf}}{B_{wf} \mu_{wf}} \nabla (p_{of} - p_{cf} + \rho_w g \sin \theta) \right) \quad (C:16)$$

$$-\phi \frac{\partial}{\partial t} (S_{wf}) + \xi_o = \nabla \left(-\frac{K_f K_{rof}}{B_{of} \mu_{of}} \nabla (p_{of} + \rho_o g \sin \theta) \right) \quad (C:17)$$

By multiplying both sides of equations (C.16) and (C.17) by the bulk volume, the equations become:

$$V_p \frac{\partial}{\partial t} (S_{wf}) - V_p \xi_o = \nabla \left(\frac{K_f K_{rof}}{B_{of} \mu_{of}} V_p \nabla (p_{of} + \rho_o g \sin \theta) \right) \quad (C:18)$$

$$-V_p \frac{\partial}{\partial t} (S_{wf}) - V_p \xi_w = \nabla \left(\frac{K_f K_{rwf}}{B_{wf} \mu_{wf}} V_p \nabla (p_{of} - p_{cf} + \rho_w g \sin \theta) \right) \quad (C:19)$$

Equations (C.18) and (C.19) do not have sink and source terms (i.e. production and injection terms); to including these terms, in the right side of these equations with the conventions of positive for production and negative for injection wells, it can be written as follows :

$$V_p \frac{\partial}{\partial t} (S_{wf}) - V_p \xi_o - q_o = \nabla \left(\frac{K_f K_{rof}}{B_{of} \mu_{of}} V_p \nabla (p_{of} + \rho_o g \sin \theta) \right) \quad (C:20)$$

$$-V_p \frac{\partial}{\partial t} (S_{wf}) - V_p \xi_w - q_w = \nabla \left(\frac{K_f K_{rwf}}{B_{wf} \mu_{wf}} V_p \nabla (p_{of} - p_{cf} + \rho_w g \sin \theta) \right) \quad (C:21)$$

C-2 Matrix flow equations

The rate of inflow into the matrix could be zero as there is no flow into the matrix; when there is a rate of outflow from the matrix into the transfer function, the conservation of mass can be written as:

$$\phi \frac{\partial}{\partial t} (S) + \xi = 0 \quad (\text{C:22})$$

$$\phi \frac{\partial}{\partial t} (S_{wm}) + \xi_w = 0 \quad (\text{C:23})$$

$$\phi \frac{\partial}{\partial t} (S_{wm}) + \xi_o = 0 \quad (\text{C:24})$$

C-3 Dual porosity

For the development of a dual porosity model, the matrix blocks act as a source term to the fracture system. Warren–Root (1963) proposed a dual porosity model based on the pseudo steady state flow in the medium of blocks. In this model, fluid does not flow directly from one matrix block to another block. It first flows into the fractures, and then it flows into another block or remains in the fractures. This is reasonable since fluid flows more rapidly in the fracture than in the matrix. The derived equations for this model are:

$$\phi \frac{\partial(\rho_w S_w)}{\partial t} = -\nabla(\rho_w u_w) \quad (\text{C:25})$$

$$\phi \frac{\partial(\rho_{po} S_o)}{\partial t} = -\nabla(\rho_{po} u_o) \quad (\text{C:26})$$

$$\phi \frac{\partial(\rho_{pg} S_o + \rho_g S_g)}{\partial t} = -\nabla(\rho_{pg} u_o + \rho_g u_g) \quad (\text{C:27})$$

where, ρ_{pg} and ρ_{po} indicate the partial densities of the gas and oil components in the oil phase respectively. The fracture equations are the same as dual porosity/permeability systems discussed in the next section.

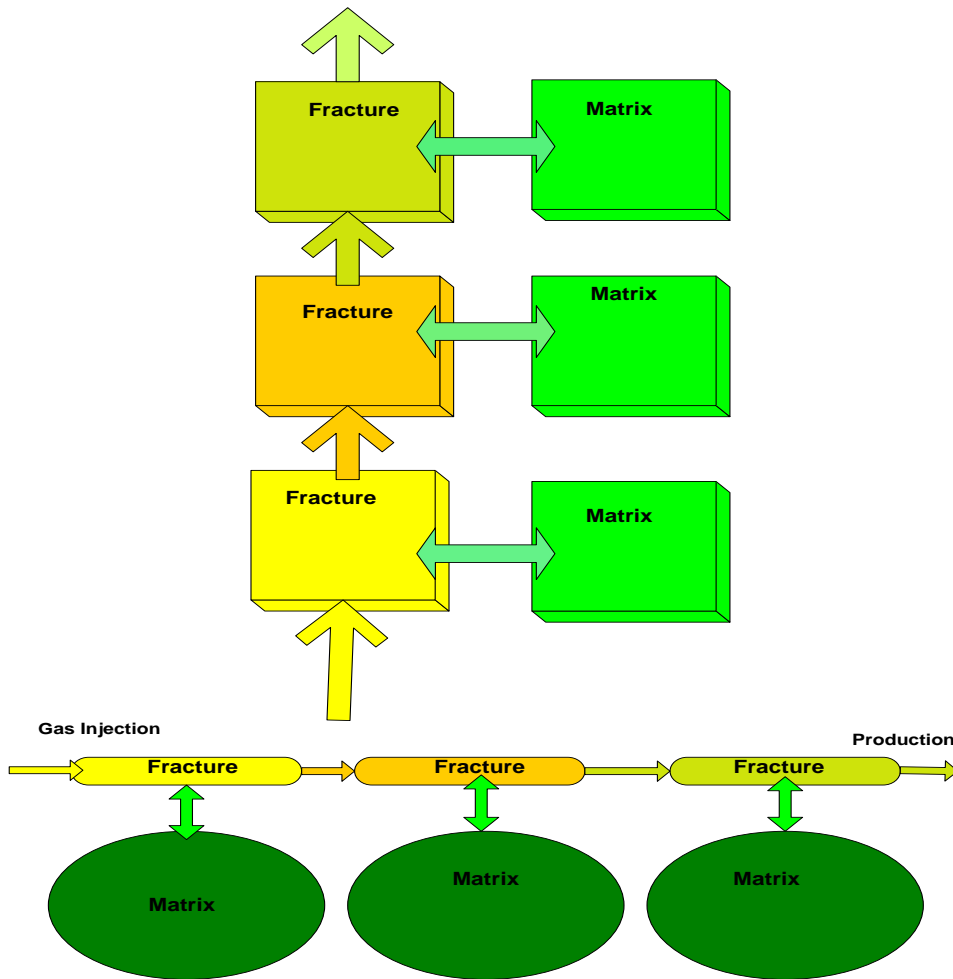


Figure C.1: Matrix fracture connectivity for dual porosity model

C-4 Dual porosity/permeability models

The concept of dual porosity/permeability has been utilised to model the flow of fluids in fracture/matrix systems (Kazemi, 1969). In this concept, the fracture system is treated as a porous structure distinct from the usual porous structure of the matrix itself. The fracture system is highly permeable, but can store very little fluid, while the matrix has opposite characteristics. When

developing a dual porosity model, it is critical to treat the flow transfer terms between the fracture and matrix systems (Figure C.2).

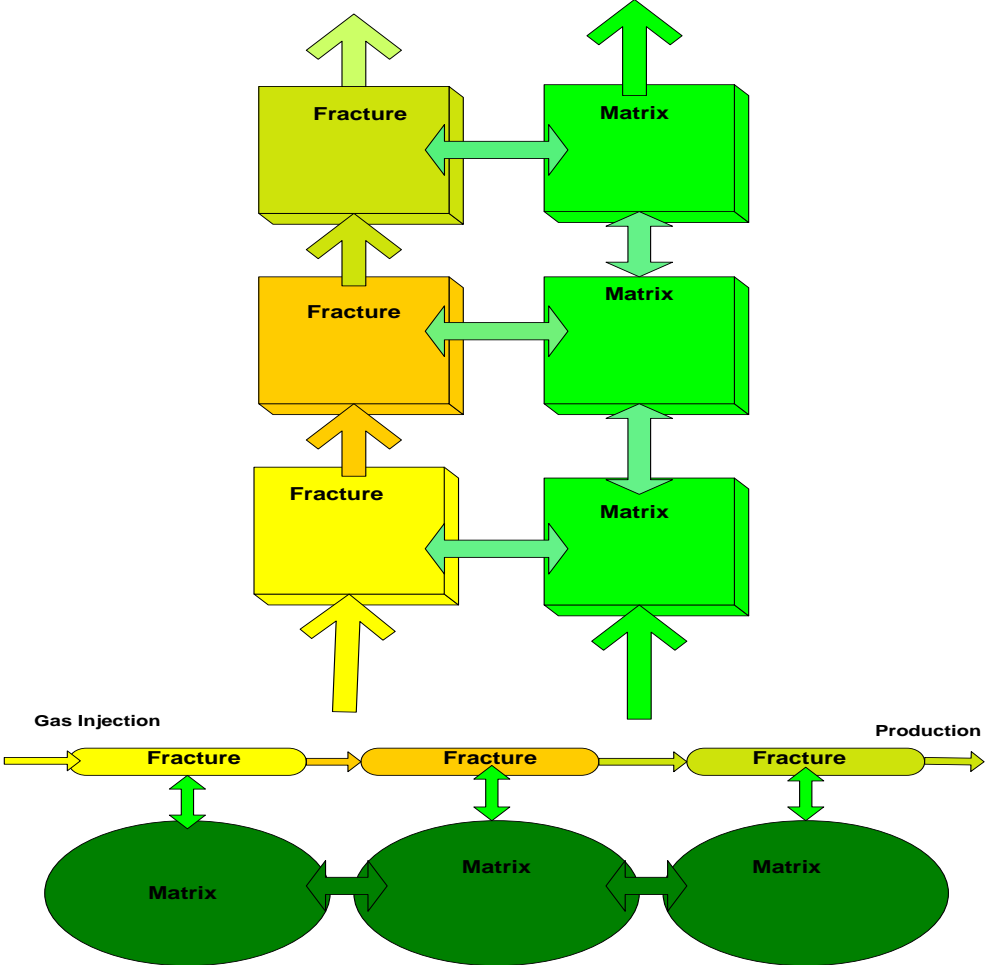


Figure C.2: Matrix fracture connectivity for the porosity/permeability model

In the mass interchange between the oil and gas phases, mass is not conserved within each phase, but rather the total mass of each component must be conserved. Thus, for the matrix system, the mass balance equations are:

$$\phi \frac{\partial(\rho_w S_w)}{\partial t} = -\nabla(\rho_w u_w) - q_{w_m} \quad (\text{C:28})$$

$$\phi \frac{\partial(\rho_{po} S_o)}{\partial t} = -\nabla(\rho_{po} u_o) - q_{o_{om}} \quad (\text{C:29})$$

$$\phi \frac{\partial(\rho_{pg} S_o + \rho_g S_g)}{\partial t} = -\nabla(\rho_{pg} u_o + \rho_g u_g) - (q_{G_{om}} + q_{G_m}) \quad (\text{C:30})$$

where, q_{w_m} , $q_{o_{om}}$, $q_{G_{om}}$, and q_{G_m} represent the matrix-fracture transfer terms:

$$S_w + S_g + S_o = 1 \quad (\text{C:31})$$

$$\phi \frac{\partial(\rho_w S_w)_f}{\partial t} = -\nabla(\rho_w u_w)_f + q_{w_m} + q_w \quad (\text{C:32})$$

$$\phi \frac{\partial(\rho_{po} S_o)_f}{\partial t} = -\nabla(\rho_{po} u_o)_f + q_{o_{om}} + q_{o_o} \quad (\text{C:33})$$

$$\phi \frac{\partial(\rho_{pg} S_o + \rho_g S_g)_f}{\partial t} = -\nabla(\rho_{pg} u_o + \rho_g u_g)_f + (q_{G_{om}} + q_{G_m}) + (q_{G_o} + q_G) \quad (\text{C:34})$$

C-5 The boundary conditions approach

The boundary conditions method treats the flow transfer term explicitly through boundary conditions on the matrix blocks. The shape factor and characteristic length considered in other methods are avoided in the boundary conditions approach. However, this approach appears to apply only to the dual porosity model and not to the dual porosity/permeability model. The formulation of the mass balance equation for each fluid phase in a fractured porous medium follows that for an ordinary medium with an additional matrix-fracture transfer term, the two overlapping continua, fractures and matrix blocks, are allowed to coexist and interact with each other. If the matrix blocks act only as

a source term to the fracture system and there is no matrix-matrix connection, the dual porosity model can be applied. If there are matrix-matrix connections, a dual porosity/permeability model can be applied for the fracture/porous medium.

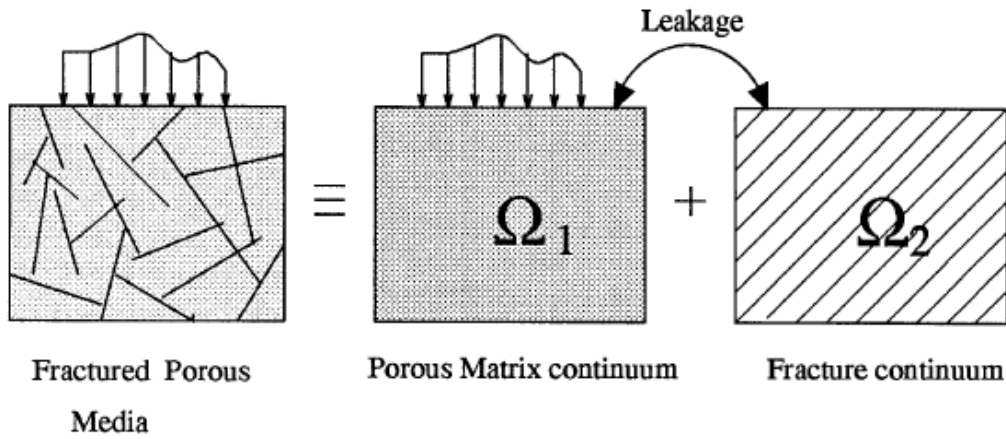


Figure 4.4: Schematic representation of a dual porosity model
(source: Lewis and Ghafori, 1997)

In this model, the fractured porous media are divided into overlapping but distinct media, the first medium represents flow and deformation in the porous matrix and the second medium represents flow in the fracture (Figure C.2). For each block (Ω_i) the following mass balance equation can be written as follows:

$$\frac{\partial(\phi\rho_w S_w)}{\partial t} = -\nabla(\rho_w u_w) \tag{C:35}$$

$$\frac{\partial(\phi \rho_{po} S_o)}{\partial t} = -\nabla(\rho_{po} u_o) \quad (C:36)$$

$$\frac{\partial(\phi \rho_{pg} S_o + \phi \rho_g S_g)}{\partial t} = -\nabla(\rho_{pg} u_o + \rho_g u_g) \quad (C:37)$$

where, ρ_{pg} , ρ_{po} are the partial molar density of the gas and oil phases, the total mass of water leaving the i^{th} matrix block Ω_i per unit time is :

$$\int_{\partial\Omega_i} \rho_w u_w v dl \quad (C:38)$$

where, v is the outward unit normal to the surface $\partial\Omega_i$ of Ω_i . By applying the divergence theorem to equation C:38 the equation becomes:

$$\int_{\partial\Omega_i} \rho_w u_w v dl = \int_{\Omega_i} \nabla(\rho_w u_w) dx = \int_{\Omega_i} \frac{\partial(\phi \rho_w S_w)}{\partial t} dx \quad (C:39)$$

The matrix-fracture, water, oil and gas transfer can be written as follows:

$$q_w = -\sum x_i(x) \frac{1}{|\Omega_i|} \int_{\Omega_i} \frac{\partial(\phi \rho_w S_w)}{\partial t} dx \quad (C:40)$$

$$q_{o_{om}} = -\sum x_i(x) \frac{1}{|\Omega_i|} \int_{\Omega_i} \frac{\partial(\phi \rho_{po} S_o)}{\partial t} dx \quad (C:41)$$

$$q_{G_{om}} + q_{G_m} = -\sum x_i(x) \frac{1}{|\Omega_i|} \int_{\Omega_i} \frac{\partial(\phi \rho_{Go} S_o)}{\partial t} dx \quad (C:42)$$

where, $|\Omega_i|$ is the volume of Ω_i and $x_i(x)$ is its characteristic function, which can be defined as follows:

$$x_i(x) = 1 \text{ if } x \text{ belong to matrix domain } (\Omega_1)$$

$$x_i(x) = 0 \text{ if } x \text{ belong to fracture domain } (\Omega_2)$$

With the definition of q_{w_m} , $q_{o_{om}}$, and $q_{G_{om}} + q_{G_m}$, boundary conditions on the surface of each matrix block can be imposed in an integral fashion, and the gravitational forces and pressure gradient effects across the block can be incorporated into the conditions (Chen, et al., 1990).

C-6 Matrix- fracture transfer functions

The matrix-fracture transfer functions are the most important parameters in the modeling of natural fracture reservoirs. Many investigators, for example Dean and Lo (1988), Lim and Aziz (1995), Kazemi (1976), and Warren and Root (1963), offered different types of transfer functions. The mechanism of this parameter is still not completely understood. This research examines more on the boundary conditions with more focus on the mass transfer phenomena. Ignoring the gravitational forces in equations (C.20) and (C.21), the transfer function has the following form for both the water and oil phases (Kazemi, 1976; Dean and Leo, 1988):

$$\xi_w = F_s k_m \lambda_{wmf} (p_{wf} - p_{wm}) \quad (C:43)$$

$$\xi_o = F_s k_m \lambda_{omf} (p_{of} - p_{om}) \quad (C:44)$$

The mobility ratios, λ_{omf} and λ_{wmf} represent the upstream mobility between fracture and matrix system and F_s is a shape factor that defines the connectivity between the matrix and the surrounding fractures:

$$p_{of} - p_{om} = \left(\frac{\lambda_{wmf}}{\lambda_{omf} + \lambda_{wmf}} \right) (p_{cf} - p_{cm}) \quad (C:45)$$

Substituting equation (C.45) into equation (C.44) yields the following transfer function:

$$\xi_o = F_s k_m \left(\frac{\lambda_{wmf} \lambda_{omf}}{\lambda_{omf} + \lambda_{wmf}} \right) (p_{cf} - p_{cm}) \quad (C:46)$$

For the rectangular matrix block with fractures on all sides, the shape factor has the following form (Kazemi et al., 1976):

$$F_s = 4 \left(\frac{1}{L_x^2} + \frac{1}{L_y^2} + \frac{1}{L_z^2} \right) \quad (C:47)$$

C-7 Expression of transfer function in terms of imbibition recovery

Deswaan (1978) proposed that the rate of imbibition into the fracture from the matrix could be expressed as:

$$\xi = R_a \lambda \int_0^t e^{-(t_D - \varepsilon)\lambda} \frac{\partial S_{wf}}{\partial \varepsilon} d\varepsilon \quad (C:48)$$

Considering the integral in equation (C.48), the transfer function for Buckley Leverett displacement in one dimension for two-phase water flooding can be written as follows:

$$\xi = R_a \lambda \sum_{i=0}^n \left\{ [S_{wf}(t_{j+1}) - S_{wf}(t_j)] \prod_{k=j}^n e^{-\lambda \Delta t_k} \right\} \quad (C:49)$$

$$\xi = R_a \lambda \left\{ Sum^{n-1} e^{-\lambda \Delta t_{Dn}} \right\} \quad (C:50)$$

where:

$$Sum^{n-1} = Sum^{n-2} + (S_{wf}^n - S_{wf}^{n-1}) e^{-\lambda \Delta t_{Dn-1}} \quad (C:51)$$

This can now be introduced into equations (C.20) and (C.21) to make this into a two-unknown two-equation problem.

C-8 Relative permeability in fractured media

A model concept frequently used for a fracture medium consists of two parallel plates which represent the fracture walls. Figure C.3 shows the natural single fracture and parallel plates. It can be applied locally, maintaining a variation in fracture aperture throughout the fracture, or globally, assuming one constant aperture for the total fracture.

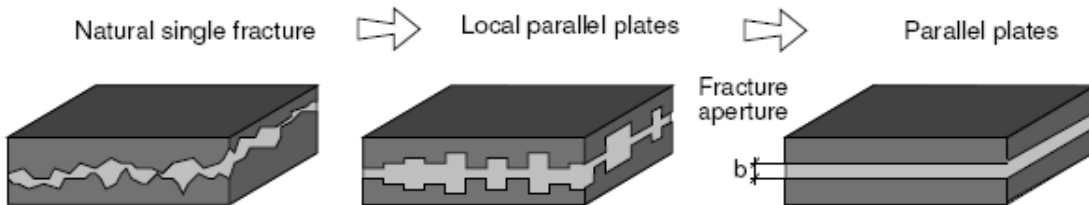


Figure C.3 From nature to parallel-plate concept
 (source: Dietrich et al, 2005)

In the parallel plate concept, the length scale l of the plates is much larger than the distance between them b ($l \gg b$). Furthermore, hydraulically smooth surface and laminar flow is assumed, where the Poiseuille fluid model can be applied. Figure C.4 shows the fluid flow with a parabola-shaped velocity profile and Navier-Stokes equation for laminar single phase flow.

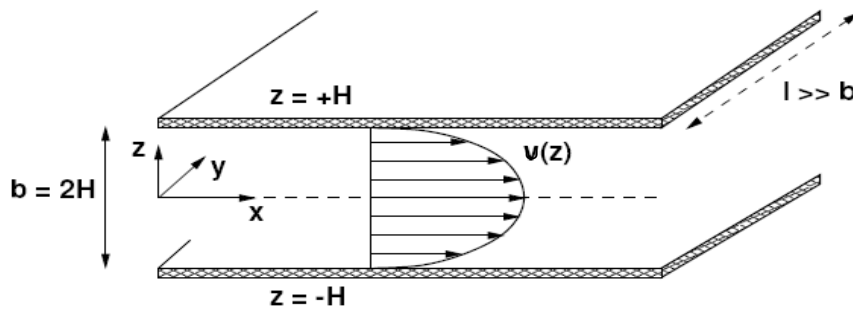


Figure C.4 The velocity profile in smoothed walls (source: Dietrich et al., 2005)

Incompressible Newtonian fluid yields the following equations as follows:

$$u(z) = \frac{\rho g}{2\mu} \left(-\frac{d}{dx} \left(\frac{p}{\rho g} + z \right) \right) (H^2 - z^2) \quad (\text{C:52})$$

The maximum velocity u_{max} at $z=0$ is:

$$u_{\max} = u(z = 0) = \frac{p}{\rho\mu} H^2 - \frac{d}{dx} \left(\frac{p}{\rho g} \right) \quad (\text{C:53})$$

The average velocity u_{ave} is derived from the maximum velocity as follows:

$$u_{ave} = \frac{3}{2} u_{\max} = \frac{\rho g}{\mu} \frac{H^2}{3} - \frac{d}{dx} \left(\frac{p}{\rho g} \right) \quad (\text{C:54})$$

Considering the distance between the two plates b ($b=2H$), the main three-dimensional velocity u_{ave} can be written as:

$$u_{ave} = \frac{b^2}{12} \frac{\rho g}{\mu} \frac{\partial h^2}{\partial x_i} = -K \frac{\partial h}{\partial x_i} \quad (\text{C:55})$$

$$k = k_1 \frac{\rho g}{\mu} \quad \text{with} \quad k_1 = \frac{b^2}{12} \quad (4.56)$$

From the above equation, it can be concluded that the permeability of a fracture, approximated by the parallel plate concept, is proportional to the square of the fracture aperture b .

Appendix D

Table of Laplace transforms

$$\bar{v}(p) = \int_0^{\infty} e^{-pt} v(t) dt$$

We write $q = \sqrt{(p/D)}$. D , x and h are always positive. α is unrestricted.

	$\bar{v}(p)$	$v(t)$
1.	$\frac{1}{p}$	1
2.	$\frac{1}{p^{\nu+1}}, \nu > -1$	$\frac{t^{\nu}}{\Gamma(\nu+1)}$
3.	$\frac{1}{p+\alpha}$	$e^{-\alpha t}$
4.	$\frac{\omega}{p^2+\omega^2}$	$\sin \omega t$
5.	$\frac{p}{p^2+\omega^2}$	$\cos \omega t$
6.	e^{-qx}	$\frac{x}{2\sqrt{(\pi Dt^3)}} e^{-x^2/4Dt}$
7.	$\frac{e^{-qx}}{q}$	$\left(\frac{D}{\pi t}\right)^{\frac{1}{2}} e^{-x^2/4Dt}$
8.	$\frac{e^{-qx}}{p}$	$\operatorname{erfc} \frac{x}{2\sqrt{(Dt)}}$
9.	$\frac{e^{-qx}}{pq}$	$2\left(\frac{Dt}{\pi}\right)^{\frac{1}{2}} e^{-x^2/4Dt} - x \operatorname{erfc} \frac{x}{2\sqrt{(Dt)}}$
10.	$\frac{e^{-qx}}{p^2}$	$\left(t + \frac{x^2}{2D}\right) \operatorname{erfc} \frac{x}{2\sqrt{(Dt)}} - x\left(\frac{t}{\pi D}\right)^{\frac{1}{2}} e^{-x^2/4Dt}$
11.	$\frac{e^{-qx}}{p^{1+n}}, n = 0, 1, 2, \dots$	$(4t)^{\frac{1}{2}n} \operatorname{erfc} \frac{x}{2\sqrt{(Dt)}}$
12.	$\frac{e^{-qx}}{q+h}$	$\left(\frac{D}{\pi t}\right)^{\frac{1}{2}} e^{-x^2/4Dt} - hD e^{hx+Dh^2}$ $\times \operatorname{erfc} \left\{ \frac{x}{2\sqrt{(Dt)}} + h\sqrt{(Dt)} \right\}$
13.	$\frac{e^{-qx}}{q(q+h)}$	$D e^{hx+Dh^2} \operatorname{erfc} \left\{ \frac{x}{2\sqrt{(Dt)}} + h\sqrt{(Dt)} \right\}$

	$\bar{v}(p)$	$v(t)$
14.	$\frac{e^{-qx}}{p(q+h)}$	$\frac{1}{h} \operatorname{erfc} \frac{x}{2\sqrt{(Dt)}} - \frac{1}{h} e^{hx+Dth^2}$ $\times \operatorname{erfc} \left\{ \frac{x}{2\sqrt{(Dt)}} + h\sqrt{(Dt)} \right\}$
15.	$\frac{e^{-qx}}{pq(q+h)}$	$\frac{2}{h} \left(\frac{Dt}{\pi} \right)^{\frac{1}{2}} e^{-x^2/4Dt} - \frac{(1+hx)}{h^2} \operatorname{erfc} \frac{x}{2\sqrt{(Dt)}}$ $+ \frac{1}{h^2} e^{hx+Dth^2} \operatorname{erfc} \left\{ \frac{x}{2\sqrt{(Dt)}} + h\sqrt{(Dt)} \right\}$
16.	$\frac{e^{-qx}}{q^{n+1}(q+h)}$	$\frac{D}{(-h)^n} e^{hx+Dth^2} \operatorname{erfc} \left\{ \frac{x}{2\sqrt{(Dt)}} + h\sqrt{(Dt)} \right\}$ $- \frac{D}{(-h)^n} \sum_{r=0}^{n-1} \{ -2h\sqrt{(Dt)} \}^r \operatorname{erfc} \frac{x}{2\sqrt{(Dt)}}$
17.	$\frac{e^{-qx}}{(q+h)^2}$	$-2h \left(\frac{D^3 t}{\pi} \right)^{\frac{1}{2}} e^{-x^2/4Dt} + D(1+hx+2h^2Dt)$ $\times e^{hx+Dth^2} \operatorname{erfc} \left\{ \frac{x}{2\sqrt{(Dt)}} + h\sqrt{(Dt)} \right\}$
18.	$\frac{e^{-qx}}{p(q+h)^2}$	$\frac{1}{h^2} \operatorname{erfc} \frac{x}{2\sqrt{(Dt)}} - \frac{2}{h} \left(\frac{Dt}{\pi} \right)^{\frac{1}{2}} e^{-x^2/4Dt}$ $- \frac{1}{h^2} \{ 1-hx-2h^2Dt \} e^{hx+Dth^2}$ $\times \operatorname{erfc} \left\{ \frac{x}{2\sqrt{(Dt)}} + h\sqrt{(Dt)} \right\}$
19.	$\frac{e^{-qx}}{p-\alpha}$	$\frac{1}{2} e^{\alpha t} \left[e^{-x\sqrt{(a/D)}} \operatorname{erfc} \left\{ \frac{x}{2\sqrt{(Dt)}} - \sqrt{(at)} \right\} \right.$ $\left. + e^{x\sqrt{(a/D)}} \operatorname{erfc} \left\{ \frac{x}{2\sqrt{(Dt)}} + \sqrt{(at)} \right\} \right]$
20.	$\frac{1}{p^{\frac{3}{2}}} e^{-qx}$	$\frac{1}{\pi} \left(\frac{x}{2tD^{\frac{1}{2}}} \right)^{\frac{1}{2}} e^{-x^2/8Dt} K_{\frac{1}{2}} \left(\frac{x^2}{8Dt} \right)$
21.	$\frac{1}{p^{\frac{3}{2}}} K_{2\nu}(qx)$	$\frac{1}{2\sqrt{(\pi t)}} e^{-x^2/8Dt} K_{\nu} \left(\frac{x^2}{8Dt} \right)$
22.	$I_{\nu}(qx') K_{\nu}(qx), \quad x > x'$ $I_{\nu}(qx) K_{\nu}(qx'), \quad x < x'$	$\frac{1}{2t} e^{-(x^2+x'^2)/4Dt} I_{\nu} \left(\frac{xx'}{2Dt} \right), \quad \nu \geq 0$
23.	$K_0(qx)$	$\frac{1}{2t} e^{-x^2/4Dt}$
24.	$\frac{1}{p} e^{x/p}$	$I_0[2\sqrt{(xt)}]$

	$\bar{v}(p)$	$v(t)$
25.	$\frac{\exp [xp - x\{(p+a)(p+b)\}^{\frac{1}{2}}]}{\{(p+a)(p+b)\}^{\frac{1}{2}}}$	$e^{-\frac{1}{2}(a+b)t+x} I_0[\frac{1}{2}(a-b)\{t(t+2x)\}^{\frac{1}{2}}]$
26.	$p^{\frac{1}{2}v-1} K_v(x\sqrt{p})$	$x^{-v} 2^{v-1} \int_{x^2/4t}^{\infty} e^{-u} u^{v-1} du$
27.	$\{p - \sqrt{(p^2 - x^2)}\}^v, \quad v > 0$	$v x^v I_v(xt)/t$
28.	$\frac{\exp [x\{(p+a)^{\frac{1}{2}} - (p+b)^{\frac{1}{2}}\}^2]}{(p+a)^{\frac{1}{2}}(p+b)^{\frac{1}{2}}[(p+a)^{\frac{1}{2}} + (p+b)^{\frac{1}{2}}]^{2v}},$ $v \geq 0$	$\frac{t^{\frac{1}{2}v} e^{-\frac{1}{2}(a+b)t} I_v\{\frac{1}{2}(a-b)t^{\frac{1}{2}}(t+4x)^{\frac{1}{2}}\}}{(a-b)^v(t+4x)^{\frac{1}{2}v}}$

Appendix E

Input data for running FlexPDE software

1-TITLE "Variation of concentration at static condition and high pressure and temperature"

COORDINATES { coordinate system, 1D,2D,3D, etc }

Ycylinder ('R','Z')

VARIABLES { system variables }

c(threshold=0.1)

P (threshold=0.1) { choose your own names }

! SELECT { method controls }

DEFINITIONS { parameter definitions }

pin=2985.3 { pressure of the systems}

Tem=648 { temperature of the system -Ranking}

V=0.00440727 { volume of the gas phase}

Ru=10.731 { universal gas constant}

Zf=0.94

Mo=40

Mol=250

!Zf=5.050e-3-2.74e-6*Pin+3.331e-8*Pin^1.5+2.198e-3*(Pin/Tem) -2.675e-5*(Pin^1.5/tem) {z
Factor of the system}

nmole=(Pin*V)/(Zf*Ru*tem)

! D=1/(6*z)*14.7e-5

conc=nmole/v

!D=0.3839e-9*tem^1.5

D=1.3678e-7*(tem^1.47*Mol^2.2)/(conc^0.5*p*Mo)

! Pt=pe+((8*Zf*Ru*tem)/10)*10*C/(((3.14*3.14))*exp(-(3.14*3.14*D)/40)

!dt(P)=(zf*Ru*tem)*D*dz(C)/15.2

Pvar=Pin-dt(P)

M = upulse(r,r-3.8)

smol=(-dt(p)*V)/(Zf*Ru*tem)

initial values

C=0

p = 2985.3

EQUATIONS {Partial Differential Equation, one for each variable}

C: $\text{div}(D*\text{grad}(C)) = dt(C)$

P: $dt(P)=(zf*Ru*tem)*D*dz(C)/44$

{ one possibility }

! CONSTRAINTS { Integral constraints }

BOUNDARIES { The domain definition }

REGION 1 { For each material region }

start (0,10)

natural (p)=p line to (3.8,10)

natural (p)=0 value (P)=pin line to (3.8,20)

natural (p) =0 value(P)= pin line to (0,20)

natural (p)=0 value(P)= pin line to close

start (0,0)

natural (p)=0 value (P)=pvar line to (3.8,0)

natural (p)=0 value (P)=pvar line to (3.8,10)

!natural (p) =p value(P)= pvar line to (0,10)

natural (p) =p value(P)= pvar line to (0,10)

```

natural (p)=0 value(P)= pvar line to close
REGION 2 { For each material region }
start (0,0)

natural (C)=0 line to (3.8,0)
natural (C)=0 line to (3.8,10)
natural (C) =conc line to (0,10)
natural (C)=0 line to close

start (0,10)

natural (C)=0 value (C)=(conc)/conc line to (3.8,10)
natural (C)=0 value (C)=(conc) /conc line to (3.8,20)
natural (C) =0 value (C)=(conc)/conc line to (0,20)
natural (C)=0 value (C)=(conc) /conc line to close

feature { a "gridding feature" to help localise the activity }
start (0,10) line to (3.8,10)

time 0 to 6000 by 60

plots

for t=1 by 60 to 6000 by 100 to endtime
contour(p) from (1.8,10) to (1.8,0)
surface(p) from (1.8,0) to (1.8,20) range (2500,3000)
contour(c) from (1.8,20) to (1.8,10)
surface(c) from (1.8,20) to (1.8,10)
! elevation(p) from (0,10) to (3.8,10)
! elevation(smol) from (0,10) to (3.8,10)
!fixed range (0, 6000)

contour(c) from (1.8,0) to (1.8,20)

```

```

    surface(c) from (1.8,0) to (1.8,20) ! viewpoint ( 1.33, 8.7, 40)
    elevation(c) from (1.8,0) to (1.8,20)
! elevation(normal(flux))

Summary

!report (p)

!report (dt(p))

!report (dz(C))

!report(dt(C))

!report (d)

!report(smol)

report (conc)

!report (nmole)

histories

!history(smol) at (1.8,11)

history(D) at (1.8,11)

!history(p) at (1.8,11) EXPORT FORMAT "#t#p#"

history(p) at (1.8,11) EXPORT FORMAT "#t#"

history(p) at (1.8,11) EXPORT FORMAT "#p#"

history(c) at (1.8,9) (1.8,8) (1.8,7) (1.8,6)(1.8,5) (1.8,4) (1.8,3) (1.8,2) (1.8,1) (1.8,0) range (0.0,1)

! history(Pvar) at (0.5,3.5) (1,3.5) (1.5,3.5) (2,3.5)(5,3.5) (8,3.5) (10,3.5) (15,3.5) (18,3.5) (20,3.5)

!history(pvar) at (0,0)

END

```

2-TITLE 'flow in porous media'

Coordinates

xCylinder ('z','r')

SELECT

smoothinit { Smooth the initial conditions a little, to minimize
 the time wasted tracking the initial discontinuity }

prefer_speed { nonlinearity is not strong - we can get away with shortcuts }

VARIABLES

s (threshold=0.1)

p (threshold=0.1) { Saturation and Pressure }

DEFINITIONS

vl=30

mug = .01826 { gas l viscosity }

muo = 15.50 { oil viscosity }

K = 4.87e-3 { Saturation-independent permeability coefficient }

Pin = 3000 { Inlet pressure }

Pout = 2500 { Outlet pressure }

!Pin = 210 { Inlet pressure }

! Pout =170

swc=0.2

s1=s/(1-swc)

M = ((1-s1)^4/muo + (2-s1)*(s1)^3)/mug { Total mobility }

f = (1-S1)^4/muo/M { Fractional flux }

kro = s1^4 { Relative permeability of water }

phi =.206 { porosity }

krp=s1^3*(2-s1)

Tem=648 {temperature of teh system -Ranking}

V=0.00440727 {volume of the gas phase}

Ru=10.731 {universal gas constant}

Zf=.94

Mo=8.439

Mol=250

nmole=(Pin*V)/(Zf*Ru*tem)

conc=nmole/v

! fl=6 {fluid velocity}

D=1.3678e-7*(tem^1.47*mol^2.2)/(conc^0.5*p*mo)

!D=2.238e-3

epsvisc = D { A little artificial diffusion helps smooth the solution }

sint = integral(s) { the total extraction integral }

! hour = 60*60

! day = hour*24 { seconds per day }

INITIAL VALUES

s = 0 { start with all oil }

p = Pin + (Pout-Pin)*z/20 { start with a rough approximation to the pressure }

EQUATIONS

! s: phi*dt(s) - div(K*krw*grad(p)) - epsvisc*div(grad(s)) = 0

! s: phi*dt(s) - div(K*krw*grad(p))-1.17e-8*div(grad(s)) = 0

s: phi*dt(s) - div(K*kro*grad(p)) - epsvisc*div(grad(s)) = 0

p: div(K*M*grad(p)) = 0

BOUNDARIES

REGION 1

{ fillet the input pipe, and define no-flow boundaries of the box }

start(0,0)

```

natural(p)=0 natural(s) = 0

line to (20,0)

    { set constant outlet pressure, and "tautological" saturation flux }

! value(p) = Pout

natural (p)=dz(p) natural(s)= -K*kro*dz(p)

line to (20,3.8)

    { reset no-flow box boundaries }

value(p) = Pin    value(s) = 1

    line to (0,3.8)

    { set constant inlet pressure and saturation }

value(p) = Pin value(s) = 1

line to close

!REGION 2

    { fillet the input pipe, and define no-flow boundaries of the box }

! start(0.0,2.95)

! value(p) = Pin    value(s) = 1

! line to (20,1.05)

! natural(p)=dz(p) natural (s) = -K*krp*dz(p)

! line to (20,3.8)

    { set constant outlet pressure, and "tautological" saturation flux }

! natural(p)=0 natural (s)=0 line to (0,3.8)

! value(p) = Pin    value(s) = 1

! line to close

!TIME 0 to 4000 by 2

TIME 0 to 50 by 1

```

MONITORS

```
for cycle=5
  contour(s) as "Saturation" range(0,1)
  contour(s) zoom as "Outflow Saturation" range(0,1)
  contour(p*14.5) zoom as "Pressure" range(2500,50000) painted
  vector(-K*M*grad(p)) norm as "Flow Velocity"
```

PLOTS

```
for t = 0 by 1 to 50
  grid(z,r)
  contour(s) as "Saturation" range(0,1) painted
  surface(s) as "Saturation" range(0,1) painted viewpoint(60,-120,30)
  contour(s) zoom as "Outflow Saturation"
  range(0,1) painted
  elevation( Krg) from (0,0) to (20,3.8) range(0,1)
  elevation( Kro) from (0,0) to (20,3.8) range(0,1)
  contour(p*14.5) as "Pressure" range(170,205) painted
  vector(-K*M*grad(p)) norm as "Flow Velocity"
  contour(K*M*magnitude(grad(p))) norm as "Flow Speed" painted
  elevation(S) from(20,0) to (20,3.8)
  elevation(S) from (0,1.8) to (20,1.8)
  !elevation (krw) on s=0.5
  !elevation(s,krw,kro) from(20,0) to (20,3.8) export format "#s#b#krw#b#kro#b#T" file "Ptable.txt"
  ! elevation(S,Kro,Krg) from(20,0) to (20,3.8) export format "#s#b#kro#b#Krg#b" file "Ptable.txt"
  elevation(kro) from(20,0) to (20,3.8) export format "#kro#b#T" file "Ptableko.txt"
  elevation(s) from(20,0) to (20,3.8) export format "#s#b#T" file "Ptables.txt"
```

elevation(krg) from(20,0) to (20,3.8) export format "#krg#b#T" file "Ptablekrg.txt"

HISTORIES

history(sint/10) at (0,0) as "% of Recovery"

history(kro,krg) at (2,3.8) (4,3.8) (6,3.8) (8,3.8)(10,3.8) (12,3.8) (14,3.8) (16,3.8) (18,3.8)(20,3.8)

history(kro/2.5,krg/2.5) at (2,0) (4,0) (6,0) (8,0)(10,0) (12,0) (14,0) (16,0) (18,0)(20,0)

history(kro,krg) at (20,0.8)

history(sint/10) at (0,0) export format "#1 #b#T" file "rec.xls"

history(kro,krg,S) at (20,3.8) (20,0) range(0,1) export format "#1#b#2#b#3" file "kpp.xls"

END

3-TITLE 'flow in Fractured media'

Coordinates

xCylinder ('z','r')

SELECT

smoothinit { Smooth the initial conditions a little, to minimize

the time wasted tracking the initial discontinuity }

prefer_speed { nonlinearity is not strong - we can get away with shortcuts }

VARIABLES

s (threshold=0.1)

p (threshold=0.1) { Saturation and Pressure }

DEFINITIONS

vl=30

mug = .01826 { gas l viscosity }

muo = 15 { oil viscosity }

$K = 4.87$ { Saturation-independent permeability coefficient }
! $P_{in} = 3000$ { Inlet pressure }
! $P_{out} = 2500$ { Outlet pressure }
 $P_{in} = 3000$ { Inlet pressure }
 $P_{out} = 2800$
 $swc = 0.2$
 $s_1 = s / (1 - swc)$
 $M = ((1 - s_1)^4 / \mu_o + (2 - s_1) * (s_1)^3) / \mu_{g1}$ { Total mobility }
 $f = (1 - S_1)^4 / \mu_o / M$ { Fractional flux }
 $k_{ro} = s_1^4$ { Relative permeability of water }
 $\phi = .206$ { porosity }
 $k_{rg} = s_1^3 * (2 - s_1)$
 $Tem = 648$ { temperature of teh system -Ranking }
 $V = 0.00440727$ { volume of the gas phase }
 $R_u = 10.731$ { universal gas constant }
 $Z_f = .94$
 $M_o = 8.439$
 $Mol = 250$
 $nmole = (P_{in} * V) / (Z_f * R_u * tem)$
 $conc = nmole / v$
! $fl = 6$ { fluid velocity }
 $D = 1.3678e-7 * (tem^{1.47} * mol^{2.2}) / (conc^{0.5} * p * mo)$
! $D = 2.238e-3$
 $epsvisc = D$ { A little artificial diffusion helps smooth the solution }
 $sint = \text{integral}(s)$ { the total extraction integral }

! hour = 60*60

! day = hour*24 { seconds per day }

INITIAL VALUES

s = 0 { start with all oil }

p = Pin + (Pout-Pin)*z/20 { start with a rough approximation to the pressure }

EQUATIONS

! s: $\phi \cdot dt(s) - \text{div}(K \cdot k_{rw} \cdot \text{grad}(p)) - \text{epsvisc} \cdot \text{div}(\text{grad}(s)) = 0$

! s: $\phi \cdot dt(s) - \text{div}(K \cdot k_{rw} \cdot \text{grad}(p)) - 1.17e-8 \cdot \text{div}(\text{grad}(s)) = 0$

s: $\phi \cdot dt(s) - \text{div}(K \cdot k_{ro} \cdot \text{grad}(p)) - \text{epsvisc} \cdot \text{div}(\text{grad}(s)) = 0$

p: $\text{div}(K \cdot M \cdot \text{grad}(p)) = 0$

BOUNDARIES

REGION 1

{ fillet the input pipe, and define no-flow boundaries of the box }

start(0,0)

natural(p)=0 natural(s) = 0

line to (20,0)

{ set constant outlet pressure, and "tautological" saturation flux }

! value(p) = Pout

natural (p)=dz(p) natural(s)= -K*kro*dz(p)

line to (20,1.0)

{ reset no-flow box boundaries }

value(p) = Pin value(s) = 1

line to (0,2.9)

{ set constant inlet pressure and saturation }

value(p) = Pin value(s) = 1

```

line to close
REGION 2
    { fillet the input pipe, and define no-flow boundaries of the box }
start(0.0,2.95)
value(p) = Pin    value(s) = 1
line to (20,1.05)
    natural(p)=dz(p) natural (s) = -K*krg*dz(p)
    line to (20,3.8)
        { set constant outlet pressure, and "tautological" saturation flux }
natural(p)=0 natural (s)=0 line to (0,3.8)
    value(p) = Pin    value(s) = 1
    line to close
TIME 0 to 7200 by 10
MONITORS
    for cycle=5
        contour(s) as "Saturation" range(0,1)
        contour(s) zoom as "Outflow Saturation"
            range(0,1)
        ! contour(p) zoom as "Pressure" range(0,1) painted
contour(p) as "Pressure"
    vector(-K*M*grad(p)) norm as "Flow Velocity"
PLOTS
    for t = 0 by 10 to 7200
        elevation (kro,krg) from (0,0) to (20,0)
        grid(z,r)

```

```

contour(s) as "Saturation" range(0,1) painted
surface(s) as "Saturation" range(0,1) painted viewpoint(60,-120,30)
contour(s) zoom as "Outflow Saturation"
contour(p) as "Pressure" painted
range(0.0,10) painted
vector(-K*M*grad(p)) norm as "Flow Velocity"
contour(K*M*magnitude(grad(p))) norm as "Flow Speed" painted
elevation(p) from (0,1.5) to (20,1.5)
elevation(S) from (0,0) to (20,0)
!elevation (krw) on s=0.5
!elevation(s,krw,kro) from(20,0) to (20,3.8) export format "#s#b#krw#b#kro#b#T" file "Ptable.txt"
!elevation(s) from(20,0) to (20,3.8) export format "#s#b#T" file "Ptables.txt"
!elevation(krw) from(20,0) to (20,3.8) export format "#krw#b#T" file "Ptable.txt"
HISTORIES
    history(sint/10) at (0,0) as "Recovery"
    export format "#b# #b#T " file "recovery.xls"
Range(0,1)
! history(kro,krw) at (2,3.8) (4,3.8) (6,3.8) (8,3.8)(10,3.8) (12,3.8) (14,3.8) (16,3.8) (18,3.8)(20,3.8)
history(kro,krw) at (2,3.8) (4,3.8) (6,3.8) (8,3.8)(10,3.8) (12,3.8) (14,3.8) (16,3.8) (18,3.8)(20,3.8)
    export format "#b# #b#T " file "kro.xls"
    export format "#b# #b#T " file "krw.xls"
    export format "#b# #b#T " file "s.xls"
END

```